Copyright Warning & Restrictions

The copyright law of the United States (Title 17, United States Code) governs the making of photocopies or other reproductions of copyrighted material.

Under certain conditions specified in the law, libraries and archives are authorized to furnish a photocopy or other reproduction. One of these specified conditions is that the photocopy or reproduction is not to be "used for any purpose other than private study, scholarship, or research." If a, user makes a request for, or later uses, a photocopy or reproduction for purposes in excess of "fair use" that user may be liable for copyright infringement,

This institution reserves the right to refuse to accept a copying order if, in its judgment, fulfillment of the order would involve violation of copyright law.

Please Note: The author retains the copyright while the New Jersey Institute of Technology reserves the right to distribute this thesis or dissertation

Printing note: If you do not wish to print this page, then select "Pages from: first page # to: last page #" on the print dialog screen

ABSTRACT

ROLES OF SURFACTANT AND BINARY POLYMERS ON DISSOLUTION ENHANCEMENT OF BCS II DRUGS FROM NANOCOMPOSITES AND AMORPHOUS SOLID DISPERSIONS

by
Md Mahbubur Rahman

Drug nanocomposites and amorphous solid dispersions (ASDs) are two major formulation platforms used for the bioavailability enhancement of BCS Class II drugs. The major drawback of nanocomposites is their inability to attain high drug supersaturation during *in vitro* (<50% relative supersaturation) and *in vivo* dissolution. On the other hand, formulating an amorphous solid dispersion (ASD) with high drug loading (>20%) that releases drug rapidly, while generating and maintaining high supersaturation over at least three hours is challenging. The goal of this thesis is to develop a fundamental understanding of the impact of anionic surfactants–polymers on *in vitro* drug release from nanocomposites and ASDs, while addressing the above challenges. To achieve this goal, the following objectives are set: (1) compare griseofulvin (GF, drug) release from spray-dried nanocomposites and ASDs with identical formulation that has low GF:polymer (HPC/Soluplus) mass ratio (1:1 to 1:5) and an anionic surfactant (SDS), (2) examine the presence/absence of SDS on drug release from nanocomposites, (3) develop rapidly supersaturating ternary ASDs of GF with HPC/Sol and SDS as a minor component, (4) investigate GF release from ternary ASDs of GF with a hydrophilic, wettability-enhancing polymer (HPC/PVP-VA64) as a minor component and an amphiphilic polymer as drug precipitation inhibitor (Soluplus), and (5) apply the fundamental knowledge generated for GF to another BCS Class II drug, itraconazole (ITZ).

Spray-drying of aqueous GF nanosuspensions with 1:5 GF:Sol–0.125% SDS has led to formation of a novel class of nanocomposites, HyNASDs, which have notable amorphous GF content (~5–20%). Their dissolution has generated 300% supersaturation within 20 min that is largely maintained after 3 h (250%). Such remarkable drug supersaturation is made possible by strong intermolecular interactions/miscibility between GF–Soluplus at 1:5 ratio and ensuing fast kinetic solubilization of GF nanoparticles upon contact of HyNASDs with water. While HyNASDs do not generate as high saturation as ASDs (480%), they can be rendered competitive to ASDs upon further optimization. The supersaturation generation by HyNASDs is affected by presence of SDS either in the formulation or in the dissolution medium, drug–polymer interactions/miscibility as well as the size of the drug (nano)crystals in the polymeric matrix. Incorporating even 1.23% SDS in Sol-based ASDs has led to dramatic increase in supersaturation (max. 570%), but it has no notable improvement for HPC-based ASDs. SDS provides Sol-based ASDs with enhanced wettability and augments Sol in solubilizing GF, without interfering with Sol's ability to inhibit GF recrystallization. Combination of Sol with HPC/VA64 has led to a trade-off between rapid drug release and high supersaturation. A strong synergistic effect exists for the ASD with 11:1 Sol:VA64. The inclusion of a hydrophilic polymer as a minor component in an amphiphilic, precipitation-inhibiting polymer of a ternary ASD exhibited optimal drug release. General findings from GF regarding HyNASD formation and impact of SDS are applicable to ITZ as well. Overall, this thesis has generated fundamental knowledge about the impact of SDS and binary polymers on improved *in vitro* release of BCS Class II drugs.

ROLES OF SURFACTANT AND BINARY POLYMERS ON DISSOLUTION ENHANCEMENT OF BCS II DRUGS FROM NANOCOMPOSITES AND AMORPHOUS SOLID DISPERSIONS

by
Md Mahbubur Rahman

A Dissertation
Submitted to the Faculty of
New Jersey Institute of Technology
in Partial Fulfillment of the Requirements for the Degree of
Doctor of Philosophy in Chemical Engineering

Otto H. York Department of
Chemical and Materials Engineering

August 2019

.

APPROVAL PAGE

ROLES OF SURFACTANT AND BINARY POLYMERS ON DISSOLUTION ENHANCEMENT OF BCS II DRUGS FROM NANOCOMPOSITES AND AMORPHOUS SOLID DISPERSIONS

Md Mahbubur Rahman

Dr. Ecevit A. Bilgili, Dissertation Advisor — Date
Associate Professor of Chemical and Materials Engineering, NJIT

Dr. Rajesh N. Davé, Committee Member — Date
Distinguished Professor of Chemical and Materials Engineering, NJIT

Dr. Robert B. Barat, Committee Member — Date
Professor of Chemical and Materials Engineering, NJIT

Dr. Murat Guvendiren, Committee Member — Date
Assistant Professor of Chemical and Materials Engineering, NJIT

Dr. Ilgaz Akseli, Committee Member — Date
Director of Pharmaceutical Science and Technology, Celgene

BIOGRAPHICAL SKETCH

Author: Md Mahbubur Rahman

Degree: Doctor of Philosophy

Date: August 2019

Undergraduate and Graduate Education:

- Doctor of Philosophy in Chemical Engineering,
  New Jersey Institute of Technology, Newark, NJ, 2019

- Master of Science in Chemical Engineering,
  North Carolina A&T State University, Greensboro, NC, 2015

- Bachelor of Science in Chemical Engineering,
  Bangladesh University of Engineering and Technology, Dhaka, Bangladesh, 2011

Major: Chemical Engineering

Presentations and Publications:

Journal Articles:

M. Rahman, A. Coelho, J. Tarabokija, S. Ahmad, E. Bilgili, Synergistic Effects of Hydrophilic Polymer–Amphiphilic Polymer Combination in Enhancing Griseofulvin Release from Amorphous Solid Dispersions, In preparation.

M. Rahman, S. Ahmad, J. Tarabokija, E. Bilgili, Impact of SDS on Griseofulvin Release from Spray-Dried Amorphous Solid Dispersions with HPC–Soluplus, In preparation.

M. Rahman, F. Arevalo, A. Coelho, E. Bilgili, Dissolution Enhancement via Drug Nanocrystal–Amorphous Solid Dispersions (HyNASDs), Eur. J. Pharm. Biopharm. (2019), Under review.

M. Rahman, A. Coelho, S. Ahmad, J. Tarabokija, E. Bilgili, Drug Release from Spray-Dried Hybrid Nanocrystal–Amorphous Solid Dispersions (HyNASDs): Impact of SDS, Powder Technol. (2019), Under review.

E. Bilgili, M. Rahman, D. Palacios, F. Arevalo, Impact of polymers on the aggregation of wet-milled itraconazole particles and their dissolution from spray-dried nanocomposites, Adv. Powder Technol., 29 (2018), 2941–2956 .

A. Bhakay, M. Rahman, R. Dave, E. Bilgili, Bioavailability enhancement of poorly water-soluble drugs *via* nanocomposites: formulation–processing aspects and challenges, Pharmaceutics, 10 (2018), 86.

Journal Articles Outside the Scope of This Dissertation:

R. Abrokwah, M. Rahman, V. Deshmane, D. Kuila, Effect of Titania Support on Fischer-Tropsch Synthesis using Cobalt, Iron, and Ruthenium Catalysts in Silicon-Microchannel Microreactor, Molecular Catalysis (2019), Under review.

M. Li, M. Rahman, C. Furey, J. Skros, O. Xu, R. Dave, E. Bilgili, Impact of Matrix Size on Dissolution Enhancement from Griseofulvin-laden Extrudates Prepared *via* Nanoextrusion, In preparation.

N. Parker, M. Rahman, E. Bilgili, A Microhydrodynamic Analysis of the Impact of Stirrer Speed and Media Loading on Breakage Kinetics during Wet Media Milling, In preparation.

Conference Proceedings:

M. Rahman, F. Arevalo, A. Coelho, S. Ahmad, J. Tarabokija, S. Bhujbal, E. Bilgili, Roles of SDS in Griseofulvin from Nanocomposites and Amorphous Solid Dispersions: A comparative Study. AIChE Annual Meeting, 2019, Orlando, FL

M. Rahman, A. Coelho, S. Ahmad, J. Tarabokija, S. Bhujbal, K. Radgman, E. Bilgili, Possible Synergistic Effects of Binary Polymers in Enhancing Release of a poorly Soluble Drug from Amorphous Solid Dispersions. AIChE Annual Meeting, 2019, Orlando, FL

N. Parker, M. Rahman, E. Bilgili, Are Crosslinked Polystyrene Beads as Effective as Zirconia Beads to Produce Drug Nanoparticles *via* Wet Stirred Media Milling? AIChE Annual Meeting, 2019, Orlando, FL

E. Bilgili, N. Parker, M. Rahman, A microhydrodynamic analysis of the impact of stirrer speed and media loading on breakage kinetics during wet media milling, 16th European Symposium on Comminution & Classification (ESCC), 2019, Leeds, UK

M. Rahman, S. Ahmad, J. Tarabokija, E. Bilgili, Release of Griseofulvin from Nanocomposites *vs.* Amorphous Solid Dispersions (ASDs): Roles of Surfactant and Drug Dose, NJPhAST, 2019, NJ

M. Rahman, A. Coelho, S. Bhujbal, E. Bilgili, Spray-dried nanocomposites and amorphous solid dispersions with identical formulation for comparative assessment of drug dissolution enhancement. AIChE Annual Meeting, Paper No: 298b, 2018, Pittsburgh, PA

M. Rahman, D. Palacios, F. Arevalo, E. Bilgili, Are low molecular weight polymers really effective for stabilization of wet-milled drug suspensions? AIChE Annual Meeting, Paper No: 170i, 2018, Pittsburgh, PA

M. Rahman, D. Palacios, F. Arevalo, E. Bilgili, Fast, immediate drug release from high drug-loaded spray-dried nanocomposites: criticality of polymer molecular weight. AIChE Annual Meeting, Paper No: 298j, 2018, Pittsburgh, PA

This dissertation is dedicated to my parents.
For their endless love, support, encouragement, and sacrifice.

আমার এই ছোট্ট অর্জনটুকূ আম্মা এবং আব্বার জন্য উৎসর্গ করিলাম।
আব্বা, অনেক ভাল থাকবেন ওপারে।
আম্মা, অনেক ভালবাসা নিবেন।
আপনাদের "মরু", "হাফজান" আজ অনেক বড় হয়ে গেছে।

ACKNOWLEDGMENTS

I would like to express my sincere gratitude to my dissertation advisor, Dr. Ecevit Bilgili, who is knowledgeable, stringent, perfectionist, considerate, and always supportive. He pushed and guided me to reach my personal best. At the same time, he is always there supporting me, defending me, encouraging me, and spending time with me throughout my Ph.D. program. He is not only an advisor in my research, but also the one doing everything in his power to guide me towards a successful future career. I am truly blessed having him as my dissertation advisor.

I would like to also express my appreciation to all my Ph.D. dissertation committee members. I especially thank Dr. Rajesh Dave for his support, constructive comments and feedback, and intellectual discussions throughout my research experience as well as allowing me to use his laboratories and instruments without which I would not have been able to generate some significant data presented here. I would like to extend my thanks to other committee members, Dr. Robert Barat, Dr. Murat Guvendiren, and Dr. Ilgaz Akseli, whose guidance, constructive feedback, and suggestions significantly helped me to reach excellence in research.

I would like to thank Ms. Clarisa Gonzalez for her time and constructive feedbacks about my dissertation formatting. I would like to recognize all the co-workers for their direct involvement in my research, either spiritually or physically: Eylul Cetindag, Guluzar Buyukgoz, Kai Zheng, Kuriakose Kunnath, Dr. Liang Chen, Nathaniel Parker, Paulina Alvarez, Danny Palacios, Faustin Arevalo, Alexander Coelho, Aron Gyorgypal, Stephanie Ahmad, James Tarabokija, and Keanu Radgman.

I am especially grateful to Dr. Meng Li for helping me to develop the skills necessary to succeed in my research and always encouraging me during my tough time.

I would like to thank all my friends who were by my side during my sorrows and joys, my ups and downs. I am fortunate enough to have such wonderful friends, seniors, and juniors. Although the list is quite long, I would like to mention some of the names to whom I am extremely grateful: Anup Saha (Dada), Shaon Bhai, Monir Bhai, Golam Morshed, Ahmed Ijaz (Saju), Plabon, Ashif Iqbal (Mickey), Dr. Toufiqur Rahman (Shopon), Hla Tun, Sourav Sagor (SMS), Lubna Apu, Dr. Farzana Rahmat, and Mehnaz Mursalat.

Finally, I would like to express my deepest gratitude to my family. To my mother, Momtaz Begum, and my father, Late Noor Muhammad, for their endless love and support at every stage of my life, my brother, Mizanur Rahman, my sisters, Noor Jahan Akhter and Noor Nahar Akhter. Without their support and encouragement this journey would not have been possible.

TABLE OF CONTENTS

TABLE OF CONTENTS

(Continued)

TABLE OF CONTENTS

(Continued)

TABLE OF CONTENTS

(Continued)

TABLE OF CONTENTS

(Continued)

Chapter **Page**

TABLE OF CONTENTS

(Continued)

TABLE OF CONTENTS

(Continued)

TABLE OF CONTENTS

(Continued)

Chapter **Page**

TABLE OF CONTENTS

(Continued)

Chapter **Page**

LIST OF TABLES

LIST OF TABLES

(Continued)

LIST OF TABLES

(Continued)

LIST OF FIGURES

LIST OF FIGURES

(Continued)

LIST OF FIGURES

(Continued)

LIST OF FIGURES

(Continued)

Figure **Page**

LIST OF FIGURES

(Continued)

LIST OF FIGURES

(Continued)

LIST OF FIGURES

(Continued)

LIST OF FIGURES

(Continued)

LIST OF FIGURES

(Continued)

LIST OF FIGURES

(Continued)

LIST OF FIGURES

(Continued)

LIST OF FIGURES

(Continued)

CHAPTER 1

INTRODUCTION

1.1 Motivation

It is estimated that approximately 40% of the marketed drugs and 75% of the new drug candidates coming out of the drug discovery pipeline are poorly water soluble (Di et al., 2009; Kipp, 2004; Lipinski, 2002). Due to their poor aqueous solubility, intestinal absorption of these drugs turns out to be rate-limiting, which leads to low bioavailability eventually (Fasano, 1998; Müllertz et al., 2010). Over the years, significant number of research has been carried out and directed toward developing various formulation/processing strategies to enhance the dissolution performance of these drugs. These strategies include production of prodrug (Rumondor et al., 2016), salt formation (Elder et al., 2013; Rahman et al., 2012), micelle formation (Letchford and Burt, 2007), cyclodextrin complexes (Aleem et al., 2008; Srivalli and Mishra, 2016), lipid-based systems (Hauss et al., 1998; Humberstone and Charman, 1997), drug nanocrystals (Li et al., 2016a; Merisko-Liversidge et al., 2003), amorphous solid dispersions (ASDs) (Nakagami, 1991; Serajuddin, 1999) etc. Among all these approaches, increasing the surface area by reducing drug particle size (drug nanocrystals) and increasing saturation solubility of the drug through the formation of ASD have achieved prevalence both in the academia and industry to enhance dissolution rate/bioavailability of poorly-water soluble drugs.

1.1.1 Background on Drug Nanocrystals and Their Production

In pharmaceutics literature, drug nanocrystals are defined as crystals with a size in the nanometer range; usually ranging from 10 nanometers to 1000 nm (Keck and Müller, 2006). Since the nanoparticles have tremendously higher specific surface area compared to the micron-sized particles, drug nanoparticles can provide significant dissolution rate and bioavailability enhancement to a multitude of poorly water-soluble drugs (Singh et al., 2011; Tanaka et al., 2012). The classical Noyes–Whitney equation (Noyes and Whitney, 1897b) could help to explain the improvement in drug dissolution rate, *dm/dt*, due to the particle size reduction and ensuing increase in surface area (Equation 1.1):

$$\left(\frac{dm}{dt}\right) = \frac{AD(C_s - C)}{h} \tag{1.1}$$

where m is mass of drug dissolved at time t, A is the surface area of the particles, D is the diffusion coefficient, h is the diffusion layer thickness, C_s is the saturation solubility, and C is the instantaneous concentration in the bulk dissolution medium. In addition to the significant enhancement of the particle surface area, the diffusion layer thickness (h) also decreases significantly as particle size decreases (Galli, 2006). Furthermore, the particle size of drugs could also influence their saturation solubility in the bulk solution, which can be explained by the Ostwald–Freundlich equation (Equation 1.2) (Shchekin and Rusanov, 2008).

$$\log\left(\frac{C_S}{C_\infty}\right) = \frac{2\sigma V}{2.303RT\rho r} \tag{1.2}$$

where C_S is saturation solubility, C_∞ is solubility of large particles, σ is interfacial tension, V is atomic volume, R is gas constant, T is absolute temperature, ρ is density

of the solid, and *r* radius of the small particle. According to Equation (1.2), the reduction of particle size especially to sizes below 100 nm increases the saturation solubility C_S (Shegokar and Müller, 2010). This indicates that not only do nanoparticles affect the dissolution rate by higher specific surface area and reduced diffusion layer thickness, but also they allow for higher saturation solubility C_S. (Kesisoglou et al., 2007) have also demonstrated 10–15% solubility increase with the reduction of drug particle size down to 100 nm. Others reported similarly higher solubility of the ultrasmall particles and nanoparticles (Junghanns and Müller, 2008b; Shegokar and Müller, 2010).

Among various methods used for the production of drug nanoparticles (Li et al., 2016a), wet stirred media milling (WSMM) has found the most common use in the pharmaceutical industry owing to its unique advantages: WSMM is organic solvent free, scalable, and environmentally benign. Moreover, WSMM allows for production of nanosuspensions with high drug loading, which exhibit low excipient side effects. Also, it has continuous processing capability and can be applied universally to any poorly water-soluble drug (Afolabi et al., 2014; Bhakay et al., 2018b; Kesisoglou et al., 2007; Li et al., 2016a; Merisko-Liversidge and Liversidge, 2008). Nanosuspensions also have the advantage of higher mass packing (higher dose) per injection volume and improved physical stability owing to the use of stabilizers such as polymers and/or surfactants (Müller and Peters, 1998; Rabinow, 2004). Several marketed products such as Rapamune® (Pfizer (Wyeth), New York City, NY, USA), Emend® (Merck, Kenilworth, NJ, USA), Tricor® (AbbVie, North Chicago, IL, USA), Megace® ES (PAR Pharmaceuticals, Woodcliff Lake, NJ, USA),

and Invega® SustennaTM (Janssen, Beerse, Belgium) made use of wet media milling.

In the common recirculating mode of WSMM operation, micron-sized drug particles in an aqueous solution of stabilizers, usually polymers and/or surfactants, circulates from a holding tank passing through the milling chamber, exiting through a screen, and returning to the holding tank. During the milling operation, the milling media (beads) are retained in the milling chamber by the screen. Due to high speed rotation of the rotor/stirrer, turbulent motion is induced in the suspension, and the mechanical power consumed is dissipated during frequent bead–bead collisions (Eskin et al., 2005). The drug particles captured between the beads are subjected to stress, which is concentrated on the cracks already present in the material and causes crack propagation, ultimately leading to breakage of the particles (Schönert, 1988) and eventually production of nanoparticles.

1.1.2 Typical Issues in the Production–Drying of Drug Nanosuspensions

Despite its advantages, WSMM is not devoid of any issues during the production of drug nanoparticles. A major issue is the aggregation–growth tendency of the milled drug particles in the aqueous suspensions during milling or storage (Li et al., 2016a). Formation of aggregated particles negates the advantage associated with the large surface area of the drug nanoparticles. Usually, two major competing mechanisms operate during the milling of the drug particles: breakage of the drug particles due to mechanical stresses and aggregation due to highly attractive inter-particle forces (van der Waals, hydrophobic forces, etc.) (Bhakay et al., 2013b). Additionally, Ostwald ripening may occur causing drug nanocrystals to grow (Bitterlich et al., 2014).

Ostwald ripening can be defined as a process where differences in solubility, as a function of particle sizes, leads to a transport of dissolved drug from small to larger particles causing growth over time. Therefore, physical stability of the drug nanosuspensions by various stabilizers (Cerdeira et al., 2010; Wu et al., 2011), also known as dispersants, is required during milling and storage for proper downstream processing and adequate shelf-life.

Selection of proper stabilizers with optimum concentration plays a major role in formulating a stable drug nanosuspension. Inadequate concentration of stabilizers may not be able to prevent aggregation of drug nanoparticles, while excess in concentration may facilitate Ostwald ripening. Electrostatic interactions, steric forces, entropic forces, and van der Waals forces among the nanoparticles usually determine the physical stability of the drug nanosuspension (Wu et al., 2011). Drug particles dispersed within a liquid continuous medium are stabilized by steric, electrostatic mechanisms or combination of both i.e., electrosteric mechanism (see Figure 1.1), owing to adsorption of polymers and/or surfactants on drug particle surfaces (Basa et al., 2008; Bilgili et al., 2016; Merisko-Liversidge and Liversidge, 2011; Van Eerdenbrugh et al., 2008c). Nonionic polymers or nonionic surfactants (e.g., poloxamers, cellulosic derivatives, polysorbates, and povidones etc.) usually provide steric stability by preventing the particles from getting into the range of attractive van der Waals forces. Electrostatic stabilization is usually imparted by ionic surfactants, e.g., sodium dodecyl sulfate (SDS), dioctyl sulfosuccinate sodium salt (DOSS), and benzethonium chloride (BKC). In electrosteric stabilization, nonionic polymers or surfactants and ionic surfactants stabilize the particles, acting simultaneously.

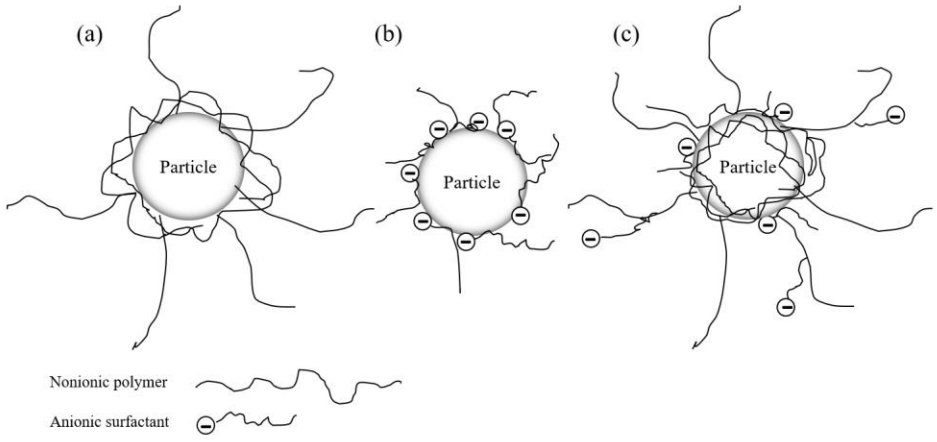

Figure 1.1 Schematic of physical stabilization mechanism in drug nanosuspensions: (a) steric stabilization imparted by nonionic polymers; (b) electrostatic stabilization imparted by anionic surfactants; and (c) electrosteric stabilization imparted by both nonionic polymers and anionic surfactants.

Usually, solid dosage forms are preferred over suspensions due to convenience and easiness of their use by patients. Therefore, nanosuspensions produced *via* WSMM are dried and converted into nanocomposites microparticles or simply nanocomposites, which are ultimately incorporated into standard dosage forms such as tablet, capsule, sachets (Basa et al., 2008; Bhakay et al., 2014a; Van Eerdenbrugh et al., 2008b), and polymeric strip films (Bhakay et al., 2016; Krull et al., 2016; Krull et al., 2015; Sievens-Figueroa et al., 2012; Susarla et al., 2015). Drying of nanosuspensions can be achieved *via* spray-freeze drying (Cheow et al., 2011; Wang et al., 2012), freeze drying (De Waard et al., 2008; Layre et al., 2006), spray drying (Azad et al., 2015b; Lee, 2003), vacuum drying (Choi et al., 2008; Kim and Lee, 2010), as well as granulation with, or coating onto, inert excipient particles (Basa et al., 2008; Bhakay et al., 2014b).

Unfortunately, drug nanoparticles tend to form aggregates during both milling and drying of the drug suspensions (Bhakay et al., 2013a; Lee, 2003), causing the loss of surface area of the drug. It must be noted that the same dispersants (soluble polymers and surfactants) used to prevent nanoparticle aggregation also act as matrix former in the dried nanocomposites and modulate drug release during dissolution/redispersion (Bhakay et al., 2018b; Li et al., 2016b; Li et al., 2016c). However, depending on the formulation, drug nanoparticles may not be fully recovered from the dried composites during redispersion and dissolution, which will slow down the drug dissolution and reduce the bioavailability from such nanoparticle-based formulations (Bhakay et al., 2013a; Bhakay et al., 2018b; Chaubal and Popescu, 2008). Here, redispersion refers to the dispersion of the drug composites in various physiologically relevant fluids like water, and preservation of the milled drug particle size. Various redispersion methods were studied extensively by Bhakay et al. (2013b, 2018a). Slow/incomplete recovery of drug nanoparticles from the nanocomposites was observed when a steric stabilizer or ionic stabilizer was used alone in the precursor griseofulvin (drug) suspension (Bhakay et al., 2013b; Lee, 2003). Drug particles were fully recovered only when steric stabilizer and ionic stabilizer were used in combination (e.g., Basa et al., 2008; Bhakay et al., 2013b)) or when swellable dispersants were co-milled along with the drug (Azad et al., 2015b; Bhakay, 2014; Bhakay et al., 2018a).

In the production of drug nanosuspensions/nanocomposites, the most widely used dispersants are the soluble polymers (Bhakay et al., 2018b; Li et al., 2016a). Among different properties of the polymers, molecular weight (MW) has a great

impact on the steric stabilization of the drug suspensions. It also regulates the suspension/solution viscosity (Adamson and Gast, 1997; Choi et al., 2008; Ploehn and Russel, 1990), mechanical properties of films (Rowe, 1986), and drug release from polymer-based dosages (Mittal et al., 2007). Similarly, use of different polymers or polymers with different MW is expected to determine the extent of aggregation in drug nanosuspensions and nanocomposites. Interestingly, only few studies examined the impact of different polymers and different MW of the same polymer on drug nanosuspension stabilization and dissolution enhancement systematically, which requires further investigation. On the other hand, despite being an effective dispersant, surfactants may pose several challenges such as aggregation of the drug nanoparticles in suspensions during milling/storage (Cerdeira et al., 2010; Knieke et al., 2013), micellar solubilization of the drug (Yalkowsky and Roseman, 1981) and particle growth *via* Ostwald ripening during milling and/or storage (Ghosh et al., 2011; Knieke et al., 2013; Verma et al., 2011). Additional challenges associated with the use of anionic surfactants include incompatibilities with other ionic molecules, sensitivity to pH, salt or temperature changes, GIT irritation (Gupta and Kompella, 2006; Liversidge and Cundy, 1995), and even toxicity when used in excess (Liversidge and Cundy, 1995), especially for inhalation applications (Lebhardt et al., 2011; Suzuki et al., 2000). In view of all the aforementioned issues, during formulation development, surfactant usage should be minimized to mitigate all potential negative impact.

Besides all the challenges mentioned above regarding the drug nanoparticle-based formulations, limited supersaturation capability of nanocomposites appears to

be the greatest impediment to the bioavailability enhancement and their competitiveness to ASDs. Throughout the thesis, supersaturation refers to relative supersaturation defined as $S = (C/C_s - 1)$, where C is the drug concentration in a dissolution medium and C_s refers to the thermodynamic aqueous solubility of the crystalline drug at the same temperature. While in the prevalent pharmaceutical terminology, particles with sizes less than 1 μm are considered nanoparticles (nanocrystals); in most published work, the median/mean size is in the range of 100–400 nm (see the review by Li et al., 2016a) and fewer publications reported true drug nanoparticles with a median/mean size below 100 nm (e.g., Li et al., 2015). As mentioned in Section 1.1.1, owing to their high curvature, nanocrystals with sizes <~100 nm tend to show high saturation solubility, which also enhances the dissolution rate, and this phenomenon can be explained *via* the Kelvin and the Ostwald–Freundlich equation (Equation 1.2) (Muller et al., 1998). The higher apparent solubility that originates from the greater curvature of <~100 nm nanocrystals than that of the micron-sized crystals was estimated to be ~10–15% (Kesisoglou and Wu, 2008); however, up to 50% increase in apparent solubility was also reported (Muller and Peters, 1998). In general, the potential benefit of nanocrystals in terms of supersaturation is mostly left without consideration in the field of bioavailability enhancement (Peltonen et al., 2018), which requires more investigation.

1.1.3 Amorphous Form of Drugs

Enhanced dissolution rate, improved bioavailability, safe dose escalation, elimination of food effects, and improved safety, efficacy and tolerability profiles are some of the

numerous advantages of drug nanocrystals (Junghanns and Müller, 2008a). However, with all these advantages, nanocrystal formulations are severely limited in their bioavailability enhancement capability due to low aqueous solubility of drug nanocrystals. Often for drugs with very low aqueous solubility, the achieved increase in dissolution rate *via* size reduction is limited and insufficient to provide significant enhancement of bioavailability (Müller et al., 2011). Another platform approach for bioavailability enhancement of poorly water-soluble drugs is the production of amorphous form of the drug. Amorphous drugs lack distinct intermolecular arrangement that leads to crystalline structure. They exhibit lower thermodynamic stability and higher apparent solubility then their crystalline counterparts. The solubility advantage of the pure amorphous compared with its crystalline form could be theoretically estimated using Equation (1.3) (Hancock and Parks, 2000):

$$\left(\frac{\sigma^{amorphous}}{\sigma^{crystal}}\right) = e^{\frac{\Delta G}{RT}} \tag{1.3}$$

where $\sigma^{amorphous}/\sigma^{crystal}$ is the ratio of the solubility of amorphous form to the stable crystalline from, ΔG is the free energy difference between the amorphous and crystalline forms, R is the universal gas constant, and T is the temperature in Kelvin. The free energy difference can be determined from Hoffman equation (Equation 1.4) (Hoffman, 1958).

$$\Delta G = \frac{\Delta H_f \times \Delta T \times T}{T_m^2} \tag{1.4}$$

where ΔH_f is the enthalpy of fusion, T is the operating temperature, T_m is the melting point temperature, and ΔT is the difference between T_m and T.

Unfortunately, taking advantage of amorphous form of poorly water-soluble drugs is challenging since pure amorphous drugs are inherently metastable: they can simply convert to crystalline form during processing and storage (recrystallization in the solid state) (Marsac et al., 2006; Shamblin et al., 1999; Wu and Yu, 2006; Yu, 2001) as well as during dissolution (recrystallization in the liquid dissolution medium) (Alonzo et al., 2010). Usually, pure amorphous products are undesirable to scale up due to their highly unstable nature and higher energy state. To resolve this stability issue, drugs are dispersed molecularly in an amorphous polymeric matrix, known as amorphous solid dispersions (ASDs), which imparts stability (prevention of recrystallization) to amorphous form of the drug during storage and dissolution. Polymers can provide stability through a number of mechanisms including reduction in the drug molecules' mobility, increase in the glass transition temperature (T_g) of amorphous drug *via* ASD formation and anti-plasticization exerted by the glassy polymer matrix (Crowley and Zografi, 2002; Cui, 2007; Shah et al., 2013; Van den Mooter et al., 2001), and strong drug–polymer intermolecular interactions such as hydrogen bonding, hydrophobic interactions, etc. (Kestur and Taylor, 2010; Kestur et al., 2011). Since the apparent solubility of the amorphous form is higher than its crystalline counterpart, ASDs can offer significant enhancement in the dissolution rate and supersaturation generation under non-sink conditions resulting in bioavailability enhancement of the drugs with very low aqueous solubility (Ambike et al., 2005; Six et al., 2004; Yamashita et al., 2003). Usually, types of the carrier matrix, molecular level interaction of drug–polymer, the extent of recrystallization inhibition during storage and dissolution, drug:polymer ratio, and manufacturing

process play important roles in the production and stabilization of ASDs (Li et al., 2017a; Qian et al., 2010; Thakral and Thakral, 2013).

1.1.4 Production of Amorphous Solid Dispersions (ASDs)

Processes used for the production of ASDs can be broadly classified into two major categories: solvent-based processes and fusion/melting-based processes (Brough and Williams, 2013). In the fusion/melting-based processes, drug and polymeric carriers are melted together at a temperature above their melting or glass transition temperature, then the molten liquid is solidified by rapid cooling. Due to the rapid cooling, drug molecules do not have sufficient time and molecular mobility to crystallize while being trapped inside the highly viscous polymeric matrix (Brough and Williams, 2013), which leads to molecular dispersion of the drug inside the polymer or formation of a solid drug–polymer solid solution. The resultant solid is then crushed or milled to obtain a desired particle size. The main advantage of the fusion/melting-based processes is that they do not require any solvent. However, an important prerequisite for ASD formation is the miscibility of the drug and polymer in the molten state to obtain a homogenous mixture. Thus, for a successful formulation, a polymeric carrier that shares similar physicochemical properties with the drug would be more suitable (Vo et al., 2013). Despite having found significant use in pharmaceutical industry, the most serious limitation of the fusion/melting-based processes is that they can only process drugs and polymers that are not thermally degradable at the elevated temperatures required for proper processing (Vasconcelos et al., 2016). Another issue is that if the drug and polymer are not miscible at the processing temperature; phase separation of the drug during cooling is

highly likely. Hot melt extrusion (HME) has become the standard fusion-based process to produce ASDs (Baghel et al., 2016).

Solvent-based processes entail preparing a solution of both drug and polymer in a single solvent or solvent mixture followed by removal of the solvent(s) to yield a solid dispersion. This technique enables molecular level mixing of the drug and polymer, which could be beneficial to the drug–polymer miscibility and stability of the product. It addresses the main issue associated with the melting method relating to the decomposition of drugs and carriers at high temperature because solvent can be removed at relatively low temperatures. An important prerequisite of the solvent-based process is the solubilization of the drug and polymer in the same solvent mixture (Leuner and Dressman, 2000). However, finding out a suitable non-toxic solvent is not always an easy task because carriers are hydrophilic in nature, whereas drugs are hydrophobic. Another disadvantage of this method is residual solvent after evaporation, which often requires a secondary drying process such as oven drying, microwave drying, etc. to achieve an acceptable solvent content required by regulations and maintain physical stability by avoiding any plasticization effect of the residual solvent (Brough and Williams, 2013; Janssens and Van den Mooter, 2009).

Spray drying (Langham et al., 2012; Paradkar et al., 2004) and freeze drying (Kagotani et al., 2013; Schersch et al., 2010) are two widely used processes for the production of ASDs in the solvent-based process. Freeze drying or lyophilization is a process comprised of freezing the drug–polymer solution followed by the reduction of surrounding pressure allowing sublimation of the frozen solvent (Brough and Williams, 2013; Van Drooge et al., 2006). In the spray drying process, a drug–

polymer solution is atomized into a hot gas chamber that causes fast evaporation of the solvent, resulting in sudden increase in viscosity and encapsulation of the drug molecules in amorphous form into the polymeric matrix (Vehring, 2008). The fast drying and presence of the amorphous polymer matrix prevents nucleation and growth of drug crystals, thus enabling molecular level dispersion of the amorphous drug in the polymeric matrix.

1.1.5 Challenges Involved with Amorphous Solid Dispersions (ASDs)

Despite several advantages of ASDs, the number of commercially available products is not as high as one would anticipate or desire (see Table 1.1). The most important problem is the poor stability of the amorphous drug during production, storage, and dissolution. In general, recrystallization of the amorphous drugs occurs in two stages: nucleation followed by crystal growth *via* diffusion or rearrangement of the drug molecules (Baird and Taylor, 2012). Thus, for the physical stability, molecular mobility of the drug–polymer is an important factor for the stability of the amorphous drug. Moisture acts as a plasticizer and often reduces the T_g of ASD and thus increases molecular mobility (Duddu and Sokoloski, 1995; Hancock and Zografi, 1994). Since polymer absorb moisture during storage, the storage at high relative humidity (RH) can accelerate drug recrystallization (Rumondor et al., 2009). High storage temperature, especially closer to the glass transition temperature of the ASD, could be another reason for accelerated recrystallization of the drug due to enhanced molecular mobility (Alhalaweh et al., 2015; Shibata et al., 2014).

Besides storage instability, maintenance of supersaturation during the dissolution of ASDs is another major challenge. During dissolution, drug may phase

separate in the form of liquid–liquid phase-separated (LLPS) droplets, or may convert to crystalline nanoparticles, which will lead to a significant reduction of the supersaturation and inability to maintain high extent of drug dissolution (Ilevbare and Taylor, 2013). Crystallization from amorphous formulations is complex and may occur either directly from the solid matrix upon contact with the dissolution medium or from a supersaturated solution generated during dissolution under non-sink conditions (Alonzo et al., 2010). Polymers play a critical role in altering the crystallization kinetics of the drug from both the matrix (Ewing et al., 2014) and solution phase (Raghavan et al., 2001), enabling supersaturation generation and maintenance when the polymer is judiciously selected in the formulation (Alonzo et al., 2011; Alonzo et al., 2010; Suzuki and Sunada, 1998). Multiple factors such as polymer type, drug–polymer miscibility and interactions, and physical stability of the amorphous drug have significant effect on the dissolution performance of ASDs (Craig, 2002; Serajuddin, 1999). Therefore, a number of complex factors needs to be considered during the evaluation of dissolution performance of ASDs including the drug:polymer ratio, the relative dissolution rate of the components, and the crystallization behavior of the drug during dissolution. In order to understand the mechanisms of drug release from ASDs and to optimize polymer selection, it is essential to evaluate the relative impact of the polymer on crystal nucleation and growth.

Table 1.1 List of Commercially Available Medicines Manufactured by Amorphous Solid Dispersion (ASD) Technique Containing Poorly Water-soluble Drugs

Trade Name	Generic Name	Processing Technology[a]	Company (Year of Approval)[b]
Cesamet®	Nabilone	SE	Meda Pharma (1985)
ISOPTIN® SR	Verapamil	ME	Ranbaxy Laboratories (1987)
Sporanox®	Itraconazole	FB bead layering	Janssen (1992)
Prograf®	Tacrolimus	SD	Astellas Pharma (1994)
NuvaRing®	Etonogestrel/ Ethinyl Estradiol	ME	Merck (2001)
Kaletra®	Lopinavir/Ritonavir	ME	AbbVie (2007)
Intelence®	Etravirin	SD	Janssen (2008)
Modigraf®	Tacrolimus	SD	Astellas Pharma (2009)
Zortress®	Everolimus	SD	Novartis (2010)
Norvir®	Ritonavir	ME	AbbVie (2010)
Onmel®	Intraconazole	ME	Merz Pharma (2010)
INCIVEK™	Telaprevir	SD	Vertex (2011)
Zelboraf®	Vemurafenib	Solvent/ anti-solvent precipitation	Roche (2011)
Kalydeco®	Ivacaftor	SD	Vertex (2012)
Noxafil®	Posaconazole	ME	Merck (2013)
Astagraf XL®	Tacrolimus	WG	Astellas Pharma (2013)
Belsomra®	Suvorexant	ME	Merck (2014)
Harvoni®	Ledipasvir/Sofosbuvir	SD	Gilead Sciences (2014)
Viekira XR™	Dasabuvir/Ombitasvir/ Paritaprevir/Ritonavir	ME	AbbVie (2014)
Epclusa®	Sofosbuvir/Velpatasvir	SD	Gilead Sciences (2016)
Orkambi®	Lumacaftor/Ivacaftor	SD	Vertex (2016)
Venclexta™	Venetoclax	ME	AbbVie (2016)
Zepatier®	Elbasvir/Grazoprevir	SD	Merck (2016)
Mavyret™	Glecaprevir/Pibrentasvir	ME	AbbVie (2017)[c]

[a]FB: Fluidized Bed; ME: Melt Extrusion; SD: Spray Drying; SE: Solvent Evaporation; WG: Wet Granulation.
[b]Based on US Food & Drug Administration (FDA), 2016 (Huang and Williams, 2018; Jermain et al., 2018).
[c]Based on European Medicines Agency: Public Assessment reports, 2016 (Huang and Williams, 2018; Jermain et al., 2018).

Although the higher free energy of the amorphous form may *theoretically* achieve a solubility level that is order of magnitude higher than that of its crystalline

counterpart, this high free energy also works as the driving force for spontaneous recrystallization from the solid state or supersaturated solution upon dissolution (Marsac et al., 2006). Usually, in the conventional ASDs, drug is molecularly dispersed or solubilized in a polymeric carrier (binary system) (Konno et al., 2008). However, significant improvement in the performance of drug ASDs has been reported recently for ternary ASDs consisting of drug–binary polymers (Xie and Taylor, 2016) or drug–polymer–surfactant (Ghebremeskel et al., 2007). Several reports have shown the improved dissolution performance and storage stability due to the presence of surfactant in the ASD formulation over the formulation w/o surfactants (Ghebremeskel et al., 2007; Goddeeris et al., 2008; Joshi et al., 2004; Li et al., 2013; Sotthivirat et al., 2013, Feng et al., 2018). It is claimed that presence of surfactant in the ASD formulation increases the drug wettability by reducing the interfacial energy barrier between the drug particles and the dissolution medium and it can inhibit drug precipitation in the aqueous medium (Jung et al., 2016). On the other hand, detrimental effects of the surfactants have also been reported in literature during dissolution of ASDs due to the competitive interaction between drug–polymer–surfactant resulting in promoted recrystallization of the drug from supersaturated solutions (Chen et al., 2016; Liu et al., 2016; Deshpande et al., 2018). In fact, sometimes by increasing the solubility and reducing the surface tension of the growing crystals, surfactants might promote precipitation *in vivo* negating the supersaturation maintenance of the drug (Rodríguez-hornedo and Murphy, 1999). Therefore, to say the least, the roles/impact of surfactant in the dissolution of drug ASDs are elusive, and the use of surfactants can be detrimental/beneficial depending

on the specific drug–polymer–surfactant system and composition. Hence, further investigation of the roles of surfactants in the wettability enhancement and recrystallization inhibition of drugs along with polymers is warranted.

Conventionally, ASD has been regarded as a simple binary component system in which the drug acts as a solute and the polymer acts as a solvent (Meng et al., 2017). However, a successful ASD formulation must be resistant to recrystallization during processing and storage. Moreover, ideally having a high drug load, it should generate and maintain high supersaturation during *in vivo* dissolution (Davis, 2018). Meeting all these criteria using a single polymer (binary ASD) could be very challenging; hence, an upsurge of research into ternary ASDs in the recent years is notable (Davis, 2018). Significant improvement in the performance of drug ASDs has already been reported recently by using ternary systems such as drug–binary polymers (e.g., Xie and Taylor, 2016a) and drug–polymer–surfactant (e.g., Ghebremeskel et al., 2007). The use of binary polymers in a ternary drug ASD has been the focus of recent studies for further improvement of drug dissolution. In the ternary ASD system (binary polymer), the dissolution profile is regulated by the characteristics of individual polymers (Ohyagi et al., 2017). Some polymers enable rapid drug release, while others can efficiently inhibit recrystallization in the polymeric matrix and the dissolution medium during the *in vitro* or *in vivo* dissolution (Zhang et al., 2018). However, in the ternary ADSs, various polymers with different hydrophilicity/amphiphilicity and drug recrystallization inhibition capability have been combined to improve the dissolution performance of ASDs (Prasad et al., 2016; Xie and Taylor, 2016a; Yoshida et al., 2012). Another driver for ternary ASDs

besides dissolution enhancement is improved storage stability and long-term drug recrystallization inhibition (Albadarin et al., 2017; Davis et al., 2018).

In the rest of Chapter 1, the remaining challenges and knowledge gaps regarding various aspects of drug nanocomposites and ASDs that are used in the dissolution enhancement of poorly water-soluble drugs are presented and how each chapter of this dissertation will address them will be indicated.

1.2 Remaining Challenges and Knowledge Gaps

1.2.1 Comparative Assessment of Various Dispersants and Their Molecular Weight in Nanosuspension Stabilization and Dissolution Rate Enhancement

Particle size growth and aggregation occur in drug suspensions during wet media milling, storage, and downstream processing, and the extent of such phenomena must be reduced as they reduce drug surface area available for dissolution (Bilgili et al., 2016; Knieke et al., 2014). To prevent gross physical instability, drug nanosuspensions are usually dried into nanocomposites that are then incorporated into standard solid dosage forms such as tablets and capsules (Basa et al., 2008; Bhakay et al., 2018b; Van Eerdenbrugh et al., 2008c). This approach also helps to achieve patient compliance because solid oral dosage forms incorporating drug nanoparticles are preferred over drug nanosuspensions. Among different drying techniques, spray-drying is preferred over other techniques due to several advantages such as its continuous and scalable nature, its ability to produce micron-sized particles with large surface area (Kemp, 2011), and its potential in producing high drug-loaded nanocomposites (Azad et al., 2015b; Bhakay et al., 2014a). Although high drug loading in dried powders can be achieved by both freeze drying and spray drying

(Azad et al., 2015b; Niwa and Danjo, 2013), spray drying is inherently continuous having a one-step process, and is more energy and time efficient compared to freeze drying (Chin et al., 2014). Hence, spray drying is selected here as the drying method for converting drug nanosuspensions into nanocomposites.

Although preparation of drug nanoparticles in the form of wet-milled suspensions and their drying into nanocomposites has been shown to be an effective approach for enhancing the dissolution rate of various poorly water-soluble drugs (Bhakay et al., 2018b; Li et al., 2016a), several challenges remain in formulation design. To prevent aggregation during milling and ensure physical stability of the suspensions, dispersants such as polymers, sugars, and surfactants are added to the suspensions where they function as stabilizers (Bhakay et al., 2018b; Chin et al., 2014; Kesisoglou et al., 2007). Unfortunately, depending on the concentration and types of dispersants used in the formulation, drug nanoparticles may still form aggregates in the wet-milled suspensions due to attractive inter-particle forces (van der Waals, hydrophobic forces, etc.) (Li et al., 2016a; Malamatari et al., 2018); further aggregation may occur during drying (Bhakay et al., 2014a; Kim and Lee, 2010; Li et al., 2016d). It must be noted that the same dispersants used to prevent nanoparticle aggregation also act as matrix former in the dried nanocomposites and modulate drug release during dissolution/redispersion (Bhakay et al., 2018b; Li et al., 2016a; Li et al., 2016b). Overall, the anticipated advantage of producing drug nanoparticles in terms of dissolution enhancement may not be achieved fully due to the aggregation of the drug particles upon milling and drying (Bose et al., 2012; Choi et al., 2008) and slow nanoparticle recovery from the nanocomposite matrix (Bhakay

et al., 2014a; Li et al., 2016b).

Among various classes of dispersants, surfactants have been commonly used because they enhance drug wettability, reduce surface tension, and provide electrostatic stabilization (Bhakay et al., 2018b; Gupta et al., 2013; Li et al., 2018a). However, there could be several issues with use of surfactants in drug nanosuspensions such as aggregation of drug nanoparticles (Knieke et al., 2013; Li et al., 2016d), particle size growth due to Ostwald ripening during milling and/or storage (Ghosh et al., 2011; Knieke et al., 2013), and micellar solubilization of the drug (Yalkowsky and Roseman, 1981). Additional challenges for anionic surfactants include incompatibilities with other ionic molecules; sensitivity to pH, salt, and temperature changes; GIT (gastro intestinal tract) irritation (Gupta and Kompella, 2006; Liversidge and Cundy, 1995); and toxicity when used in excess (Liversidge and Cundy, 1995), especially for the inhalation applications (Lebhardt et al., 2011; Suzuki et al., 2000). Various formulation strategies can be used to mitigate these issues with surfactants. One strategy is to use a combination of a surfactant with a water-soluble adsorbing polymer, thereby reducing surfactant usage (Bhakay et al., 2018b; Bilgili and Afolabi, 2012; Bilgili et al., 2016; Niwa et al., 2011). Another strategy is to develop surfactant-free formulations that contain other classes of dispersants either alone or in combination (Bhakay et al., 2018b; Chin et al., 2014). For example, water-soluble polymers such as hydroxypropyl cellulose (HPC), hydroxypropyl methyl cellulose (HPMC), polyvinylpyrrolidone (PVP), and polyethylene glycol (PEG) can be used alone or in combination with other water-soluble dispersants such as sugars (e.g., sucrose, lactose) and sugar alcohols (e.g.,

mannitol, sorbitol) (Abdelwahed et al., 2006; Chin et al., 2014; Kesisoglou et al., 2007), water-insoluble dispersants such as microcrystalline cellulose, anhydrous dicalcium phosphate, and montmorillonite (Van Eerdenbrugh et al., 2008a), and swellable crosslinked polymers such as sodium starch glycolate and croscarmellose sodium (Azad et al., 2015b; Bhakay et al., 2014b).

Polymers are the most widely used dispersants in drug nanosuspensions/nanocomposites (Bhakay et al., 2018b; Li et al., 2016a). Polymer molecular weight (MW) affects steric stabilization in drug suspensions and suspension/solution viscosity (Adamson and Gast, 1997; Choi et al., 2008; Ploehn and Russel, 1990), mechanical properties of films (Rowe, 1986), and drug release from polymer-based dosages (Mittal et al., 2007). More specifically, use of different polymers or polymers with different MW is expected to determine the extent of aggregation in drug nanosuspensions and nanocomposites. Interestingly, only few studies examined the impact of different polymers and different MW of the same polymer on drug nanosuspension stability systematically. For example, ITZ was wet ball-milled for 4 days in aqueous solution of HPC with MW in the range ~10–50 kg/mol inside a vial (Choi et al., 2008). This study concluded that lower MW HPC is more effective for faster particle size reduction, while suspensions with all HPC grades were stable. However, they did not study the impact of MW on drug dissolution. Nabumetone and halofantrine suspensions with HPMC and PVP were wet media milled for 6 h in a mixer mill (Sepassi et al., 2007); however, drying of the suspensions and dissolution testing were not performed. Their study suggests that only lower MW HPMC (<50 kg/mol) led to drug suspensions having mean particle

sizes less than 1 μm. Unfortunately, studies like (Choi et al., 2008; Sepassi et al., 2007) that used low-energy mills as opposed to high-energy (wet stirred media) mills do not truly reflect the impact of different polymers or MW on steric stabilization and reduction of drug aggregate formation. In wet media milling, breakage kinetics and extent of drug particle breakage depend on the viscosity of the drug suspensions, which is affected by the type/MW of the polymer (Li et al., 2016a). The use of higher MW polymer and/or higher polymer concentration causes more pronounced viscous dampening and slower breakage (Bilgili and Afolabi, 2012; Sepassi et al., 2007). While viscous dampening occurs in any wet media mill, low-energy mills are particularly sensitive to viscous dampening; drug nanoparticles may not even be produced with high MW polymers even after prolonged milling (see e.g., Sepassi et al., 2007). Hence, such studies drew somewhat confounded conclusions about the impact of polymer MW due to significant impact of viscous dampening. In the study presented in Chapter 2, a wet stirred media mill was used instead, which reduces the sensitivity to viscous dampening and helps to better elucidate the roles of polymer MW.

Itraconazole (ITZ), an antifungal drug, has been used for the treatment of local and systemic mycoses. As it is a hydrophobic model BCS Class II drug with high permeability and poor water solubility (<1 ng/mL) (Peeters et al., 2002), several research groups (Azad et al., 2016; De Smet et al., 2014; Parmentier et al., 2017; Sarnes et al., 2014; Van Eerdenbrugh et al., 2008d) produced ITZ-loaded nanocomposites to improve its dissolution rate. These studies used surfactants along with other dispersants in the nanocomposite formulations; the highest drug loading

that achieved immediate drug release (>80% in 20 min) was 63% (Van Eerdenbrugh et al., 2008d). Therefore, in Chapter 2, the impact of various polymers/MW on ITZ nanosuspension stabilization and ITZ release from spray-dried ITZ nanosuspensions is investigated. This investigation could yield significant insight into the roles of polymers and allow for design of high-drug loaded, fast-dissolving, surfactant-free nanocomposites.

1.2.2 Drug Nanocomposites With High Supersaturation Capability and Their Comparison to ASDs in Dissolution Enhancement

As mentioned in Section 1.1.2, hydrophilic/amphiphilic polymers and/or surfactants are added to the suspensions as stabilizers to suppress the aggregation during and after WSMM (Li et al., 2016b; Wang et al., 2013). In general, drug:stabilizer mass ratio has been optimized based on several considerations. At low concentration of stabilizers, drug nanoparticle aggregation cannot be suppressed (Knieke et al., 2013; Li et al., 2016c); while if used in excess, stabilizers especially surfactants may promote Ostwald ripening (Ghosh et al., 2011; Verma et al., 2011). Also depending on the molecular weight of the polymer, too high concentration of the polymer can cause significant viscous dampening, leading to slower breakage kinetics during milling (Bilgili and Afolabi, 2012; Knieke et al., 2013) as well as downstream processing issues (Bhakay et al., 2018). Finally, stabilizer concentration should be minimized to achieve high drug loading in the final solid dosages, while still achieving physical stability in the milled suspensions (Bhakay et al., 2018b; Li et al., 2016b). In view of these considerations, it is no surprise to find that a drug:polymer mass ratio much higher than 1 has been widely reported in several papers: 1:0.5 to 1:0.05 (Kesisoglou et al., 2007; Wang et al., 2013), 1:0.8 to 1:0.02 (Chang et al.,

2015), and 1:1 to 1:0.02 (Van Eerdenbrugh et al., 2008c). A quick review of recent literature (see Table 1.2) also suggests a similarly high drug:polymer mass ratio, i.e., 1:1 to 1:0.01, in drug nanosuspensions used in the preparation of spray-dried nanocomposites.

As mentioned in Section 1.1.2, drug nanosuspensions prepared *via* WSMM are usually dried and converted into nanocomposite microparticles or shortly nanocomposites. Pharmaceutical formulators need to resolve two major issues regarding the drug release from nanocomposites. First, depending on the stabilizer formulation in the precursor nanosuspensions, primary drug nanoparticles may not be effectively recovered from the nanocomposites during the dissolution (Azad et al., 2015b; Bilgili et al., 2018). This may be attributed to the poor physical stability of the drug nanosuspensions (extensive aggregation) prepared by WSMM and/or inability of the nanocomposite matrix to release drug nanoparticles fast enough (Azad et al., 2015b; Bhakay et al., 2013a; Bilgili et al., 2018; Li et al., 2016c). These issues have been largely addressed (see Bhakay et al., 2018b and the references cited therein), e.g., by using strongly adsorbing/interacting polymers (Bilgili et al., 2018), soluble excipients like sugars and sugar-alcohols (Iurian et al., 2017; Medarević et al., 2018), combination of a polymer with a surfactant (Bhakay et al., 2014a; Li et al., 2016b), and combining an adsorbing polymer with colloidal superdisintegrants (Azad et al., 2015b; Li et al., 2018b).

Table 1.2 Formulations and Drug–Polymer Content of Nanosuspensions Used for the Preparation of Spray-Dried Nanocomposites in Recent Studies

Drug	Drug content (% w/v)	Polymeric stabilizer[b]	Drug:polymer mass ratio	References
Naproxen	1.0	HPMC	1:0.5	Kumar et al. (2014)
Lovastatin	0.5[a]	PVP K12, K30, K17, and PVA	1:0.2	Zhang et al. (2014)
Griseofulvin	10[a]	HPC SL	1:0.25	Azad et al. (2015)
Naproxen	1.0, 3.0, and 5.0	HPMC E15	1:0.2–1:0.6	Kumar et al. (2015)
Griseofulvin	5.0	HPC SL	1:0.25	Shah et al. (2016)
Allisartan Isoproxil	5.0	PVP K30	1:0.01–1:0.03	Hou et al. (2017)
Mefenamic Acid	5.0[a]	HPC SSL	1:0.15	Konnerth et al. (2017)
Aprepitant	2.5	Pharmacoat 603 and HPC SSL	1:0.5, 1:1	Toziopoulou et al. (2017)
Carvedilol	8.3	HPC SL	1:0.1–1:0.4	Medarevic et al. (2018)
Fenofibrate	10.0[a]	HPC	1:0.25	Aleandri et al. (2018)
Itraconazole	10.0[a]	HPC SL	1:0.25–1:0.65	Li et al. (2018)
Itraconazole	10.0[a]	HPC L and HPC SL	1:0.45	Bilgili et al. (2018)

[a]With respect to the total weight of the suspension liquid (% w/w); [b]HPMC: hydroxypropyl methylcellulose, HPC: hydroxypropyl cellulose, PVA: polyvinyl alcohol, PVP: polyvinylpyrrolidone.

Unfortunately, the second major challenge, i.e., the low supersaturation generation capability of drug nanocomposites in *in vitro* and *in vivo* dissolution has not been resolved. Interestingly, even though all studies mentioned in Table 1.2 reported significant increase in drug release from the spray-dried nanocomposites as compared with as-received drug micro-crystals and their physical mixtures with the excipients, none of these studies investigated or reported any supersaturation generation in the dissolution tests. In fact, the low drug supersaturation from nanocomposites is the primary reason for pharmaceutical formulators to opt for ASDs for bioavailability enhancement of high-dose poorly soluble drugs. As mentioned in Section 1.1.3, as the apparent solubility of the amorphous form is much greater than its crystalline counterpart, ASDs provide high extent of drug release above thermodynamic solubility and significant supersaturation (Ambike et al., 2005; Six et al., 2004; Yamashita et al., 2003) unlike drug nanocomposites.

Surprisingly, although both drug nanocomposites and ASDs have been used as two major platforms for dissolution enhancement, a *head-to-head* comparison of *in vitro* drug release from these two solid dosage forms having *identical formulation* is not available in the literature. Typically, to establish the dissolution enhancement owing to the use of nanocrystals, nanocomposites were compared with the as-received crystalline drug as well as physical mixtures of the as-received drug with the same formulation of the nanocomposites (Bhakay et al., 2014a; Hecq et al., 2005). Likewise, ASDs were compared to the as-received drug microparticles and/or drug microparticles in tablets/capsules in terms of dissolution enhancement (Jung et al., 1999; Six et al., 2004). In some cases, nanosuspensions, not dried nanocomposites,

were compared with ASDs, but not in a head-to-head manner. For instance, Fakes et al. (2009) investigated the bioavailability enhancement of a BCS class II drug, BMS-488043, using a 10% (w/w) drug nanosuspension with 2% (w/w) hydroxypropyl cellulose (HPC-SL) and 0.1% (w/w) sodium lauryl sulfate (SLS). They also prepared the drug ASD by spray drying and flash evaporation techniques at different drug:polymer (polyvinyl pyrrolidone, PVP) ratios. In the case of spray drying, 40:60 drug:PVP was used for the formulation development and further characterization, whereas 90:10 drug:PVP ratio was selected in the case of flash evaporation. The nanosuspension and two amorphous formulations containing 20% and 40% drug were compared to a wet-milled crystalline drug in a capsule in a crossover beagle dog study. While having different formulations, the ASDs showed superior bioavailability enhancement compared with the nanosuspension, as expected from the relatively high drug supersaturation capability of the ASDs with respect to the nanosuspension. In a recent study (Li et al., 2017), a nanoextrusion process was used to compare griseofulvin (GF) nanocomposites with ASDs. GF nanosuspensions prepared *via* WSMM were extruded with additional polymers and simultaneously dried in a twin-screw extruder. This nanoextrusion process with two different polymers, i.e., HPC (partially miscible with GF) and Soluplus (Sol, miscible with GF), led to the formation of GF nanocomposite and GF ASD, respectively. The researchers demonstrated that for 100 mg GF dose, GF–Sol ASD led to 340% (relative) supersaturation whereas GF–HPC nanocomposite only achieved 60% supersaturation. While this finding corroborates the well-known shortcoming of nanocomposites *vs.* ASDs in drug supersaturation generation, a direct and scientifically fair *head-to-head*

comparison of drug release from nanocomposites *vs.* ASDs having *identical polymer/formulation* is still lacking in the literature. Finally, none of the previous studies on spray-dried GF nanocomposites (Azad et al., 2015b; Bhakay et al., 2014a; Shah et al., 2016) reported or investigated GF supersaturation in the dissolution medium.

Chapter 3 presents how drug nanocomposites and ASDs with identical formulation can be prepared using the spray drying process, which enables us to compare their drug release in a head-to-head manner, unlike all previously mentioned studies. The main objective is to improve the supersaturation capability of drug nanocomposites in dissolution tests significantly using a relatively low drug:polymer mass ratio (high polymer loading), i.e., 1:1 and 1:3, as compared with high drug:polymer mass ratio like 3:1 in typical nanosuspension formulations (Table 1.1), and compare their dissolution performances to those of the ASDs.

1.2.3 Roles of Surfactant in Drug Release from Spray-Dried Nanocomposites

A quick review of recent literature on spray-dried drug nanosuspensions that contain polymer–anionic surfactants as stabilizers (see Table 1.3) suggests a high drug:polymer mass ratio, i.e., 1:0.5 to 1:0.1, with minimal use of anionic surfactants with respect to drug (1:0.1 to 1:0.0025). Selection of such low concentrations of anionic surfactants, usually below their critical micelle concentration (CMC), has been mostly driven by two considerations: (i) significant growth of drug nanoparticles could occur due to Ostwald ripening above CMC (Ghosh et al., 2011; Verma et al., 2011) and (ii) anionic surfactants are relatively toxic and can cause gastrointestinal tract irritation, if used at high concentrations (Gupta and Kompella, 2006; Liversidge

and Cundy, 1995).

As discussed in Section 1.2.2, the low supersaturation generation capability in dissolution tests has not been resolved or addressed adequately. For example, even though all studies reported in Table 1.3 indicated significant increase in drug release from the spray-dried nanocomposites with surfactants as compared with as-received drug micro-crystals and/or their physical mixtures with the excipients, they, except Zuo et al. (2013), did not investigate or report any supersaturation generation in the dissolution tests. The dissolution data in Zuo et al. (2013) suggest up to ~50% (relative) supersaturation of fenofibrate from spray-dried nanocomposites in 0.15% sodium dodecyl sulfate (SDS) solution, which is in line with supersaturation levels from traditional nanocomposites (Li et al., 2017b; Müller and Peters, 1998). It is fair to assert that low drug supersaturation from nanocomposites is still the primary reason for pharmaceutical formulators to opt for ASDs for bioavailability enhancement of poorly soluble drugs. Hence, a new approach for boosting the supersaturation capability of nanocomposites to make them competitive to ASDs is warranted.

Being motivated by the use of low drug:polymer mass ratios from 1:1 to 1:9 in drug ASDs (Baghel et al., 2016; Singh and Van den Mooter, 2016) unlike the high drug:polymer ratios (1:0.8 to 1:0.02) in traditional drug nanocomposites (Chang et al., 2015; Kesisoglou et al., 2007; Van Eerdenbrugh et al., 2008c; Wang et al., 2013), as also depicted in Table 1.3, in Chapter 4, drug nanocomposites with relatively high polymer loading are presented. Judicious choice of polymers that have relatively low aqueous viscosities even at high concentrations allowed for preparation of drug

nanosuspensions and their spray-drying without processing issues. To avoid potential toxicity issues associated with anionic surfactants, SDS, the most common anionic surfactant, was used at 0.125% w/v in the drug suspensions, below its CMC (0.24% w/v (Moroi et al., 1974)). Chapter 4 also presents the impact of SDS during *in vitro* drug release from the nanocomposites.

Table 1.3 Formulations and Drug–Polymer–Anionic Surfactant Content of Aqueous Drug Nanosuspensions Used for the Preparation of Spray-Dried Nanocomposites in Recent Studies

Drug	Drug content (% w/w)	Polymeric stabilizer and grade[b]	Surfactant[b]	Drug:polymer: surfactant mass ratio (–)	References
Miconazole	20	HPC LF, HPMC E15	SDS	1:0.25:0.0025	Cerdeira et al. (2013)
Itraconazole	20	HPC LF, HPMC E15	SDS	1:0.25:0.0025	Cerdeira et al. (2013)
Fenofibrate	10[a]	HPMC E5	SDS	1:0.2:0.003	Zuo et al. (2013)
Griseofulvin	10	HPC SL	SDS	1:0.25:0.05	Bhakay et al. (2014)
Azodicarbonamide	10	HPC SL	SDS	1:0.25:0.05	Bhakay et al. (2014)
Lovastatin	0.5	PVP K12/K17/K30, PVA	SDS	1:0.2:0.05	Zhang et al. (2014)
Griseofulvin	10	HPC SL	SDS	1:0.25:0.05	Azad et al. (2015)
Itraconazole	1[a]	PVP K40	SDS	1:0.1:0.01–1:0.3:0.05	Kumar et al. (2015)
Griseofulvin	5[a]	HPC SL	DS	1:0.25:0.01	Shah et al. (2016)
Hesperetin	1	HPMC	SC	1:0.5:0.1	Liu et al. (2018)
Glibenclamide	1	HPMC	SC	1:0.5:0.1	Liu et al. (2018)
Resveratrol	1	HPMC	SC	1:0.5:0.1	Liu et al. (2018)
Rutin	1	HPMC	SC	1:0.5:0.1	Liu et al. (2018)
Quercetin	1	HPMC	SC	1:0.5:0.1	Liu et al. (2018)
Aprepitant	2.5[a]	HPMC E15, HPC SSL	SDS	1:0.5:0.1, 1:1:0.04	Toziopoulou et al. (2017)
Carvedilol	8.3[a]	HPC SL	SDS	1:0.1:0.01–1:0.4:0.01	Medarevic et al. (2018)
Fenofibrate	10	HPC	SDS	1:0.25:0.05	Aleandri et al. (2018)
Itraconazole	10	HPC L, HPC SL	SDS	1:0.25:0.02	Bilgili et al. (2018)

[a]With respect to the total volume of the suspension liquid (% w/v); [b]DS: docusate sodium; HPMC: hydroxypropyl methylcellulose, HPC: hydroxypropyl cellulose, PVA: polyvinyl alcohol, PVP: polyvinylpyrrolidone; SC: sodium cholate; SDS: sodium dodecyl sulfate.

1.2.4 Roles of an Anionic Surfactant in Drug Release from Spray-Dried ASDs

In most of the recent studies (see Table 1.4), anionic surfactants like sodium dodecyl sulfate (SDS) have been used as a carrier along with polymers in ASDs so as to solubilize the drug; hence, surfactants form a high mass fraction of the ASDs. This is not surprising as the use of surfactants and surfactants–polymers as carriers has been an emerging trend in the last two decades (Vasconcelos et al., 2007). When polymers alone cannot achieve high kinetic solubilization, they are augmented with copious amounts of surfactants which can solubilize drugs through micellar solubilization and surfactant–polymer complex formation (Jung et al., 2016; Liu et al., 2016; Xia et al., 2016). Although the role of anionic surfactants in wettability enhancement of drugs is commonly accepted and mentioned, Table 1.4 suggests that this aspect either for anionic surfactants like SDS alone or along with polymers has been rarely examined and quantified, especially in relation to the drug release from ASDs. For example, (Lu et al., 2014) investigated the impact SDS, the most commonly used anionic surfactant, in the wettability enhancement of simvastatin (SV) and its relation to the dissolution rate of the SV–polyvinyl pyrrolidone (PVP) solid dispersion *via* separate measurements of contact angle and water absorption into a packed powder bed. While they reported the positive impact of SDS inclusion on drug wettability and drug release form the solid dispersions, they did not investigate the impact of SDS on the supersaturation maintenance/recrystallization kinetics. Similarly, the impact of anionic surfactants on drug supersaturation maintenance has not been routinely studied in separate desupersaturation–recrystallization kinetic studies unlike in Chen et al. (2018), Deshpande et al. (2018) and Feng et al. (2018). Moreover, several

studies have indicated that SDS had deleterious impact on drug supersaturation maintenance as it promoted drug recrystallization in the presence of polyvinyl pyrrolidone-vinyl acetate (PVP-VA) (Liu et al., 2016) and crystal growth in the presence of PVP (Mosquera-Giraldo et al., 2014).

As SDS was intended as a carrier/solubilizer in most of the studies in Table 1.4, the drug:SDS mass ratios in ASDs are typically in the range of 1:0.2 to 1:3, except in few studies (Dave et al., 2013; Kim et al., 2018; Lu et al., 2014; Truong et al., 2015; Yan et al., 2012) that did not investigate the impact of SDS on drug wettability and recrystallization kinetics. In other words, SDS has been rarely used as a minor component, e.g., 1:0.05 or 20:1 drug:polymer mass ratio. In view of the existing literature, it is fair to state that the impact of SDS, as a *minor component* of the ASD, on both drug wettability enhancement and drug crystallization inhibition/supersaturation maintenance in the presence of polymers, specifically hydroxypropyl cellulose (HPC) and Soluplus (Sol), has not been systematically examined. It is hypothesized that the use of SDS as a minor component along with a drug-miscible polymer, which can provide solubilization and supersaturation maintenance, could boost supersaturation from the ASDs *via* mainly wettability enhancement and some additional drug solubilization, without having any deleterious effect on drug recrystallization. Another driver for the use of SDS as a minor component of ASDs is that anionic surfactants are relatively toxic and can cause gastrointestinal tract irritation (Gupta and Kompella, 2006; Kim et al., 2016), especially if used at high concentrations in ASDs with high drug doses.

Table 1.4 The Formulation Composition of Drug ASDs with Sodium Dodecyl Sulfate (SDS) in Recent Studies and Survey of the Use of Wettability and Desupersaturation Tests

Drug	Drug loading[a] (% w/w)	Polymer[b]	Drug:Polymer:SDS	Wettability testing	DeS testing[c]	References
Ketoprofen	10%	PEG	1:8:1	No	No	Mura et al. (2005)
Tacrolimus	10%	CMC-Na	3:24:3	No	No	Park et al. (2009)
Docetaxel	5–9%	PVP K30	1:9:1–1:19:1	No	No	Moes et al. (2011)
Valsartan	50–67%	HPMC	3:1.25:0.25–3:2:1	No	No	Yan et al. (2012)
Sulfathiazole	33–50%	PVP K29/32	1:1:0.1–1:1:1	No	No	Dave et al. (2013)
Simvastatin	33%	PVP K29/32	1:3:0.02–1:3:0.06	Yes	No	Lu et al. (2014)
Sorafenib	20–50%	Soluplus	1:0.9:0.1–1:4.5:0.5	No	No	Truong et al. (2015)
Tacrolimus	20–33%	HPMC	1:1:1–1:1:3	No	No	Jung et al. (2016)
Felodipine	23%	Soluplus	1:3:0.2–1:3:0.4	No	Yes	Chen et al. (2018)
Itraconazole	50%	Soluplus, PVP VA64	2:1:1	No	Yes	Deshpande et al. (2018)
Itraconazole	20%	HPMC-AS	1:3.75:0.25–1:2.75:1.25	No	Yes	Feng et al. (2018)
Sirolimus	16–48%	HPMC	1:1:0.05–1:5:0.1	No	No	Kim et al. (2018)
Nifedipine	14–40%	Kolliphor, Soluplus	1:1:0.5–1:4:2	No	No	Muralichand and Bhikshapathi, (2018)

[a]% w/w with respect to the total weight of the total solid content.
[b]CMC-Na: Carboxymethylcellulose-sodium; HPMC: hydroxypropyl methylcellulose; HPMC-AS: hydroxypropyl methylcellulose-acetyl succinate; PEG: polyethylene glycol; PVP: polyvinyl pyrrolidone; PVP-VA: polyvinyl pyrrolidone-vinyl acetate.
[c]DeS testing: Desupersaturation testing

Unlike all previous studies, the study presented in Chapter 5 aims to examine the impact of a common anionic surfactant, SDS, as a minor component of a drug–polymer–SDS ASD, on *in vitro* drug release while elucidating its roles in wettability enhancement and recrystallization inhibition in the presence of HPC/Sol.

1.2.5 Synergistic Effects of Binary Polymers in ASDs in Drug Supersaturation

Several recent reports (see Table 1.5) have shown improved dissolution performance and storage stability of the ternary ASDs (binary polymers with drug) over binary ASDs (single polymer with drug). Al-Obaidi and Buckton (2009) studied the dissolution performance and storage stability of binary and ternary griseofulvin (GF) ASDs produced by hydroxypropyl methylcellulose acetate succinate (HPMCAS) and poly[N-(2-hydroxypropyl) methacrylamide] (PHPMA) in the dissolution performance and storage stability. Although the ternary ASD provided significant storage stability due to the stronger GF interactions with both HPMCAS and PHPMA *via* hydrogen bonding, there was no improvement observed during dissolution compared to the binary ASDs. Xie and Taylor (2016b) optimized the dissolution performance of a high drug loaded ASD containing celecoxib (CXB) by using binary polymers. Polyacrylic acid (PAA), a hydrophilic polymer, was used to achieve rapid drug release, while hydroxypropyl methylcellulose (HPMC) or HPMCAS were used to inhibit CXB recrystallization, thus maintaining the supersaturation during dissolution. The ternary ASDs with certain ratios of HPMC and PAA achieved rapid release as well as crystallization inhibition at 30% CXB loading. The optimum formulation was reported to have 3:6:1 mass ratio for both CXB–PAA–HPMCAS and CXB–PAA–HPMC, which achieved fast CXB release and high supersaturation generation–

maintenance. Xie and Taylor (2016a) also investigated the effectiveness of polyvinyl pyrrolidone (PVP) K12, PVP K29/32, HPMC, and HPMCAS in inhibiting CXB crystallization *via* desupersaturation experiments and compared the CXB release rate and crystallization tendency of CXB in various binary and ternary ASDs. HPMC and HPMCAS were more effective than PVP K12 or PVP K29/32 in maintaining supersaturation. The dissolution results from binary ASDs suggest that the CXB release was substantially faster from PVP-based ASDs than HPMC/HPMCAS-based ASDs. However, poor crystallization inhibition ability of PVP K12 and PVP K29/32 resulted in faster desupersaturation compared to HPCM/HPMCAS. Ternary ASD with 4:1 PVP:HPMCAS/HPMC exhibited slower CXB release than PVP-based binary ASD, but no desupersaturation was observed during dissolution time period (16 h).

Table 1.5 Binary Polymers Used in the Preparation of Ternary Drug ASDs *via* Solvent Evaporation Techniques

Drug	Drug loading[a] (% w/w)	Polymer1 (P1)[b]	Polymer2 (P2)[b]	Drug:P1:P2 Mass Ratio (–)[c]	Wettability study	DeS test[d]	References
Griseofulvin	50	HPMCAS	PHPMA	1:0.5:0.5	No	No	Al-Obaidi and Buckton, (2009)
Cilostazol	20	HPMC	PVP	1:2:2–1:3:1	No	No	Park et al. (2013)
API	30	PVP	PLGA	1:1.5:0.8	No	No	Meeus et al. (2015)
Celecoxib	50	PVP	HPMCAS	1:0.8:0.2	No	Yes	Xie and Taylor, (2016a)
Celecoxib	50	PVP	HPMC	1:0.8:0.2	No	Yes	Xie and Taylor, (2016a)
Celecoxib	10–50	PAA	HPMCAS	1:0.4:0.6–1:8:1	No	Yes	Xie and Taylor, (2016b)
Celecoxib	30–50	PAA	HPMC	1:0.5:0.5–1:2:0.3	No	Yes	Xie and Taylor, (2016b)
Itraconazole	10–30	Soluplus	HPMCP	1:4.5:4.5–1:1.3:1	No	No	Davis et al. (2017)
Griseofulvin	20	HPMC	EUD	1:2:2	No	Yes	Ohyagi et al. (2017)
Ibuprofen	20	PVP VA64	HPMCP	1:2:2	No	No	Ziaee et al. (2017)
Itraconazole	30	Soluplus	HPMCP	1:1.3:1	No	No	Davis et al. (2018)
Lovastatin	25	Soluplus	HA	1:1.5:1.5	No	Yes	Guan et al. (2019b)
Lacidipine	16.7	Soluplus	GA	1:3.75:1.25	No	Yes	Guan et al. (2019a)

[a]% w/w with respect to the total weight of the solid content.

[b]EUD: Eudragit, GA: gum Arabic, HA: hyaluronic acid; HPMC, hydroxypropyl methylcellulose, HPMCAS: hydroxypropyl methyl cellulose acetate succinate, HPMCP: hydroxypropyl methyl cellulose phthalate, PEG: polyethylene glycol, PHPMA: poly [N-(2-hydroxypropyl)methacrylate], PLGA: Poly(lactic-co-glycolic acid), PAA: polyacrylic acid, PVP: polyvinyl pyrrolidone, PVP VA: polyvinyl pyrrolidone-vinyl acetate.

[c]The ratios refer to the polymer1:polymer2 mass ratio. All formulations had 1:3 drug:total polymer mass ratio whether a single polymer or binary polymers were used.

[d]DeS test: desupersaturation test.

Guan et al. (2019b) investigated the synergistic effect of Soluplus (Sol) and hyaluronic acid (HA) on the *in vivo* and *in vitro* dissolution and supersaturation maintenance of lovastatin (LOV). In their study, HA was used as a crystal growth inhibitor and the Sol was used as a nucleation inhibitor. Desupersaturation test confirmed the synergistic effect of HA–Sol combination on the supersaturation maintenance of LOV. Significant enhancement in the dissolution performance was achieved by the ASD with binary polymers (Sol–HA) than the ASDs with single polymer. The possible reason for the synergistic effect of the binary polymer was explained by the Sol–HA complex formation where HA could insert into the Sol micelles and interact with Sol *via* hydrogen bonds providing both electrostatic and steric stabilization against nucleation and crystal growth from the supersaturated drug solutions. Guan et al. (2019a) investigated the synergistic effect of a nucleation inhibitor (Sol) and a crystal growth inhibitor (gum arabic, GA) on the *in vitro–in vivo* performance of lacidipine from ASD formulation. Although significant improvement in supersaturation maintenance was not observed, synergistic effect in equilibrium solubility enhancement and dissolution performance was observed with Sol–GA mass ratio 3:1 even after 3 months of accelerated storage condition. The authors explained that the complex micelle of Sol–GA could provide a softer core with improved solubilizing ability, resulting in improved equilibrium solubility of the drug. Davis et al. (2017) produced ternary ASDs of ITZ–Sol–HPMCP and studied the storage stability and dissolution performance by varying the drug–polymer compositions. After one year of storage at accelerated condition, all the ternary formulations had amorphous ITZ confirming storage stability. Dissolution studies indicated that the

formulations with higher Sol content exhibited faster dissolution and higher extent of ITZ supersaturation. Ohyagi et al. (2017) investigated the synergistic role of polymer blending on dissolution performance of GF ASDs. The ternary ASD of GF–HPMC–Eudragit (EUD) showed faster drug release with a significantly higher supersaturation than the GF–HPMC and GF–EUD ASDs. In their study, to produce a ternary ASD, first a polymer blend was produced by spray drying of HPMC and EUD, and then this spray-dried polymer blend was spray-dried again with GF to produce ternary ASD. The authors reasoned that the hydrogen bond formation due to the intermolecular interactions between HPMC and EUD likely helped to improve the dissolution performance of ternary ASDs over binary ASDs.

The recent studies overall suggest that ternary ASDs that make judicious use of binary polymers can outperform binary ASDs with a single polymer in one or more of the following performance metrics: storage stability, rapid drug release, and high supersaturation generation with prolonged maintenance. Among all studies, the work of Xie and Taylor, (2016a, b) is quite intriguing and has offered a new strategy for ternary ASDs. The inclusion of an effective crystallization inhibitor (HPMC, HPMCAS) as a *minor component* in a hydrophilic polymer (PVP, PAA), which enables rapid drug release, of a ternary drug ASD can achieve both rapid drug release and high, sustained drug supersaturation during *in vitro* dissolution. The study presented in Chapter 6 explores if this strategy works for ternary griseofulvin (GF) ASDs with binary polymer combination of HPC/PVP-VA64 (hydrophilic polymer) and Sol (amphiphilic polymer, possible crystallization inhibitor).

1.3 Dissertation Outline

This dissertation has been organized into various chapters as follows:

1) Chapter 2 assesses the impact of polymers on the aggregation of wet-milled itraconazole and their dissolution from spray-dried nanocomposites. The aim is to understand the impact of polymer type and molecular weight on nanoparticle stabilization and drug release from the nanocomposites. The fundamental knowledge generated could help formulators guide the rational formulation design of surfactant-free, stable nanosuspensions and fast dissolving spray-dried nanocomposites.
2) Chapter 3 examines drug supersaturation generation during the dissolution of spray-dried griseofulvin nanocomposites *vs.* ASDs, which contain a low drug:polymer mass ration (high polymer loading). The characterization of the nanocomposites suggests the formation of molecularly dispersed drug surrounding the drug nanocrystals, a special class of nanocomposites we called hybrid nanocrystal–ASD (HyNASD).
3) Impact of an anionic surfactant (SDS) in the formation and dissolution performance of HyNASDs with various drug:polymer mass ratios and different drug doses has been investigated and results/discussion are presented in Chapter 4. The criticality of the anionic surfactant in high supersaturating HyNASDs has been indicated.
4) In Chapter 5, impact of surfactant as a minor component of ASDs on drug release has been systematically investigated for various drug:polymer ratios and different drug doses. Despite being a minor component, anionic surfactant played a major

role in supersaturation from ASDs.

5) In Chapter 6, synergistic effect of binary polymer combination in the drug supersaturation generation and maintenance from ASDs has been examined using combinations of two hydrophilic polymers that provide rapid drug release and an amphiphilic polymer that generates supersaturation and inhibits drug recrystallization.
6) To generalize the observations and understanding from Chapters 3–5 that focused on griseofulvin, in Chapter 7, another poorly water-soluble drug, itraconazole (ITZ), has been used in HyNASDs and ASDs. HyNASD formation and its significant supersaturation effect as well as positive impact of SDS as a minor component of HyNASDs/ASDs has been corroborated.
7) Finally, Chapter 8 provides the conclusions and recommendations for future work that originate from interesting research questions/issues identified during the course of this investigation.

CHAPTER 2

IMPACT OF POLYMERS ON THE AGGREGATION OF WET-MILLED ITRACONAZOLE AND THEIR DISSOLUTION FROM SPRAY-DRIED NANOCOMPOSITES

We explore the impact of various polymers and their molecular weight on the stabilization of wet-milled suspensions of itraconazole (ITZ), a poorly soluble drug, and its dissolution from spray-dried suspensions. To this end, ITZ suspensions with SSL, SL, and L grades of hydroxypropyl cellulose (HPC) having molecular weights (MWs) of 40, 100, and 140 kg/mol, respectively, hydroxypropyl methyl cellulose (HPMC E3 with 10 kg/mol), polyvinylpyrrolidone (PVP K30 with 50 kg/mol), sodium dodecyl sulfate (SDS, surfactant), and HPC SL–SDS were wet media milled and spray-dried. Laser diffraction results show that 2.5% HPC SL–0.2% SDS led to the finest ITZ nanosuspension, whereas without SDS, only 4.5% HPC with SL/L grades ensured minimal aggregation. Rheological characterization reveals that aggregated suspensions exhibited pronounced pseudoplasticity, whereas stable suspensions exhibited near Newtonian behavior. Spray-drying yielded nanocomposites with 60–78% mean ITZ loading and acceptable content uniformity. Severe aggregation occurred during milling/drying when 4.5% polymers with MW ≤ 50 kg/mol were used; their nanocomposites exhibited incomplete redispersion due to slow matrix erosion and released ITZ slowly during dissolution test. Overall, high drug-loaded, surfactant-free ITZ nanocomposites that exhibited immediate release (>80% dissolved in 20 min) were prepared *via* spray-drying of wet-milled ITZ with 4.5% HPC SL/L.

2.1 Materials and Methods

2.1.1 Materials

ITZ was purchased from Jai Radhe Sales (Ahmedabad, India). HPC, HPMC, and PVP are commonly used hydrophilic, water-soluble polymers that serve as steric stabilizers and dispersants in the preparation of drug nanosuspensions and nanocomposites (Bhakay et al., 2018b; Li et al., 2016a). SSL, SL, and L grades of HPC with MW of 40, 100, and 140 kg/mol, respectively, donated by Nisso America Inc. (New York, NY, USA), were used to examine the impact of MW. HPMC (Methocel E3 grade with 10 kg/mol MW) and PVP (Kollidon K30 grade with 50 kg/mol MW) were donated by Dow Chemical (Midland, MI, USA) and BASF Corporation (Florham Park, NJ, USA), respectively. PVP K30 was selected because it has slightly higher MW than HPC SSL, while E3 grade of HPMC was used because such low MW HPMC (E3/E5) was commonly used in prior studies (e.g., (Bhakay et al., 2018b; Tuomela et al., 2014)). SDS, purchased from Sigma Aldrich (Milwaukee, WI, USA), is a commonly used anionic surfactant. Zirmil Y grade wear-resistant yttrium-stabilized zirconia (YSZ) with a median size of 430 µm (400 µm nominal size) was used as the milling media and purchased from Saint Gobain ZirPro (Mountainside, NJ, USA).

2.1.2 Rational for Formulation Design and Wet Stirred Media Milling Process

The formulations used in the preparation of drug suspensions are provided in Table 2.1. Unless otherwise indicated, suspensions and nanocomposites are labeled with the concentration–type of the dispersants in the suspensions. All percentages (%) refer to w/w with respect to the total weight of deionized water (200 g). ITZ concentration

was kept constant at 10%. Formulations F1–F3 allow us to examine the impact of HPC SL–SDS combination, which is known to be effective for stabilizing multiple drug nanosuspensions due to its synergistic effect (e.g., (Bilgili et al., 2016)), with the respective controls (SDS alone and HPC SL alone). Various surfactant-free suspensions with different polymers/grades having 4.5% concentration were also prepared (F4–F8). A higher polymer concentration (>4.5%) would reduce drug loading in the nanocomposites below 50%; hence, it was not considered.

Table 2.1 Formulation of the Milled Suspensions and Drug Content in the Nanocomposites

ID[a]	Polymer type/grade	MW[b] (kg/mol)	Suspension content[a]		Theoretical drug content (% w/w) [d]	Actual drug content, RSD (% w/w, %) [d]
			Polymer (% w/w) [c]	SDS (% w/w) [c]		
F1	-	-	0	0.2	98.0	NM[e]
F2	HPC SL	100	2.5	0	80.0	77.8, 3.6
F3	HPC SL	100	2.5	0.2	78.7	78.3, 4.7
F4	HPC SL	100	4.5	0	69.0	68.3, 2.9
F5	HPC SSL	40	4.5	0	69.0	61.0, 4.8
F6	HPC L	140	4.5	0	69.0	67.4, 4.4
F7	HPMC E3	10	4.5	0	69.0	59.5, 2.5
F8	PVP K30	50	4.5	0	69.0	62.9, 5.1

[a] ID is formulation identity
[b] MW is Molecular Weight of the polymers
[c] All suspensions have 10% ITZ. %w/w is with respect to the weight of deionized water (200g).
[d] %w/w is the weight of ITZ with respect to the weight of nanocomposites;
[e] Not measured.

A shear mixer (Fisher Scientific Laboratory Stirrer, Catalog No. 14-503, Pittsburgh, PA) was used to disperse ITZ particles in aqueous dispersant solution. The resultant ITZ pre-suspensions were transferred to the holding tank of a Netzsch wet stirred media mill (Microcer, Fine Particle Technology LLC, Exton, PA, USA) (Figure 2.1a). Selection of the milling conditions was guided by our prior studies on wet media milling (Afolabi et al., 2014; Bilgili et al., 2016). 50 mL of the chamber

was filled with zirconia beads, and a screen with 200 µm opening was used to hold the beads in the chamber. The suspension was recirculated through the chamber at a rate of 126 mL/min *via* a peristaltic pump and was milled at a rotor speed of 4000 rpm for 65 min. The milling chamber and holding tank were cooled by a chiller (Advantage Engineering Greenwood, IN, USA). Particle sizes of samples taken at the exit of the mill chamber were measured at different time intervals. A portion of each suspension was separated in a vial and stored for 7 days at 8 °C to assess the short-term physical stability.

2.1.3 Preparation of Nanocomposites *via* Spray Drying

The milled ITZ suspensions were dried following one-day storage using a spray dryer (4M8-Trix, Procept, Zelzate, Belgium) running in a co-current flow set up (Figure 2.1b). The length and the diameter of the spray dryer are 1.59 m and 0.15 m, respectively. The operating conditions were adapted from Azad et al. (2015b). The suspensions were atomized at 2 bar atomizing pressure using a bi-fluid nozzle having 0.6 mm tip diameter. In each run, ~120 g milled suspensions were sprayed at 1.3–1.6 g/min spray rate using a peristaltic pump (Makeit-EZ, Creates, Zelzate, Belgium). Drying air at 120 °C was fed co-currently at the top of the column at a rate of 0.37–0.40 m^3/min. The residence time was calculated to be ~4 s. After attainment of steady-state in about 15 min, the outlet temperature was measured to be 35–38 °C in different runs due to variable solids loading in different formulations (refer to Table 2.1). A cyclone separator was used at 54–70 mbar differential pressure to separate the particles from the outlet air stream and divert them into a glass jar. The dried powders, i.e., the nanocomposites, were used for further characterization.

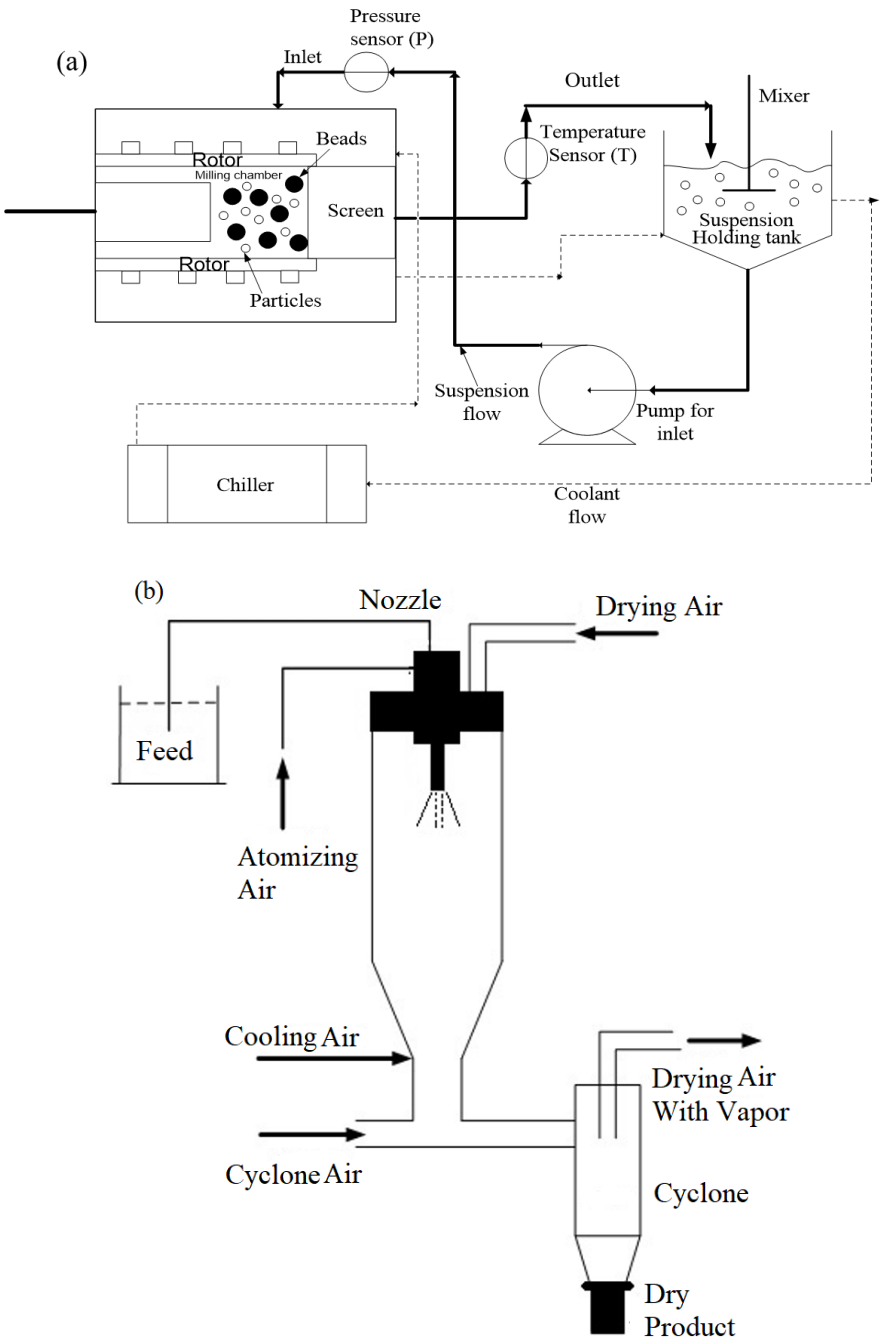

Figure 2.1 (a) Schematic of a wet stirred media mill in recirculation mode of operation and (b) schematic of a co-current spray dryer. (Figures are not drawn to scale.).

2.1.4 Particle Sizing and Imaging

Particle size distributions (PSDs) of the suspensions were measured at various times during milling as well as after 1-day and 7-day refrigerated storage by laser diffraction using Coulter LS 13 320 (Beckman Coulter, Miami, FL). The steps involved in measuring PSDs of the suspensions were adopted from ref. (Bilgili et al., 2016). During sample addition, intensity was maintained between 40–45%, while obscuration was below 8%. Mie scattering theory was used to compute the volume-based PSDs in the software with refractive index value 1.68 for ITZ and 1.33 for deionized water (medium). Before each measurement, 2 mL suspension sample was diluted with 5 mL of the respective stabilizer solution using a vortex mixer (Fisher Scientific Digital Vortex Mixer, Model No: 945415, Pittsburgh, PA) at 1500 rpm for 1 min.

PSDs of the nanocomposites were measured by Rodos/Helos laser diffraction (LD) system (Sympatec, NJ, USA) based on Fraunhofer theory using the dry powder dispersion module. About 1 g of the sample was placed on the sample chute of the Rodos dispersing system. The chute was vibrated at 100% setting to feed the sample, and 1.0 bar dispersion pressure was imposed to suck in the falling powder through the sample cell of the laser diffraction system. In addition, nanocomposite particles were placed on a glass slide and visualized by Axio Scope.A1 polarized light microscope (Carl Zeiss Microscopy GmbH, Göttingen, Germany).

Images of as-received ITZ and milled F3 suspension were taken using a LEO 1530 SVMP (Carl Zeiss, Inc., Peabody, MA, USA) SEM. For dry as-received ITZ particles, a carbon tape was placed on an SEM stub and then the particles were placed

on top of the carbon tape. For F3 suspension, approximately 1.0 mL aliquot of the suspension sample was diluted to 30 mL with deionized water, mixed for 30 s with a vortex mixer, mounted on top of a silicon chip (Ted Pella Inc., Redding, CA, USA), and then placed on a carbon specimen holder (Li et al., 2016c). This sample was placed into a desiccator for overnight drying under vacuum condition. The final samples were then sputter coated with carbon using BAL-TEC MED020 (BAL-TEC, Balzers, Switzerland) to reduce possible charging during imaging.

2.1.5 Apparent Shear Viscosity, Density, and Zeta Potential of the Suspensions

The apparent shear viscosity of the milled suspensions was measured using R/S plus rheometer (Brookfield Engineering, Middleboro, MS, USA) with a water jacket assembly Lauda Eco (Lauda-Brinkmann LP, Delran, NJ, USA) (Afolabi et al., 2014). A coaxial cylinder with jacketed setup was used to impart a controlled shear rate on the samples from 0 to 1000 1/s in 60 s. The jacket temperature was kept constant at 25 ± 0.5 °C. The raw data were analyzed using the Rheo3000 software (Brookfield Engineering, Middleboro, MA, USA). The viscosities of selected dispersant (stabilizer) solutions were also measured as they are needed in wettability study. For the 2.5% HPC SL–0.2% SDS sample with viscosity <10 cP, a rheometer with higher sensitivity/accuracy (Kinexus Ultra Plus Rotational Rheometer, Malvern Panalytical, Southborough, MA, USA) was used. 40 mm rotational parallel plates with 0.75 mm gap were used to provide a controlled shear rate on the sample from 0 to 1000 1/s. The simple power-law model was fitted to measured viscosity profiles of all suspensions (Equation 2.1):

$$\eta = \eta(\dot{\gamma}) = a\dot{\gamma}^{n-1} \tag{2.1}$$

where η and $\dot{\gamma}$ are the apparent shear viscosity and shear rate, respectively, while *a* and *n* are the consistency index and power-law index, respectively. This model shows that $n = 1$ represents Newtonian flow behavior, $n < 1$ represents shear-thinning (pseudoplastic) behavior, and $n > 1$ represents shear-thickening (dilatant) behavior. The density (ρ) was measured thrice by weighing a 60 mL glass cylinder filled with the suspension and dividing by the volume.

Using a Delsa Nano C zeta potential analyzer (Delsa Nano C, BeckmanCoulter, USA), zeta potentials of wet-milled ITZ particles and the milled suspensions with 2.5% HPC SL, 2.5% HPC SL–0.2% SDS, and 4.5% HPC SL were measured. The Delsa Nano C uses electrophoretic light scattering (ELS) for zeta potential determination; electrophoretic movement of charged particles was determined from the Doppler shift of scattered light under an applied electric field.

2.1.6 X-Ray Powder Diffraction (XRPD)

The crystallinity of as-received ITZ, physical mixture corresponding to F4 formulation, and F4–F8 nanocomposites was analyzed using PXRD (PANalytical, Westborough, MA, USA), equipped with Cu Kα radiation (λ = 1.5406 Å). The samples were scanned at a rate 0.165 s^{-1} for 2θ ranging from 5 to 40°. To detect characteristic peaks more distinctly, another set of samples were prepared: wet-milled suspensions were centrifuged (Compact II centrifuge, Clay Adams® Brand, Sparks, MD, USA) at 3200 rpm for 90 min to separate the drug from the aqueous phase with excess polymer. The resultant solid phase was redispersed in deionized water

followed by another centrifugation. The final solid phase was overnight-dried in a vacuum hood before XRPD analysis.

2.1.7 Thermal Characterization

Thermograms of a physical mixture corresponding to F4 formulation as well as F2 and F4–F8 nanocomposites were obtained by a Mettler–Toledo differential scanning calorimeter (DSC) (PolyDSC, Columbus, OH, USA). About 6 mg sample was placed in a sealed aluminum pan and loaded into the DSC. The samples were heated at a rate of 10 °C/min from 25 °C to 220 °C. Nitrogen gas was used as the purge gas and protective gas at a flow rate of 50 mL/min and 150 mL/min, respectively. Using the integrated software (STARe 10), peak melting point temperature T_m and fusion enthalpy ΔH_m were determined. For the characterization of the residual water in the spray-dried nanocomposites, thermogravimetric analysis (TGA) was performed using a TGA/DSC1/SF Stare system (Mettler Toledo, Inc., Columbus, OH). About 6 mg of F4/F8 nanocomposites was placed in a ceramic crucible and heated from 25 °C to 150 °C at a constant rate of 10 °C/min under nitrogen flow.

2.1.8 Drug Wettability

Drug wettability was investigated by analyzing the penetration rate of dispersant solutions into a packed bed of ITZ particles inside a cylindrical column according to the Washburn method (Hołownia et al., 2008; Washburn, 1921). An Attension Sigma 700 (Biolin Scientific, Linthicum, MD, USA) set-up was used. Experimental method was adapted from Li et al. (2017), and readers are referred to Appendix A for details. Dispersant concentrations in the solutions were identical to those in the respective wet-milled suspensions in Table 2.1. The apparent shear viscosity η and surface

tension γ of the liquids were measured using R/S Plus Rheometer (Brookfield Engineering, Middleboro, MA, USA) and Attension Sigma 700 (Biolin Scientific, Linthicum, MD, USA), respectively. Only for the solutions having viscosity <10 cP (2.5% HPC SL, 4.5% HPC SSL and 4.5% PVP K30), η was measured using a Kinexus Ultra Plus Rotational Rheometer (Malvern Panalytical, Southborough, MA, USA). The ratio of the cosine of contact angles $\cos\theta_{ds}/\cos\theta_{w}$ that does not require a separate measurement of the constant C was calculated using the modified Washburn equation (Li et al., 2017). Here, θ_{ds} and θ_{w} are the contact angles between ITZ and the dispersant solutions and between ITZ and deionized water, respectively. This ratio or its logarithmic value provides a rough measure of the drug wettability enhancement upon use of various dispersants in water.

2.1.9 Redispersion of the Drug Nanocomposites

The redispersion of the spray-dried powders was performed following the method in refs. (Bhakay et al., 2014a; Li et al., 2016b). About 0.5 g of nanocomposites was weighed and dispersed in a 60 mL beaker containing 30 mL of 3 g/L aqueous SDS solution (the same concentration as that of the dissolution medium) and stirred with a paddle-stirrer (CAT R18, Scientific Instrument Center Limited, Winchester, UK) at 400 rpm for 60 min. ~0.5 mL aliquot of redispersed sample was taken at 2, 10 and 60 min while stirring, and particle size was measured using laser diffraction. A droplet of each redispersion sample was dropped on a glass slide and dried immediately using a hot air gun. The Zeiss Axio Scope.A1 polarizing microscope was used to capture the image of the dried samples. 30 mL medium was selected purposefully so that the dispersants can fully dissolve, while releasing the ITZ nanoparticles/clusters

with minimal dissolution. Indeed, the maximum amount of ITZ that can dissolve is small (e.g., 0.11% of ITZ in F3 nanocomposites).

2.1.10 Drug Content and Dissolution Performance of the Nanocomposites

Actual drug content of the nanocomposite powders was measured by assay testing. 100 mg of the spray-dried powders was dissolved in 20 mL dichloromethane (DCM), sonicated for 50 min to ensure complete dissolution of ITZ, and then stored overnight to settle any undissolved particles. An aliquot of 100 µl was taken from the supernatant and diluted to 10 mL with DCM. The absorbance of all the samples was measured at 260 nm wavelength *via* Ultraviolet (UV)-spectrophotometer (Agilent, Santa Clara, CA, USA). Six replicates were tested for each formulation to calculate mean drug content and percent relative standard deviation (RSD).

Dissolution of as-received ITZ and spray-dried ITZ nanocomposites was performed *via* a Distek 2100C dissolution tester (North Brunswick, NJ, USA) according to the USP II paddle method. The dissolution medium was 1000 mL SDS buffer with 3.0 g/L concentration. This solution was selected because it provides a good discrimination of ITZ release among the nanocomposite formulations (Azad et al., 2016). The medium was maintained at 37 °C and stirred by a paddle at 50 rpm. Nanocomposites, equivalent to a dose of 20 mg of ITZ, were added to the medium, and 4 mL samples were taken manually at 1, 2, 5, 10, 20, 30, and 60 min. The absorbance of dissolved ITZ was measured *via* UV-spectroscopy (Agilent, Santa Clara, CA, USA) at 260 nm wavelength. Aliquots of the samples were filtered using a 0.1 µm PVDF membrane type syringe filter to avoid any effect of undissolved drug during UV-spectroscopy. The medium solution without drug was used as the blank.

The amount of drug dissolved was measured using a calibration curve generated from drug concentration *vs.* absorbance (R^2 = 0.9995 with $p < 0.0001$). ITZ release was reported as a function of dissolution time for an average of six replicates. >80% drug release in 20 min was regarded as a stringent criterion for immediate drug release (Azad et al., 2016; Bhakay et al., 2014b).

ITZ dissolution data was fitted by Korsmeyer–Peppas model (Ritger and Peppas, 1987a, b):

$$M_t / M_\infty = kt^n \tag{2.2}$$

where k is a constant incorporating structural and geometric characteristics of the drug dosage form, n is the release exponent, indicative of the drug release mechanism, and M_t/M_∞ is fractional drug release. While this model has been used to assess drug release mechanisms, it was simply used as an empirical kinetic model here because some of the assumptions behind the mechanistic model were not satisfied, which may potentially confound the interpretation of the release mechanisms. Since the drug release rate ($\mathrm{d}(M_t/M_\infty)/\mathrm{d}t$) is proportional to kn (Peppas, 1985), kn provides a quantitative measure for comparing initial release rates from different dispersant formulations.

Dissolution profiles of all nanocomposites were compared to those of F3 and F4 nanocomposites, separately, using difference (f_1) and similarity (f_2) factors (Boateng et al., 2009; Costa and Lobo, 2001). f_1 values up to 15 (0–15) and f_2 values greater than 50 (50–100) suggest statistical similarity of two profiles.

2.2 Results and Discussion

2.2.1 Apparent Breakage Kinetics During Wet Media Milling

The ITZ suspensions with various dispersants listed in Table 2.1 were wet milled in a stirred media mill. Figure 2.2 presents the temporal evolution of median particle size d_{50} and 90% passing size d_{90} of the milled suspensions, while Table 2.2 presents d_{50} and d_{90} of the final (65 min) milled suspensions and their sizes after 7-day refrigerated storage.

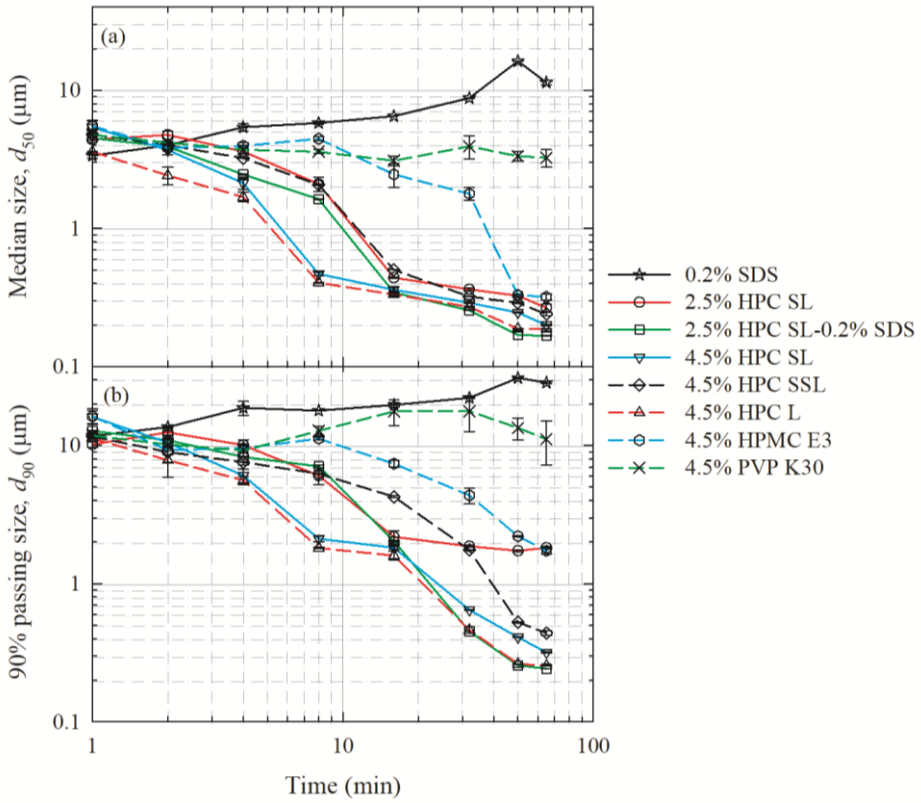

Figure 2.2 Temporal evolution of (a) median size d_{50} and (b) 90% cumulative passing size d_{90} during the milling of ITZ suspensions with 0.2% SDS (F1), 2.5% HPC SL (F2), 2.5% HPC SL–0.2% SDS (F3), 4.5% HPC SL (F4), 4.5% HPC SSL (F5), 4.5% HPC L (F6), 4.5% HPMC E3 (F7), and 4.5% PVP K30 (F8), respectively.

As-received ITZ particles (Figure 2.3) had d_{50}: 15.5 µm and d_{90}: 45.8 µm, measured *via* Rodos/Helos laser diffraction system. When milled with 2.5% HPC SL–0.2% SDS, the best stabilizing formulation in this study, d_{50} and d_{90} of ITZ particles monotonically decreased and attained a limiting, plateau size at 0.17 and 0.24 µm, respectively (Figure 2.2). Figure 2.3a and 2.3b visually confirms the dramatic size reduction during high energy wet stirred media milling, which allows us to prepare ~230 g ITZ nanosuspension within 65 min *vs.* ~8 g ITZ suspension in several days by ball milling in a vial (Choi et al., 2008). Qualitative similarity between the particle sizes observed in Figure 2.3b and laser diffraction measurement signifies minimal aggregation in this suspension due to effective stabilization.

During wet media milling, two mechanisms act simultaneously: breakage of the drug particles, fragments of already broken particles as well as aggregates (deaggregation) and aggregation of the particles (Bilgili et al., 2004; Choi et al., 2008; Sommer et al., 2006). The PSD and characteristic particle sizes like d_{50} and d_{90} evolve in accordance with the competition between the rates of these two opposing mechanisms, i.e., breakage and aggregation. The monotonic decrease in particle size for 2.5% HPC SL–0.2% SDS suggests that breakage was the dominant mechanism during the milling owing to efficient stabilization. On the contrary, aggregation of ITZ particles was the dominant mechanism during the milling with 0.2% SDS and 4.5% PVP, and d_{50} and d_{90} either changed in a non-monotone fashion or even increased (Figure 2.2). Such interesting size increase and non-monotone behavior were also observed in previous wet media milling studies where either poor stabilization with dispersants occurred or no stabilizers were used (Bhakay et al.,

2011; Bilgili and Afolabi, 2012). Previous studies (Bhakay et al., 2011; Monteiro et al., 2013) reported that *primary* drug nanoparticles, which were examined by SEM imaging, were produced by wet media milling even in the absence of dispersants, while large aggregates formed in the suspensions were measured by laser diffraction. For suspensions with other dispersants, the aggregation appeared to be slower than the breakage, and d_{50} and d_{90} decreased in time, but all suspensions showed varying extent of aggregation depending on the dispersant used (Figure 2.2). Without SDS, only 4.5% HPC (any grade) could ensure a d_{90} below 1 μm. It should be noted that suspensions may undergo additional aggregation during the storage, which is discussed below.

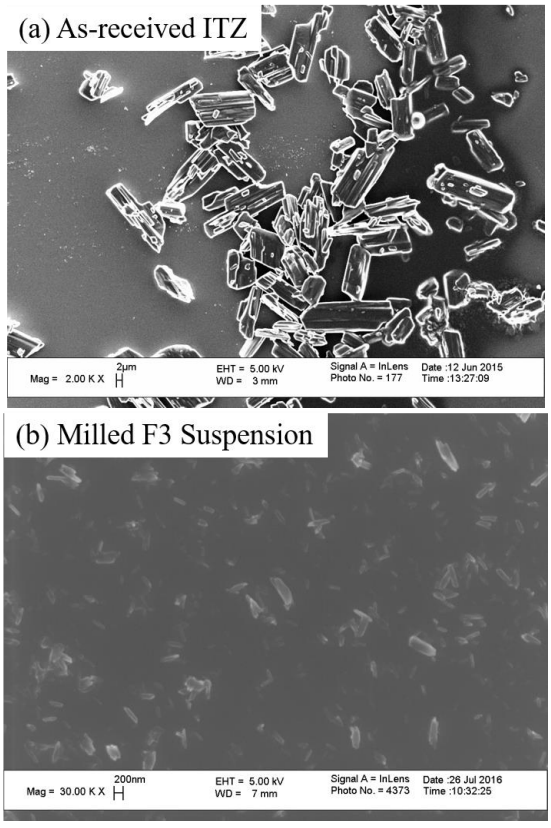

Figure 2.3 SEM images of ITZ particles: (a) before milling (marker size: 2 μm, 2 K× magnification) and (b) after milling (F3, 2.5% HPC SL–0.2% SDS) (marker size: 200 nm, 30 K× magnification).

2.2.2 Stabilization Mechanisms

Let us now examine the impact of dispersants on the final milled particle sizes and their 7-day stability (Table 2.2). When 0.2% SDS (an anionic surfactant) was used as a stabilizer, an aggregated, coarse suspension with d_{50}: 11.4 μm was formed. Apparently 0.2% SDS was not sufficient to provide strong electrostatic stabilization, and it also imparted lowest wettability enhancement among all the dispersants studied (Table 2.3). The use of 2.5% HPC SL led to submicron median size in the final suspension with d_{90}: 1.82 μm, which could be explained by the adsorption of HPC on ITZ particles and ensuing steric stabilization (Choi et al., 2008) and slow-down of aggregation during milling. However, 2.5% HPC SL was not sufficient to prevent further aggregation that results from Brownian motion during the storage, and ITZ particle size dramatically increased over 7-day storage (Figure 2.4). Other suspensions did not exhibit such a drastic change in particle size upon 7-day storage. Zeta potentials of the wet-milled ITZ particles, the milled ITZ suspensions with 2.5% HPC SL and 4.5% SL were measured to be 0.25, –2.2, and 0.34 mV, respectively. Overall, the electrostatic charge of the ITZ particles in the milled suspensions was very low: nearly neutral particles within experimental accuracy. Considering that even short-term stability requires an absolute value of zeta potential greater than 20 mV (Lakshmi and Kumar, 2010; Riddick, 1968), steric stabilization appears to be the dominant stabilization mechanism upon use of the polymeric dispersants in this study. An increase in HPC SL concentration from 2.5% to 4.5% likely allowed for greater HPC adsorption and formation of a thicker polymer layer on ITZ particles, which reduced aggregation potential of colliding particles. Adsorption of cellulosic

polymers (HPMC and HPC) onto drug nanoparticles are known to follow Langmuir or Freundlich adsorption isotherms (Bilgili and Afolabi, 2012; Knieke et al., 2013), which display greater adsorption at higher polymer concentration in the bulk solution. In addition, significant wettability enhancement upon use of HPC SL (Table 2.3) could have facilitated deaggregation during the milling. Overall, the use of 4.5% HPC SL largely mitigated aggregation and led to formation of a relatively stable suspension over 7 days (Figure 2.4).

As compared with 4.5% HPC SL suspension, 4.5% HPMC E3 and 4.5% PVP K30 suspensions had larger ITZ aggregates, which could be explained by lower extent of polymer adsorption onto ITZ particles and ensuing poorer steric stabilizing action by the respective polymers. In fact, adequate stabilization of wet-milled ITZ suspensions required the use of 0.05%–0.2% SDS when HPMC E3 was used (Azad et al., 2016). Besides, while 4.5% PVP K30 has slightly higher MW (50 kg/mol) than 4.5% HPC SSL (40 kg/mol), its stabilizing capability was inferior to HPC SSL, which suggests that the ITZ–specific polymer interaction through their functional groups determine the extent of polymer adsorption and modulate steric stabilization (Choi et al., 2008). While polymer adsorption on ITZ particles was not studied here, our results suggest that HPC appears to be a better steric stabilizer than PVP and HPMC.

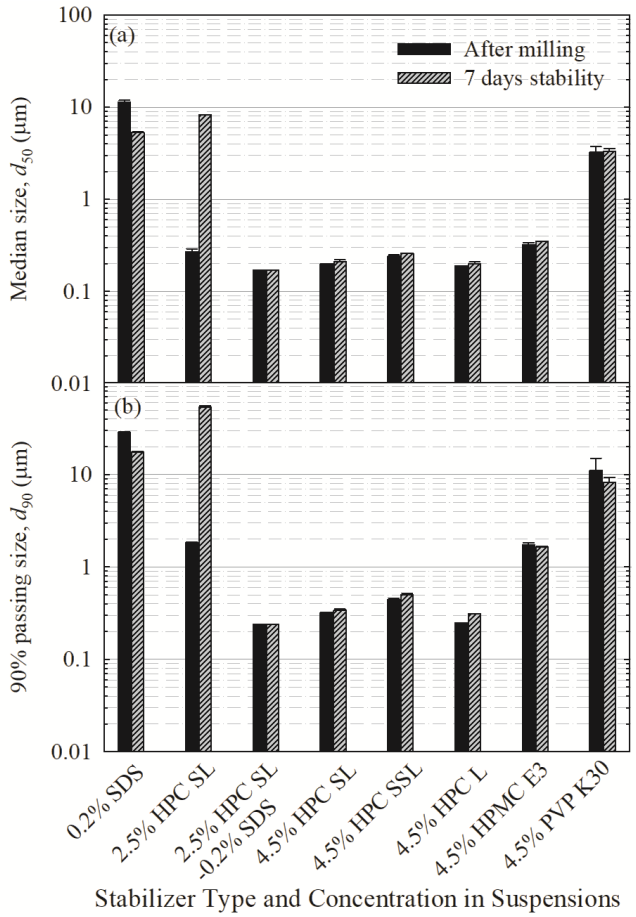

Figure 2.4 Volume-based particle size statistics of the ITZ suspensions with 0.2% SDS (F1), 2.5% HPC SL (F2), 2.5% HPC SL–0.2% SDS (F3), 4.5% HPC SL (F4), 4.5% HPC SSL (F5), 4.5% HPC L (F6), 4.5% HPMC E3 (F7), and 4.5% PVP K30 (F8) after milling (65 min) and 7-day storage at 8 °C: (a) Median particle size d_{50} and (b) 90% cumulative passing size d_{90}.

Table 2.2 Particle Size Statistics of the Drug Suspensions After Milling and 7-day Storage and Those of the Spray-dried Nanocomposites

Formulation ID	Suspension composition [a]	Particle size of the suspensions after milling (μm)		Particle size of the suspensions after 7 days (μm)		Nanocomposite particle size (μm)	
		d_{50}±SD	d_{90}±SD	d_{50}±SD	d_{90}±SD	d_{50}±SD	d_{90}±SD
F1	0.2% SDS	11.4±0.44	28.5±0.57	5.32±0.10	17.4±0.41	8.43±1.18	18.7±1.80
F2	2.5% HPC SL	0.27±0.02	1.82±0.04	8.23±0.02	53.5±2.40	13.9±0.04	26.4±0.11
F3	2.5% HPC SL–0.2% SDS	0.17±0.00	0.24±0.00	0.17±0.00	0.24±0.00	11.3±0.26	21.2±0.33
F4	4.5% HPC SL	0.20±0.00	0.32±0.00	0.21±0.00	0.34±0.01	16.2±0.01	32.3±0.17
F5	4.5% HPC SSL	0.24±0.01	0.44±0.02	0.26±0.00	0.50±0.02	14.0±0.11	29.4±0.06
F6	4.5% HPC L	0.19±0.00	0.25±0.00	0.20±0.01	0.31±0.00	23.5±0.18	49.2±0.67
F7	4.5% HPMC E3	0.32±0.02	1.73±0.09	0.35±0.00	1.64±0.02	17.7±0.10	39.8±0.12
F8	4.5% PVP K30	3.25±0.47	11.1±3.92	3.33±0.20	8.24±1.08	15.2±0.11	27.9±0.21

[a]All suspensions have 10% ITZ. %w/w is with respect to the weight of deionized water (200g).

Table 2.3 Wetting Effectiveness Factor Calculated Using the Modified Washburn Method for Various ITZ–stabilizer Solution Pairs

Formulation of the stabilizer solution[a]	Slope (g^2/s)	R^2 (-)	Viscosity η(cP)	Density ρ (g/mL)	Surface tension γ (mN/m)	log ($\cos\theta_{ds}/\cos\theta_w$) (-)
Water	6.47×10^{-06}	0.995	0.89[b]	1.00	70.8	0
0.2% SDS	1.20×10^{-03}	0.999	0.94[c]	1.00	32.8	2.69
2.5% HPC SL	5.00×10^{-04}	0.999	4.59	1.01	42.4	2.81
2.5% HPC SL–0.2% SDS	8.00×10^{-04}	0.999	17.4	1.03	38.2	3.63
4.5% HPC SL	2.20×10^{-03}	0.999	13.4	1.01	42.3	3.92
4.5% HPC SSL	5.10×10^{-03}	0.999	4.13	1.00	43.0	3.78
4.5% HPC L	1.40×10^{-03}	0.998	24.3	1.02	41.8	3.98
4.5% HPMC E3	3.40×10^{-03}	0.999	6.10	1.01	42.8	3.77
4.5% PVP K30	3.20×10^{-03}	0.998	1.66	1.01	50.7	3.10

[a] %w/w is with respect to the weight of deionized water.
[b] Taken from ref. (Korson et al., 1969).
[c] Taken from ref. (Kushner et al., 1952).

The combination of 2.5% HPC SL and 0.2% SDS led to the finest ITZ particles and a 7-day stable suspension. HPC–SDS provides synergistic stabilization during milling and storage for a multitude of BCS Class II drugs due to combined electrostatic stabilization (zeta potential of –9.7 mV) by negatively charged SDS and steric stabilization by adsorbed HPC, i.e., electrosteric stabilization (Bilgili and Afolabi, 2012; Bilgili et al., 2016; Peltonen and Hirvonen, 2010; Shete et al., 2016) besides wettability enhancement of the lipophilic drug (see Table 2.3) and associated deaggregation effectiveness provided by the combination (Li et al., 2018a). The significantly higher wetting enhancement ratio for 2.5% HPC SL–0.2% SDS as compared with 0.2% SDS and 2.5% HPC SL (Table 2.3) corroborates the synergy. Such synergistic effects have been reported previously (Basa et al., 2008; Lee et al., 2008; Ryde and Ruddy, 2002). HPC and SDS interact, forming aggregates or micelle-like SDS clusters bound to HPC (Winnik and Winnik, 1990). The formation of such clusters could be deduced from the higher viscosity of 2.5% HPC SL–0.2% SDS aqueous solution than those of 0.2% SDS and 2.5% HPC SL aqueous solutions (Table 2.3). These clusters can co-adsorb on particle surfaces (Berglund et al., 2003a, b; Evertsson and Nilsson, 1997), potentially facilitating adsorption of HPC (Cerdeira et al., 2010) and enabling electrosteric stabilization. It should be noted that in the absence of SDS, only HPC SL/L led to stable particle sizes close to those of the HPC–SDS combination (Figure 2.4).

A comparison of the final milled particle sizes (Table 2.2) for suspensions with SSL, SL, and L grades of 4.5% HPC with 40, 100, and 140 kg/mol MW, respectively, suggests that higher MW HPC led to finer and more stable ITZ

suspensions. The apparent breakage was faster for the higher MW HPC than lower MW (Figure 2.2) because the rate of aggregation was slower in higher MW HPC. These findings suggest higher MW HPC is more effective for the stabilization of ITZ, which is in contrast with ref. (Choi et al., 2008). The authors of ref. (Choi et al., 2008) highlight a thermodynamic consideration that polymers of higher MW have less entropy loss related to their freedom of motion, which results in a higher affinity to the drug surface and thus stronger adsorption and slower desorption (Morrison and Ross, 2002; Ploehn and Russel, 1990). Therefore, according to this thermodynamic consideration, a polymer with higher MW should provide better stabilization, which is contrary to the findings in ref. (Choi et al., 2008), but in line with our study. As argued in Introduction, unfortunately, studies like (Choi et al., 2008; Sepassi et al., 2007) that used low-energy mills do not truly reflect the impact of different polymers or MW on steric stabilization and reduction of drug aggregate formation. The use of higher MW polymer and/or higher polymer concentration causes more pronounced viscous dampening (Bilgili and Afolabi, 2012), which slows down the breakage in low-energy mills more profoundly than in high-energy mills. Hence, such studies drew somewhat confounded conclusions about the impact of polymer MW due to pronounced impact of viscous dampening. Not only did high-energy, wet stirred media milling enabled faster production of ITZ nanoparticles than low energy mills used in ref. (Choi et al., 2008) for ITZ–HPC, but also it allowed us to elucidate the role of polymer MW in stabilization of drug nanoparticles, which in line with the thermodynamic consideration of polymer adsorption.

2.2.3 Rheology of the Milled Suspensions

To further assess the aggregation state of the precursor suspensions, rheological characterization of the ITZ suspensions was performed as an orthogonal characterization method, similar to (Azad et al., 2015a; Li et al., 2018a). Figure 2.5 illustrates the apparent shear viscosity profiles of the milled suspensions. The power-law model was fitted to the apparent shear viscosity profiles, and the fitted consistency index a, power-law index (n), and R^2 values are reported in Table 2.4. The p-values for the model fit and the estimated parameters are less than 0.05 and R^2 values are in the range of 0.94–0.99, which suggest that overall the power-law model fitted the data fairly well and both the model and its parameters were statistically significant. Milled ITZ suspensions that had high extent of aggregation, as revealed by laser diffraction measurement results (see Table 2.2), exhibited pronounced pseudoplastic behavior, as shown by the sharp decrease in viscosity with an increase in shear rate (Figure 2.5), $n < 1$ (~0.2–0.3), and high a values (Azad et al., 2015a; Li et al., 2018a). The milled suspensions with smaller aggregates (HPC SL/L) exhibited slight pseudoplasticity, tending toward near-Newtonian behavior (n ~0.9–1). Suspensions with higher HPC MW had smaller aggregates and displayed less pseudoplasticity (higher n and lower a). During the rheological characterization, suspension samples were subjected to increasing shear rate, and any aggregates present were deaggregated upon an increase in shear rate (Barthelmes et al., 2003; Bernhardt et al., 1999). Usually, aggregates occlude liquid in their void spaces, which raises the effective volume fraction of the solid in a suspension with fixed solids amount. Hence, deaggregation during the characterization upon an increase in shear

rate reduces the apparent shear viscosity (pseudoplasticity), and this effect was more pronounced for suspensions that exhibited a higher extent of aggregation. Overall, the rheological characterization supports our earlier finding that higher MW HPC is more favorable for ITZ stabilization because smaller aggregates formed during the milling, which led to less remarkable pseudoplasticity for the respective suspensions.

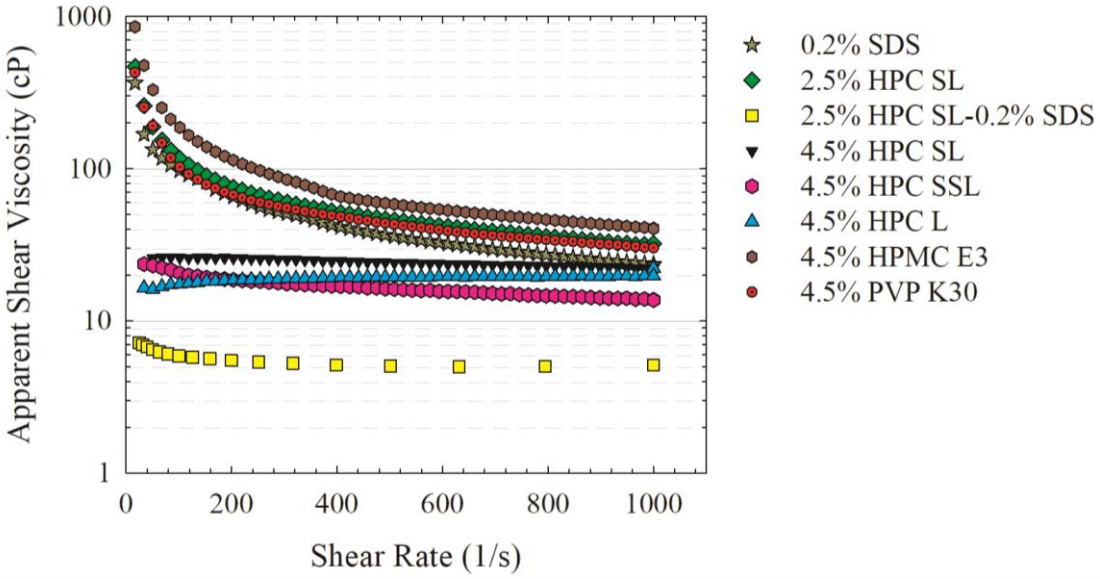

Figure 2.5 Semi-log plots for apparent shear viscosity *vs.* shear rate of the milled ITZ suspensions with 0.2% SDS (F1), 2.5% HPC SL (F2), 2.5% HPC SL–0.2% SDS (F3), 4.5% HPC SL (F4), 4.5% HPC SSL (F5), 4.5% HPC L (F6), 4.5% HPMC E3 (F7), and 4.5% PVP K30 (F8), respectively.

Table 2.4 Power-law Model Parameters Obtained from Fitting the Apparent Shear Viscosity Profiles of Various Milled ITZ Suspensions

Formulation ID	Suspension composition [a]	*n* (-)	*a* (cP.s^n)	R^2 (-)
F1	0.2% SDS	0.33	2230	0.974
F2	2.5% HPC SL	0.30	3180	0.989
F3	2.5% HPC SL–0.2% SDS	0.90	9.80	0.950
F4	4.5% HPC SL	0.91	41.1	0.954
F5	4.5% HPC SSL	0.84	44.0	0.984
F6	4.5% HPC L	1.05	14.4	0.940
F7	4.5% HPMC E3	0.24	6620	0.994
F8	4.5% PVP K30	0.30	2960	0.988

[a]All suspensions have 10% ITZ. %w/w is with respect to the weight of deionized water (200g).

2.2.4 Properties of the ITZ Nanocomposites

The milled ITZ suspensions were spray-dried to prepare nanocomposites using a co-current spray dryer. High ITZ loaded nanocomposites (60–78%) were produced *via* spray-drying (Table 2.1), and most of the nanocomposites had higher ITZ loading than those reported earlier (Azad et al., 2016; De Smet et al., 2014; Parmentier et al., 2017; Sarnes et al., 2014; Van Eerdenbrugh et al., 2008d). All nanocomposites had RSDs less than 6.0%, suggesting pharmaceutically acceptable content uniformity. There was a slight variation in the theoretical and actual drug content, which can be attributed to preferential drug loss during handling/transfer after milling, poor separation of finer particles in the cyclone of the spray drier, and presence of some residual moisture after drying (Azad et al., 2015b). By measuring weight loss of the selected nanocomposites (F4 and F8) *via* TGA, mean moisture contents were determined. F4 and F8 nanocomposites had a residual moisture content of 2.1 ± 0.2% w/w and 1.8 ± 0.3% w/w, respectively, which confirms removal of most of the water from the milled suspensions during spray drying.

The optical microscope images (Figure 2.6) illustrate that rounded and nearly spherical nanocomposite particles were formed upon spray drying. The characteristic sizes of the nanocomposite particles, as measured by laser diffraction, display few trends (see Table 2.2). First, a comparison of F1–F3 nanocomposites to F4–F8 nanocomposites suggests that the lower dispersant loading led to smaller nanocomposites. Formation of coarser nanocomposites upon use of higher dispersant loading was also observed in previous spray drying studies (Sun et al., 2015; Vatanara, 2015). For different grades of 4.5% HPC, the nanocomposites with a higher MW HPC had larger particles, especially for HPC L grade. Among F4–F8 nanocomposites with 4.5% polymer (identical dispersant and total solids loading), the median sizes did not vary greatly (14–18 μm), with the exception for HPC L having the highest MW (24 μm).

In DSC thermograms, the physical mixture with F4 formulation (10% ITZ–4.5% HPC SL) and the nanocomposites exhibited a distinguished endothermic peak correspond to the melting of ITZ (Figure 2.7). The melting point temperature T_m and the fusion enthalpy ΔH_m were lower for the nanocomposites than for the physical mixture. The observed reduction in T_m and ΔH_m is most likely due to defect formation and accumulation during milling (Azad et al., 2015b; Monteiro et al., 2013). Moreover, according to Gibbs–Thomson equation (Wu and Nancollas, 1998), the melting temperature of a material is proportional to its cohesive energy, which indicates that nanoparticles with reduced cohesive energy require less energy for melting, thus, exhibiting lower T_m and ΔH_m as compared to as-received microparticles. The reduction in T_m and ΔH_m was more pronounced for HPMC E3

and PVP K30, which might be due to some amorphization on the surface of the drug particles and suppressed recrystallization during drying in the presence of these polymers. Kayaert and Mooter (Kayaert and Van den Mooter, 2012) also reported similar amorphization on the surface of drug nanoparticles during drying, depending on the drug–polymer interaction.

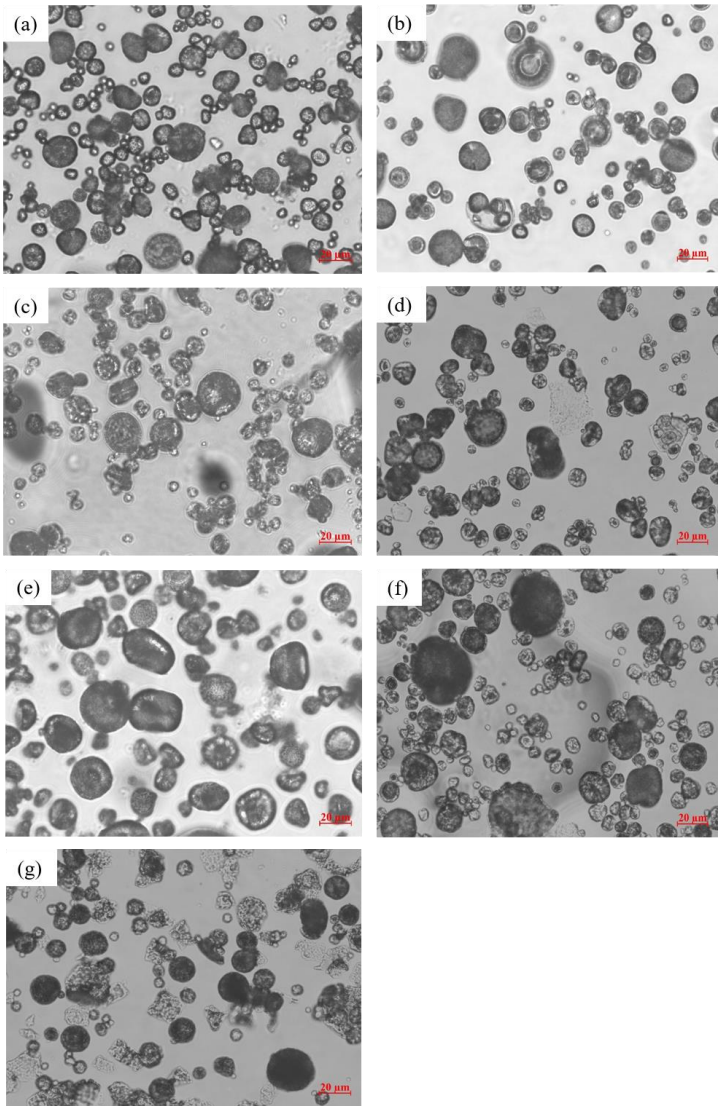

Figure 2.6 Optical microscope images of the nanocomposites prepared from the milled ITZ suspensions with (a) 2.5% HPC SL (F2), (b) 2.5% HPC SL–0.2% SDS (F3), (c) 4.5% HPC SL (F4), (d) 4.5% HPC SSL (F5), (e) 4.5% HPC L (F6), (f) 4.5% HPMC E3 (F7), and (g) 4.5% PVP K30 (F8), respectively. The marker size is 20 µm in all images.

In DSC thermograms, the physical mixture with F4 formulation (10% ITZ–4.5% HPC SL) and the nanocomposites exhibited a distinguished endothermic peak correspond to the melting of ITZ (Figure 2.7). The melting point temperature T_m and the fusion enthalpy ΔH_m were lower for the nanocomposites than for the physical mixture. The observed reduction in T_m and ΔH_m is most likely due to defect formation and accumulation during milling (Azad et al., 2015b; Monteiro et al., 2013). Moreover, according to Gibbs–Thomson equation (Wu and Nancollas, 1998), the melting temperature of a material is proportional to its cohesive energy, which indicates that nanoparticles with reduced cohesive energy require less energy for melting, thus, exhibiting lower T_m and ΔH_m as compared to as-received microparticles. The reduction in T_m and ΔH_m was more pronounced for HPMC E3 and PVP K30, which might be due to some amorphization on the surface of the drug particles and suppressed recrystallization during drying in the presence of these polymers. Kayaert and Mooter (2012) also reported similar amorphization on the surface of drug nanoparticles during drying, depending on the drug–polymer interaction.

XRPD diffractograms (Figure 2.8a) illustrate distinct, sharp peaks for as-received crystalline ITZ *vs.* lack of peaks for the (amorphous) polymers. Regardless of the preparation procedure, milled ITZ suspensions after drying exhibited the same peaks as those of the as-received ITZ and the physical mixture with F4 formulation (10% ITZ–4.5% HPC SL) (Figure 2.8b and 2.8c). However, the peak intensities were reduced along with broadening after milling–drying, which could be attributed to the smaller drug particle sizes and high stresses imparted by the milling process (Van

Eerdenbrugh et al., 2008d) and coverage of ITZ by the polymeric matrix. Similar observations were reported for loviride nanoparticles (Van Eerdenbrugh et al., 2007). Removal of excess polymer in the milled suspensions by centrifugation followed by drying led to slightly sharper peaks with higher intensity, signifying the role of the excess polymer (Figure 2.8c *vs.* Figure 2.8b). Overall, XRPD and DSC results together suggest that the crystalline nature of ITZ was preserved after milling and drying despite the formation of defects and potentially small fraction of amorphous drug.

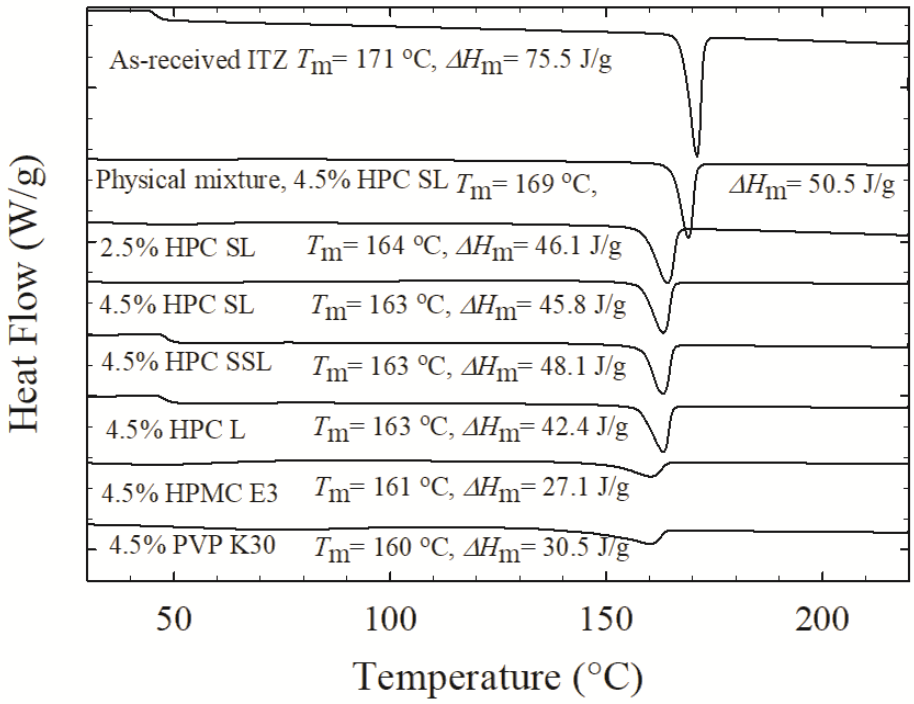

Figure 2.7 DSC thermograms of as-received ITZ, physical mixture of F4 (blend of 10% ITZ–4.5% HPC SL), as well as the nanocomposites prepared *via* spray-drying of the milled ITZ suspensions with 2.5% HPC SL (F2), 4.5% HPC SL (F4), 4.5% HPC SSL (F5), 4.5% HPC L (F6), 4.5% HPMC E3 (F7), and 4.5% PVP K30 (F8), respectively.

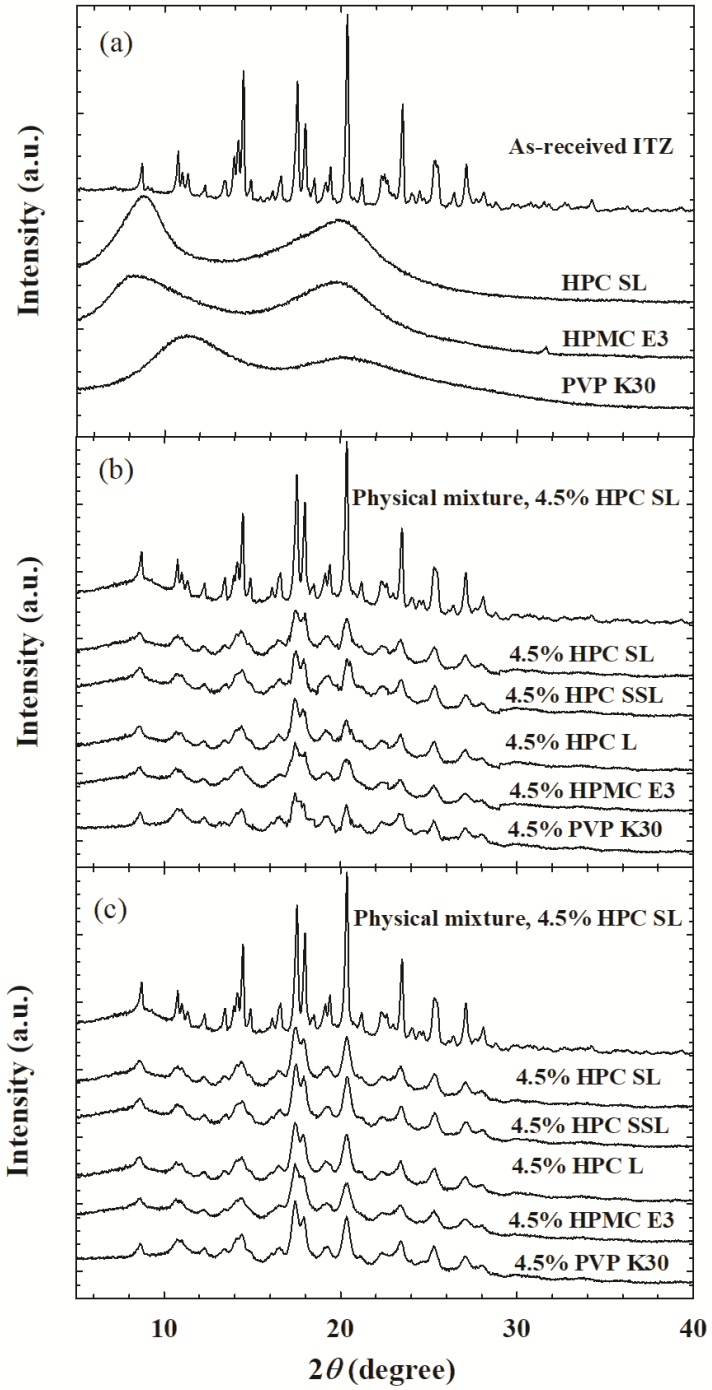

Figure 2.8 XRD diffractograms of (a) as-received ITZ, HPC SL, HPMC E3, and PVP K30; (b) physical mixture of F4 (blend of 10% ITZ–4.5% HPC SL) and spray-dried milled ITZ suspensions with 4.5% HPC SL (F4), 4.5% HPC SSL (F5), 4.5% HPC L (F6), 4.5% HPMC E3 (F7), and 4.5% PVP K30 (F8); and (c) physical mixture of F4 (blend of 10% ITZ–4.5% HPC SL) and centrifuged–oven-dried milled ITZ suspensions with 4.5% HPC SL (F4), 4.5% HPC SSL (F5), 4.5% HPC L (F6), 4.5% HPMC E3 (F7), and 4.5% PVP K30 (F8).

2.2.5 Redispersibility of the Nanocomposites

Figure 2.9 presents the characteristic particle sizes after 2 min, 10 min, and 60 min redispersion of the nanocomposites in the redispersion medium as well as the particle sizes of the ITZ suspensions after milling and one-day storage (prior to spray-drying). Figure A3 of Appendix A presents the optical microscope images of the above-mentioned redispersed samples. Ideally, during the redispersion test, the dispersant (polymeric) matrix should erode fast while dissolving in water and release the ITZ particles/clusters. Note that the dissolution of ITZ particles was negligible during the redispersion test by design, unlike that in dissolution testing. The nanocomposite particles with 2.5% HPC SL, 4.5% HPC SSL, 4.5% HPMC E3, and 4.5% PVP K30 did not erode at all or eroded extremely slowly, keeping their large size and morphology intact during the 60 min redispersion (Figure 2.9 and Figure A3). These dispersants all had MW ≤ 50 kg/mol. Only the nanocomposites with 4.5% HPC (SL/L grades with 100/140 kg/mol MW) and 2.5% HPC–0.2% SDS exhibited fast erosion and recovered ITZ nanoparticles/clusters. The optical microscope images in Figure A3 qualitatively support the redispersion behavior quantified by the laser diffraction results. When redispersion was slow and incomplete, the rounded/spherical nanocomposite particles appeared in the images even after 60 min, whereas fast redispersion was associated with complete erosion of the nanocomposite matrix, leading to disappearance of the nanocomposite particles in the images.

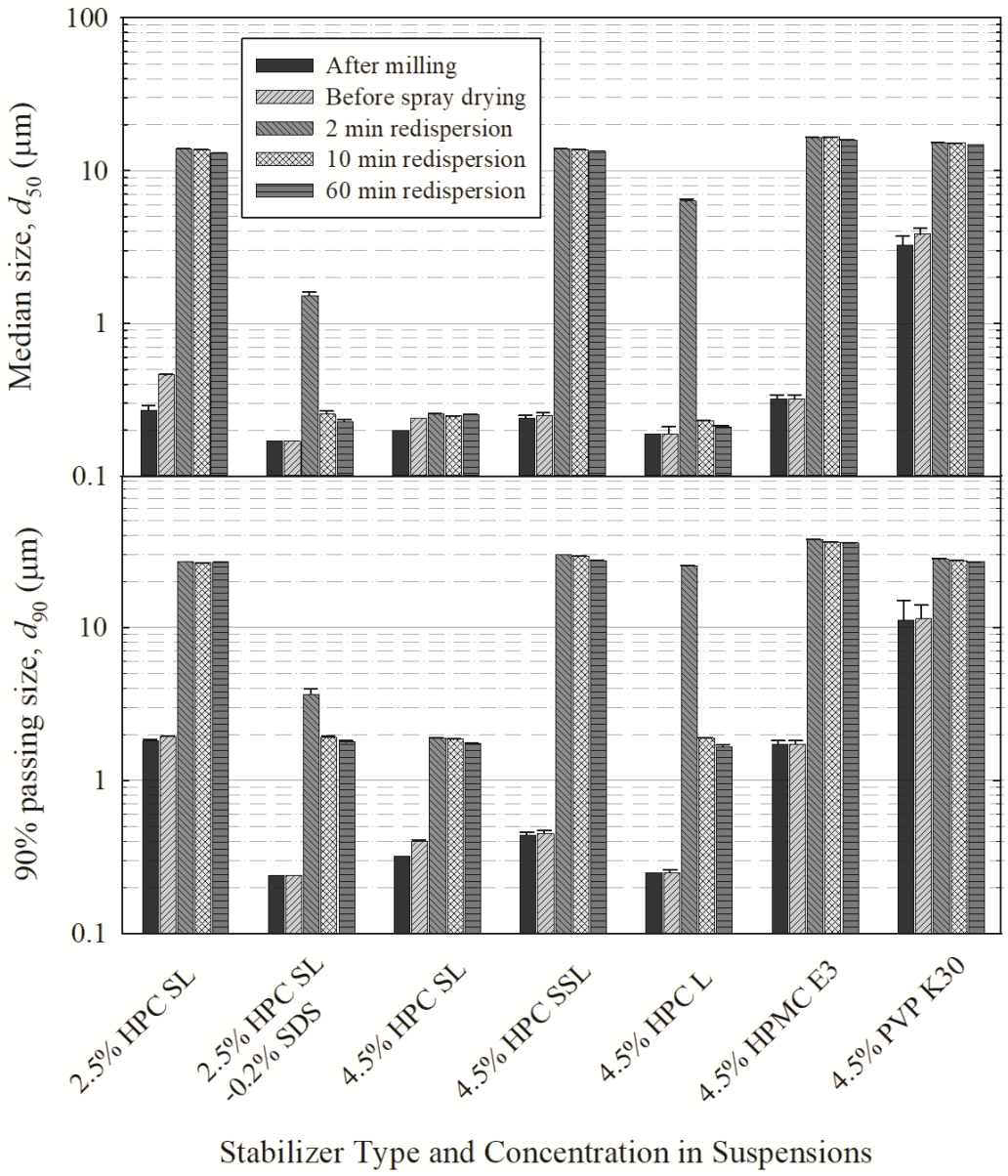

Figure 2.9 Volume-based particle size statistics of the ITZ suspensions after milling (65 min), before spray drying (after 1 day of milling), and the nanocomposites redispersed in 3 g/L SDS solution for 2 min, 10 min, and 60 min: (a) Median particle size d_{50} and (b) 90% passing size d_{90}. Suspension formulations contain 2.5% HPC SL(F2), 2.5% HPC SL–0.2% SDS (F3), 4.5% HPC SL (F4), 4.5% HPC SSL (F5), 4.5% HPC L (F6), 4.5% HPMC E3 (F7), and 4.5% PVP K30 (F8).

An interesting question arises as to how hydrophilic and freely water-soluble dispersants used in this study could not achieve fast redispersion for all nanocomposite formulations. Indeed, according to the modified Washburn

experiments (see Figure A1 of Appendix A), the polymeric dispersant solutions penetrated into pores of a packed ITZ bed much faster than water and improved ITZ wettability drastically as per higher values of the wetting effectiveness factor, i.e., $\log(\cos\theta_{ds}/\cos\theta_{w})$ (Table 2.3). Accordingly, upon use of dispersants in the nanocomposites, one would expect that (i) the redispersion/dissolution medium could penetrate into the pores of the nanocomposite particles generated upon dissolution of the water-soluble dispersants fast and (ii) any ITZ aggregates released from the nanocomposites could redisperse/dissolve in the redispersion/dissolution medium. However, the redispersion tests (see Figure 2.9) suggest that the significant wettability enhancement upon use of dispersants observed in the modified Washburn experiments (Table 2.3) did not translate into fast redispersion of the nanocomposites and fast recovery of the ITZ nanoparticles for some dispersants. For example, while the use of dispersants with high $\log(\cos\theta_{ds}/\cos\theta_{w})$ in the nanocomposites led to recovery of ultrafine particles during the redispersion (e.g., 2.5% HPC SL–0.2% SDS), this was not the case for 4.5% HPC SSL.

In the Washburn method, a polymeric dispersant solution penetrated through the void space of packed ITZ particles, whereas in the redispersion test, the polymeric solution is expected to locally form around the nanocomposite upon dissolution of the polymeric matrix. It is likely that the polymer at the surfaces of the nanocomposite particles with 2.5% HPC SL, 4.5% HPC SSL, 4.5% HPMC E3, and 4.5% PVP K30 did not locally dissolve to provide the "theoretical" wettability enhancement. Since ITZ is a highly hydrophobic drug, which is indicated by the log-partition coefficient (logP) value of 8.5 (Van Eerdenbrugh et al., 2008b), and it comprises 60%–78% of

the nanocomposites, the nanocomposite surface could be hydrophobic despite the presence of hydrophilic dispersants especially if the drug nanoparticles are not well-dispersed in the polymeric dispersant matrix due to formation of aggregates. Note that the aforementioned nanocomposites had aggregated ITZ particles that were already formed in the precursor suspensions during milling–storage (Figure 2.9) and that were likely formed during the drying (for 4.5% HPC SSL). Aggregation of drug nanoparticles during drying have been reported by other researchers (Li et al., 2016c; Van Eerdenbrugh et al., 2008b): when used at insufficiently low concentration, dispersants (e.g., 2.5% HPC SL) could not provide a sufficient physical barrier between drug nanoparticles and their existing aggregates, and larger clusters, sometimes called agglomerates or hard aggregates, can form (Li et al., 2016c; Van Eerdenbrugh et al., 2008b). Although the exact mechanism leading to nanoparticle aggregation during drying is unknown (Van Eerdenbrugh et al., 2008b), the capillary pressure theory suggests that aggregation is due to the capillary forces encountered during the drying process (Wang et al., 2005); others attributed aggregation to polymer chain entanglement and/or potential micro-phase separation of polymeric stabilizer from particles upon increase in particle concentration with reduced water content (Kim and Lee, 2010; Lee et al., 2009; Vehring, 2008). In summary, the aggregates of hydrophobic ITZ particles on the surface of the nanocomposites appear to have prevented solubilization of the polymer, thus negating any potential wettability improvement thereupon, and leading to negligible/slow erosion. The nanocomposites with 4.5% HPC (SL/L grades with 100/140 kg/mol MW) and 2.5% HPC–0.2% SDS did not have small aggregates in the precursor suspensions; hence, it

is expected that the hydrophobic ITZ nanoparticles/aggregates were well-dispersed in the hydrophilic polymeric matrix, and the matrix wetted and eroded fast upon contact with the aqueous media, thus releasing the ITZ nanoparticles fast.

2.2.6 ITZ Dissolution Enhancement

The dissolution profiles of the as-received ITZ, the physical mixture of formulation F4, and the nanocomposites with various dispersants are presented in Figures 2.10 and 2.11. The *p*-values for the Korsmeyer–Peppas model fit and the estimated parameters are less than 0.05, and R^2 values are in the range of 0.92–0.99 (Table 2.5), both of which suggest that overall the model fitted the data fairly well and both the model and its parameters were statistically significant. The *kn* value was used to compare initial dissolution rates of various nanocomposites, while >80% ITZ release in 20 min was used as the main discriminating criterion for immediate release. The f_1–f_2 statistics suggest that the dissolution profiles of F3 and F4 nanocomposites were similar; all dissolution profiles were statistically different from those of F3 and F4 nanocomposites (Section A.4 of Appendix A).

Table 2.5 Korsmeyer–Peppas Model Parameters Obtained From Fitting the Dissolution Data

Formulation ID [a]	Formulation composition [b]	Korsmeyer–Peppas model			
		n (-)	k (%min^{-n})	R^2 (-)	kn (%min^{-n})
F1	0.2% SDS	0.47	7.67	0.963	3.59
F2	2.5% HPC SL	0.50	6.15	0.992	3.08
F3	2.5% HPC SL–0.2% SDS	0.30	48.2	0.929	14.4
F4	4.5% HPC SL	0.23	49.1	0.942	11.1
F5	4.5% HPC SSL	0.42	14.2	0.978	5.96
F6	4.5% HPC L	0.35	30.4	0.923	10.6
F7	4.5% HPMC E3	0.37	17.6	0.982	6.55
F8	4.5% PVP K30	0.54	10.7	0.952	5.71

[a] Formulation is labeled based on the composition of the respective milled ITZ suspension formulation.
[b]All precursor suspensions have 10% ITZ. w/w is w.r.t. the weight of deionized water (200 g).

2.2.6.1 General Trends. Figure 2.10 shows that only 7.3% of as-received ITZ was released (dissolved) after 60 min. The slow ITZ dissolution was due to low surface area of as-received, coarse ITZ crystals (d_{50}: 15.5 μm) and lipophilic nature of ITZ. The nanocomposites produced by spray drying of wet-milled ITZ suspensions led to significantly higher ITZ dissolution for any dispersant used as compared with as-received ITZ (Figures 2.10 and 2.11). Considering that only limited dissolution improvement was observed for a physical mixture of as-received, coarse ITZ particles–4.5% HPC SL, it is evident that ultrafine ITZ particles in the form of nanoparticles and, to some extent, their aggregates (refer to Table 2.2) present in a hydrophilic nanocomposite matrix, account for the significant dissolution rate enhancement. In general, the nanocomposites that exhibited fast erosion and redispersion (Figure 2.9) of the polymeric matrix released ITZ faster as compared with those that exhibited slow redispersion (Figures 2.10 and 2.11), which originated from the presence of aggregates in the respective nanocomposites. It is also important

to note that the redispersion of the nanocomposites with any dispersant formulation is expected to be faster in the dissolution test than in the redispersion test because the ITZ particles on the surface of the nanocomposites can dissolve in the dissolution test with 1000 mL medium, thus facilitating the redispersion. This explains why >75% of ITZ dissolved from the nanocomposites with 4.5% HPC SSL/HPMC E3/PVP K30 at 60 min (Figure 2.11) despite their slow erosion during 60 min redispersion test (Figure 2.9).

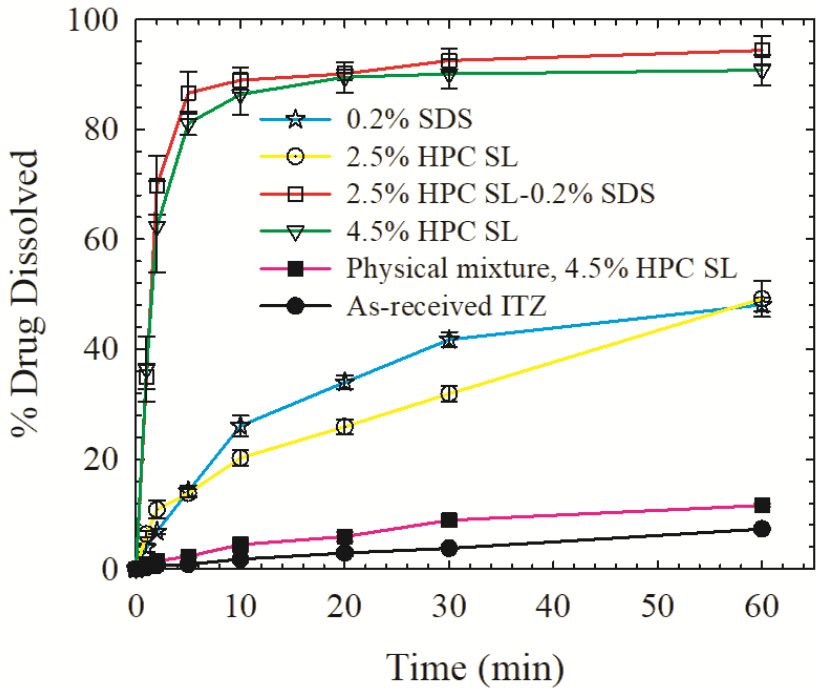

Figure 2.10 Drug dissolution from the nanocomposites prepared *via* spray-drying of the milled ITZ suspensions with 0.2% SDS (F1), 2.5% HPC SL (F2), 2.5% HPC SL–0.2% SDS (F3), and 4.5% HPC SL (F4) as well as from physical mixture of formulation F4 (blend of 10% ITZ–4.5% HPC SL) and as-received ITZ.

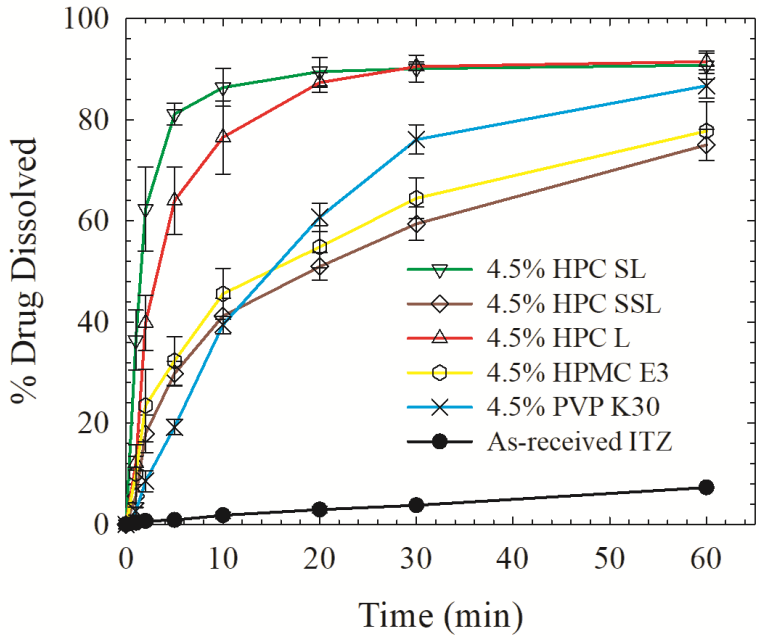

Figure 2.11 Drug dissolution from the nanocomposites prepared *via* spray-drying of the milled ITZ suspensions with 4.5% concentration of HPC SL (F4), HPC SSL (F5), HPC L (F6), HPMC E3 (F7), and PVP K30 (F8) as well as from as-received ITZ.

While the ITZ particle size in the nanocomposites is clearly a dominant factor in ITZ dissolution enhancement, a question arises as to whether nanocomposite particle size (refer to Table 2.2) can significantly affect the dissolution results. Note that 0.2% SDS nanocomposites (smallest nanocomposites) and 4.5% HPC L (biggest nanocomposites) exhibited one of the slowest (kn = 3.59 $\%min^{-0.47}$) and the fastest ITZ release (kn = 10.6 $\%min^{-0.35}$), respectively, among all nanocomposites, contrary to what one would expect if the nanocomposite particle size itself is a dominant factor for ITZ release. To answer this question more precisely, we also spray-dried the milled 4.5% HPC SL suspension (F4) using a larger nozzle tip opening (1.2 mm *vs.* 0.6 mm) at lower atomization pressure (1.5 bar *vs.* 2.0 bar) as compared with the baseline drying conditions. The so-formed nanocomposite particles were coarser (d_{50}: 20.7 µm and d_{90}: 40.6 µm) than the baseline 4.5% HPC SL nanocomposites (d_{50}: 16.2

μm and d_{90}: 32.3 μm), both having identical dispersant formulation. The dissolution profiles (see Figure A.2 of Appendix A) indicate that despite ~30% increase in d_{50} and d_{90}, there is no statistically significant impact of the nanocomposite particle size on ITZ release (f_1 = 0.93 and f_2 = 91.8) within the particle size range studied. Hence, while there may be some confounding effect of the nanocomposite particle size, it is expected that the milled ITZ (aggregate) particle size and dispersant type/concentration have more dominant effects on the drug release.

2.2.6.2 Impact of Various Dispersants. Figure 2.10 shows that the nanocomposites with 0.2% SDS and 2.5% HPC SL released 48.1% and 49.2% of ITZ at 60 min, respectively. However, the drug release from both nanocomposites was still slow and immediate release (>80% in 20 min) was not achieved. On the other hand, immediate release was achieved when combination of HPC and SDS (F3) or higher concentration of HPC SL (F4) was used. In fact, the dissolution profile of 4.5% HPC SL formulation is statistically similar to that of 2.5% HPC–0.2% SDS, which suggests the feasibility of preparing an equivalent surfactant-free nanocomposite. The dispersants were ranked-ordered based on the initial ITZ release rates, quantified by *kn*, as follows: 2.5% HPC–0.2% SDS > 4.5% HPC SL > 0.2% SDS > 2.5% HPC SL. These results can be explained by the faster redispersion behavior of the 4.5% HPC SL and 2.5% HPC–0.2% SDS nanocomposites and the smaller aggregate sizes in the respective milled/stored precursor suspensions.

Figure 2.11 compares the ITZ release from the nanocomposites prepared with 4.5% polymer alone in the milled suspensions. The nanocomposites were ranked-ordered based on ITZ release in 20 min as follows: HPC SL ≅ HPC L > PVP K30 >

HPMC E3 > HPC SSL. Only HPC SL/L grades with 100 kg/mol and 140 kg/mol MW, respectively, achieved immediate release because they had small aggregates in their precursor suspensions and exhibited faster redispersion than the other polymers and HPC SSL (Figure 2.9). These observations for HPC were also confirmed by the *kn* values of the respective nanocomposites: HPC SL > HPC L > HPMC E3 > HPC SSL > PVP K30. It appears that there is an optimum HPC MW for the fastest ITZ release. Although the precursor suspension with HPC L had slightly smaller aggregates than that with HPC SL, the former exhibited slower ITZ release perhaps due to slower redispersion (see Figure 2.9). This may also be partly explained by the confounding effect of the nanocomposite particle size as HPC L nanocomposites were the biggest among all. The nanocomposites with low MW polymers, i.e., HPC SSL (40 kg/mol), PVP K30 (50 kg/mol), and HPMC E3 (10 kg/mol) exhibited slower ITZ release than HPC SL/L because of the large aggregates formed during milling, storage, and drying and the ensuing slower redispersion (Figure 2.9). Finally, the lowest extent of ITZ release at 20 and 60 min with HPC SSL could be related to formation of hard aggregates during drying, slow redispersion of the nanocomposites, and slow deaggregation of the hard ITZ aggregates in the dissolution medium (Li et al., 2016c). While the precursor suspension with PVP K30 had large ITZ aggregates, it appears that the aggregates emanating from the nanocomposites were dispersed in the dissolution test, leading to higher ITZ release in 20 and 60 min as compared with HPC SSL.

2.3 Conclusions

This study has demonstrated that wet-milled stable 10% ITZ nanosuspensions showing near-Newtonian flow behavior can be prepared with 4.5% HPC SL/L (100 and 140 kg/mol MW, respectively). At 4.5% concentration, HPC SSL (40 kg/mol), HPMC E3 (10 kg/mol), and PVP K30 (50 kg/mol) could not suppress ITZ nanoparticle aggregation, leading to significant pseudoplastic behavior. Contrary to previous studies that highlight the favorability of low MW polymers (Choi et al., 2008; Sepassi et al., 2007) (specifically <50 kg/mol for ITZ–HPC (Choi et al., 2008)), our study demonstrated that higher MW HPC (100 and 140 kg/mol) is more favorable for ITZ nanosuspension stabilization, which in line with the thermodynamic considerations of polymer adsorption. Spray drying of the ITZ suspensions yielded nanocomposites with 60–78% mean ITZ loading, which is higher than that in the ITZ nanocomposites produced in prior studies, and acceptable content uniformity. Severe aggregation occurred during the milling/drying when 4.5% polymers with MW ≤ 50 kg/mol were used. Their nanocomposites did not redisperse into ITZ nanoparticles/aggregates due to negligible/slow matrix erosion in the redispersion test; thus, they did not exhibit immediate release during the dissolution test. While the use of higher MW HPC (100 and 140 kg/mol) was more favorable from both nanosuspension stabilization and ITZ release perspectives, there exists an optimal MW. The fastest ITZ dissolution among the nanocomposites with 4.5% polymer was achieved by HPC SL (100 kg/mol). Moreover, the viscous dampening effect even in a wet stirred media mill could detrimentally slow down the breakage rate if polymers with higher MW (e.g., >150 kg/mol) were used. Overall, high drug-

loaded, surfactant-free ITZ nanocomposites that exhibited fast redispersion and immediate release were prepared *via* spray-drying of wet-milled ITZ with 4.5% HPC SL/L. In a future study, higher MW grades (> 50 kg/mol) of HPMC and PVP will be used to examine if they could improve nanosuspension stability and ITZ release similar to HPC. Moreover, HPC with MW above 150 kg/mol will be used to examine the limits of wet stirred media milling in producing drug nanosuspensions fast, as such limiting conditions could occur due to pronounced viscous dampening.

CHAPTER 3

DISSOLUTION ENHANCEMENT *VIA* DRUG HYBRID NANOCRYSTAL–AMORPHOUS SOLID DISPERSION (HYNASD) *VS.* ASD

As has been indicated in Chapter 1, drug nanocomposites (nanoparticle-based dosage form) and amorphous solid dispersions (ASDs) are two major approached to enhance the bioavailability of the poorly water-soluble drugs, both approaches have some advantages and disadvantages. A major shortcoming of drug nanocomposites as compared with amorphous solid dispersions (ASDs) is their limited supersaturation capability in the dissolution media. Chapter 3 aims to address this limitation of the drug nanocomposites by introducing a new class of drug nanoparticles called hybrid nanocrystal–amorphous solid dispersions (HyNASDs) and compare their performance to ASDs. A wet-milled griseofulvin (GF, BCS II drug) nanosuspension and a GF solution, both containing the same dissolved polymer–surfactant (SDS: sodium dodecyl sulfate) with 1:1 and 1:3 GF:polymer mass ratios, were spray-dried. Hydroxypropyl cellulose (HPC) and Soluplus (Sol) were used as matrix-forming polymers. XRPD, DSC, and Raman spectroscopy reveal that ASDs were formed upon spray-drying the solution-based feed, whereas nanocomposites and nanocomposites with >10% amorphous content, HyNASDs, were formed with the nanosuspension-based feed. Sol provided higher GF relative supersaturation, up to 180% and 360% for HyNASDs and ASDs, respectively, in the dissolution tests than HPC (up to 50% for both) owing to Sol's stronger intermolecular interactions and miscibility with GF and its recrystallization inhibition. Besides the higher kinetic solubility of GF in Sol, presence of GF nanoparticles *vs.* micron-sized particles in the

nanocomposites enabled fast supersaturation. This study demonstrates successful preparation of fast supersaturating (190% within 20 min) HyNASDs, which renders nanoparticle formulations competitive to ASDs in bioavailability enhancement of poorly soluble drugs.

3.1 Materials and Methods

3.1.1 Materials

BP/EP grade micronized griseofulvin (GF) was purchased from Letco Medical (Decatur, AL, USA) and used as a challenging Biopharmaceutics Classification System (BCS) Class II drug because GF nanocrystals exhibit severe aggregation in suspensions, if improperly stabilized (Bilgili and Afolabi, 2012), and it is known to be a fast crystallizing drug (Baird et al., 2010). Its solubility in deionized (DI) water is ~8.9 mg/L at 25 °C and ~14.2 mg/L at 37 °C; it has a melting point T_m of 220 °C and a glass transition temperature T_g of 89 °C (Baird et al., 2010). Hydroxypropyl cellulose (HPC, SSL grade, Nisso America Inc., New York, NY) is a semi-crystalline polymer with low crystallinity and amorphous domains of very low T_g. It is widely used as a stabilizer during milling and matrix former in the nanocomposites (Azad et al., 2015b; Bhakay et al., 2014a). Soluplus (Sol, BASF, Tarrytown, NY)) is an amphiphilic graft copolymer produced from polyvinyl caprolactam–polyvinyl acetate–polyethylene glycol having a single glass transition temperature of 73 ± 2 °C (Terife et al., 2012). Sol has been commonly used to produce ASDs of various poorly water-soluble drugs (Ha et al., 2014). An anionic surfactant, sodium dodecyl sulfate (SDS), purchased from GFS Chemicals, Inc. (Columbus, OH) was used as a wetting

agent, which also helps to stabilize GF nanosuspensions. Acetone (ACS reagent, ≥ 99.5%) was purchased from BDH Analytical chemicals, (VWR, GA) and used as a solvent to prepare solution-based feed to the spray dryer. In WSMM, Yttrium zirconia beads (Zirmil Y, Saint Gobain ZirPro, Mountainside, NJ, USA) with a median size of 430 µm were used.

3.1.2 Preparation of Spray-Dried Powders

Aqueous suspension-based (W:water) feeds and organic solution-based (S:solvent) feeds of GF were fed to the spray dryer for the preparation of drug nanocomposites and ASDs, respectively (Figure 3.1). Table 3.1 presents the formulations used in the precursor feeds. Drug concentration was kept constant at 2.5% (w/v). The GF concentration was calculated w.r.t. the total volume of the water in the suspension-based feeds and the total volume of the solvent mixture (acetone–water) in the solution-based feeds, which was fixed at 240 mL. GF nanosuspensions were prepared with two different polymers (HPC/Sol) at 1:1 and 1:3 drug:polymer mass ratios to examine the impact of polymer type and polymer loading on GF release in dissolution tests. To elucidate the role of Sol, a nanosuspension with 3:1 GF:Sol (W-Sol-3:1) and a suspension of as-received (micronized) GF with 1:3 GF:Sol (W-M-Sol-1:3) were also prepared. In all formulations, SDS concentration was kept constant below the critical micelle concentration (CMC, 0.23%, w/v) at 0.125% (w/v) to minimize Ostwald ripening (Knieke et al., 2013).

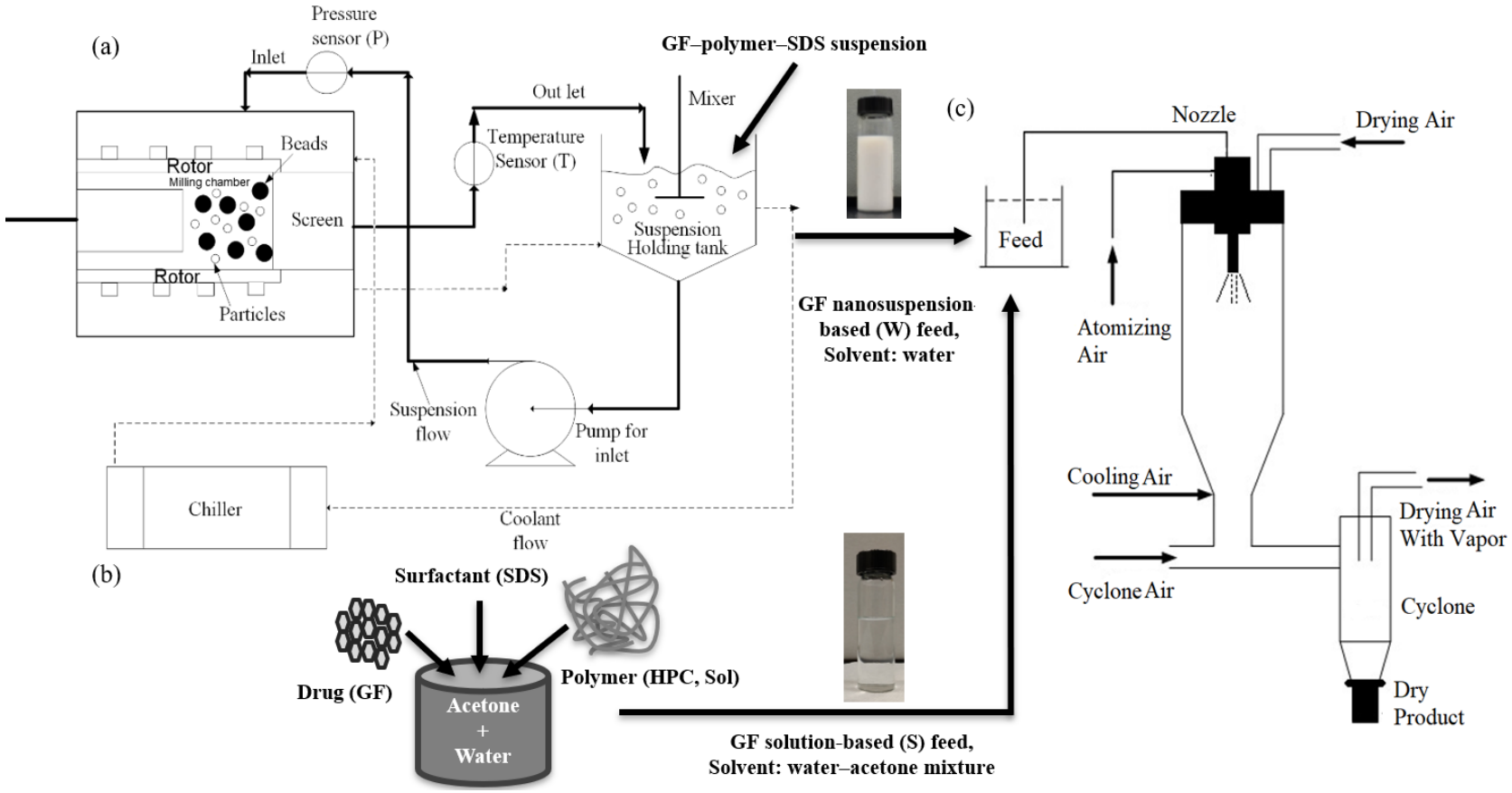

Figure 3.1 Schematic illustration of the process setup: (a) wet-stirred media milling (WSMM) of drug in aqueous solution of polymer–surfactant for the preparation of the drug nanosuspension-based (W) feed, (b) mixing of drug, polymer, and surfactant in acetone–water mixture for the preparation of the drug solution-based (S) feed, and (c) co-current spray drying of each feed separately. Diagrams are not drawn to scale.

Table 3.1 Formulations of the Suspension-based (W) Feeds and Solution-based (S) Feeds Used in Spray Drying

Formulation[a]	GF (% w/v)[b]	Polymer (% w/v)[b]	SDS (% w/v)[b]	Water (mL)	Acetone (mL)
W-Sol-1:3	2.5	7.5	0.125	240	0
W-Sol-1:1	2.5	2.5	0.125	240	0
W-Sol-3:1	2.5	0.8	0.125	240	0
W-HPC-1:3	2.5	7.5	0.125	240	0
W-HPC-1:1	2.5	2.5	0.125	240	0
S-Sol-1:3	2.5	7.5	0.125	40	200
S-Sol-1:1	2.5	2.5	0.125	40	200
S-HPC-1:3	2.5	7.5	0.125	40	200
S-HPC-1:1	2.5	2.5	0.125	40	200

[a]S denotes solution-based feed; W denotes nanosuspension-based feed; Sol denotes Soluplus; the ratios refer to the drug:polymer mass ratios. All formulations have 0.125% w/v SDS.
[b]% w/v with respect to the total volume (240 mL) of the liquid (water/solvent).

In the preparation of nanosuspension-based (W) feeds, a shear mixer (Fisher Scientific Laboratory Stirrer, Catalog No. 14-503, Pittsburgh, PA) was used to disperse as-received GF particles in the aqueous dispersant (HPC/Sol–SDS) solutions first. The resultant GF pre-suspensions were transferred to the holding tank of a Microcer wet stirred media mill (WSMM) (Netzsch Fine Particle Technology, LLC, Exton, PA, USA) with 80 mL milling chamber (Figure 3.1a). Milling conditions were adopted from our prior work on WSMM (Afolabi et al., 2014; Bilgili et al., 2016). 50 mL of the milling chamber was filled with zirconia beads, and to hold the beads in the chamber a screen with 200 μm opening was used at the outlet of the chamber. The pre-suspension was recirculated through the chamber at a rate of 126 mL/min *via* a peristaltic pump and was milled at a rotor speed of 3200 rpm for 64 min. A portion of each suspension was separated in a vial and stored for 7 days at 8 °C to assess the short-term physical stability. Also, the milled suspensions were refrigerated at 8 °C for overnight before spray drying.

To prepare the solution-based (S) feeds, a mixture of acetone–water was purposefully selected to dissolve all components of the formulation (Figure 3.1b). To ensure a *head-to-head* comparison of the nanocomposites with ASDs, the formulations of the solution-based (S) feeds are kept identical to those of the suspension-based (W) feeds. 40 mL of deionized water was added to 200 mL acetone to prepare a total of 240 mL solvent mixture. After dissolving the drug–polymer–surfactant into the binary solvent mixture using a magnetic stirrer, the solutions were sonicated for 30 min before feeding to the spray dryer.

Using a spray dryer (4M8-Trix, Procept, Zelzate, Belgium) having a co-current flow set-up (Figure 3.1c), GF suspensions and drug–polymer solutions were dried. The total length and the diameter of the spray dryer are 1.59 m and 0.15 m, respectively. To ensure complete drying, inlet temperature was selected above the boiling temperature of the respective pure liquids. Drying air at 120 °C flowing at 0.37–0.40 m^3/min and drying air at 75 °C flowing at rate of 0.27–0.30 m^3/min were fed co-currently at the top of the dryer column to dry W feeds and S feeds (see Table 2), respectively. 200 g suspension/solution of each formulation was sprayed at 2.0 g/min rate using a peristaltic pump (Make-it-EZ, Creates, Zelzate, Belgium). A cyclone separator was used to separate the dried particles from the outlet stream into a glass jar. Atomizing air pressure of 2.0 bar, a bi-fluidic nozzle with tip diameter of 0.6 mm, and cyclone pressure of 55–60 mbar were selected based on prior experience (Azad et al., 2015b) and exploratory experiments. The dried particles obtained from the collection jar were transferred into double plastic bags and stored in a vacuum-desiccator at room temperature for further characterization.

3.2 Characterization Techniques

3.2.1 Particle Sizing

Drug particle size distributions (PSDs) in the suspensions were measured by laser diffraction (LS 13 320, Beckman Coulter, Miami, FL) based on Mie scattering theory following the procedure described in ref. (Bilgili et al., 2016) at various times: right after milling, after 1-day and 7-day storage at 8 °C to in a refrigerator. The intensity was maintained between 40–50% while the obscuration was maintained below 8.0% for all measurements. Refractive index values are 1.65 for GF (drug) and 1.33 for deionized water (medium). Before each measurement, a 2.0 mL suspension sample was dispersed into 5.0 mL of the respective stabilizer solution using a vortex mixer (Fisher Scientific Digital Vortex Mixer, Model No: 945415, Pittsburgh, PA) at 1500 rpm for one min prior to each measurement.

The particle sizes of the spray-dried powders were measured by a Rodos/Helos laser diffraction system (Sympatec, NJ, USA) based on Fraunhofer theory following the procedure described in ref. (Li et al., 2016b). About 1 g of the powder sample was placed on top of the sample chute of the Rodos dispersing system and the sample chute was vibrated at a 100% setting, and 0.1 bar dispersion pressure was used to suck in the falling powder through the sample cell of the laser diffraction system. For further confirmation of the particle sizes, spray-dried particles were placed on a glass slide and observed by Axio Scope.A1 polarized light microscope (PLM, Carl Zeiss Microscopy GmbH, Göttingen, Germany).

3.2.2 Solid State Characterization and Drug–Polymer Interactions

To analyze the crystallinity of the as-received GF, HPC, Sol, spray-dried powders, and physical mixtures of GF–polymer–SDS (same formulation as stated in Table 3.1), X-ray powder diffraction (XRPD) (PANanalytical, Westborough, MA, USA), provided with Cu K_α radiation (λ= 1.5406 Å) was used. The samples were scanned at a rate of 0.165 s^{-1} for 2θ ranging from 5° to 40°. The total area under three distinct, non-overlapping peaks of GF at characteristic diffraction angles of 13.2°, 14.6°, and 16.5° was calculated for both the physical mixtures and the spray-dried powders using the equipment's HighScore Plus software, which was then used to estimate the crystallinity.

Differential scanning calorimetry (DSC) of the as-received GF, Sol, HPC, physical mixtures of GF–polymer–SDS, and spray-dried powders was performed using a Mettler-Toledo polymer analyzer (PolyDSC, Columbus, OH, USA) with integrated STARe 10 software. ~6.0–7.0 mg powder sample was placed in an aluminum pan with a hole in the lid and loaded into the DSC machine. As-received GF was heated at a rate of 10 °C/min from 25 °C to 250 °C. All other samples were heated from 25 °C to 70 °C and the temperature was held for 2 min at 70 °C, then cooled back to 25 °C to remove any residual solvent in the sample. In the final step, the samples were heated from 25 °C to 250 °C at 10 °C/min. Nitrogen gas was used as the purge gas and protective gas at a flow rate of 50 mL/min and 150 mL/min, respectively. Thermogravimetric analysis (TGA) was performed to measure the residual water/solvent content using a TGA/DSC1/SF Stare system (Mettler Toledo, Inc., Columbus, OH). ~6.0–7.0 mg of each spray-dried sample was placed in a

ceramic crucible and heated from 25 °C to 150 °C at a heating rate of 10 °C/min under nitrogen flow.

Raman spectroscopy was conducted using a Fergie Imaging Spectrometer System (Princeton Instruments, Trenton, NJ) with a 500-mW external diode laser processing at 785 nm wavelength. Data acquisition time for all spectra was 15 s per scanned spectrum (100–1800 cm^{-1}) and each spectrum acquired was averaged over two scans. The data was presented for the range of 1550–1800 cm^{-1} wavenumber.

3.2.3 Characterization of Drug Recrystallization

To elucidate the role of drying rate on drug recrystallization during drying, a droplet of 20 µL of the solution prepared for the solution-based (S) feed was put onto a hot glass slide at 75 °C and kept for drying in quiescent air. After about one min drying, the slides were placed under the polarized light microscope (PLM) to observe if any drug recrystallization occurred. To elucidate GF recrystallization in the presence of water, a small portion of the spray-dried powders prepared using the solution-based (S) feed (S-HPC-1:3 and S-Sol-1:3) was gently pressed to form a loose compact, which was then mounted onto a microscopic glass slide, and placed under the PLM. 20 µL of deionized water was added to the sample and the PLM images were captured at 0, 1, 2, and 5 min from the moment of water addition.

3.2.4 Study of Nanoparticle Recovery From the Nanocomposites

Aqueous redispersion of the nanocomposites was performed following a previously established method (Bilgili et al., 2018; Li et al., 2016b). About 0.5 g of the spray-dried powders prepared using the nanosuspension-based (W) feeds was dispersed in 30 mL of deionized water inside a 60 mL beaker and stirred at 500 rpm for 60 min

with a paddle-stirrer (CAT R18, Scientific Instrument Center Limited, Winchester, UK). ~1.0 mL aliquot of redispersed sample was taken at 2, 10 and 60 min while stirring, and particle size was measured using laser diffraction (LS 13 320, Beckman Coulter, Miami, FL). At the same collection times, a droplet of each redispersed sample was taken and dried immediately by dropping on a preheated glass slide on a hot plate at 100 °C. After drying, the PLM was used to capture images of the redispersed particles. The details of the experimental methods and results are presented in Appendix B.

3.2.5 Drug Content and Dissolution Performance of the Spray-Dried Powders

The drug content in the dried powders varied based on the drug:polymer mass ratios. To measure the actual drug content in the spray-dried powders, an assay testing was performed by dissolving 100 mg of the sample powders in 20 mL methanol under 30 min of sonication, followed by overnight storage to ensure complete solubilization of the GF particles. An aliquot of 100 µL was taken from the GF solution and diluted up to 10 mL using methanol. The absorbance of the samples was measured at 292 nm using UV spectrophotometer (Agilent, Santa Clara, CA, USA), and the drug concentration was calculated from a pre-established calibration curve. Six replicates were tested for each formulation to calculate mean drug content along with the relative standard deviation (RSD).

Drug release from the spray-dried powders and various physical mixtures (PMs) prepared by blending was determined *via* a Distek 2100C dissolution tester (North Brunswick, NJ, USA), following the USP II paddle method. 1000 mL deionized water at 37 °C was stirred at 50 rpm paddle speed. Spray-dried powder

samples containing 100 mg GF (above the thermodynamic solubility of as-received GF particles) were weighed and added to the dissolution medium and 4 mL samples were taken out manually at 1, 2, 5, 10, 20, 30, 60, 120, 180, and 210 min. These aliquots were filtered through 0.1 µm PVDF membrane-type syringe filter before UV-spectroscopy measurements (similar to Bhakay et al. (2014a) and Li et al. (2017)). The filtered samples were diluted with 37 °C deionized water at a ratio of 1 to 5 before UV measurement. Dissolved GF amount was measured by UV spectroscopy at 296 nm wavelength and calculated using a pre-established calibration curve. Deionized water was used as the blank before UV measurement and six replicates of each sample were performed. In this paper, relative % supersaturation is reported based on GF concentration at 210 min and thermodynamic solubility of as-received GF particles, unless otherwise indicated.

3.2.6 Supersaturation Maintenance Ability of the Polymers

The supersaturation maintenance ability of HPC/Sol was examined in a separate desupersaturation test (similar to ref. (Konno et al., 2008)). A concentrated solution of GF in acetone was prepared by dissolving 100 mg of as-received GF in 20 mL acetone. This solution was subsequently added to 1000 mL of pre-dissolved HPC–SDS/Sol–SDS solution with 100 µg/mL and 300 µg/mL polymer concentration, which maintained 1:1 and 1:3 drug:polymer mass ratio, respectively, in the USP II paddle type dissolution tester. The addition resulted in 92–99 µg/mL supersaturated solutions of GF initially, and any subsequent desupersaturation during the following 210 min was tracked *via* GF concentration measurements. The experimental

conditions and concentration measurement were identical to those in the dissolution test. All measurements were carried out in triplicate.

3.3 Results and Discussion

3.3.1 Properties of GF Nanosuspensions Prepared *via* Wet Stirred Media Milling

Four different GF suspensions were wet media milled using HPC/Sol at 1:1 and 1:3 drug:polymer mass ratios in the presence of SDS. The median particle size d_{50} and 90% passing size d_{90} of the final milled suspensions (after 64 min), after 1-day and 7-day storage are presented in Figure 3.2. Unless properly stabilized, GF nanoparticles severely aggregate in aqueous suspensions, forming micron-sized particles (Bilgili and Afolabi, 2012). The wet-milling of as-received (micronized) GF particles with d_{50}: 9.74 µm and d_{90}: 27.4 µm yielded nanosuspensions with d_{50} in the range of 0.14–0.19 µm. The small changes in d_{50} and d_{90} during the 7-day storage suggest that the suspensions did not undergo drastic aggregation/growth during milling and storage. On the other hand, an increase in HPC concentration led to smaller aggregates and finer sizes. In a previous study, HPC–SDS was reported to have synergistic stabilizing effect on GF suspensions during milling and storage (Bilgili and Afolabi, 2012) and stabilized multiple BCS Class II drug nanosuspensions (Bilgili et al., 2016). HPC and Sol imparted steric stabilization by adsorbing on drug nanoparticles (Bilgili and Afolabi, 2012; Yang et al., 2014), while the anionic surfactant (SDS) enhanced GF wettability/deaggregation and helped to stabilize the GF nanosuspensions *via* electrostatic repulsion (Bilgili and Afolabi, 2012; Bilgili et al., 2016).

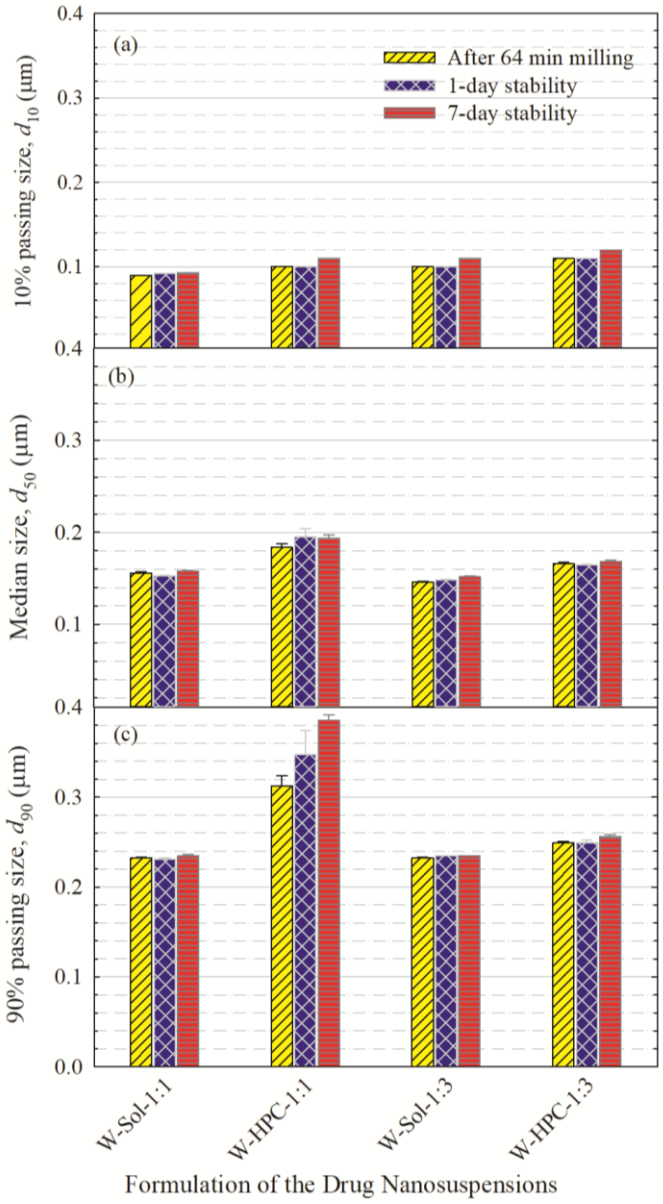

Figure 3.2 Volume-based particle size statistics of the milled GF suspensions with 1:1 and 1:3 GF:polymer mass ratios after milling (64 min) as well as 1-day storage and 7-day storage at 8 °C: (a) 10% cumulative passing size d_{10}, (b) median particle size d_{50} and (c) 90% cumulative passing size d_{90}. All suspensions have 2.5% w/v GF and 0.125% w/v SDS.

3.3.2 Size, Morphology, and Drug–Moisture Content of The Spray-Dried Powders

Drug nanosuspension-based (W) feeds produced by WSMM and drug–polymer solution-based (S) feeds with identical formulations were spray-dried separately. The

residence time in the spray dryer was short, i.e., 4.0 s and 5.0 s, for W feeds and S feeds, respectively. Despite the relatively short residence time, the spray-dried powders were completely dried, as indicated by the TGA, which shows weight loss of ~2.0% for the samples. The extremely large surface area generated by atomization of the feed coupled with the fast-convective heat–mass transfer at high air temperature enabled fast drying of the droplets. The mean (actual) drug content after spray-drying was higher for feeds with higher drug:polymer mass ratio (Table 3.2). RSD values were below 6%: 0.73–3.14%, which signifies pharmaceutically acceptable content uniformity. The slightly lower drug content as compared with the theoretical value can be attributed to preferential drug loss during handling/transfer after milling, poor separation of finer particles in the cyclone separator of the spray dryer, and presence of the residual moisture after drying (Azad et al., 2015b; Bilgili et al., 2018). The median sizes of the spray-dried powders were measured to be in the range of 6.89–19.0 μm and 11.0–15.8 μm (Table 3.2) for W feeds and S feeds, respectively. An increase in polymer loading led to formation of coarser particles due to increase in total solids loading and higher viscosity of the feed (Basa et al., 2008; Bilgili et al., 2018; Li et al., 2018b). The microscopic images (Figure 3.3) illustrate that spray-dried particles have rounded–donut shapes, and their sizes are in rough agreement with the ranges mentioned in Table 3.2.

Table 3.2 Particle Size Statistics of the Spray-Dried Powders and Their Drug Content

Formulation[a]	Particle size statistics of the spray-dried particles (μm)			Actual drug content, RSD (% w/w, %)	Theoretical drug content (% w/w)
	d_{10}±SD	d_{50}±SD	d_{90}±SD		
W-Sol-1:3	9.29±0.1	19.0±0.1	33.6±0.1	21.2, 1.50	24.7
W-Sol-1:1	4.48±0.1	10.1±0.1	21.9±0.2	42.0, 1.73	48.8
W-Sol-3:1	1.66±0.1	6.89±0.3	15.3±0.4	64.4, 0.51	72.3
W-HPC-1:3	6.37±0.1	16.5±0.6	40.0±0.1	22.3, 3.14	24.7
W-HPC-1:1	5.24±0.1	12.9±0.1	34.2±0.1	42.5, 2.83	48.8
S-Sol-1:3	4.11±0.0	12.3±0.0	33.2±0.1	21.5, 2.02	24.7
S-Sol-1:1	5.03±0.1	11.0±0.1	20.2±0.0	42.3, 2.21	48.8
S-HPC-1:3	6.48±0.0	15.8±0.6	31.3±1.0	24.4, 2.56	24.7
S-HPC-1:1	7.05±0.2	13.0±0.9	26.9±0.8	41.7, 0.73	48.8

[a]S denotes solution-based feed, W denotes nanosuspension-based feed, Sol denotes Soluplus; the ratios refer to the drug:polymer mass ratios. All formulations have 0.125% w/v SDS.

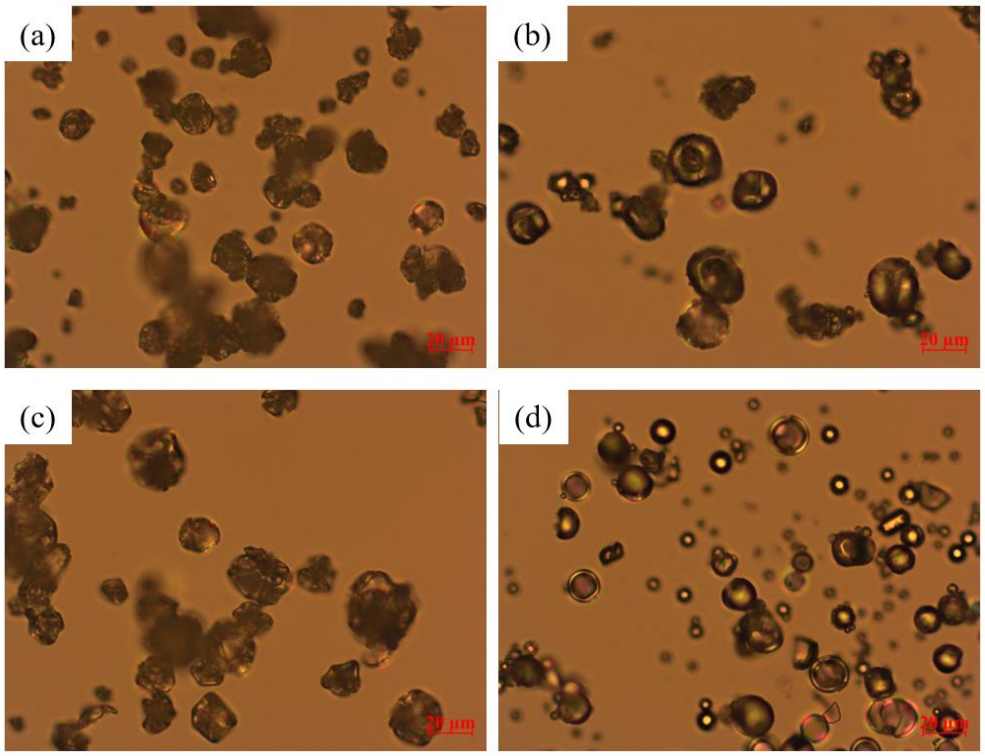

Figure 3.3 Polarized light microscope images of the spray-dried particles prepared using the GF nanosuspension-based (W) feed and the GF solution-based (S) feed with 1:3 GF:polymer mass ratios: (a) W-HPC-1:3, (b) S-HPC-1:3, (c) W-Sol-1:3, and (d) S-Sol-1:3. All images were taken at 50X magnification (scale bar: 20 μm).

3.3.3 Formation of Drug Nanocomposites/HyNASDs *vs.* ASDs Upon Spray Drying

The solid state of GF in the spray-dried powders was investigated *via* XRPD (see Figure 3.4) and DSC (see Figure 3.5). Table 3.3 presents the summary of DSC thermal events and estimated crystallinity *via* XRPD. X-ray diffractograms depict that as-received GF exhibited intense peak characteristics of a crystalline material, whereas HPC/Sol exhibited halo pattern indicating amorphous structure (Figure 3.4a). The physical mixtures (PMs), prepared by blending, exhibited peaks at the same diffraction angles as those of as-received GF, albeit with reduced peak intensity (Figure 3.4b and 3.4c), which can be attributed to the dilution and surface coverage of GF microparticles with HPC/Sol, and the reduction is more discernible with increasing polymer concentration. Similar XRPD diffractograms to those of the PMs were observed for the spray-dried powders prepared using the suspension-based (W) feeds confirming that spray-drying of W feeds led to formation of nanocomposites that are mostly crystalline (Figure 3.4b and 3.4c). Interestingly, the diffractograms of the spray-dried powders with W feeds especially those with higher polymer loading (lower GF:polymer ratio) show clear peak broadening and peak intensity reduction as compared with those of PMs, beyond the aforementioned dilution effect. Surprisingly, wet milling followed by spray-drying led to reduction of crystallinity and formation of notable (~5–20%) amorphous drug (see Table 3.3). To the best knowledge of the authors, this level of amorphous content in drug nanocomposites is not common. It is well-established that wet media milling does not cause any detectable amorphization of as-received GF, in the absence of stabilizers, due to plasticization effect of water (Monteiro et al., 2013). In the presence of high polymer

loading in the nanosuspensions here, however, amorphization of GF took place during the spray drying.

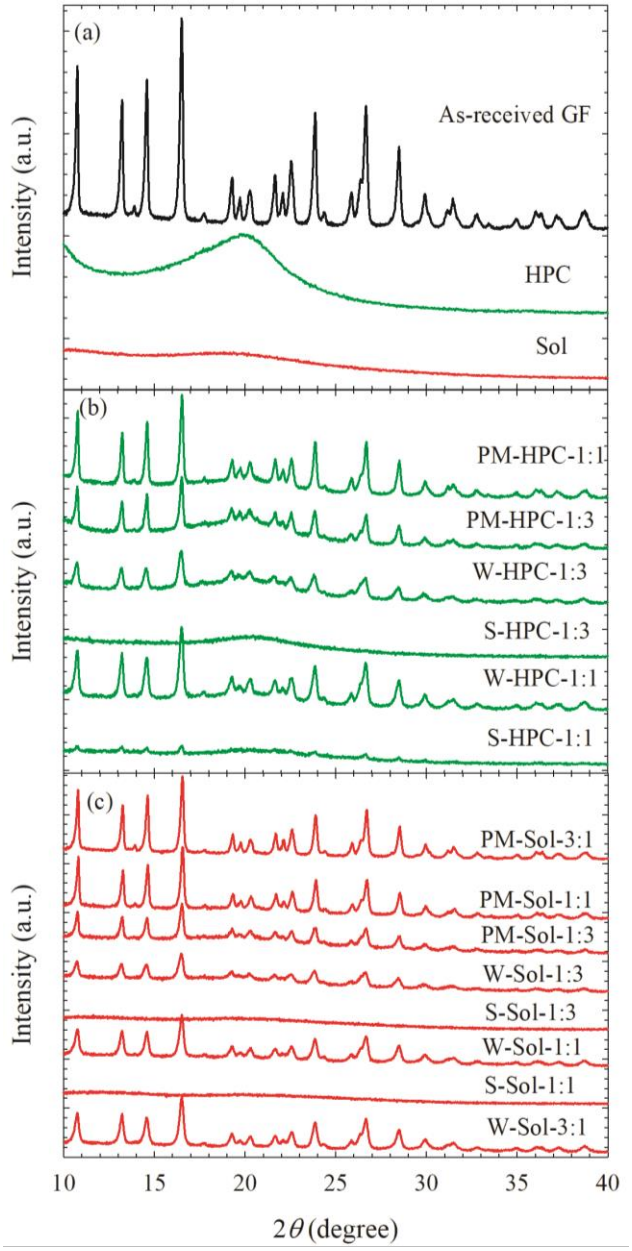

Figure 3.4 X-ray diffractograms of as-received GF, HPC, and Sol (a); physical mixtures (PMs) of GF–polymer–SDS and the spray-dried powders prepared using the GF nanosuspension-based (W) feed and GF solution-based (S) feed with various GF:polymer mass ratios: (b) HPC as the polymer and (c) Sol as the polymer.

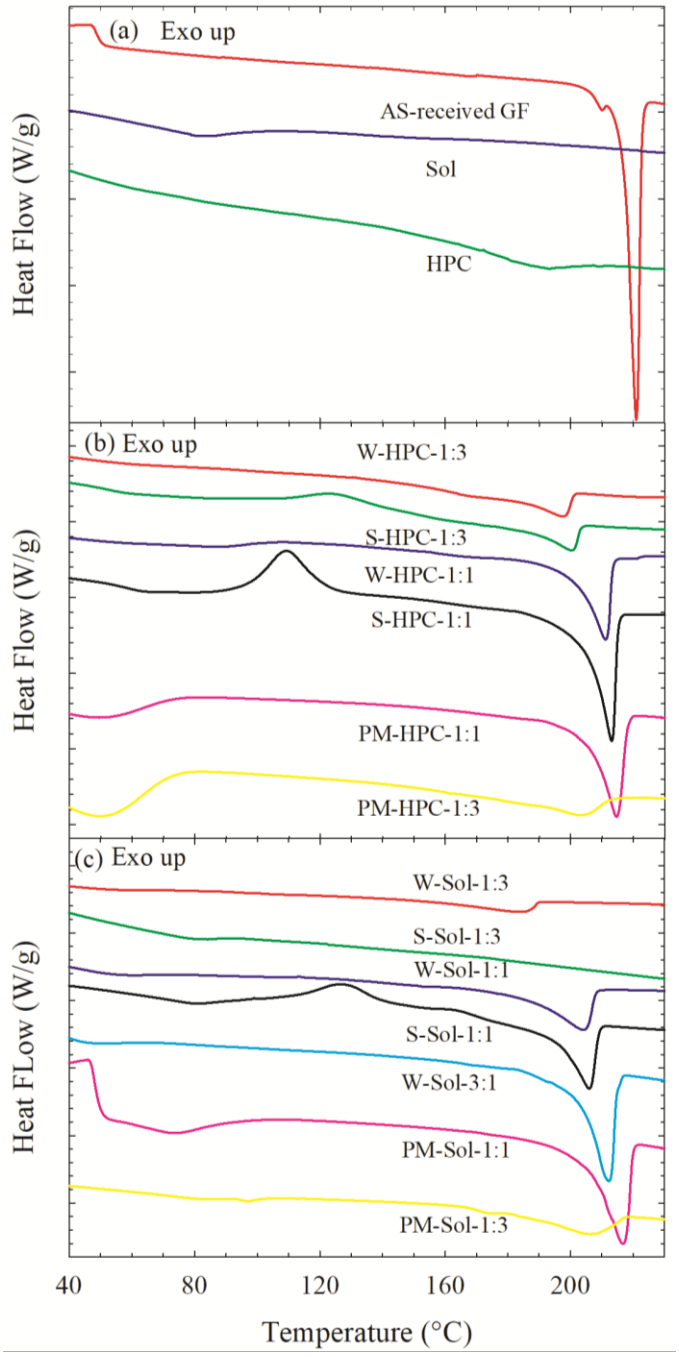

Figure 3.5 DSC thermograms of as-received GF, HPC, and Sol (a); physical mixtures (PMs) of GF–polymer–SDS and the spray-dried powders prepared using the GF nanosuspension-based (W) feed and GF solution-based (S) feed with various GF:polymer mass ratios: (b) HPC as the polymer and (c) Sol as the polymer.

Table 3.3 Characteristic Temperatures–Enthalpy Values Obtained From DSC Thermograms and Crystallinity Estimated From XRPD Diffractograms

Formulation[a]	T_g (°C)[a,b]	T_{rc} (°C)[a,b]	ΔH_{rc} (J/g)[a,b]	T_m (°C)[a,b]	ΔH_f (J/g)[a,b]	Crystallinity (%)[b]
S-HPC-1:1	58.9	109	–20.0	213	40.6	6.5
W-HPC-1:1	ND	ND	ND	211	28.7	95.5
S-HPC-1:3	57.7	124	–1.71	200	10.5	ND
W-HPC-1:3	ND	ND	ND	198	12.7	86.5
W-Sol-3:1	ND	ND	ND	212	47.0	92.1
S-Sol-1:1	74.6	127	–9.26	206	25.4	ND
W-Sol-1:1	ND	ND	ND	204	22.7	86.3
S-Sol-1:3	80.0	ND	ND	ND	ND	ND
W-Sol-1:3	ND	ND	ND	186	7.37	81.3

[a]S denotes solution-based feed, W denotes nanosuspension-based feed, Sol denotes Soluplus; the ratios refer to the drug:polymer mass ratios. All formulations have 0.125% w/v SDS. Other symbols: T_g, T_{rc}, and T_m stand for temperature for glass transition, recrystallization transition, and melting point, respectively, while ΔH_{rc} and ΔH_f respectively stand for recrystallization enthalpy and fusion enthalpy.
[b]ND: not detected.

Table 3.3 shows that despite being largely crystalline, the amorphous content in the spray-dried powders prepared *via* nanosuspension-based (W) feeds increased upon an increase in the polymer loading in the nanosuspensions. Moreover, higher amorphous content was observed in the Sol formulations than in the HPC formulations at the same drug:polymer mass ratio. These findings suggest that amorphous GF was formed due to GF–polymer molecular interactions and/or solubilization of the surface layer of nanoparticles by the polymer during the spray-drying. It is likely that presence of GF nanoparticles with large surface area could have facilitated the formation of amorphous content around the GF nanoparticles. In other words, the polymeric matrix of the spray-dried particles encapsulates drug nanocrystals, surrounded by a layer of amorphous GF ASD in the polymeric matrix (see Figure 3.6b). Formation of amorphous content upon drying of drug nanosuspensions was first observed by (Kayaert and Van den Mooter, 2012), albeit to

a much lower extent; however, the impact of such amorphous content on drug release from the nanocomposites has not been studied at all. As the dissolution tests will reveal below, despite being largely crystalline, these nanocomposites with high polymer loading (low drug:polymer ratio) allow for much higher supersaturation than traditional nanocomposites; hence, we refer to them as hybrid nanocrystal–ASD (HyNASD). The higher amorphous content in the Sol than in the HPC formulations could be related stronger molecular interactions of Sol with GF than HPC with GF and GF–Sol miscibility. It is suggested that if the solubility parameter difference between a drug and polymer is <7.0 $MPa^{1/2}$, they are likely to be miscible; if the difference is >10 $MPa^{1/2}$, they are considered immiscible (Forster et al., 2001; Greenhalgh et al., 1999). The solubility parameters of GF, HPC, and Sol are 12.2 (Thakral and Thakral, 2013), 24.0 (Choi et al., 1994), and 19.4 (Kolter et al., 2012) $MPa^{1/2}$, respectively. The solubility parameter differences between GF–Sol and GF–HPC are 7.2 and 11.8 $MPa^{1/2}$, respectively, which suggests that GF–Sol is borderline miscible (or at least partially miscible), whereas GF–HPC is most likely immiscible. While being useful, the solubility parameters do not account for all drug–polymer interactions such as contributions from hydrogen bonding, hydrophobic interactions, etc., and hence should be used with caution as rough estimates of drug–polymer miscibility.

XRPD diffractograms (Figure 3.4b and Figure 3.4c) of the spray-dried powders prepared using the solution-based (S) feeds showed halo pattern instead of any characteristic diffraction peaks of GF (except S-HPC-1:1). These halo patterns confirm that amorphous GF dispersed molecularly into the polymer matrix forming

amorphous solid dispersions (ASDs). Despite the immiscibility of HPC with GF, fast drying of acetone–water in 1:3 GF–HPC solution led to molecular dispersion and arrested amorphous GF in the HPC matrix kinetically. On the other hand, the peaks in the XRPD diffractogram of S-HPC-1:1 and 6.5% crystalline GF could be explained by the insufficient HPC concentration to ensure complete dispersion of GF molecules in the polymer matrix; hence, recrystallization of GF during spray-drying occurred.

The DSC thermograms in Figure 3.5a show an endothermic peak associated with melting of as-received GF, with a T_m of 220.1 °C and ΔH_f of 101.8 J/g; a glass transition for Sol (amorphous) at 72.4 °C, and a slight endothermic event around 170–200 °C for HPC likely due to the melting of the small crystalline domain of largely amorphous HPC (Sarode et al., 2013) (crystallinity was undetectable by XRPD). The T_g of HPC could not be measured (in the range of –25 to 0 °C (Sarode et al., 2013)) due to limitation of our equipment. For spray-dried powders prepared using solution-based (S) feeds, a single T_g was observed for all the formulations confirming the formation of molecular level dispersion (Luebbert et al., 2017; Wlodarski et al., 2015) (see Table 3.3 and ASD schematic in Figure 3.6c). While S-Sol-1:3 exhibited only a glass transition, all other ASDs exhibited a glass transition followed by an exothermic event due to re-crystallization of amorphous GF followed by the melting of the recrystallized GF (Figure 3.5b and 3.5c). The (absolute value) enthalpy of recrystallization was lower for Sol than for HPC formulations and was lower when a higher polymer loading was used (in line with other studies e.g., (Wlodarski et al., 2015)). Recrystallization occurred during the heating step of DSC scan because above T_g amorphous drug molecules and amorphous polymer had

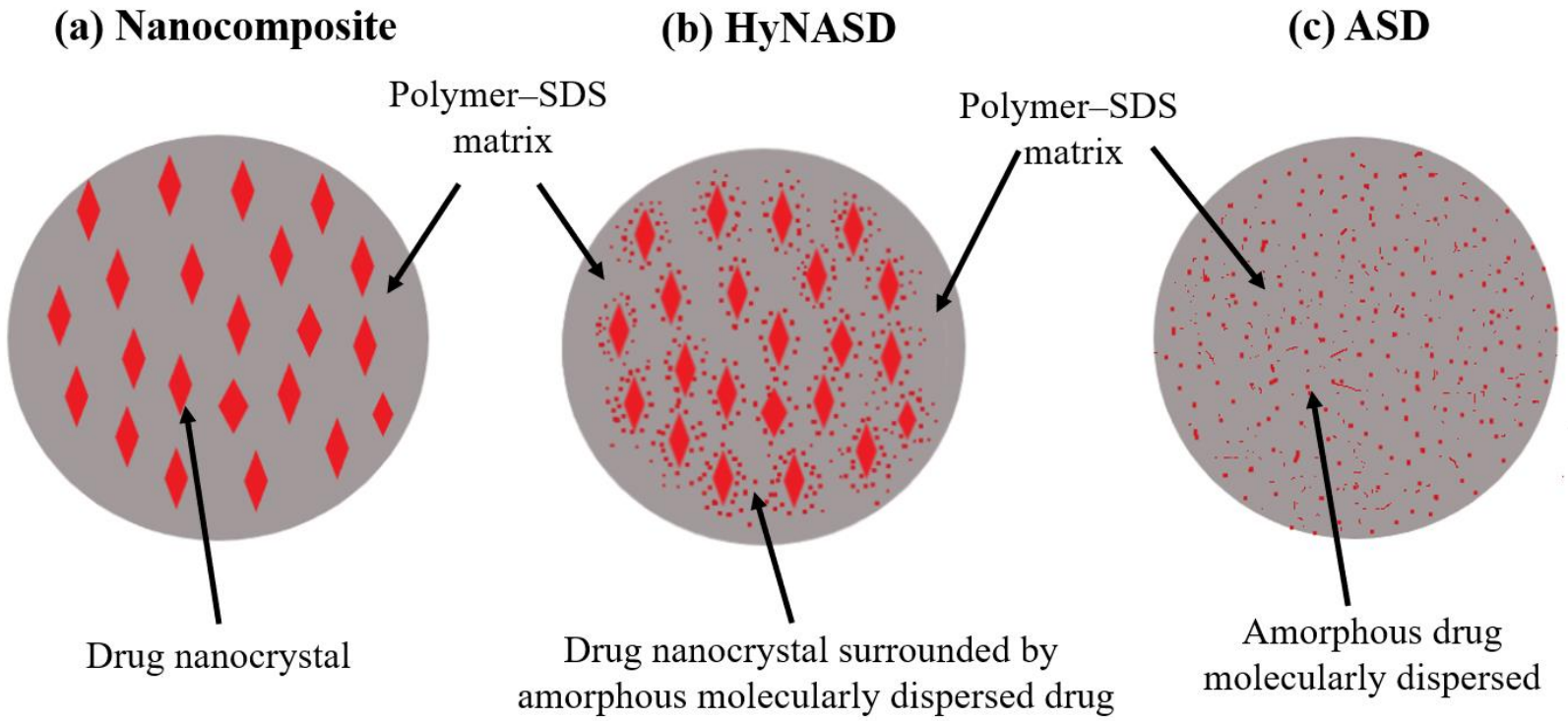

Figure 3.6 Schematic illustration of the solid state of the drug (GF) in (a) GF nanocomposite, (b) GF hybrid nanocrystal–amorphous solid dispersion (HyNASD), and (c) GF amorphous solid dispersion (ASD). Figure is not drawn to scale.

higher mobility, leading to GF recrystallization. Due to stronger molecular interactions and miscibility of Sol with GF, S-Sol-1:3 with high Sol loading was able to inhibit recrystallization even at high temperatures during the DSC scan.

The spray-dried powders prepared using the suspension-based (W) feeds, i.e., the nanocomposites including HyNASDs, exhibited a melting endotherm only (Figure 3.5b and 3.5c). The T_m and fusion enthalpy ΔH_f of these spray-dried powders were lower than those of the respective physical mixtures (Table 3.3). Moreover, higher polymer loading (1:3 *vs.* 1:1 W formulations) led to lower T_m and ΔH_f, similar to the lower peaks and crystallinity in XRPD. The observed reduction in T_m and ΔH_f of HyNASDs, as compared with the physical mixtures, may be partly attributed to defect formation and accumulation during milling. However, only a slight reduction in T_m and ΔH_f occurred upon wet media milling of GF without stabilizers (Monteiro et al., 2013). Hence, the reduction in T_m and ΔH_f was mostly attributed to amorphization of GF on the surface of the drug nanocrystals (Kayaert and Van den Mooter, 2012) or its solubilization in the polymer upon spray-drying as well as the solubilization during the DSC scan. Compared with the thermogram of as-received GF, the thermograms of the physical mixtures also show a significant reduction of T_m and ΔH_f, which can be explained by the solubilization of GF in molten polymer at high temperatures during the DSC scan. Finally, the lower T_m and ΔH_f of the W-Sol formulations than those for the W-HPC formulations could again be explained by the higher miscibility and stronger molecular interaction of Sol with GF than HPC with GF.

The observed Raman lines in Figure 3.7a for as-received GF and PMs of GF are largely in agreement with Fourier transform Raman data of ref. (Feng et al., 2008) and Raman data of ref. (Żarów et al., 2011) for crystalline GF. The Raman spectra of S-Sol-1:3 (Figure 3.7c) show that the GF line at 1606 cm^{-1} disappeared, and the lines at other characteristic frequencies shifted to new positions that are characteristic of amorphous GF, e.g., the line shift from 1712 to 1715 cm^{-1} (see Zarow et al. (Żarów et al., 2011)), signifying formation of amorphous GF and strong molecular interactions between GF and Sol in the ASD. While the GF line at 1606 cm^{-1} disappeared in the Raman spectra of S-HPC-1:3 (Figure 3.7b), the shifts in other lines were subtler than those for the Raman spectra of S-Sol-1:3, which could suggest stronger molecular interactions between GF and Sol than GF and HPC. While the W-Sol-1:3 and W-HPC-1:3 powders (HyNASDs) did not show disappearance of lines or line shifts, unlike S-Sol-1:3 and S-HPC-1:3 powders (ASDs), their spectra clearly show broadening of the characteristic GF lines and peak intensity reduction as compared with the spectra of the respective PMs due to GF–polymer interactions and presence of amorphous domains in these powders. In contrast, the spectra of W-Sol-3:1 (nanocomposite), having $1/9^{th}$ of Sol content compared with W-Sol-1:3, did not show as much line broadening compared to the spectra of its respective PM.

The XRPD, DSC, and Raman spectroscopy results overall suggest that spray-drying of GF–polymer solutions (S feeds) led to formation of ASDs, whereas spray-drying of GF–polymer nanosuspensions (W feeds) led to formation of drug nanocomposites/HyNASDs. Although a hard and crisp distinction between traditional nanocomposites and HyNASDs is not intended here, HyNASDs appear to have

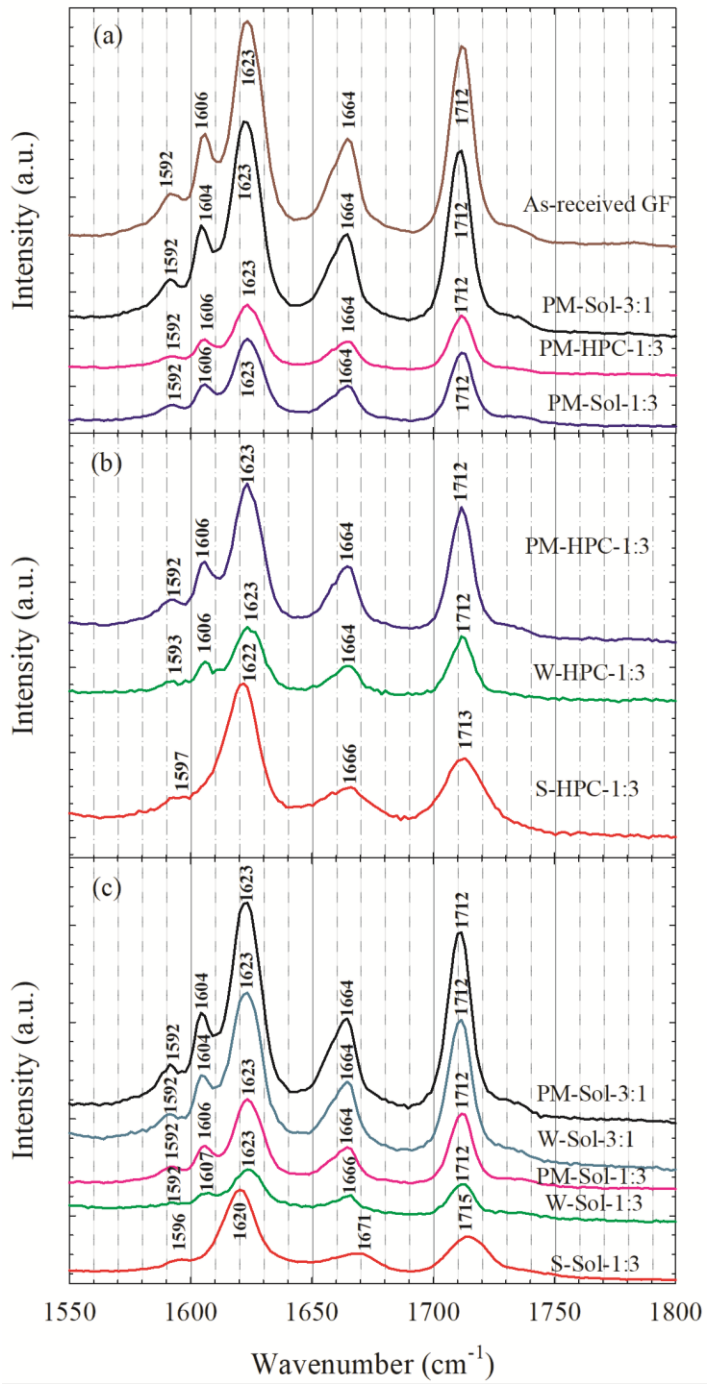

Figure 3.7 Raman spectra of as-received GF, physical mixtures (PMs) of GF–Sol–SDS at 3:1 and 1:3 GF:Sol mass ratios and GF–HPC–SDS at 1:3 GF:HPC mass ratio (a); physical mixtures of GF–polymer–SDS and the spray-dried powders prepared using the GF nanosuspension-based (W) feed and GF solution-based (S) feed with 1:3 GF:polymer mass ratio: (b) HPC as the polymer and (c) Sol as the polymer. W-Sol-3:1 stands for the spray-dried powder with 3:1 GF:Sol mass ratio.

notable amorphous content (>%10 in XRPD) and/or exhibit significant T_m depression–ΔH_f reduction and GF Raman peak broadening as compared with the respective physical mixtures. As a general observation, we note that spray-drying a drug nanosuspension with a lower drug:polymer mass ratio (1:1, 1:3) than typically used (see e.g., Table 1.2) and the use of a miscible polymer, i.e., Sol, that interacts with the drug nanoparticles strongly and potentially solubilizes them during the spray drying favor the formation of HyNASDs *vs.* nanocomposites (W-Sol-1:3 *vs.* W-Sol-3:1). Moreover, as will be shown in Section 3.3.5, nanocomposites and HyNASDs may behave quite differently in their functional responses such as drug release *in vitro*.

3.3.4 Impact of Drying Rate and Drug–Polymer Interactions/Miscibility

In the solution-based (S) feeds, GF, polymer, and SDS were completely dissolved in acetone–water mixture, which allowed molecular level interaction in the solution before spray drying. Due to fast evaporation of the solvents in the spray dryer, viscosity increases rapidly causing entrapment of the drug molecules in the polymer matrices, which appears to have retarded phase separation even in the case of GF–HPC (immiscible) and enables the ASD formation. In the nanosuspension-based (W) feeds, GF exists as nanocrystalline particles while polymer and SDS were dissolved in water. However, due to large surface area of GF nanocrystals and presence of relatively high polymer loading (1:1 and 1:3 GF:polymer), GF was partially solubilized or molecularly dispersed, especially in Sol, as the evaporation proceeds,

leading to formation of GF molecularly dispersed in the polymer matrix surrounding the GF nanocrystals (refer to Figure 3.6b).

To demonstrate the criticality of drying rate and drug–polymer interactions/miscibility, we have devised a slower drying method: a single droplet of GF–HPC–SDS solution on a heated glass slide at 75 ºC, same temperature as that of hot air in the spray-drying. However, the droplet was dried in quiescent air, which makes external mass transfer of solvent vapor in air controlling the evaporation rate, making drying slower compared to spray drying. The drying took less than 40 s, whereas the drying occurred less than ~5 s in the spray dryer. The PLM images in Figure 3.8 illustrate that GF crystals formed during the slow drying of all solutions. On the other hand, the drying of S-Sol-1:3 solution yielded few small crystals, whereas that of S-Sol-1:1 solution yielded significant number of needle-shaped crystals. The extent of recrystallization was much higher in HPC than in Sol. HPC could not inhibit the nucleation/crystal growth of GF from the supersaturated solution as evaporation proceeded during the spray-drying. Since only S-HPC-1:1 spray-dried powder had 6.5% crystalline GF and others solution-based (S) spray-dried samples did not have detectable GF crystals, it is concluded that the relatively fast evaporation during the spray drying enabled ASD formation.

It is known that the phase separation and recrystallization involve diffusion and nucleation of drug molecules, both of which require molecular mobility and can be restricted by polymer molecules as inhibitor (Baghel et al., 2016). Strong drug–polymer interactions can reduce the molecular mobility and delay crystallization onset time and the extent of crystallization (Mistry et al., 2015). This is in line with

earlier work, e.g., (Kothari et al., 2015), where the recrystallization time of nifedipine increased with an increase in polymer (PVP) concentration. To gain additional insights into the GF recrystallization inhibition capability of Sol/HPC in solutions, desupersaturation experiments were performed. The GF desupersaturation curves indicate the superior GF recrystallization inhibition and supersaturation maintenance capability of Sol over HPC, and even at 1:1 drug:Sol mass ratio, Sol is an effective inhibitor (Figure 3.9). Figure 3.9 also corroborates the fast recrystallization tendency of GF (Baird et al., 2010) and establishes negligible role of SDS alone on supersaturation maintenance. Again, these findings from the desupersaturation experiments can be explained by adequate GF–Sol miscibility based on solubility parameter differences and stronger GF–Sol molecular interactions than GF–HPC interactions, based on Raman spectroscopy (Figure 3.7).

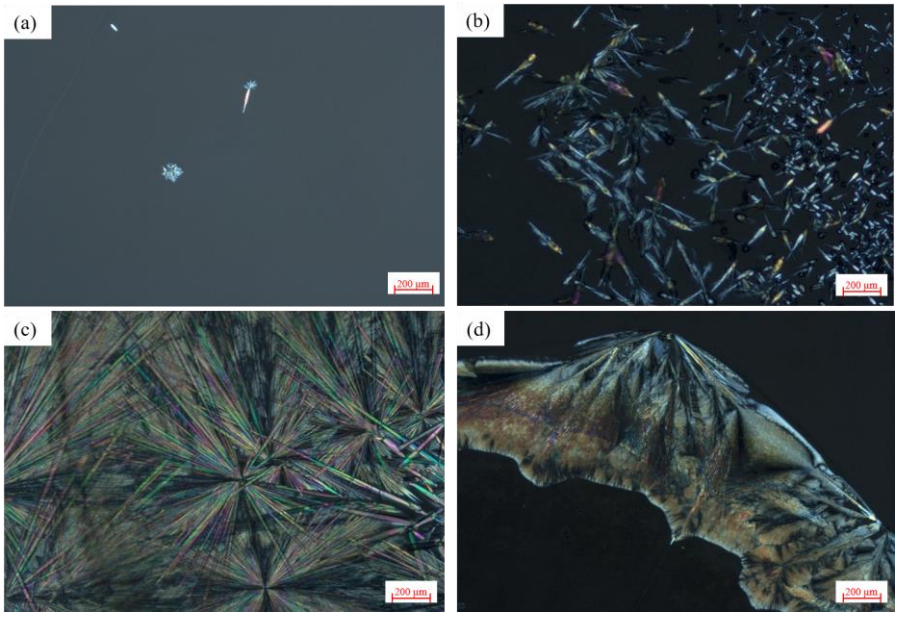

Figure 3.8 Polarized light microscope images of a droplet of GF solution-based (S) feed, i.e., (a) S-Sol-1:3, (b) S-Sol-1:1, (c) S-HPC-1:3, and (d) S-HPC-1:1, dried on a hot glass slide at 75 °C. All images were taken at 5X zoom (scale bar: 200 µm).

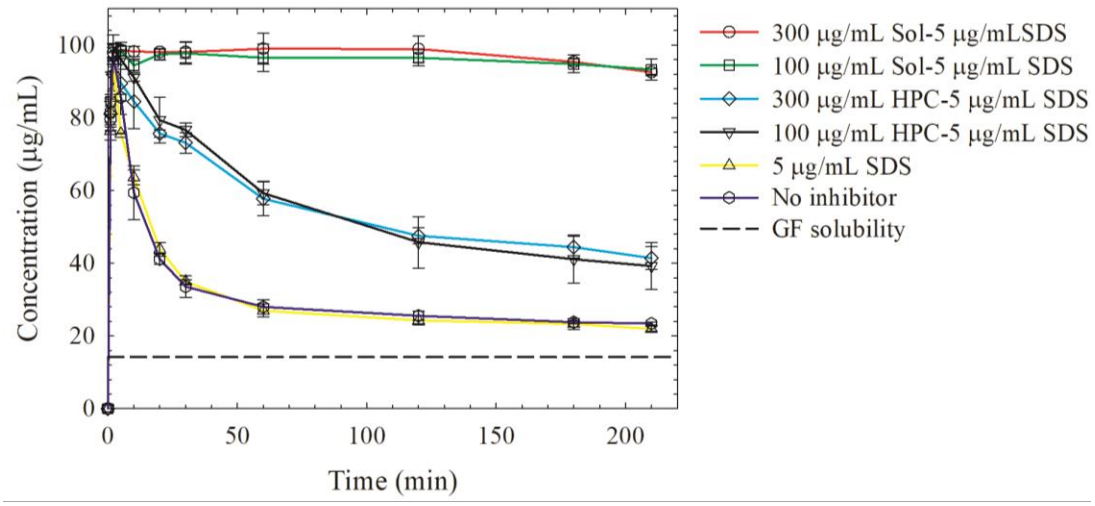

Figure 3.9 GF desupersaturation curves for a supersaturated 20 mL GF–acetone solution mixed with 1000 mL aqueous solution of 300 µg/mL and 100 µg/mL of HPC/Sol–5 µg/mL SDS (equivalent to S-formulations with 1:3 and 1:1 drug:polymer mass ratios, respectively), 5 µg/mL SDS only, and in the absence of any recrystallization inhibitor. The initial GF concentration right after mixing ranged from 92–99 µg/mL.

3.3.5 Dissolution Performance of the Spray-Dried Powders

The temporal evolution of GF release from the spray-dried powders and their corresponding PMs containing 100 mg equivalent GF dose in 1000 mL deionized water was investigated. We note from Figures 3.10 and 3.11 that the mere presence of HPC/Sol–SDS could slightly increase the extent and rate of GF release without any prior processing of the as-received micronized GF particles. This could be partly explained by the wetting enhancement of the hydrophobic drug (GF) in the presence of HPC/Sol–SDS and deaggregation of the large drug aggregates present in the as-received drug (Li et al., 2017) and partly by the higher solubility in the dissolution medium. The thermodynamic solubility of the GF microparticles at 37 °C was measured to be 14.2 mg/L, 17.8 mg/L, and 18.3 mg/L in the deionized water, aqueous

medium of Sol–SDS (1:3 drug:polymer ratio), and aqueous medium of HPC–SDS (1:3 drug:polymer ratio), respectively.

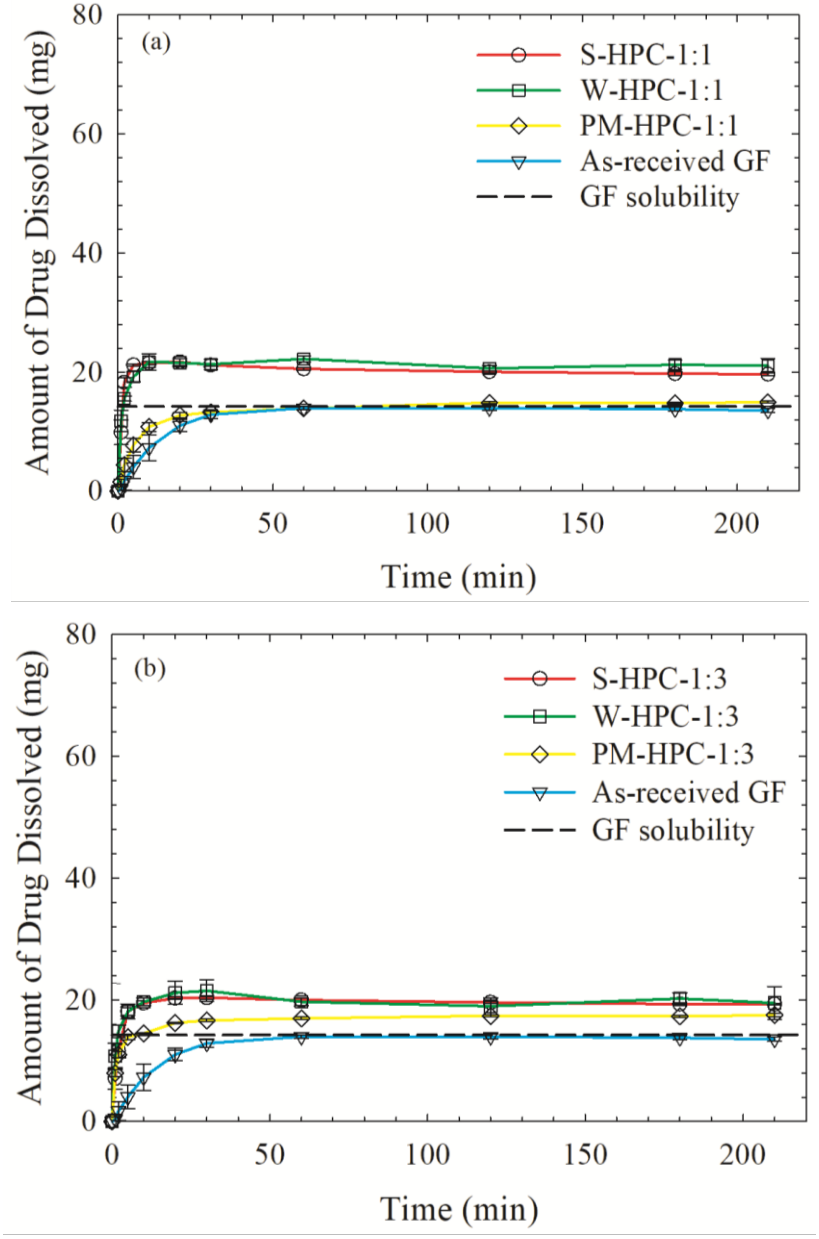

Figure 3.10 Evolution of drug release from as-received GF, physical mixture (PM) of GF–HPC–SDS, and spray-dried powders with two different GF:HPC mass ratios: (a) 1:1 GF:HPC and (b) 1:3 GF:HPC. Dissolution sample size is equivalent to 100 mg GF dose.

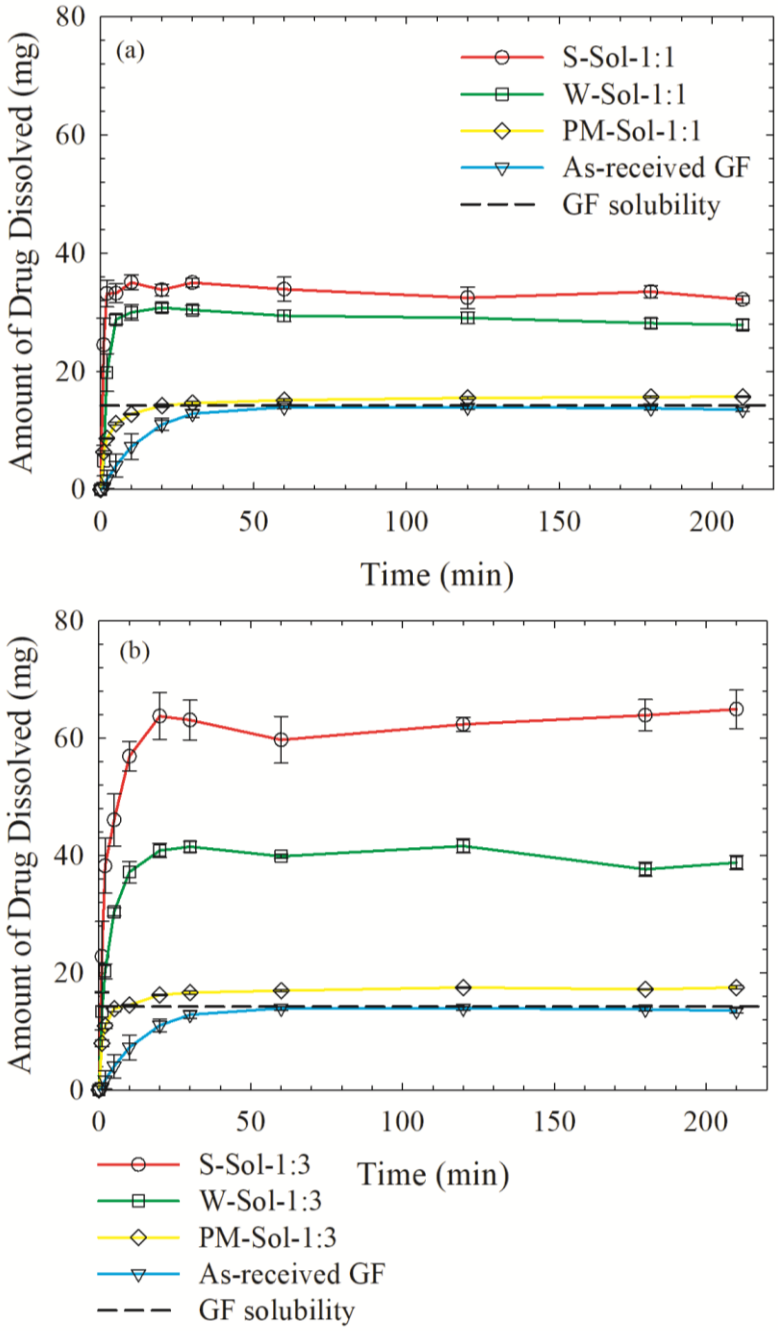

Figure 3.11 Evolution of drug release from as-received GF, physical mixture (PM) of GF–Sol–SDS, and spray-dried powders with two different GF:Sol mass ratios: (a) 1:1 GF:Sol and (b) 1:3 GF:Sol. Dissolution sample size is equivalent to 100 mg GF dose.

Figures 3.10 and 3.11 also show that both GF HyNASDs and ASDs prepared *via* spray-drying of the suspension-based (W) and solution-based (S) feeds,

respectively, enhanced the dissolution rate and the extent of GF release as compared to the as-received GF and the physical mixtures (PM). However, even a cursory look at the Figure 3.10 *vs.* Figure 3.11 reveals a drastic difference between HPC-based formulations and Sol-based formulations: the former provided an order of magnitude lower (relative) supersaturation than the latter, i.e., ~50% (for both HyNASDs and ASDs) *vs.* 360% (S-Sol-1:3, ASD) and 180% (W-Sol-1:3, HyNASD). Another interesting general observation is that there was little impact of polymer loading or drug:polymer ratio on the supersaturation for HPC-based formulations, whereas supersaturation significantly increased upon increase in polymer loading (lower drug:polymer ratio) for Sol-based formulations.

HPC-based HyNASDs and ASDs performed equally poorly in enhancing supersaturation (Figure 3.10), but for different reasons, as compared with Sol-based HyNASDs and ASDs (Figure 3.11). S-HPC-1:1 and S-HPC-1:3 powders are ASDs that have respectively 94% and 100% XRPD-amorphous GF, which has order of magnitude higher apparent (kinetic) solubility than its crystalline counterpart. Unfortunately, depending on the polymer–drug miscibility and interactions, amorphous drugs may phase-separate and recrystallize upon contact of ASDs with water in the dissolution medium (Alonzo et al., 2011; Chen et al., 2015) because once imbibed into the ASD matrix, water acts as a plasticizing agent, reducing the T_g of the ASD and enhancing the mobility of the drug molecules (Chen et al., 2015). HPC-SSL has sub-ambient T_g (Sarode et al., 2013) (lower than T_g of Sol: 73 ± 2 °C) and its ASDs have lower T_g than Sol-based ASDs (see Table 3.3). Moreover, due to HPC immiscibility with GF, its relatively weak molecular interactions with GF as

compared with Sol (miscible with GF), as well as its poor GF nucleation/crystal growth inhibition (refer to Figure 3.9), it is no surprise that the amorphous GF recrystallized from HPC-based ASDs during the dissolution test, which also explains the drastic differences between the HPC-based ASDs *vs.* Sol-based ASDs. PLM images of a loose compact of the ASD particles in Figure 3.12 also corroborate the formation of GF crystals from S-HPC-1:3 ASD upon its exposure to water, whereas no recrystallization was observed for S-Sol-1:3. The HPC-based HyNASDs also performed poorly. Although they released GF nanocrystals upon redispersion (see Appendix B), these GF nanocrystals have limited supersaturation capability. Moreover, the small amorphous content of the HyNASDs probably recrystallized in water similar to amorphous GF in HPC-based ASDs. While HPC has been used in both marketed drug nanocrystal products and in academia for preparation of drug nanosuspensions and drug nanocomposites (Bhakay et al., 2018b; Li et al., 2016b), we find here that it is not a suitable polymer for preventing GF recrystallization and achieving high GF supersaturation.

What is remarkable about the dissolution results in Figure 3.11 is neither the 360% supersaturation obtained with the S-Sol-1:3 ASD nor the higher Sol loading (1:3 *vs.* 1:1 GF:Sol ratio) achieving higher supersaturation. ASDs are well-known to generate significant supersaturation (Alonzo et al., 2011; Jackson et al., 2015) due to amorphous nature of the molecularly dispersed drug, and the polymer provides solubilization of the drug within the swollen GF–Sol matrix and recrystallization inhibition. Sol has a T_g of 73 ± 2 °C and strong molecular interactions with GF (GF Raman line shifts in Figure 3.7); it is miscible with GF and is an excellent GF

nucleation/crystal growth inhibitor, as evidenced by the small desupersaturation after ~3 h (Figure 3.9) and absence of crystals in the PLM image (Figure 3.12b). During the PLM imaging of S-Sol-1:3 (see Figure 3.12b), the compact with the Sol matrix got swollen after the addition of water while eroding slowly (not shown in the images). Even after 5 min of water imbibition, no recrystallization of the amorphous GF was observed, which supports how high supersaturation was reached in this ASD.

What we found surprising is that W-Sol-1:3 provides 180% GF supersaturation (Figure 3.11). It is well-known that drug nanocomposites have limited supersaturation capability, typically up to 10–15% (Kesisoglou and Wu, 2008), and supersaturation capability of nanocomposites has not even been studied in depth (Azad et al., 2015b; Bhakay et al., 2014a; Shah et al., 2016). Note that W-Sol-1:3 is not a traditional nanocomposite: while largely composed of drug nanocrystals, it has about 20% amorphous GF and in water it provided 180% supersaturation. In this paper, we refer to such nanocomposites as HyNASDs (Figure 3.6b) to differentiate them from nanocomposites (Figure 3.6a) and ASDs (Figure 3.6b). Another remarkable finding is that W-Sol-1:3 (HyNASD) generated more supersaturation than S-Sol-1:1 (ASD), i.e., 180% *vs.* 130%. Although this mainly resulted from the HyNASD having more Sol than the ASD and this comparison is not head-to-head, there is no similar result in literature where a formulation consisting of ~80% nanocrystals outperforms an ASD with 100% amorphous drug. Clearly, HyNASDs boost the supersaturating capabilities of traditional nanocomposites.

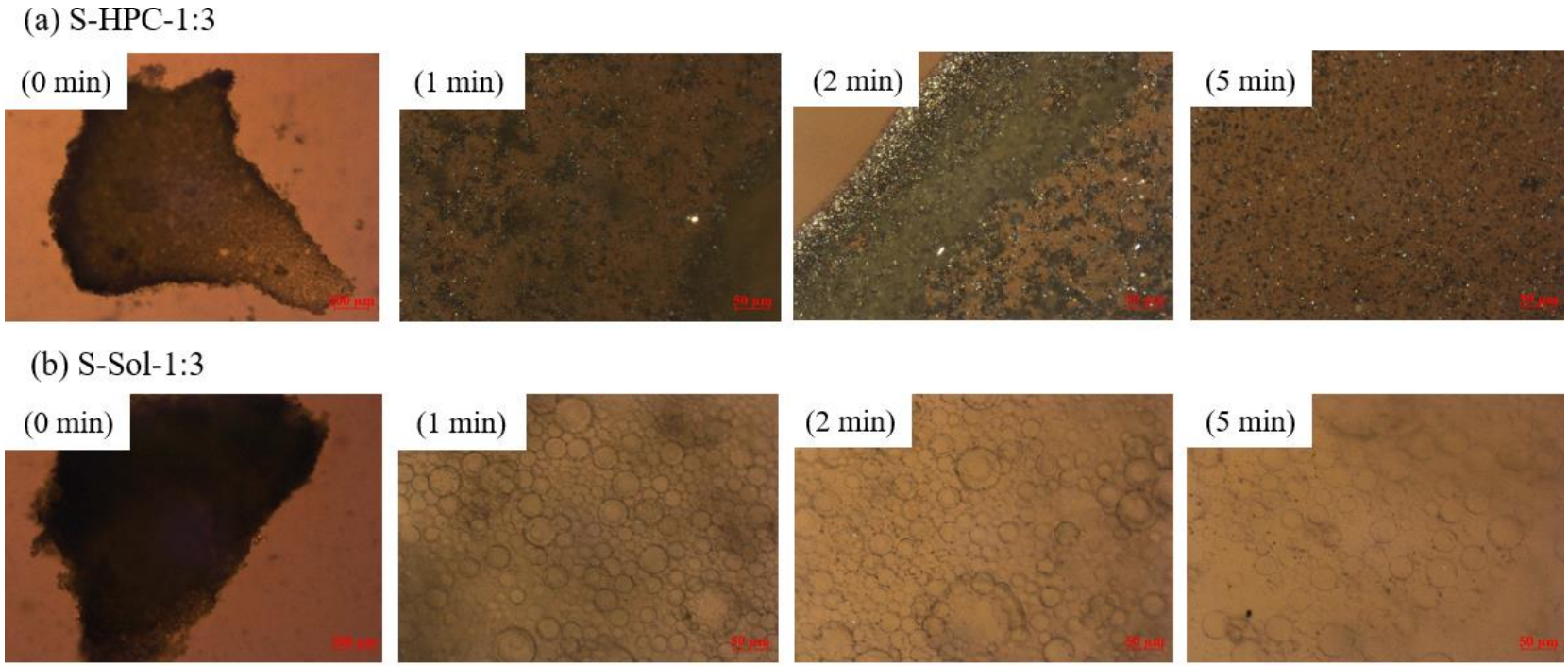

Figure 3.12 Polarized light microscope images of a loose compact of the ASD particles (S-formulations) with (a) 1:3 GF:HPC mass ratio and (b) 1:3 GF:Sol mass ratio in 20 µL deionized water. The images were taken at 0 (before adding water), 1, 2, and 5 min after the addition of deionized water addition. Except 0 min image (5X magnification, scale bar: 200 µm), which focused on the compact, all other images focused on particles that emanated from the surface, which were captured at 20X magnification (scale bar: 50 µm).

Additional dissolution experiments were carried out with various spray-dried powders prepared using suspension-based (W) feeds in order to elucidate the significant functional performance difference between traditional nanocomposites (e.g., W-Sol-3:1 with low Sol loading) and HyNASDs (W-Sol-1:1 and W-Sol-1:3 with high Sol loading) (see Figure 3.13). W-Sol-3:1, like any traditional nanocomposite, provided low (30%) supersaturation, whereas the two HyNASDs, i.e., W-Sol-1:1 and W-Sol-1:3, provided 100% and 180% supersaturation, respectively. There is a clear trend: an increase in Sol loading led to higher amorphous content and higher GF supersaturation/drug release. During dissolution of the HyNASDs, the amorphous GF dissolves and diffuses through swollen Sol matrix (Li et al., 2017), while additional GF could dissolve into the swollen Sol matrix and supersaturate upon water imbibition. It is also likely that higher Sol loading helps the solubilization in the dissolution medium. Not only did the higher Sol content lead to HyNASDs having higher amorphous content upon spray drying (see Table 3.3), but also the higher Sol loading enabled solubilization of additional GF within the swollen Sol matrix and/or in the dissolution medium. Both mechanisms contributed to the high supersaturation from HyNASDs. The contribution of amorphous GF and GF solubilization by Sol within the swollen Sol matrix to supersaturation follows the order: W-Sol-1:3 (180%) > W-Sol-1:1 (eq. 1:3) (130%) > W-Sol-1:1 (100%). Note that W-Sol-1:1 (eq. 1:3) has the same total Sol content as in W-Sol-1:3, but 2/3rd of Sol was pre-dissolved in the dissolution medium and it was not part of the W-Sol-1:1 matrix. Incorporating the whole Sol in the spray-dried matrix achieved higher supersaturation than keeping 1/3rd of Sol in the matrix and pre-dissolving 2/3rd in the

medium. Apparently, having all Sol in the spray-dried matrix allowed for more amorphous GF generated during the spray-drying, while also helping the solubilization of GF within the swollen Sol matrix. On the other hand, having additional Sol in the dissolution medium generated more supersaturation, as inferred from the dissolution of W-Sol-1:1 (eq. 1:3) *vs.* W-Sol-1:1.

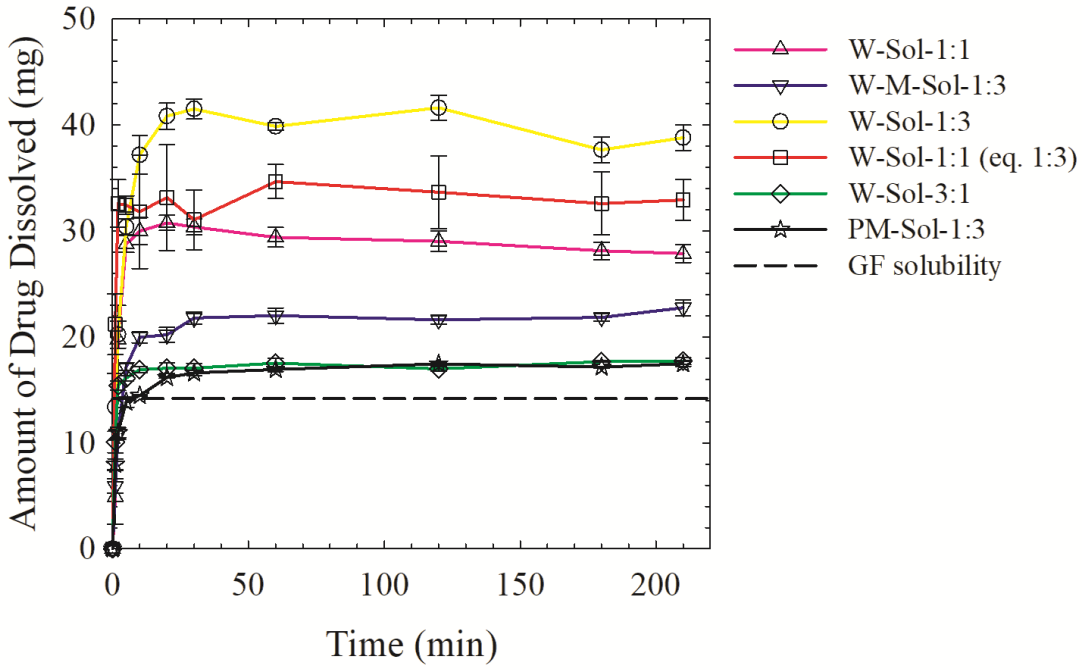

Figure 3.13 Evolution of GF dissolution from physical mixture (PM) of GF–Sol–SDS with 1:3 GF:Sol, spray-dried W-formulations with 1:1, 1:3, and 3:1 GF:Sol, as well as W-Sol-1:1 (eq. 1:3), which has the same total Sol content as in W-Sol-1:3, but 2/3rd of Sol was pre-dissolved in the dissolution medium and the remaining 1/3rd was in W-Sol-1:1 (eq. 1:3). W-M-Sol-1:3 stands for the spray-dried powder prepared using a suspension-based feed of as-received (micronized) GF. Dissolution sample size is equivalent to 100 mg GF dose.

It may be argued that the higher supersaturation in HyNASDs as compared with traditional nanocomposites is solely about GF–Sol interactions/miscibility and GF solubilization by Sol. W-M-Sol-1:3 was prepared by spray-drying the aqueous suspension of as-received (micronized, d_{50}: 9.74 µm) GF microcrystals with Sol–

SDS. W-Sol-1:3 (HyNASD), which contains drug nanocrystals with d_{50}: 0.14 µm and ~20% amorphous GF, generated thrice as much supersaturation as W-M-Sol-1:3, demonstrating the importance of crystal size in HyNASD for supersaturation generation. The solubilization of GF particles (microparticles or nanoparticles) in the Sol matrix and supersaturation generation during the dissolution is a kinetically-driven process, which is limited by the size of the particles: faster solubilization and higher supersaturation occurred when GF nanoparticles were encapsulated by the Sol matrix (HyNASD) as compared with the micronized GF particles owing to approximately 70-times larger surface area of the nanoparticles.

3.4 Conclusions

Spray-drying of an aqueous GF nanosuspension with 1:1 and 1:3 GF:Sol/HPC mass ratios in the presence of SDS led to formation HyNASDs, which have notable amorphous GF content unlike traditional drug nanocomposites that typically have 1:0.8 to 1:0.02 drug:polymer mass ratio. To ensure a fair, head-to-head comparison of HyNASDs to ASDs, ASDs with identical composition were prepared by spray-drying the organic solution of GF–Sol/HPC–SDS in acetone–water mixture. All spray-dried powders had acceptable content uniformity. XRPD–DSC–Raman spectroscopy shed light on the nanocomposite/HyNASD and ASD formation. HPC-based HyNASDs and ASDs performed equally poorly in enhancing GF supersaturation (50%) in dissolution tests, whereas Sol-based ones achieved significant supersaturation: up to 360% for ASD and 180% for HyNASD. These results were explained by higher T_g of Sol than that of HPC, GF–Sol miscibility, stronger molecular interactions between

Sol–GF than HPC–GF, and excellent nucleation/crystal growth inhibition by Sol as compared to HPC. The supersaturation generation capability of HyNASDs is largely controlled by drug–polymer interactions/miscibility as well as the size of the drug (nano)crystals in the polymeric matrix. Overall, the most striking finding from this study is that despite having ~80% nanocrystals, HyNASDs provided fast drug supersaturation (~190% within 20 min) unlike traditional nanocomposites (30%), which could render nanoparticle formulations more attractive in bioavailability enhancement of poorly soluble drugs. While HyNASDs did not generate as high saturation as ASDs, they can be rendered competitive to ASDs upon further formulation–process optimization. Future research efforts will include (i) investigation of the storage stability of HyNASDs *vs.* ASDs under various environmental conditions, (ii) preparation of HyNASDs with various drug–polymer pairs and their comparative assessment, (iii) systematic examination of the impact of various surfactants, and (iv) impact of various drug nanoparticle sizes in the range of 50–1000 nm on drug supersaturation.

CHAPTER 4

DRUG RELEASE FROM SPRAY-DRIED HYBRID NANOCRYSTALS–AMORPHOUS SOLID DISPERSIONS (HyNASDs): IMPACT OF SDS

As discussed in Chapter 1, limited supersaturation generation capability is a major limitation of the drug nanocomposites compared to the ASD formulations. To address this limitation, a new class of drug nanocomposites called HyNASDs has been introduced in Chapter 3, which provided significant supersaturation generation in the dissolution medium. In Chapter 4, we prepared hybrid nanocrystal–amorphous solution dispersions (HyNASDs) in order to boost the drug release performance of traditional nanocomposites while elucidating the impact of a common anionic surfactant, sodium dodecyl sulfate (SDS), on drug release in dissolution tests. To this end, 2.5% wet-milled griseofulvin (GF, BCS Class II drug) suspensions containing 1:1, 1:3, and 1:5 GF:polymer mass ratios, with 0.125% SDS (below CMC) and without SDS, were spray-dried. Hydroxypropyl cellulose (HPC) and Soluplus (Sol) were used as suspension stabilizers and matrix-forming polymers. Examination of particle sizes in the milled suspensions revealed the criticality of SDS in the synergistic stabilization of GF nanoparticles. XRPD and DSC results suggest that nanocomposites and nanocomposites with notable amorphous GF (>10%), HyNASDs, were formed upon spray-drying. Redispersion of the spray-dried powders revealed the criticality of SDS in nanoparticle recovery from the nanocomposites/HyNASDs, which could be explained by GF wettability enhancement by SDS, as inferred from the modified Washburn experiment. Results from *in vitro* dissolution tests with low (9 mg) GF dose suggest that enhanced

wettability with SDS and smaller spray-dried particle sizes led to faster GF release. For 100 mg GF dose (above thermodynamic solubility), Sol provided higher GF relative supersaturation, e.g., 250% for the HyNASDs (1:5 GF:Sol with SDS) *vs.* 30% for the nanocomposites (3:1 GF:Sol with SDS), than HPC (up to 50%) owing to Sol's stronger intermolecular interactions–miscibility with GF and its kinetic solubilization–recrystallization inhibition of GF. Higher polymer loading led to higher supersaturation. SDS provided Sol-based HyNASDs with enhanced wettability and augmented Sol in solubilizing SDS, leading to fast supersaturation (max. 300% within 20 min). This study demonstrates how drug release from traditional nanocomposites could be boosted upon incorporating a drug-miscible, solubilizing polymer with a low GF:polymer mass ratio and an anionic surfactant.

4.1 Materials and Methods

4.1.1 Materials

BP/EP grade, micronized griseofulvin (GF) purchased from Letco Medical (Decatur, AL, USA) was used as a challenging Biopharmaceutics Classification System (BCS) Class II drug because GF nanocrystals exhibit severe aggregation in suspensions, if improperly stabilized (Bilgili and Afolabi, 2012), and it is known to be a fast crystallizing drug (Baird et al., 2010). Its solubility is ~8.9 mg/L at 25 °C and ~14.2 mg/L at 37 °C, melting point T_m 220 °C, and a glass transition temperature T_g of 89 °C (Baird et al., 2010). Hydroxypropyl cellulose (HPC, SSL grade, Nisso America Inc., New York, NY) is a semi-crystalline polymer with low crystallinity and amorphous domains of very low T_g. It is widely used as a stabilizer during milling

and matrix former in the nanocomposites (Azad et al., 2015b; Bhakay et al., 2014a). Soluplus® (Sol) is an amphiphilic graft copolymer produced from polyvinyl caprolactam–polyvinyl acetate–polyethylene glycol having a single glass transition temperature of 73 ± 2 °C (Terife et al., 2012). Even 15% w/v aqueous solutions of both polymers have less than 60 cP viscosity at 25 °C, which allowed us to perform milling and spray drying without any processing issue. Sodium dodecyl sulfate (SDS), an anionic surfactant with a CMC of 8.0 mM at ambient temperature, purchased from GFS Chemicals, Inc. (Columbus, OH) was used as a wetting agent, which also helps to stabilize GF nanosuspensions. Wear resistant yttrium zirconia beads (Zirmil Y, Saint Gobain ZirPro, Mountainside, NJ, USA) with a median size of 430 µm was used as the milling media.

4.1.2 Milling and Spray Drying of Drug Suspensions

Aqueous suspension-based (W:water) feeds of GF prepared by wet milling were fed to the spray dryer for the preparation of drug nanocomposites. Table 4.1 presents the formulations used in the precursor feeds. The concentration of GF and SDS was kept at 2.5% w/v and 0.125% w/v, respectively, in all suspensions. The concentration was calculated with respect to the 240 mL suspension liquid (deionized water). GF suspensions were prepared with two polymers (HPC and Sol) with three drug:polymer mass ratios of 1:1, 1:3, and 1:5 to examine the impact of polymer type and polymer loading on GF release in the dissolution tests. To prepare a traditional nanocomposite, a GF nanosuspension with 3:1 GF:Sol (W-Sol-3:1, SDS) was also prepared. Finally, to investigate the impact of SDS in the stabilization of the milled GF suspensions and GF release during dissolution tests, surfactant-free suspensions

having the same drug:polymer mass ratios were also prepared for comparative analysis.

Table 4.1 Formulations and Compositions of the Aqueous (W) Suspension-Based Feeds Used in Spray Drying Experiments

ID	Formulation[a]	GF (% w/v)[b]	Polymers (% w/v)[b]	SDS (% w/v)[b]	Water (mL)
W1	W-Sol-1:5	2.5	12.5	0	240
W2	W-Sol-1:3	2.5	7.5	0	240
W3	W-Sol-1:1	2.5	2.5	0	240
W4	W-Sol-1:5, SDS	2.5	12.5	0.125	240
W5	W-Sol-1:3, SDS	2.5	7.5	0.125	240
W6	W-Sol-1:1, SDS	2.5	2.5	0.125	240
W7	W-HPC-1:5	2.5	12.5	0	240
W8	W-HPC-1:3	2.5	7.5	0	240
W9	W-HPC-1:1	2.5	2.5	0	240
W10	W-HPC-1:5, SDS	2.5	12.5	0.125	240
W11	W-HPC-1:3, SDS	2.5	7.5	0.125	240
W12	W-HPC-1:1, SDS	2.5	2.5	0.125	240
W13	W-Sol-3:1, SDS	2.5	0.8	0.125	240

[a]W denotes suspension-based feed; Sol denotes Soluplus; the ratios refer to the drug:polymer mass ratios.
[b]% w/v with respect to the volume (240 mL) of the deionized water.

In each milling experiment, a shear mixer (Fisher Scientific Laboratory Stirrer, Catalog No. 14-503, Pittsburgh, PA) was used to disperse as-received GF particles in aqueous stabilizer (HPC/Sol) solutions with and w/o SDS. The resultant GF pre-suspensions were transferred to the holding tank of a Microcer wet stirred media mill (WSMM) (Netzsch Fine Particle Technology, LLC, Exton, PA, USA) having 80 mL chamber. Milling conditions were adapted from our prior work on wet media milling (Afolabi et al., 2014; Bilgili et al., 2016). 50 mL of the milling chamber was filled with zirconia beads, and a screen with 200 μm opening was used in the outlet of the chamber to hold the beads in the chamber. A peristaltic pump was used to recirculate the suspension through the chamber at a rate of 126 mL/min and

the suspension was milled for 64 min at a rotor speed of 3200 rpm. A chiller (Advantage Engineering Greenwood, IN, USA) was used to maintain the milling chamber temperature below 35 °C throughout the milling. A portion of each suspension was separated in a vial and stored for 7 days at 8 °C to assess the short-term physical stability. Also, the milled suspensions were refrigerated at 8 °C overnight before spray drying.

Milled GF suspensions were dried using a spray dryer (4M8-Trix, Procept, Zelzate, Belgium) having a co-current flow set-up. The total length and the diameter of the spray dryer are 1.59 and 0.15 m, respectively. To ensure complete drying, inlet temperature was selected above the boiling temperature of the water. Drying air at 120 °C were fed at 0.37–0.40 m^3/min at the top of the dryer column to dry the milled GF nanosuspensions, while 200 g milled suspension of each formulation was fed at 2.0 g/min rate using a peristaltic pump (Make-it-EZ, Creates, Zelzate, Belgium) and atomized by a bi-fluidic nozzle at the top of the column concurrently to air flow. A cyclone separator was used to separate the dried particles from the outlet stream into a glass jar. The residence time was calculated to be ~4.0 s for the feeds. Atomizing air pressure of 2.0 bar, a bi-fluidic nozzle with tip diameter of 0.6 mm, and cyclone pressure of 55–60 mbar were selected based on prior experience (Azad et al., 2015b) and exploratory experiments. The dried particles obtained from the collection jar were transferred into double plastic bag and stored into a vacuum-desiccator at room temperature for further characterizations.

4.2 Characterization Techniques

4.2.1 Particle Size Measurement

Drug particle size distributions (PSDs) in the suspensions were measured using a laser diffraction (LS 13 320, Beckman Coulter, Miami, FL) based on Mie scattering theory following the procedure described in Bilgili et al. (2016). Particle sizes were measured at various time points: right after milling, after 1-day and 7-day storage at 8 °C to in a refrigerator. During the measurement, the intensity was maintained 40–50% while the obscuration was maintained below 8.0%. Refractive index values are 1.65 for GF (drug) and 1.33 for deionized water (medium). For each measurement, a 2.0 mL suspension sample was diluted with 5.0 mL of the respective stabilizer solution and mixed using a vortex mixer (Fisher Scientific Digital Vortex Mixer, Model No: 945415, Pittsburgh, PA) at 1500 rpm for 1 min.

The particle sizes of the spray-dried powders were measured by a Rodos/Helos laser diffraction system (Sympatec, NJ, USA) based on Fraunhofer theory following the procedure described in Li et al. (2016b). About 1 g of the powder sample was placed on top of the sample chute of the Rodos dispersing system and the sample chute was vibrated at a 100% setting, and 0.1 bar dispersion pressure was used to suck in the falling powder through the sample cell of the laser diffraction system. For further confirmation of the particle sizes, spray-dried particles were placed on a glass slide and observed by Axio Scope.A1 polarized light microscope (PLM, Carl Zeiss Microscopy GmbH, Göttingen, Germany).

4.2.2 Solid State Characterization and Drug–Polymer Interactions

To analyze the crystallinity of the as-received GF, HPC, Sol, spray-dried powders, and physical mixtures of GF–polymer with or w/o SDS, X-ray powder diffraction (XRPD) (PANanalytical, Westborough, MA, USA), provided with Cu K_α radiation (λ= 1.5406 Å) was used. The samples were scanned at a rate of 0.165 s^{-1} for 2θ ranging from 5° to 40°. The total area under three distinct, non-overlapping peaks of GF at characteristic diffraction angles of 13.2, 14.6, and 16.5º was calculated for both the physical mixtures and the spray-dried powders using the equipment's HighScore Plus software, which was then used to estimate the crystallinity.

Differential scanning calorimetry (DSC) of the as-received GF, Sol, HPC, and spray-dried powders was performed using a Mettler-Toledo polymer analyzer (PolyDSC, Columbus, OH, USA) with integrated STARe 10 software. ~6.0–7.0 mg powder sample was placed in an aluminum pan with a hole in the lid and loaded into the DSC machine. As-received GF was heated at a rate of 10 °C/min from 25 °C to 250 °C. All other samples were heated from 25 °C to 70 °C and the temperature was held for 2 min at 70 °C, then cooled back to 25 °C to remove any residual solvent in the sample. In the final step, the samples were heated from 25 °C to 250 °C at 10 °C/min. Nitrogen gas was used as the purge gas and protective gas at a flow rate of 50 mL/min and 150 mL/min, respectively. Thermogravimetric analysis (TGA) was performed to measure the residual water/solvent content using a TGA/DSC1/SF Stare system (Mettler Toledo, Inc., Columbus, OH). ~6.0–7.0 mg of each spray-dried sample was placed in a ceramic crucible and heated from 25 °C to 150 °C at a heating rate of 10 °C/min under nitrogen flow.

Raman spectroscopy was conducted using a Fergie Imaging Spectrometer System (Princeton Instruments, Trenton, NJ) with a 500-mW external diode laser processing at 785 nm wavelength. Data acquisition time for all spectra was 15 s per scanned spectrum (100–1800 cm^{-1}) and each spectrum acquired was averaged over two scans. The data was presented for the range of 1550–1800 cm^{-1} wavenumber.

4.2.3 Nanoparticle Recovery From the Nanocomposites

Aqueous redispersion of the spray-dried powders was performed following the method in refs. (Bhakay et al., 2014a; Li et al., 2016b). About 0.5 g of the spray-dried powders produced from nanosuspension-based (W) feeds was dispersed in 30 mL of deionized water inside a 60 mL beaker and stirred at 500 rpm for 60 min with a paddle-stirrer (CAT R18, Scientific Instrument Center Limited, Winchester, UK). ~1.0 mL aliquot of redispersed sample was collected at 2, 10 and 60 min while stirring, and particle size was measured using laser diffraction (LS 13 320, Beckman Coulter, Miami, FL). At the same time, a droplet of each redispersed sample was dried immediately by dropping on a preheated glass slide at 100 °C using a hot plate. After drying, the polarized light microscope (PLM) was used to capture the images of the redispersed particles. The details of the experimental methods and PLM images are presented in Section C.2 of the Appendix C.

4.2.4 Drug Content in the Spray-Dried Powders and *In Vitro* Dissolution Tests

The drug content in the dried powders varied based on the drug:polymer mass ratios. To measure the actual drug content, an assay testing was performed by dissolving 100 mg of the sample powders in 20 mL methanol under 30 min of sonication, followed by overnight storage to ensure complete solubilization of the GF particles. An aliquot

of 100 µL was taken from the GF solution and diluted up to 10 mL using methanol. The absorbance of the samples was measured at 292 nm using UV spectrophotometer (Agilent, Santa Clara, CA, USA), and the drug concentration was calculated from a pre-established calibration curve. Six replicates were tested for each formulation to calculate the mean drug content along with the relative standard deviation (RSD).

Drug release from the spray-dried powders and physical mixtures (PMs) prepared by blending was determined *via* a Distek 2100C dissolution tester (North Brunswick, NJ, USA), following the USP II paddle method. 1000 mL deionized water at 37 °C was selected as the dissolution medium and stirred at 50 rpm paddle speed. Considering the thermodynamic aqueous solubility of GF, i.e., 14.2 mg/L at 37 °C, a typical low (8.9 mg) dose and high dose (100 mg) of GF would allow for non-supersaturating and supersaturating dissolution conditions. Although the low dose may not arouse as much interest as the high dose, a low dose like 8.9 mg may emulate potent poorly soluble drugs. The spray-dried powders were poured into the dissolution medium and 4 mL samples were taken out manually at 1, 2, 5, 10, 20, 30, and 60 min. These aliquots were filtered with a 0.1 µm PVDF membrane-type syringe filter before UV-spectroscopy measurements to minimize any confounding effect of the undissolved coarse drug aggregates (Bhakay et al., 2014a; Li et al., 2016b). In separate dissolution tests, 100 mg equivalent GF was used to allow for supersaturation in the bulk dissolution medium, which was conducted with additional sampling at 120, 180, and 210 min. The filtered samples were diluted with deionized water kept at 37 °C at a ratio of 1 to 5 before UV measurement. Dissolved GF amount was measured by UV-vis spectroscopy at 296 nm wavelength and calculated

using a pre-established calibration curve. Deionized water was used as blank before UV measurement, and six replicates were performed for each sample. In this paper, relative % supersaturation is reported based on GF concentration at 210 min and thermodynamic solubility of as-received GF particles, unless otherwise indicated.

4.2.5 Drug Wettability Enhancement by Sol and HPC Solutions With or W/O SDS

GF wettability was investigated by analyzing the penetration rate of stabilizer solutions into a packed bed of GF particles inside a cylindrical column according to the Washburn method (Hołownia et al., 2008; Washburn, 1921). Attension Sigma 700 (Biolin Scientific, Linthicum, MD, USA) set-up was used to measure the mass of the liquid penetrated the GF powder bed as a function of time. Experimental methods were adapted from Bilgili et al. (2018) and Li et al. (2017) and the details can be found in Section C.1 of the Appendix C. In the current study, liquids and powder refer to GF-saturated aqueous solutions of 15% Sol/HPC with 0.125% SDS or w/o SDS and as-received GF, respectively. All percentages are (% w/w) with respective to deionized water. The aqueous solution of the stabilizers and deionized water were saturated with griseofulvin (GF) and stirred overnight. After overnight stirring, the saturated solutions were used for further characterization. The apparent shear viscosity and surface tension of the liquids were measured using R/S Plus Rheometer (Brookfield Engineering, Middleboro, MA, USA) and Attension Sigma 700 (Biolin Scientific, Linthicum, MD, USA), respectively. The ratio of the cosine of contact angles $\cos\theta_{ss}/\cos\theta_{w}$ was calculated using the modified Washburn equation and used as a wetting effectiveness factor. Here, θ_{ss} is the contact angle between GF and the stabilizer solutions and θ_{w} is the contact angle between GF and deionized water. The

ratio was used as a rough measure of the drug wettability enhancement upon use of different stabilizers (HPC/Sol and HPC/Sol–SDS) in water with respect to the GF–water wettability.

4.2.6 Drug Supersaturation Maintenance Ability of the Polymers

Drug (GF) supersaturation maintenance ability of HPC/Sol with and w/o SDS was examined in separate desupersaturation tests (similar to Konno et al. (2008)). A concentrated solution of GF was prepared by dissolving 100 mg of as-received GF into 20 mL of acetone *via* sonication for 40 min. This solution was subsequently added to a 1000 mL of pre-dissolved HPC/Sol solution having 100 and 300 µg/mL concentrations to maintain 1:1 and 1:3 drug:polymer ratios (similar to the formulations in Table 4.1), respectively, with or w/o SDS in the USP II paddle type dissolution tester. The addition resulted in 92–99 µg/mL supersaturated solution of GF initially (target: 100 µg/mL, corresponding to complete dissolution of 100 mg drug during dissolution testing). Any subsequent desupersaturation during the following 210 min was tracked *via* GF concentration measurements. The experimental conditions and concentration measurements were identical to those in the dissolution test. All measurements were carried out in triplicate.

4.3 Results and Discussion

4.3.1 Properties of GF Suspensions Prepared *via* Wet Stirred Media Milling

Twelve GF suspensions with HPC/Sol at 1:1, 1:3, and 1:5 drug:polymer mass ratios and 0.125% SDS and without SDS were wet media milled. Figure. 4.1 presents the characteristic particle sizes of the 64 min milled suspensions and the suspensions after

1-day and 7-day storage. As-received GF (unmilled) particles had d_{50}: 9.74 ± 0.23 µm and d_{90}: 27.4 ± 0.1 µm. After milling for 64 min, median particle sizes d_{50} were in the range of 0.146–0.155 µm for W4–W6 (Sol–SDS) and 0.166–0.184 µm for W10–W12 (HPC–SDS) formulations. Unless properly stabilized, GF nanoparticles are known to form micron-sized aggregates in aqueous suspensions (Bilgili and Afolabi, 2012). Figure 4.1 suggests that only with SDS, GF nanosuspensions with median sizes d_{50} less than 200 nm were formed, and the small changes in their d_{50} and d_{90} during the 7-day storage suggest that these suspensions were physically stable. With SDS, Sol-based suspensions were insensitive to Sol loading, whereas finer aggregates were formed with lower GF:HPC mass ratio (higher polymer loading). On the other hand, without SDS, Sol-based suspensions with 1:1 and 1:3 GF:Sol exhibited severe nanoparticle aggregation with a 4 µm median size, whereas submicron median sizes were observed for HPC-based suspensions. These suspensions also exhibited notable size increase upon 7-day storage. An increase in polymer concentration led to finer aggregates.

Due to their relatively neutral charge, stabilizing capability of Sol/HPC solely depends on their steric effects, which in turn is modulated by their adsorption onto GF nanoparticle surfaces. The adsorption is dependent on free polymer concentration

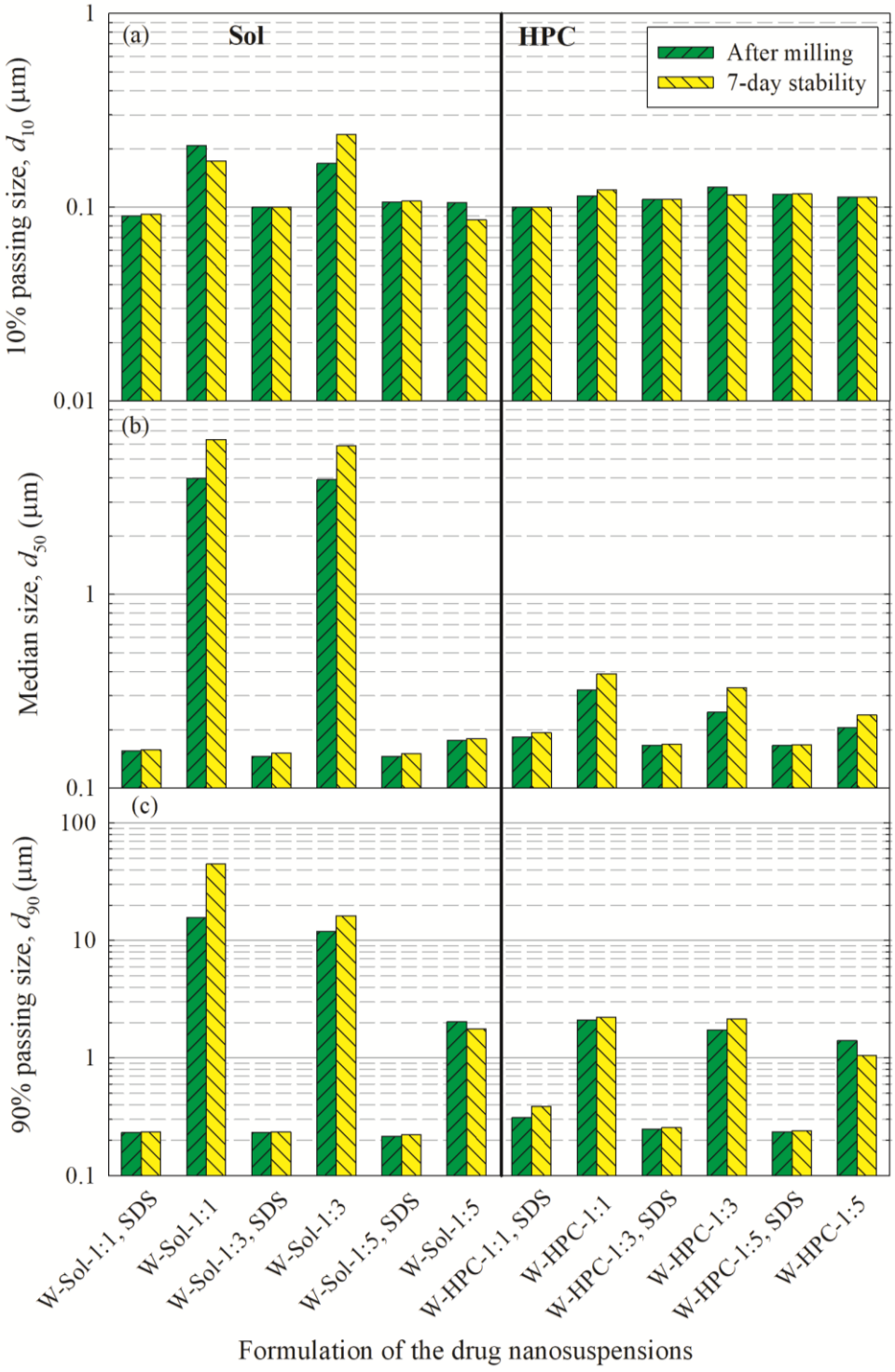

Figure 4.1 Volume-based particle size statistics of the milled GF suspensions with 1:1, 1:3, and 1:5 GF:polymer mass ratios and 0.125% SDS/without SDS after milling (64 min) as well as 7-day storage at 8 °C: (a) 10% cumulative passing size d_{10}, (b) median particle size d_{50} and (c) 90% cumulative passing size d_{90}.

in the suspension, and usually increases as polymer concentration increases. The finer aggregates and lower extent of aggregation can be explained by greater polymer adsorption at higher polymer adsorption, which was already established in an earlier HPC–GF adsorption study (Bilgili and Afolabi, 2012). Clearly, presence of 0.125% in the suspensions had the most dramatic effect on the extent of nanoparticle aggregation. HPC–SDS was reported to have synergistic stabilizing effect on GF suspensions during milling and storage (Konno et al., 2008) and stabilized multiple BCS Class II drug nanosuspensions (Bilgili et al., 2016). HPC and Sol imparted steric stabilization by adsorbing on drug nanoparticles (Bilgili and Afolabi, 2012; Yang et al., 2014), while the anionic surfactant (SDS) enhanced GF wettability/deaggregation and helped to stabilize the GF nanosuspensions *via* electrostatic repulsion (Bilgili and Afolabi, 2012; Bilgili et al., 2016). As can be seen from Table 4.2, both polymers and polymer–SDS reduced the surface tension and enhanced the GF wettability by water. As indicated by the higher wetting effectiveness factor, HPC (hydrophilic polymer) rendered GF more wettable by water than Sol (amphiphilic polymer), and SDS enhanced the wettability even further when used in combination with both polymers. The wettability is important to the deaggregation of the aggregates formed during milling, which allows for full exposure of GF particle surfaces for polymer adsorption. The lower wettability of GF by Sol as compared with HPC could be one reason for the large aggregates in Sol-based suspensions. On the other hand, with SDS, finer suspensions were obtained with Sol than with HPC, which suggests differing interactions between polymer–SDS.

Table 4.2 Properties of Drug-Saturated Deionized Water–Aqueous Stabilizer Solutions and Wetting Effectiveness Factor Determined Using the Modified Washburn Method

Formulation	η (cP)	ρ (g/mL)	γ (mN/m)	Slope, (g^2/s)	R^2	$\cos\theta_{ss}/\cos\theta_w$
Water	0.89	1.00	66.5	7.0×10^{-3}	0.990	1.00[a]
Sol	8.76	1.01	41.4	1.2×10^{-3}	0.989	2.65
Sol–SDS	13.5	1.01	40.5	1.5×10^{-3}	0.991	4.65
HPC	53.2	1.01	39.9	1.5×10^{-3}	0.998	20.9
HPC–SDS	58.3	1.01	34.8	2.4×10^{-3}	0.999	42.1

[a]The slope of the water penetration data was used as reference for wettability enhancement by the stabilizer solutions.

4.3.2 Size, Morphology, and Drug–Moisture Content of the Spray-Dried Powders

Despite the relatively short residence time (4 s), the powders were completely dried, as indicated by TGA, which shows weight loss of 2.0 ± 0.3% for the samples. The extremely large surface area generated by atomization of the suspension feed coupled with the convective heat–mass transfer at high air temperature enabled fast drying of the droplets in the drying chamber. The mean (actual) drug content after spray-drying was higher for feeds with higher drug:polymer mass ratio (Table 4.3). All RSD values were below 6%: 0.51–4.71%, which signifies pharmaceutically acceptable content uniformity. The lower drug content as compared with the theoretical value can be attributed to preferential drug loss during handling/transfer of the suspensions after milling, poor separation of finer particles in the cyclone separator of the spray dryer, and presence of the residual moisture after drying (Azad et al., 2015b; Bilgili et al., 2018). An increase in polymer loading (lower drug:polymer mass ratio) led to formation of coarser particles due to increase in total solids loading and higher viscosity of the precursor feed (Bilgili et al., 2018; Li et al., 2018b; Poozesh and Bilgili, 2019). Compared to the significant impact of polymer loading on particle size,

the impact of SDS was weak and did not exhibit a clear trend. The microscopic images (Figure 4.2) illustrate that spray-dried particles are somewhat aggregated due to their cohesive nature and individual particles have rounded–shriveled morphology.

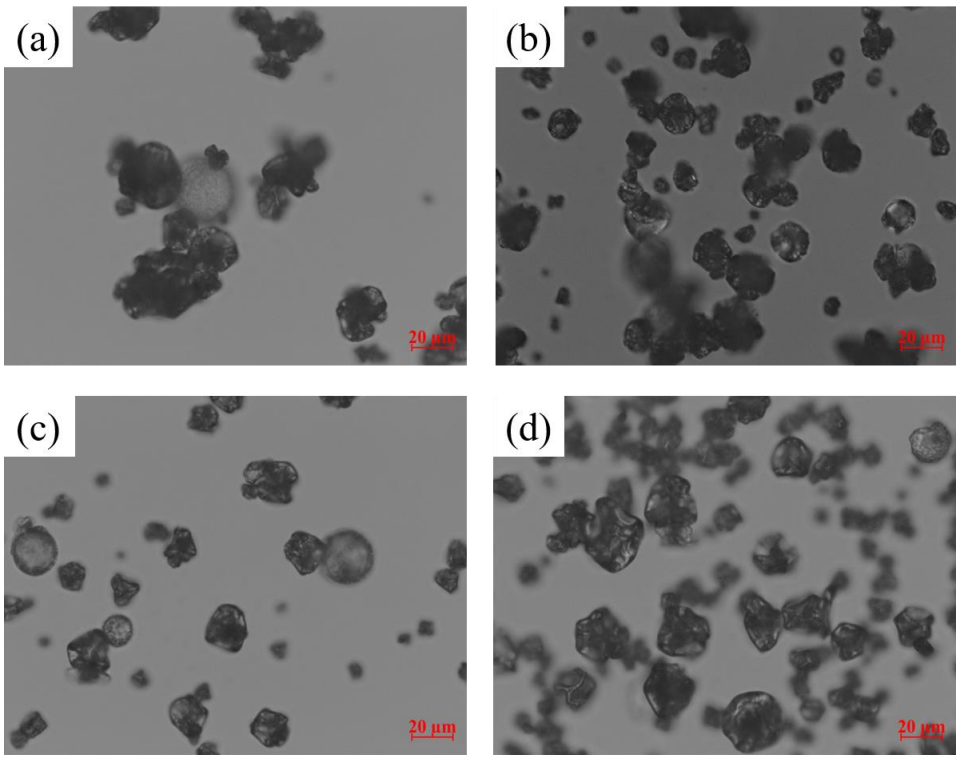

Figure 4.2 Polarized light microscope images of the spray-dried particles prepared using the GF suspension-based (W) feed with 1:3 GF:polymer mass ratios and 0.125% SDS/without SDS: (a) W-HPC-1:3 (b) W-HPC-1:3, SDS, (c) W-Sol-1:3, and (d) W-Sol-1:3, SDS. All images were taken at 50X magnification (scale bar: 20 µm).

4.3.3 Formation of Drug Nanocomposites/HyNASDs

Figure 4.3 illustrates the XRPD diffractograms of the spray-dried powders, while Table 4.4 presents their crystallinity. X-ray diffractograms depict that as-received GF exhibited intense peak characteristics of a crystalline material, whereas HPC/Sol exhibited halo pattern indicating amorphous structure. The physical mixtures (PMs), prepared by blending of as-received GF with HPC/Sol or HPC/Sol–SDS powders,

Table 4.3 Particle Size Statistics of the Spray-Dried Powders and Their Drug Content

ID	Formulation[a]	Particle size statistics of the spray-dried particles (μm)			Theoretical drug content (% w/w)[b]	Actual drug content, RSD (% w/w, %)[b]
		d_{10}±SD	d_{50}±SD	d_{90}±SD		
W1	W-Sol-1:5	10.8±0.4	21.8±0.3	39.8±0.5	16.7	15.4, 2.34
W2	W-Sol-1:3	5.68±0.1	16.2±0.0	31.9±0.1	25.0	22.3, 4.47
W3	W-Sol-1:1	4.02±0.2	10.4±0.1	20.0±0.0	50.0	44.1, 4.31
W4	W-Sol-1:5, SDS	10.3±0.1	20.3±0.1	36.4±0.3	16.5	14.9, 3.47
W5	W-Sol-1:3, SDS	9.29±0.1	19.0±0.1	33.6±0.1	24.7	21.2, 1.50
W6	W-Sol-1:1, SDS	4.48±0.1	10.1±0.1	21.9±0.2	48.8	42.0, 1.73
W7	W-HPC-1:5	9.73±0.3	22.3±0.4	46.0±0.7	16.7	14.9, 4.71
W8	W-HPC-1:3	6.41±0.1	20.3±0.1	41.8±0.3	25.0	22.8, 4.60
W9	W-HPC-1:1	4.61±0.1	14.9±0.4	35.8±0.6	50.0	45.4, 1.77
W10	W-HPC-1:5, SDS	8.32±0.2	21.0±0.8	44.3±0.8	16.5	15.3, 1.48
W11	W-HPC-1:3, SDS	6.37±0.1	16.5±0.6	40.0±0.1	24.7	22.3, 3.14
W12	W-HPC-1:1, SDS	5.24±0.1	12.9±0.1	34.2±0.1	48.8	42.5, 2.83
W13	W-Sol-3:1, SDS	1.66±0.1	6.89±0.3	15.3±0.4	72.3	64.4, 0.51

[a]W denotes suspension-based feed; Sol denotes Soluplus; the ratios refer to the drug:polymer mass ratios.
[b][b]% w/w with respect to the total weight of the spray-dried powder.

exhibited peaks at the same diffraction angles as those of as-received GF, albeit with reduced intensity. The diffractograms of the spray-dried powders without SDS (Figure 4.3a) and with SDS (Figure 4.3b) did not remarkably differ, except for peak intensities; they exhibit a similar pattern regarding the impact of polymer loading. The peak intensities of GF in the PMs were lower than those of the as-received GF powder, which can be attributed to the dilution and surface coverage of GF microparticles with HPC/Sol, and the reduction is more discernible with increasing polymer concentration. Similar XRPD diffractograms to those of the PMs were observed for the spray-dried powders confirming that spray-drying of the milled suspensions led to formation of nanocomposites that are largely crystalline. Interestingly, the diffractograms of the spray-dried powders displayed reduced peak intensities as compared with their respective PMs, beyond the aforementioned dilution effect of the polymer, which becomes more pronounced upon an increase in polymer loading (lower drug:polymer mass ratio). Surprisingly, wet milling followed by spray-drying led to reduction of crystallinity and formation of notable (up to 21%) amorphous GF (see Table 4.4). To the best knowledge of the authors, this level of amorphous content in drug nanocomposites is not common.

It is well-known that wet media milling does not cause any detectable amorphization of as-received GF, in the absence of stabilizers, due to plasticization effect of water (Monteiro et al., 2013; Żarów et al., 2011). XRPD diffractograms of the wet-media milled GF and as-received GF were almost identical (Monteiro et al., 2013) In the presence of high polymer loading in the suspensions here, however,

amorphization of GF took place during the spray drying. Table 4.4 shows that despite being largely crystalline, the spray-dried powders had higher amorphous GF when

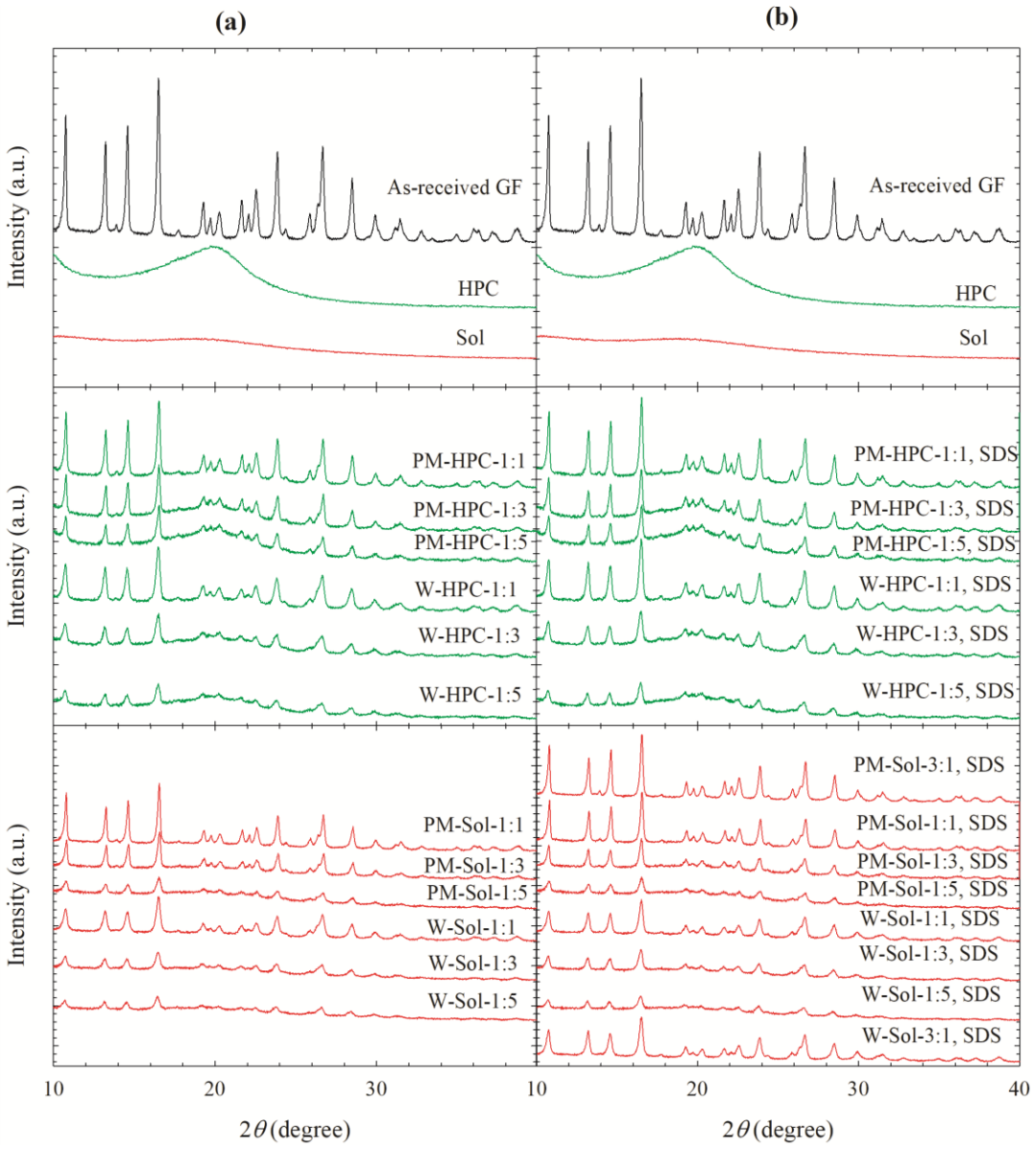

Figure 4.3 X-ray diffractograms of as-received GF, HPC, Sol, physical mixtures (PMs) of GF–HPC/Sol and the spray-dried powders prepared using the GF suspension-based (W) feed with 1:1, 1:3, and 1:5 drug:polymer mass ratios: (a) without SDS and (b) with 0.125% SDS in the suspension. W-Sol-3:1, SDS and PM-Sol-3:1, SDS stand for the spray-dried powder prepared using a suspension-based feed with 3:1 GF:Sol mass ratio and 0.125% SDS and its corresponding physical mixture, respectively.

Table 4.4 Melting Point Temperature and Fusion Enthalpy of the Spray-Dried Powders Obtained From DSC Thermograms and Crystallinity Estimated From XRPD Diffractograms

ID	Formulation[a]	T_m (ºC)[b]	ΔH_f (J/g)[b]	ΔT_m (ºC)[b]	Crystallinity (%)
W1	W-Sol-1:5	171	1.56	49.1	80.3
W2	W-Sol-1:3	181	3.23	39.1	86.8
W3	W-Sol-1:1	205	19.6	15.1	93.9
W4	W-Sol-1:5, SDS	168	2.46	52.1	78.8
W5	W-Sol-1:3, SDS	186	7.37	34.1	81.3
W6	W-Sol-1:1, SDS	204	22.7	16.1	86.3
W7	W-HPC-1:5	189	8.34	31.1	80.8
W8	W-HPC-1:3	199	12.0	21.1	82.7
W9	W-HPC-1:1	211	28.0	9.1	99.2
W10	W-HPC-1:5, SDS	172	3.54	48.1	81.8
W11	W-HPC-1:3, SDS	198	12.7	22.1	86.5
W12	W-HPC-1:1, SDS	211	28.7	9.1	95.5
W13	W-Sol-3:1, SDS	212	47.0	8.1	92.1

[a]W denotes nanosuspension-based feed, Sol denotes Soluplus; the ratios refer to the drug:polymer mass ratios.

[b]T_m stands for melting point temperature, ΔT_m stands for melting point depression, and ΔH_f stands for fusion enthalpy.

the polymer loading in the precursor suspension was higher. In general, more amorphous GF formed in the Sol formulations than in the HPC formulations at the same drug:polymer mass ratio with/without SDS except for 1:3 GF:polymer without SDS. These findings imply that (i) amorphous GF formed due to GF–polymer molecular interactions and/or solubilization of the surface layer of nanoparticles by the polymer during the spray-drying and (ii) Sol appears to favor the amorphization of GF more than HPC, which implies stronger Sol–GF molecular interactions/miscibility than HPC–GF. It is likely that presence of GF nanoparticles and their aggregates with large surface area and higher polymer loading (more GF–polymer interactions and higher GF solubilization in the polymer) could have favored the formation of amorphous GF. Based on these findings and ref. (Kayaert and Van den Mooter, 2012), it is proposed that the polymeric matrix of the spray-dried

particles encapsulates drug nanocrystals/aggregates, surrounded by a layer of amorphous GF molecularly dispersed in the polymer (see Figure 4.4b). Formation of amorphous content upon drying of drug nanosuspensions was first noted in (Kayaert and Van den Mooter, 2012), albeit to a lower extent, and was regarded as "unfavorable". Nonetheless, the impact of such amorphous content on drug release from the nanocomposites has not been studied at all. As the dissolution tests will reveal, despite being largely crystalline, these nanocomposites with relatively high polymer loading (low drug:polymer ratio) allow for much higher supersaturation than traditional nanocomposites, similar to the supersaturation levels observed for ASDs; hence, we coin the term hybrid nanocrystal–ASD (HyNASD) for this special class of nanocomposites.

The DSC thermograms in Figure 4.5 show an endothermic peak associated with melting of as-received GF, with a melting point temperature T_m of 220.1 °C and a fusion enthalpy ΔH_f of 101.8 J/g; a glass transition for Sol (amorphous) at 72.4 °C; and a slight endothermic event around 170–200 °C for HPC likely due to the melting of the small crystalline domain of largely amorphous HPC (Sarode et al., 2013) (crystallinity was undetectable by XRPD). The T_g of HPC could not be measured (in the range of –25 to 0 °C (Sarode et al., 2013)) due to limitation of our equipment. The spray-dried powders exhibited a melting endotherm only, corresponding to the fusion of their GF crystals. The absence of any recrystallization event during the heating could suggest that the amorphous GF in HyNASDs did not recrystallize due to GF–

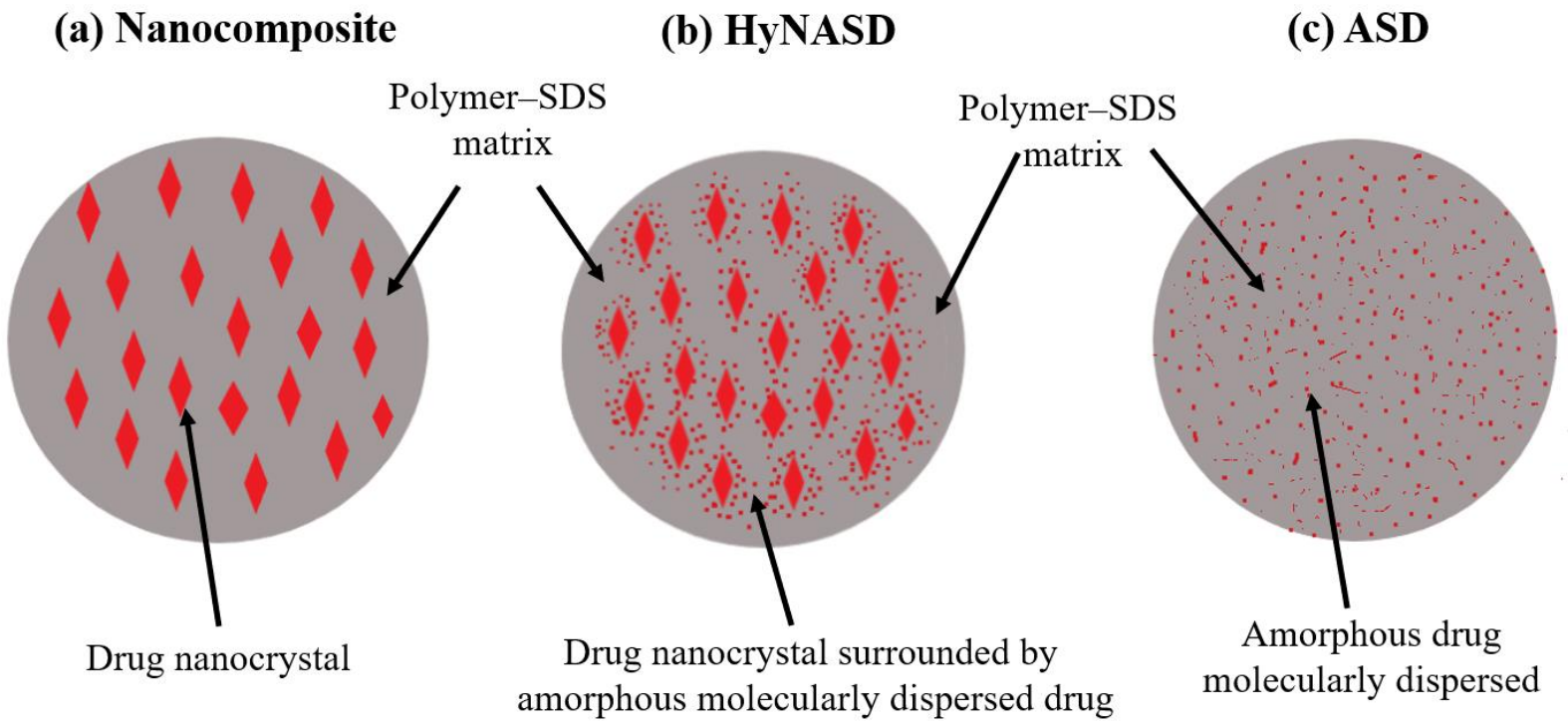

Figure 4.4 Schematic illustration of the solid state of the drug (GF) in (a) GF nanocomposite, (b) GF hybrid nanocrystal–amorphous solid dispersion (HyNASD), and (c) GF amorphous solid dispersion (ASD). Figure is not drawn to scale.

polymer molecular interactions as the small amorphous GF was in the ASD surrounding the drug crystals (see Figure 4.4b).

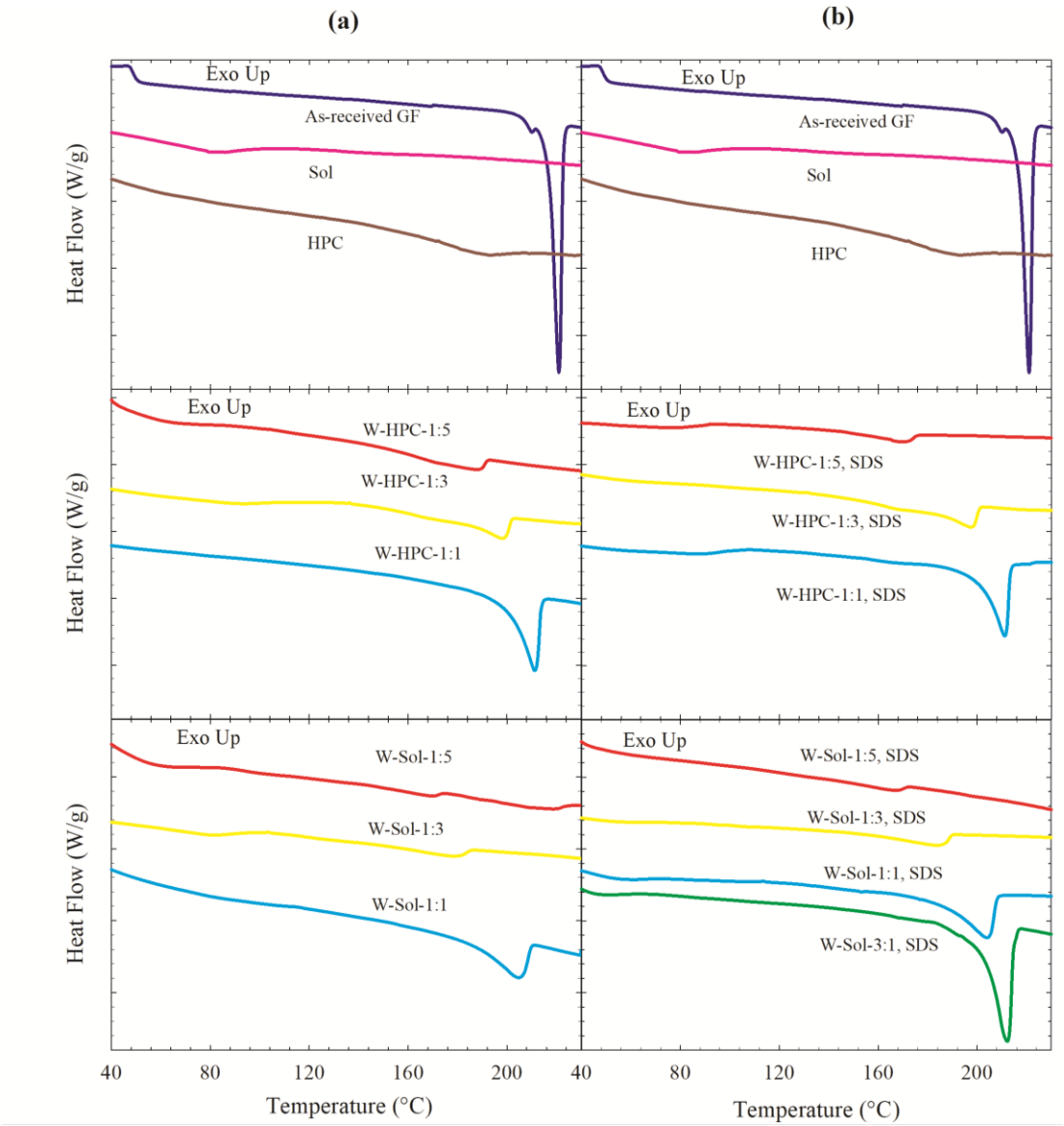

Figure 4.5 DSC thermograms of as-received GF, HPC, Sol, and the spray-dried powders prepared using the GF suspension-based (W) feed with 1:1, 1:3, and 1:5 drug:polymer mass ratios: (a) without SDS and (b) with 0.125% SDS in the suspension. W-Sol-3:1, SDS stands for the spray-dried powder prepared using a suspension-based feed with 3:1 GF:Sol mass ratio and 0.125% SDS.

Wet media milling of as-received GF without any stabilizers depressed T_m by less than 1 ºC (Monteiro et al., 2013). On the other hand, Figure 4.5 and Table 4.4 show that spray-drying of GF suspensions with polymers led to drastic melting point depression (high ΔT_m), up to 52 ºC, and reduction of ΔH_f even if the ΔH_f values were corrected for dilution with polymer and reduced crystallinity (not shown for brevity). The significant melting point depression in drug–polymer mixtures is indicator of drug–polymer miscibility (Baird and Taylor, 2012; Newman et al., 2008). In general, higher polymer loading (lower GF:polymer mass ratio) led to lower T_m as compared with the as-received GF crystals, higher ΔT_m, and lower ΔH_f, regardless of the presence/absence of SDS, which signifies significant GF–polymer molecular interactions. Moreover, without exceptions, having identical polymer/SDS composition, the spray-dried powders with Sol had higher ΔT_m and lower ΔH_f than those with HPC, which could be explained by (i) stronger GF–Sol interactions and miscibility, (ii) higher initial amorphous content in the Sol-based spray-dried powders, and (iii) higher extent of solubilization of GF in the polymer melt at high temperatures due to the thermal treatment during the DSC scan. Compared with the clear trends regarding the impact of polymer loading for formulations with/without SDS, the trends for SDS impact were not as strong and as clear. For HPC-based formulations, the impact of SDS was small and only notable for the highest HPC loading (1:5), which exhibited higher ΔT_m and lower ΔH_f with SDS than without SDS, implying increased solubilization of GF in the presence of SDS. For Sol-based formulations, the impact of SDS was small at 1:1 GF:Sol loading. While lower ΔH_f without SDS than with SDS was noted for all GF:Sol powders, ΔT_m did not follow a

clear trend. The relatively low impact of SDS could be related to the small amount of SDS in the formulations (1:0.05 GF:SDS).

4.3.4 Raman Spectroscopy and Drug–Polymer Miscibility

The observed Raman lines in Figure 4.6 for as-received GF and PMs of GF are largely in agreement with Fourier transform Raman data of ref. (Feng et al., 2008) and Raman data of ref. (Żarów et al., 2011) for crystalline GF. While the W-Sol-1:3 and W-HPC-1:3 powders did not show disappearance of any lines characteristic of GF, their spectra clearly show broadening of the characteristic GF lines, peak intensity reduction, and line shifts as compared with the spectra of the respective PMs due to GF–polymer interactions (Meng et al., 2015) and presence of amorphous domains in these powders (Baird et al., 2010). In contrast, the spectra of W-Sol-3:1 with SDS, having $1/9^{th}$ of Sol content compared with W-Sol-1:3 with SDS, did not show as much line broadening and line shift compared to the spectra of its respective PM. Finally, the line at 1606 cm^{-1} does not exist in amorphous GF (Żarów et al., 2011); hence, intensity reduction and line broadening/slight line shift at 1606 cm^{-1} could originate from the presence of amorphous GF content.

It is suggested that if the solubility parameter difference between a drug and polymer is <7.0 $MPa^{1/2}$, they are likely to be miscible; if the difference is >10 $MPa^{1/2}$, they are considered immiscible (Forster et al., 2001; Greenhalgh et al., 1999). The solubility parameters of GF, HPC, and Sol are 12.2 (Thakral and Thakral, 2013), 24.0 (Choi et al., 1994), and 19.4 (Kolter et al., 2012) $MPa^{1/2}$, respectively. The solubility parameter differences between GF–Sol and GF–HPC are 7.2 and 11.8 $MPa^{1/2}$, respectively, which suggests that GF–Sol is borderline miscible, whereas GF–HPC is

immiscible. Despite being useful, a caveat about the solubility parameters is worth-noting: the theoretical models of this approach are applicable for simple molecular

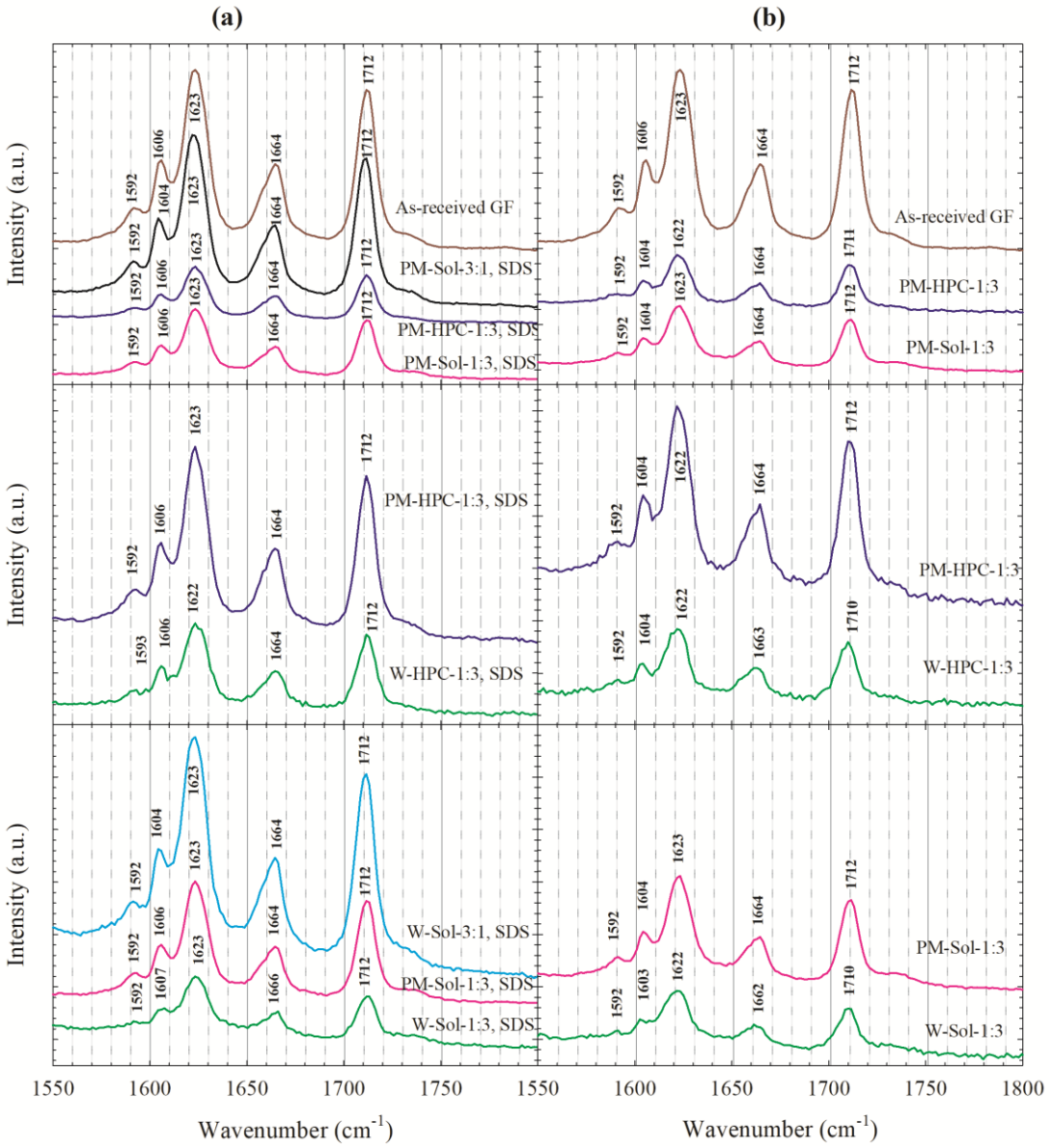

Figure 4.6 Raman spectra of as-received GF, physical mixtures (PMs) of GF–HPC/Sol at 1:3 drug:polymer ratio, and the spray-dried powders prepared using the GF suspension-based (W) feed with 1:3 GF:polymer mass ratio: (a) with SDS and (b) without SDS in the suspensiom. W-Sol-3:1, SDS and PM-Sol-3:1, SDS stand for the spray-dried powder prepared using a suspension-based feed with 3:1 GF:Sol mass ratio and 0.125% SDS and its corresponding physical mixture, respectively.

structures wherein van der Waals force plays a predominant role, while for drug–polymer systems which are known to form highly directional interactions (e.g., hydrogen bonding) or long-range interactions (e.g., ionic interaction), this approach can be erroneous (Baird et al., 2010; Meng et al., 2015). Indeed, the formation of amorphous GF upon spray-drying with HPC-based suspensions, drastic melting point depression and reduced ΔH_f in the spray-dried powders (even after corrected for crystallinity and GF loading) and the Raman spectroscopy results above suggest that HPC molecularly interacts with GF, resulting in partial miscibility unlike the prediction from the solubility parameters. However, the solubility parameters correctly predicted the higher Sol–GF–miscibility than the HPC–GF miscibility, which is in in line with the DSC and XRPD results.

The XRPD, DSC, and Raman spectroscopy results overall suggest that spray-drying of GF–polymer nanosuspensions with/without SDS led to formation of drug nanocomposites/HyNASDs. Although a hard and crisp distinction between traditional nanocomposites and HyNASDs is not intended here, HyNASDs appear to have notable amorphous content (>%10 in XRPD) and/or exhibit significant T_m depression–ΔH_f reduction and GF Raman peak broadening as compared with the respective physical mixtures. As a general observation, we note that spray-drying a drug nanosuspension with a lower drug:polymer mass ratio (1:3 and 1:5) than typically used (see e.g., Table 1.3) and the use of a strongly miscible polymer that interacts with the drug nanoparticles and solubilizes them during the spray drying favor the formation of HyNASDs *vs.* nanocomposites (W-Sol-1:3 *vs.* W-Sol-3:1). Moreover, as will be shown in Section 4.3.7, nanocomposites and HyNASDs may

behave quite differently in their functional responses such as *in vitro* drug release.

4.3.5 Redispersibility of the Spray-Dried Powders

Spray-dried powders were dispersed in 30 mL of deionized water inside a 60 mL beaker and stirred at 500 rpm for 60 min, and particle sizes of the suspension samples taken 2, 10, and 60 min into redispersion are presented in Figures 4.7 and 4.8 for HPC-based and Sol-based formulations, respectively. Ideally, the redispersion of the powders should yield particles with sizes similar to those in the milled suspensions. A cursory look at these figures suggests that redispersion of the powders with SDS achieved this ideal expectation: fast recovery of the drug nanoparticles that have similar sizes to those in the precursor suspensions. The only exception was W-Sol-1:1, SDS, which has the lowest Sol loading and had d_{90} above 1 μm. Without SDS, most spray-dried powders exhibited slow or incomplete redispersion. Among Sol-based powders only W-Sol-1:5 (with the highest Sol loading) exhibited complete redispersion, whereas W-Sol-1:1 and W-Sol-1:3 redispersed extremely slowly (incomplete redispersion). On the other hand, even without SDS, all HPC-based powders were able to redisperse to different extents. Note that GF is a relatively hydrophobic drug (Muster and Prestidge, 2005), while HPC is hydrophilic, and Sol is amphiphilic. Based on modified Washburn method and results presented in Table 4.2, we note (i) the higher wettability enhancement by HPC as compared with Sol in aqueous solutions and (ii) higher wettability enhancement when SDS was present along with the polymer in the aqueous solutions. Hence, the wettability of the spray-dried powder largely controls the redispersion behavior. Although the spray-dried powders encapsulate the drug crystals/amorphous GF, depending on the polymer

loading, the surface will still have hydrophobic GF exposed to water. The dissolving polymer/SDS in the microenvironment of the particles enhances wettability of the hydrophobic drug and allows for faster imbibition/absorption of water in the particle, which facilitates the redispersion.

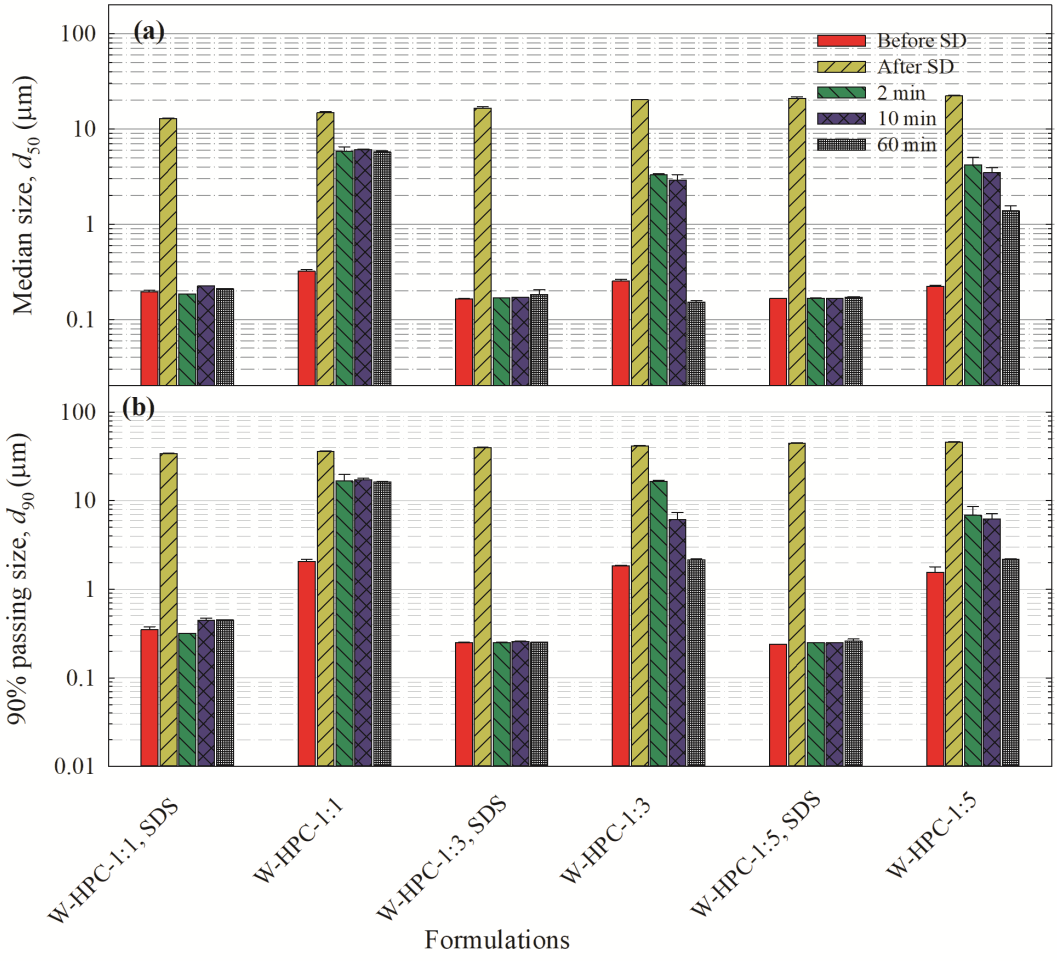

Figure 4.7 Volume-based particle size statistics of the GF suspension-based (W) feeds with 1:1, 1:3, and 1:5 GF:HPC mass ratios and 0.125% SDS/without SDS before spray drying (SD) (after 1 day of milling), after spray drying (spray-dried powders), and the spray-dried particles after redispersion in deionized water for 2 min, 10 min, and 60 min: (a) median particle size d_{50} and (b) 90% passing size d_{90}.

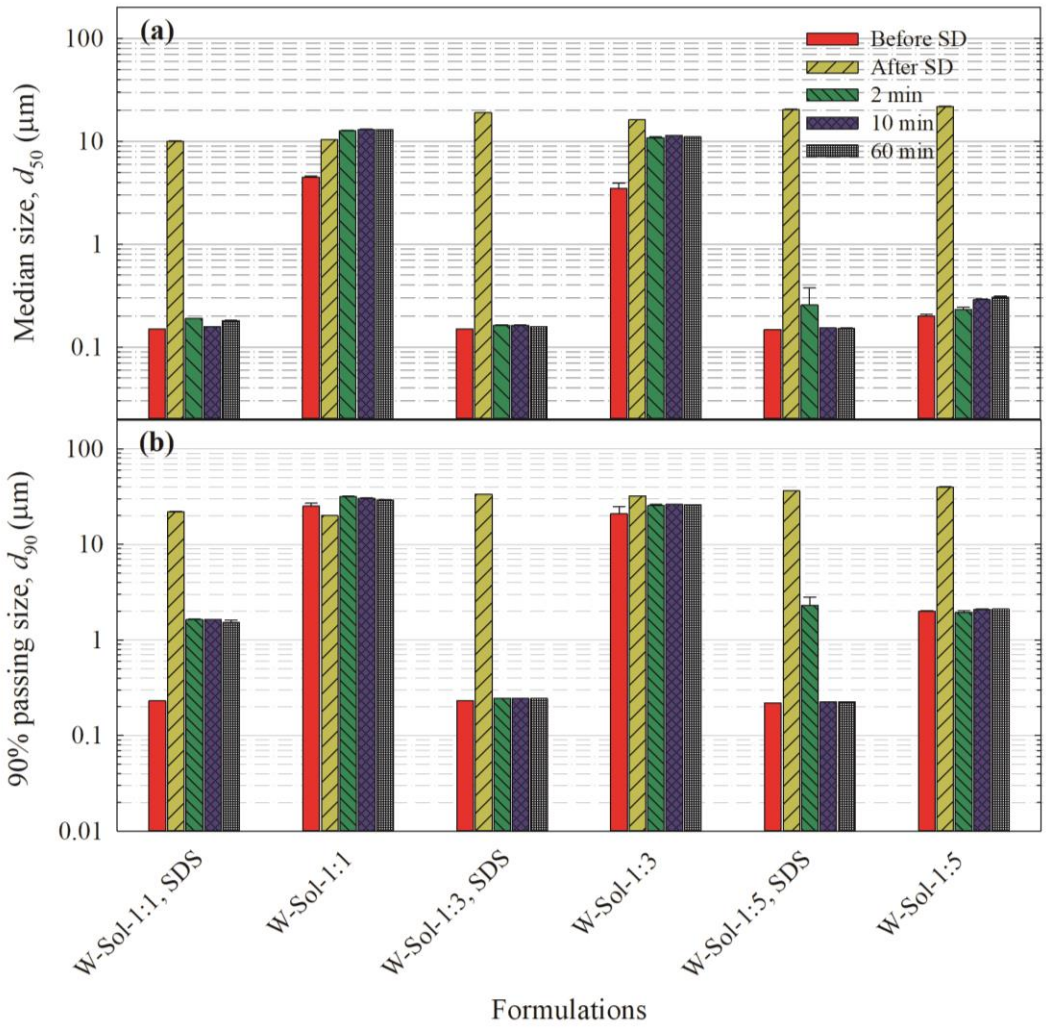

Figure 4.8 Volume-based particle size statistics of the GF suspension-based (W) feeds with 1:1, 1:3, and 1:5 GF:Sol mass ratios and 0.125% SDS/without SDS before spray drying (SD) (after 1 day of milling), after spray drying (spray-dried powders), and the spray-dried particles after redispersion in deionized water for 2 min, 10 min, and 60 min: (a) median particle size d_{50} and (b) 90% passing size d_{90}.

4.3.6 Dissolution Performance of the Spray-Dried Powders in Non-Supersaturating Condition

The temporal evolution of GF release from the spray-dried powders and the PM with the highest polymer loading (1:5 GF:polymer) containing 8.9 mg equivalent GF dose in 1000 mL deionized water at 37 ºC was investigated. The bulk dissolution medium will not supersaturate for this low drug dose as the GF solubility is 14.2 mg/L. We

note from Figure 4.9 that the mere presence of HPC/Sol (1:5 GF:polymer mass ratio)/SDS could increase GF release rate without any wet-milling–spray drying of the as-received (micronized) GF particles. This could be partly explained by the wetting enhancement of the hydrophobic drug (GF) in the presence of HPC/Sol–SDS (Table 4.2), deaggregation of the large drug aggregates present in the as-received drug (Li et al., 2017b), and partly by the higher solubility of GF in the dissolution medium due to dissolution of PM's polymer/SDS in the dissolution medium. For example, the thermodynamic solubility of the GF microparticles at 37 °C was measured to be 14.2 mg/L, 17.8 mg/L, and 18.3 mg/L in the deionized water, aqueous

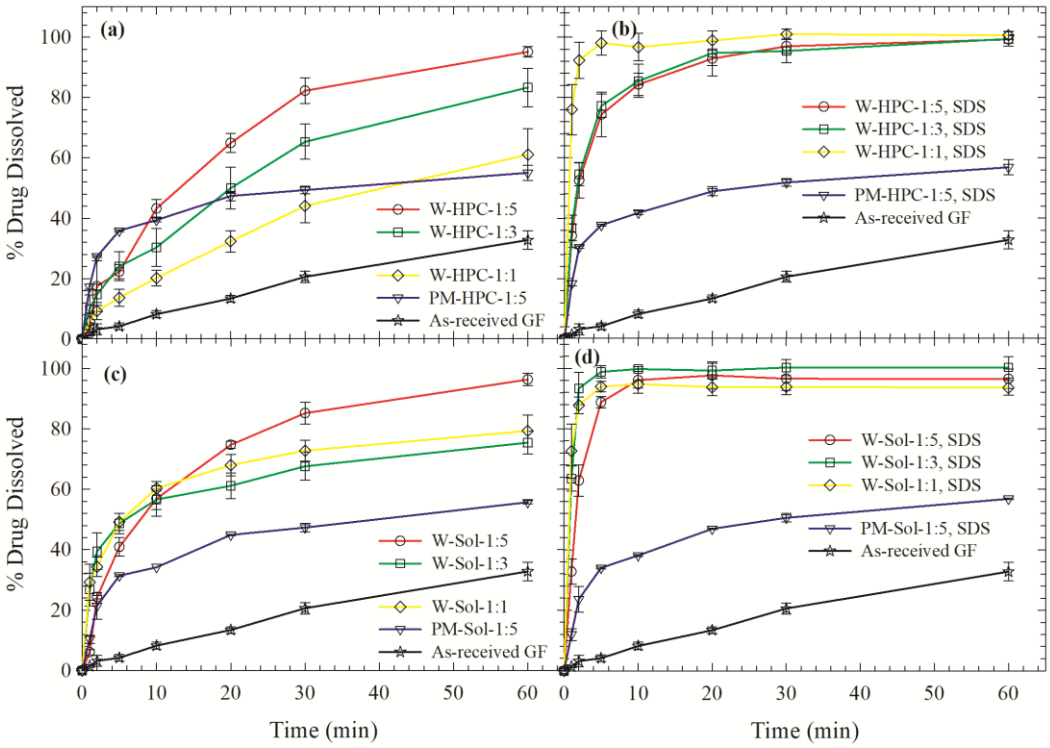

Figure 4.9 Evolution of drug release from as-received GF, physical mixture (PM) with 1:5 GF:polymer mass ratio, and spray-dried powders prepared using GF suspension-based (W) feeds with 1:1, 1:3, and 1:5 drug:polymer mass ratios: (a) HPC without SDS, (b) HPC with SDS, (c) Sol without SDS, and (d) Sol with SDS. Dissolution sample size equivalent to 8.9 mg GF dose (low dose, non-supersaturating condition in the bulk dissolution medium).

medium of 1:3 GF:Sol with SDS, and aqueous medium of 1:3 GF:HPC with SDS, respectively. However, the spray-dried powders released GF faster than the PM owing to the presence of GF nanoparticles/aggregates with larger surface area than drug microcrystals and amorphous GF that has higher kinetic solubility than crystalline GF.

A quick comparison of Figure 4.9b to 4.9a and Figure 4.9d to 4.9c reveals that the spray-dried powders with SDS dissolved faster than those without SDS, which is in accordance with the expectations from the redispersion results and the wetting effectiveness factors presented in Table 4.2. The dissolution profiles of the powders with SDS all exhibited fast, immediate drug release (>80% GF release in 20 min) and their dissolution profiles are hard to differentiate. The presence of SDS imparted wettability enhancement to the spray-dried powders, allowed for their faster redispersion and recovery of the nanoparticles with small extent of aggregation, and ultimately faster GF release. For powders with SDS, wettability may not be the rate-limiting process in drug dissolution; hence, other factors such as spray-dried particle size might have played a role. For example, the fastest-dissolving powder, i.e., W-HPC-1:1, SDS in Figure 4.9b had the smallest spray-dried particles. Without SDS, the HPC-based powders exhibited faster GF release at higher HPC loading despite larger size of the particles; whereas such monotonic behavior was not observed for the Sol-based powders: 1:1 GF:Sol released GF faster than 1:3 GF:Sol, while 1:5 GF:Sol achieved the fastest drug release. These somewhat nuanced trends resulted from differing spray-dried particle sizes, redispersibility, and drug particle sizes in the precursor suspensions, and cannot be predicted by the redispersion results in Figure

4.7 and Figure 4.8 also because of the different volume and microhydrodynamics in the redispersion and dissolution tests. Owing to 1000 mL volume in the dissolution test *vs.* 30 mL in the redispersion test, drug dissolution simultaneously occurred along with erosion of the polymeric matrix in the dissolution test, which allowed redispersion of 1:1 and 1:3 GF:Sol particles without SDS in the dissolution test, whereas these powders did not redisperse much over 60 min in the redispersion test.

4.3.7 Dissolution Performance of the Spray-Dried Powders in Supersaturating Condition

The temporal evolution of GF release from the spray-dried powders and the PM with the highest polymer loading (1:5 GF:polymer) containing 100 mg equivalent GF dose in 1000 mL deionized water at 37 ºC was investigated. The bulk dissolution medium could supersaturate for this high drug dose as the GF solubility is 14.2 mg/L. Unless otherwise specified, all supersaturation values are relative to aqueous thermodynamic solubility of GF and calculated at 210 min. Considering that the major shortcoming of traditional drug nanocomposites with low polymer loading (like W-Sol-3:1, SDS) as compared with amorphous solid dispersions (ASDs) is their limited supersaturation capability in dissolution media, the examination of drug dissolution under supersaturating condition is critical. A cursory look at Figure 4.10 reveals immediately various general trends: (i) the spray-dried powder could generate GF superstation more than the corresponding PM for 1:5 GF:polymer, (ii) the GF supersaturation was higher for spray-dried powders with SDS than those without SDS, and (iii) Sol-based formulations generated much higher supersaturation than HPC-based formulations especially when the formulation included SDS. These results point to the criticality of the wet-media milling in preparing drug nanoparticles

especially in the presence of SDS, wettability of the spray-dried powder, which was enhanced by SDS (Table 4.2), GF–polymer miscibility (refer to Section 4.3.4), and solubilization of the GF by the polymer/SDS.

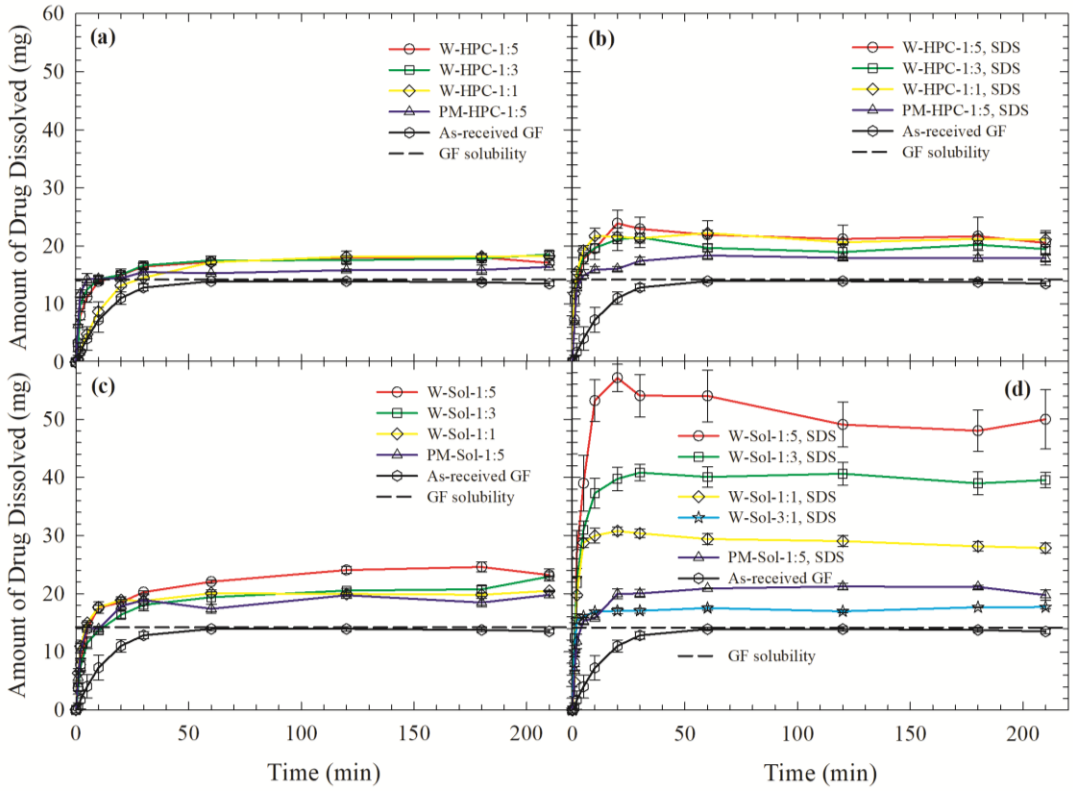

Figure 4.10 Evolution of drug release from as-received GF, physical mixture (PM) with 1:5 GF:polymer mass ratio, and spray-dried powders prepared using GF suspension-based (W) feeds with 1:1, 1:3, and 1:5 drug:polymer mass ratios: (a) HPC without SDS, (b) HPC with SDS, (c) Sol without SDS, and (d) Sol with SDS. Dissolution sample size equivalent to 100 mg GF dose (high dose, supersaturating condition in the bulk dissolution medium). W-Sol-3:1, SDS stands for the spray-dried powder prepared using a suspension-based feed with 3:1 GF:Sol mass ratio with 0.125% SDS.

During the dissolution test, as water wets and imbibes into the spray-dried particles, their polymer dissolves and the particles redisperse into smaller GF–polymer/SDS clusters depending on the wettability, while their amorphous GF fraction contributes to the dissolution fast. In the polymer/SDS-rich

microenvironment of the particles and clusters released, GF could be solubilized by the polymer/SDS, and the rate of this process depends on the cluster/particle size, GF particle size inside these clusters as well as the drug:polymer mass ratio and presence/absence of SDS. Unfortunately, depending on the polymer–drug miscibility and interactions, amorphous content of the HyNASDs (see Table 4.4 for the crystallinity) may phase-separate and recrystallize upon contact with water in the dissolution medium (Alonzo et al., 2011; Chen et al., 2015) because water acts as a plasticizing agent, reducing the glass transition of the ASD component of HyNASDs and enhancing the mobility of the drug molecules (Chen et al., 2015). Finally, the supersaturated GF in the dissolution medium and the released drug nanoparticles form a metastable system, and GF could recrystallize on existing GF nanoparticles and cause their growth, with ensuing GF desupersaturation in time. Strong drug–polymer interactions can reduce the drug molecular mobility and delay recrystallization onset time and the extent of recrystallization (Mistry et al., 2015). Similarly, ref. (Kothari et al., 2015) found that the recrystallization time of nifedipine increased with an increase in polymer (PVP) concentration. To gain additional insights into the GF recrystallization inhibition capability of Sol/HPC–SDS in solutions, independent desupersaturation experiments were performed. Figure 4.11 presents the GF desupersaturation curves. Supersaturation was attained fast upon mixing a GF solution with deionized water and aqueous HPC/Sol/SDS solutions. The supersaturation was largely maintained up to ~210 min with Sol and Sol–SDS, signifying the superior inhibition capability of Sol. GF without any inhibitor and with SDS alone recrystallized fast as GF is a fast recrystallizing compound (Baird et al.,

2010). HPC and HPC–SDS could not maintain supersaturation long unlike Sol.

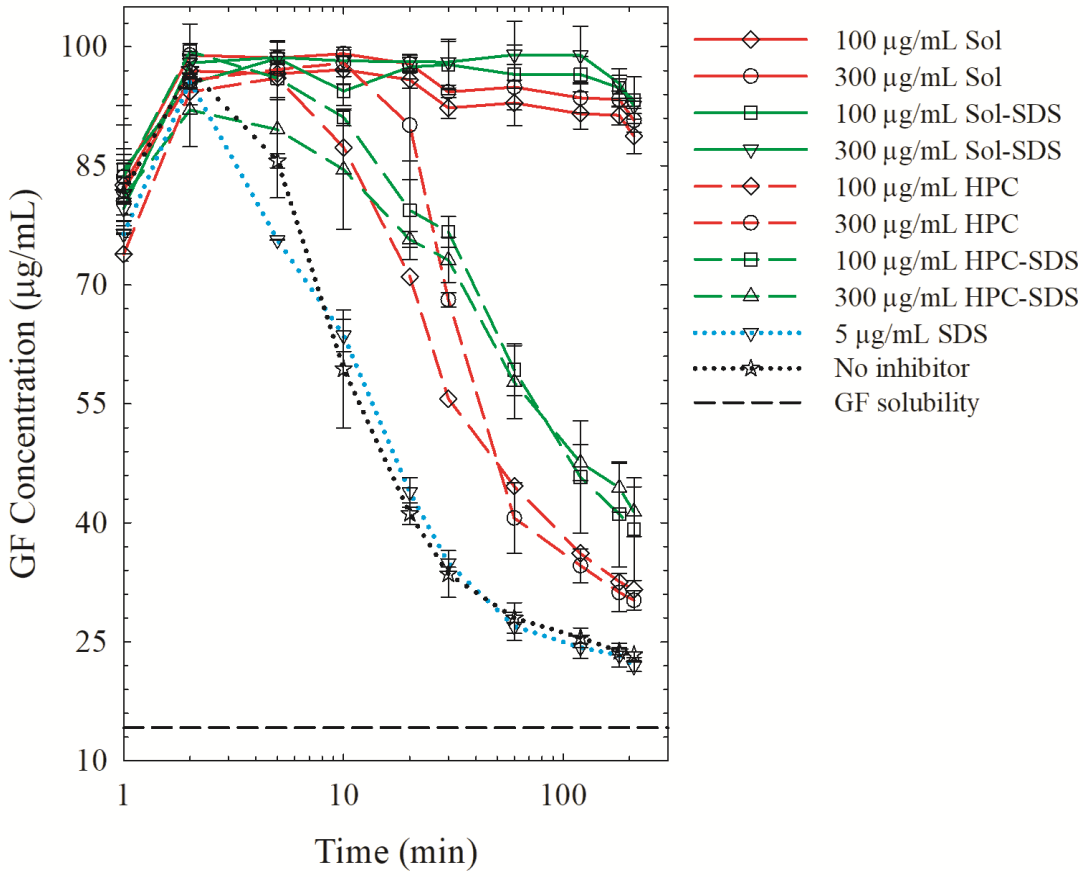

Figure 4.11 GF desupersaturation curves for a supersaturated 20 mL GF–acetone solution mixed with 1000 mL aqueous solutions of 300 µg/mL and 100 µg/mL of HPC/Sol–5 µg/mL SDS or w/o SDS (corresponding to 1:3 and 1:1 polymer:drug formulations), 5 µg/mL SDS only, and deionized water (without any recrystallization inhibitor). The initial concentration of GF right after mixing was targeted at 100 µg/mL.

A comparison of Figure 4.10a *vs.* 4.10b and wetting effectiveness factors in Table 2.2 suggest that wetting enhancement with SDS helped to increase the GF release, but even with SDS, the HPC-based spray-dried powders did not generate more than ~50% supersaturation. HPC-SSL has sub-ambient glass transition temperature T_g (Sarode et al., 2013) (much lower than T_g of Sol: 73 ± 2 °C) and the

amorphous GF molecularly dispersed in HPC matrix of the HyNASDs may have recrystallized due to plasticizing action of water. Moreover, due to HPC's partial miscibility with GF, its relatively weak molecular interactions with GF as compared with Sol, as well as its poor GF nucleation/crystal growth inhibition (refer to Figure 4.11), HPC-based HyNASDs did not generate significant supersaturation even at 1:5 GF:HPC with SDS. While HPC has been used in both marketed drug nanocrystal products and in academic research for preparation of drug nanosuspensions and drug nanocomposites (Bhakay et al., 2018b; Li et al., 2016a), we find here that its SSL grade is not effective in solubilizing GF, preventing GF recrystallization, and achieving high GF supersaturation.

What is remarkable about the dissolution results in Figure 4.10c and 4.10d is that Sol-based HyNASDs with SDS could generate high GF supersaturation fast (up to 300% within 20 min), which is not common in pharmaceutical nanotechnology literature. HyNASDs (1:5 GF:Sol with SDS) achieved 250% GF supersaturation *vs.* 30% achieved by the traditional nanocomposites with low polymer loading (3:1 GF:Sol with SDS). Traditional nanocomposites with drug:polymer mass ratios in the 1:0.8–1:0.02 range usually generate supersaturation up to 50% (see e.g., (Bhakay et al., 2014a; Müller et al., 2011; Zuo et al., 2013)). The high supersaturation achieved by HyNASDs was not possible without SDS because HyNASDs without SDS exhibited retarded release of GF nanoparticles due to poor wettability (see Table 4.2) and they had significant fraction of GF nanoparticle aggregates; both can be inferrred from the poorer redispersibility (Figures 4.7 and 4.8) and the coarser GF particle sizes in the precursor suspensions without SDS (Figure 4.1). Sol was responsible for the

high supersaturation owing to its stronger intermolecular interactions–miscibility with GF affording kinetic solubilization of GF and its inhibition of GF recrystallization (refer to Figure 4.11). Finally, with a T_g of 73 ± 2 °C, Sol prevented recrystallization of amorphous GF molecularly dispersed in the HyNASD during the dissolution test. Another trend in Figure 4.10d was evident: an increase in Sol loading led to higher GF supersaturation/drug release. One reason for this is the higher amorphous content in HyNASDs at higher polymer loading (Table 4.4), which contributed to the faster supersaturation generation, as in ASDs. Moreover, higher Sol loading with respect to GF helped the solubilization of smaller GF nanocrystals within the Sol matrix of the spray-dried particles and drug–Sol clusters emanating from them in the dissolution medium.

Besides its drastic effect on wettability and drug particle size in Sol-based formulations, SDS also helped to delay GF crystallization, despite the fact that SDS alone could not suppress GF recrystallization (Figure 4.11). Presence of SDS might have contributed to the solubilization of GF in the Sol–SDS matrix during the spray drying and the dissolution. To better elucidate the roles of SDS, SDS was added to the dissolution medium to form 0.0005% and 0.125% w/v solutions. Then, the spray-dried powder without SDS (W-Sol-1:5) was dissolved in such media and its dissolution was compared with that of W-Sol-1:5, SDS in water. Here, 0.0005% corresponds to SDS level that would be achieved upon complete dissolution of W-Sol-1:5, SDS powder, while 0.125% (still below CMC) was present in the precursor drug nanosuspensions, whose examination may reveal the impact of high SDS within or in the neighborhood of the swollen spray-dried particles. The analysis of external

addition of SDS to the dissolution medium *vs.* internal addition of SDS to the formulation allowed us to elucidate if there is any other effect of SDS besides its wettability enhancement. Figure 4.12 shows that adding SDS externally to the dissolution medium improved the GF release from W-Sol-1:5 significantly and higher SDS concentration achieved higher supersaturation, which can be explained by wettability enhancement and redispersion of the GF nanoparticle aggregates of W-Sol-1:5 in the dissolution medium. On the other hand, W-Sol-1:5, SDS (SDS internally added as part of the formulation) achieved the highest GF supersaturation

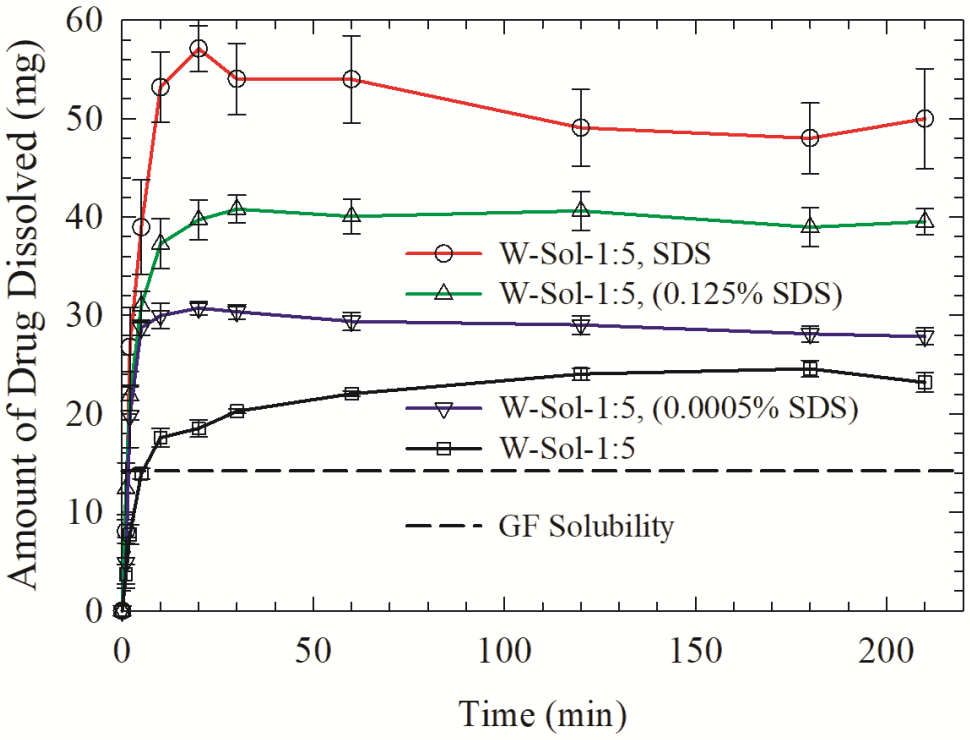

Figure 4.12 Evolution of drug release from spray-dried powders prepared using GF suspension-based (W) feeds with 1:5 drug:polymer mass ratio and SDS and without SDS in the formulation. Deionized water was used as the dissolution medium for the formulation with SDS (W-Sol-1:5, SDS). For the formulation without SDS (W-Sol-1:5), aqueous solution of 0.125% w/v SDS, aqueous solution of 0.0005% w/v SDS, and deionized water were used as dissolution media. Dissolution sample size equivalent to 100 mg GF dose (high dose, supersaturating condition in the bulk dissolution medium).

in water, implying that internal addition of SDS helped Sol in solubilizing GF during the spray-drying and dissolution besides its favorable effect on the wetting/deaggregation of GF aggregates. Such solubilizing effect of SDS has been reported in earlier studies on drug ASDs (Lu et al., 2014; Sjökvist et al., 1991).

4.4 Conclusions

Spray-drying of wet-milled GF suspensions with high polymer loading (1:1 to 1:5 GF:polymer mass ratio) with HPC/Sol as polymer and with/without SDS led to formation of a special class of nanocomposites, HyNASDs, which contain drug nanocrystals and aggregates surrounded by notable amorphous content (5%–21%) molecularly dispersed in the polymeric matrix. All spray-dried powders had acceptable content uniformity. XRPD–DSC–Raman spectroscopy shed light on the nanocomposite/HyNASD formation and revealed higher GF miscibility–stronger molecular interactions for Sol–GF than for HPC–GF. Redispersion of the HyNASD powders indicated the critical need for wettability enhancement by SDS. The HyNASDs with SDS exhibited fast, immediate release in non-supersaturating dissolution condition; the ones without SDS exhibited slower GF release, whose profile depended on polymer loading and spray-dried particle size. Under supersaturating dissolution conditions (high GF dose), HPC-based HyNASDs performed poorly in enhancing GF supersaturation (up to 50% even with SDS), whereas Sol-based ones with SDS achieved fast supersaturation: up to 300% within 20 min and maintained supersaturation at 250% after 3 h. These results were explained by higher T_g of Sol than that of HPC, higher GF–Sol miscibility, stronger

molecular interactions between Sol–GF than HPC–GF, excellent nucleation/crystal growth inhibition by Sol as compared to HPC as well as wettability–solubilization enhancement by SDS. The supersaturation generation capability of HyNASDs was largely controlled by presence of SDS either in the formulation or in the dissolution medium, drug–polymer interactions/miscibility as well as the size of the drug (nano)crystals in the polymeric matrix. Overall, the most striking finding from this study is that despite having ~80% nanocrystals, Sol-based HyNASDs with SDS provided fast drug supersaturation and maintained it at 250% unlike traditional nanocomposites (10%–60%), which could render nanoparticle formulations more attractive in bioavailability enhancement of poorly soluble drugs. In a forthcoming paper, we will compare the dissolution performance of HyNASDs with ASDs having identical formulation. Future research efforts will include investigation of the storage stability of HyNASDs under various environmental conditions and preparation of HyNASDs with various drug–polymer–surfactants and their comparative assessment.

CHAPTER 5

IMPACT OF SDS ON GRISEOFULVIN RELEASE FROM SPRAY-DRIED AMORPHOUS SOLID DISPERSIONS WITH HPC–SOLUPLUS

In Chapter 4, impact of an anionic surfactant, sodium dodecyl sulphate (SDS) was investigated in the stabilization of GF nanosuspensions and production of HyNASDs and dissolution enhancement under supersaturating condition. Significant improvement in the drug release rate and in supersaturation generation was achieved while using SDS in the formulation. Since the mechanism of drug release and supersaturation generation–maintenance mechanisms are different from drug nanocomposites and ASDs, it is important to investigate the impact of surfactant in the production and dissolution performance of ASDs. The goal of this chapter was to elucidate the impact of a common anionic surfactant, sodium dodecyl sulfate (SDS), on drug release from amorphous solution dispersions (ASDs) while elucidating its roles in wettability enhancement and recrystallization inhibition along with polymers. To this end, hydroxypropyl cellulose (HPC) and Soluplus (Sol) were used as matrix-forming polymers of the ASDs. 2.5% griseofulvin (GF, BCS Class II drug) and HPC/Sol with 1:1, 1:3, and 1:5 GF:polymer mass ratios, along with 0.125% SDS and without SDS, were dissolved in acetone–water and spray-dried. XRPD, DSC, and Raman spectroscopy results suggest that Sol had stronger interactions and better miscibility with GF than HPC and formed XRPD-amorphous GF, while HPC-based ASDs, except the ASD with1:5 GF:HPC/SDS, had crystalline GF. SDS helped to reduce the fraction of GF crystals in HPC-based ASDs, suggesting its role in GF solubilization within the polymer matrix. Modified Washburn experiments revealed

significant wettability enhancement when SDS was used along with the polymer and better wettability enhancement by HPC (hydrophilic) than Sol (amphiphilic). Results from *in vitro* dissolution tests with low (9 mg) GF dose suggest that enhanced wettability with SDS led to faster GF release. For 100 mg GF dose (above thermodynamic solubility), without SDS, ASDs provided limited GF supersaturation due to poor wettability of Sol-based ASDs (max. 250%) and extensive GF recrystallization in HPC-based ASDs (max. 50%). Microscopic imaging of a loose ASD compact imbibed with water confirmed formation of GF crystals in HPC-based ASDs. Incorporating even 0.83% SDS in Sol-based ASDs led to dramatic increase in supersaturation (max. 570%), but it had no notable improvement for HPC-based ASDs. SDS provided Sol-based ASDs with enhanced wettability and augmented Sol in solubilizing GF, without interfering with Sol's ability to inhibit GF recrystallization, as confirmed by desupersaturation experiments. While elucidating the roles of SDS, this study demonstrates the dramatic positive impact of incorporating SDS as a minor component of ASDs unlike its common use as a carrier for solubilization in most recent studies.

5.1 Materials and Methods

5.1.1 Materials

BP/EP grade, micronized griseofulvin (GF) purchased from Letco Medical (Decatur, AL, USA) was used as a challenging Biopharmaceutics Classification System (BCS) Class II drug, which is known to be a fast crystallizing drug (Baird et al. 2010). Its aqueous solubility is ~8.9 mg/L at 25 °C and ~14.2 mg/L at 37 °C, and has a melting

point temperature T_m of 220 °C and a glass transition temperature T_g of 89 °C (Baird et al., 2010). Hydroxypropyl cellulose (HPC, SSL grade, Nisso America Inc., New York, NY) is a semi-crystalline polymer with low crystallinity and amorphous domains of very low T_g (Sarode et al., 2013) Soluplus® (Sol) is an amphiphilic graft copolymer produced from polyvinyl caprolactam–polyvinyl acetate–polyethylene glycol having a single glass transition temperature of 73 ± 2 °C (Terife et al., 2012). Sodium dodecyl sulfate (SDS), an anionic surfactant, purchased from GFS Chemicals, Inc. (Columbus, OH) was used as a surface-active agent. Acetone (ACS reagent, ≥ 99.5%) was purchased from BDH Analytical chemicals, (VWR, GA) and used as a solvent to prepare solution-based feed to the spray dryer

5.1.2 Preparation of Spray-Dried Powders

Organic solution-based (S:solvent) feeds of GF were fed to the spray dryer for the preparation of drug ASDs. Table 5.1 presents the formulations used in the precursor feeds. The drug concentration was kept constant at 2.5% (w/v) in all formulations. The drug concentration was calculated with respect to the total volume of the solvent mixture (acetone–water) in the solution-based feeds, which was fixed at 240 mL. A mixture of acetone–water was purposefully selected to dissolve all components of the formulation. 2.5% griseofulvin (GF, BCS Class II drug) and HPC/Sol with 1:1, 1:3, and 1:5 GF:polymer mass ratios, along with 0.125% SDS (20:1 GF:SDS mass ratio) and without SDS, were dissolved in acetone–water using a magnetic stirrer and spray-dried to prepare the ASDs. The rationale for selecting of 0.125% SDS is as follows: when fully dissolved, ASD will provide 0.0005% SDS in the dissolution medium, i.e., water, which is well below the critical micelle concentration of SDS (8 mM, 0.23%

w/v at 25 ºC) (Sharma et al., 1996). Hence, the micellar solubilization of GF by SDS in the dissolution medium is purposefully avoided. After dissolving the drug–polymer–surfactant into the binary solvent mixture, the solutions were sonicated for 30 min before feeding to the spray dryer.

Table 5.1 Formulations of the GF–HPC/Sol Solutions With or Without SDS Fed to the Spray Dryer

ID	Formulation[a]	GF (% w/v)[b]	Polymers (% w/v)[b]	SDS (% w/v)[b]	Water (mL)	Acetone (mL)
S1	S-Sol-1:5	2.5	12.5	0	40	200
S2	S-Sol-1:3	2.5	7.5	0	40	200
S3	S-Sol-1:1	2.5	2.5	0	40	200
S4	S-Sol-1:5, SDS	2.5	12.5	0.125	40	200
S5	S-Sol-1:3, SDS	2.5	7.5	0.125	40	200
S6	S-Sol-1:1, SDS	2.5	2.5	0.125	40	200
S7	S-HPC-1:5	2.5	12.5	0	40	200
S8	S-HPC-1:3	2.5	7.5	0	40	200
S9	S-HPC-1:1	2.5	2.5	0	40	200
S10	S-HPC-1:5, SDS	2.5	12.5	0.125	40	200
S11	S-HPC-1:3, SDS	2.5	7.5	0.125	40	200
S12	S-HPC-1:1, SDS	2.5	2.5	0.125	40	200

[a]S denotes solution-based feed; Sol denotes Soluplus; the ratios refer to the drug:polymer mass ratios.
[b]% w/v with respect to the total volume (240 mL) of the solvent mixture (acetone + deionized water).
[c]% w/w with respect to the total weight of the solid content.

Using a spray dryer (4M8-Trix, Procept, Zelzate, Belgium) having a co-current flow set-up, solution-based feeds were dried. The total length and the diameter of the spray dryer are 1.59 m and 0.15 m, respectively. To ensure complete drying, inlet temperature was selected above the boiling temperature of the respective pure liquids. Drying air at 75 °C flowing at a rate of 0.27–0.30 m^3/min were fed co-currently at the top of the dryer column to dry the solution-based feeds. 200 g solution of each formulation was sprayed at 2.0 g/min rate using a peristaltic pump (Make-it-EZ, Creates, Zelzate, Belgium). A cyclone separator was used to separate the dried

particles from the outlet stream into a glass jar. Atomizing air pressure of 2.0 bar, a bi-fluidic nozzle with tip diameter of 0.6 mm, and cyclone pressure of 55–60 mbar were selected based on prior experience (Azad et al., 2015b) and exploratory experiments. The dried particles obtained from the collection jar were transferred into double plastic bags and stored in a vacuum-desiccator at room temperature for further characterization.

5.1.3 Particle Size and Morphology of the Spray-Dried Powders

The particle size of the spray-dried powders was measured by a Rodos/Helos laser diffraction system (Sympatec, NJ, USA) based on Fraunhofer theory following the procedure described in Li et al. (2016b). About 1 g of the powder sample was placed on top of the sample chute of the Rodos dispersing system and the sample chute was vibrated at a 100% setting, and 0.1 bar dispersion pressure was used to suck in the falling powder through the sample cell of the laser diffraction system. Spray-dried particles were placed on a glass slide and observed by Axio Scope.A1 polarized light microscope (PLM, Carl Zeiss Microscopy GmbH, Göttingen, Germany).

5.1.4 Solid Sate Characterization and Drug–polymer Interactions

To analyze the crystallinity of the as-received GF, HPC, Sol, spray-dried powders, and physical mixtures of GF–polymer with or w/o SDS (same formulation as stated in Table 5.1), XRPD (PANanalytical, Westborough, MA, USA), provided with Cu K_α radiation (λ= 1.5406 Å), was used. The samples were scanned at a rate of 0.165 s^{-1} for 2θ ranging from 5° to 40°. The total area under three distinct, non-overlapping peaks of GF at characteristic diffraction angles of 13.2, 14.6, and 16.5º was calculated for

both the physical mixtures and the spray-dried powders using the equipment's HighScore Plus software, which was then used to estimate the crystallinity.

DSC of the as-received GF, Sol, HPC, and spray-dried powders was performed using a Mettler-Toledo polymer analyzer (PolyDSC, Columbus, OH, USA) with integrated STARe 10 software. ~6.0–7.0 mg powder sample was placed in an aluminum pan with a hole in the lid and loaded into the DSC machine. As-received GF was heated at a rate of 10 °C/min from 25 °C to 250 °C. All other samples were heated from 25 °C to 70 °C and the temperature was held for 2 min at 70 °C, then cooled back to 25 °C to remove any residual solvent in the sample. In the final step, the samples were heated from 25 °C to 250 °C at 10 °C/min. Nitrogen gas was used as the purge gas and protective gas at a flow rate of 50 mL/min and 150 mL/min, respectively. Thermogravimetric analysis (TGA) was performed to measure the residual water/solvent content using a TGA/DSC1/SF Stare system (Mettler Toledo, Inc., Columbus, OH). ~6.0–7.0 mg of each spray-dried sample was placed in a ceramic crucible and heated from 25 °C to 150 °C at a heating rate of 10 °C/min under nitrogen flow.

Raman spectroscopy was conducted using a Fergie Imaging Spectrometer System (Princeton Instruments, Trenton, NJ) with a 500-mW external diode laser processing at 785 nm wavelength. Data acquisition time for all spectra was 15 s per scanned spectrum (100–1800 cm^{-1}) and each spectrum acquired was averaged over two scans. The data was presented for the range of 1550–1800 cm^{-1} wavenumber.

5.1.5 Drug Content in the Spray-Dried Powders and *In Vitro* Dissolution Tests

The drug content in the dried powders varied based on the drug:polymer mass ratios. To measure the actual drug content in the spray-dried powders, an assay testing was performed by dissolving 100 mg of the sample powders in 20 mL methanol under 30 min of sonication, followed by overnight storage to ensure complete solubilization of the GF particles. An aliquot of 100 µL was taken from the GF solution and diluted up to 10 mL using methanol. The absorbance of the samples was measured at 292 nm using UV spectrophotometer (Agilent, Santa Clara, CA, USA), and the drug concentration was calculated from a pre-established calibration curve. Six replicates were tested for each formulation to calculate mean drug content along with the relative standard deviation (RSD).

Drug release from the spray-dried powders and physical mixtures (PMs) prepared by blending was determined *via* a Distek 2100C dissolution tester (North Brunswick, NJ, USA), following the USP II paddle method. 1000 mL deionized water at 37 °C was stirred at 50 rpm paddle speed during the test. Two different doses i.e., 8.9 mg (non-supersaturating condition) and 100 mg (supersaturating condition) were tested for the dissolution performance of the spray-dried powders. Since the solubility of GF is 14.2 mg/L in water at 37 °C, a relatively low dose, i.e., 8.9 mg was selected to ensure non-supersaturating condition in the dissolution medium, which also could emulate low-dose (potent) drugs. The spray-dried powders were poured into the dissolution medium and 4 mL samples were taken out manually at 1, 2, 5, 10, 20, 30, and 60 min. These aliquots were filtered with a 0.1 µm PVDF membrane-type syringe filter before UV-spectroscopy measurements to minimize any confounding effect of undissolved drug. In a separate dissolution tests, 100 mg equivalent GF was

used to allow for supersaturation in the bulk dissolution medium, which was conducted for 210 min with additional sampling at 120, 180, and 210 min. The filtered samples were diluted with deionized water kept at 37 ºC at a ratio of 1 to 5 before UV measurement. Dissolved GF amount was measured by UV-vis spectroscopy at 296 nm wavelength and calculated using a pre-established calibration curve. Deionized water was used as blank before UV measurement, and six replicates were performed for each sample. In this paper, relative % supersaturation is reported based on GF concentration at 210 min and thermodynamic solubility of as-received GF particles, unless otherwise indicated.

5.1.6 Drug Wettability Enhancement by Sol and HPC Solutions With or W/O SDS

GF wettability by water, the dissolution medium, was investigated by analyzing the penetration rate of aqueous polymer/SDS solutions into a packed bed of GF particles inside a cylindrical column according to the modified Washburn method (Hołownia et al., 2008; Washburn, 1921). An Attension Sigma 700 (Biolin Scientific, Linthicum, MD, USA) was used to measure the mass of test liquid penetrated into the GF powder bed as a function of time. Experimental methods were adapted from Bilgili et al. (2018) and Li et al. (2017) (refer to Appendix D for details). In the current study, liquids and powder refer to GF-saturated aqueous solutions of 15% Sol/HPC with 0.125% SDS–w/o SDS, 0.125% SDS alone and as-received GF, respectively. All percentages are (% w/w) with respective to deionized water. The aqueous solution of the stabilizers and deionized water were saturated with griseofulvin (GF) and stirred overnight. After overnight stirring, the saturated solutions were used for further characterization. The apparent shear viscosity and surface tension of the liquids were measured using R/S

Plus Rheometer (Brookfield Engineering, Middleboro, MA, USA) and Attension Sigma 700 (Biolin Scientific, Linthicum, MD, USA), respectively. The ratio of the cosine of contact angles $\cos\theta_{ss}/\cos\theta_{w}$ was calculated using the modified Washburn equation and used as a wetting effectiveness factor. Here, θ_{ss} is the contact angle between GF and the GF-saturated polymer/SDS solutions and θ_{w} is the contact angle between GF and GF-saturated deionized water. This ratio was used as a rough measure of the drug wettability enhancement upon use of polymers (HPC/Sol) and SDS in water taking water as a basis of comparison.

5.1.7 Characterization of Drug Recrystallization in the Presence of Aqueous Medium

To elucidate GF recrystallization in the presence of water, a small portion of the spray-dried powders prepared using the solution-based (S) feed (S-HPC-1:3 and S-Sol-1:3) with and w/o SDS was gently pressed to form a loose compact, which was then mounted onto a microscopic glass slide, and placed under the polarized light microscope (PLM). 20 µL of deionized water was added to the sample and the PLM images were captured at 0, 1, 2, and 5 min from the moment of water addition.

5.2 Results and Discussion

We present and discuss the properties of the spray-dried powders (Section 5.2.1), solid state characterization of the drug and ASD formation in spray-dried powders (Section 5.2.2), as well as *in vitro* drug release from the ASDs and impact of SDS–polymer loading under non-supersaturating (Section 5.2.3) and supersaturating dissolution conditions (Section 5.2.4).

5.2.1 Size, Morphology, and Drug–Moisture Content of the Spray-Dried Powders

Although the residence time in the spray dryer is short, complete drying of the feed is expected due to the fast evaporation of the solvents from fine droplets, which originated from atomization of the feed suspension/solution at a higher temperature than the boiling point of the liquid at the inlet. Residual moisture content in the spray-dried powders was measured by TGA based on weight loss. Weight loss of 2.0 ± 0.3% was measured with TGA for all the samples, which confirmed that most of the solvents were removed during the spray drying. The actual (mean) drug content after spray-drying ranged from 14.6–15.1% for 1:5 GF:polymer powders, 21.5–24.4% for 1:3 GF:polymer powders, and 42.3–44.9% for 1:1 GF:polymer powder (refer to Table 5.2). As expected, an increase in polymer loading in the feed solutions led to lower drug content in the powders. The slight variation in the theoretical and actual drug content can be attributed to preferential drug loss during handling, poor separation of finer particles in the cyclone separator of the spray dryer, and presence of some residual moisture after drying (Azad et al., 2015b; Bilgili et al., 2018). The relative standard deviation (RSD) of drug content in all powders was less than 6.0%, signifying pharmaceutically acceptable content uniformity. The median sizes d_{50} of the spray-dried powders ranged from 10.9–22.6 μm (Table 5.2). An increase in polymer loading led to formation of coarser particles due to increase in total solids loading and higher viscosity of the feed (Bilgili et al., 2018; Li et al., 2018b; Poozesh and Bilgili, 2019). Unlike this clear and strong impact of polymer loading, the impact of SDS was weak: for a given polymer type/loading, the powders with SDS had slightly greater median sizes than the powders without SDS, except for S:Sol-1:3.

The microscopic images (Figure 5.1) illustrate that spray-dried particles have rounded–donut shapes, and their sizes are in rough agreement with the ranges mentioned in Table 5.2.

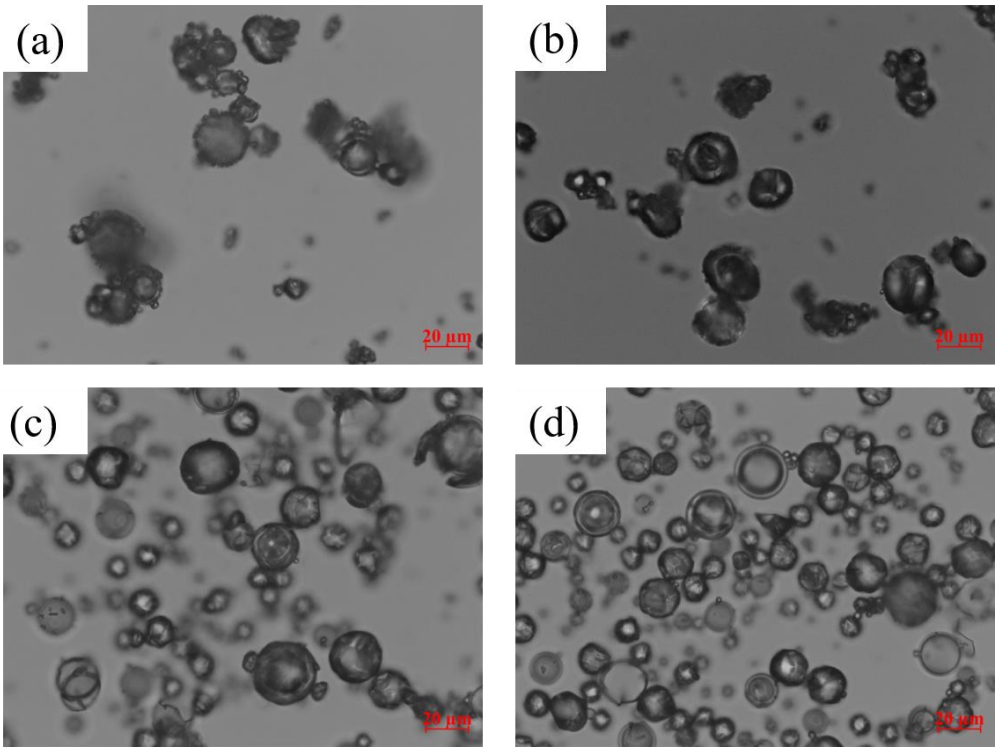

Figure 5.1 Light microscope images of the spray-dried particles prepared using the GF solution-based (S) feed with 1:3 GF:polymer mass ratio and 0.125% SDS/without SDS: (a) S-HPC-1:3, (b) S-HPC-1:3, SDS, (c) S-Sol-1:3, and (d) S-Sol-1:3, SDS. All images were taken at 50X magnification (scale bar: 20 µm).

Table 5.2 Particle Size Statistics of the Spray-Dried Powders and Their Drug Content

ID	Formulation[a]	Particle size statistics of the spray-dried particles (μm)			Theoretical drug content (% w/w)[b]	Actual drug content, RSD (% w/w, %)[b]
		d_{10}±SD	d_{50}±SD	d_{90}±SD		
S1	S-Sol-1:5	7.03±0.2	18.3±0.2	38.3±0.1	16.7	14.8, 1.79
S2	S-Sol-1:3	6.08±0.1	14.3±0.0	32.4±0.1	25.0	22.1, 1.76
S3	S-Sol-1:1	3.46±0.2	10.9±0.1	21.5±0.0	50.0	44.8, 3.46
S4	S-Sol-1:5, SDS	6.23±0.1	20.8±0.1	40.1±0.2	16.5	14.6, 4.45
S5	S-Sol-1:3, SDS	4.11±0.0	12.3±0.0	33.2±0.1	24.7	21.5, 2.02
S6	S-Sol-1:1, SDS	5.03±0.1	11.0±0.1	20.2±0.0	48.8	42.3, 2.21
S7	S-HPC-1:5	6.48±0.2	21.5±0.4	42.3±0.2	16.7	15.0, 2.65
S8	S-HPC-1:3	5.87±0.1	15.4±0.3	33.5±0.1	25.0	24.0, 1.51
S9	S-HPC-1:1	5.28±0.1	12.7±0.2	30.3±1.2	50.0	44.9, 1.67
S10	S-HPC-1:5, SDS	7.10±0.2	22.6±0.2	40.3±0.3	16.5	15.1, 3.30
S11	S-HPC-1:3, SDS	6.48±0.0	15.8±0.6	31.3±1.0	24.7	24.4, 2.56
S12	S-HPC-1:1, SDS	7.05±0.2	13.0±0.9	26.9±0.8	48.8	42.7, 0.73

[a]S denotes solution-based feed; Sol denotes Soluplus; the ratios refer to the drug:polymer mass ratios.
[b]% w/w with respect to the total weight of the solid content.

5.2.2 Formation of Drug ASDs Upon Spray Drying

To confirm the crystalline state of the drug (GF) in the final spray-dried powders, as-received GF (microparticles), polymers (HPC/Sol), spray-dried powders, and corresponding physical mixtures (PM) of the spray-dried powders were analyzed using XRPD (Figure 5.2) and DSC (Figure 5.3). Table 5.3 presents the summary of DSC thermal events and estimated crystallinity *via* XRPD. X-ray diffractograms (Figure 5.2) depict that as-received GF (microparticles) exhibited intense peak characteristics of a crystalline material, whereas HPC/Sol exhibited halo pattern indicating amorphous structure. The physical mixtures (PMs), prepared by blending, exhibited peaks at the same diffraction angles as those of as-received GF, albeit with reduced peak intensity, which can be attributed to the dilution and surface coverage of GF microparticles with HPC/Sol/SDS. On the other hand, XRPD diffractograms of all Sol-based spray-dried powders with and without SDS, regardless of polymer loading, showed halo pattern instead of any characteristic peaks of GF. These halo patterns confirm the formation of amorphous solid dispersion (ASD). Small peaks were visible in the XRPD diffractograms of S-HPC-1:3, S-HPC-1:1, and S-HPC-1:1, SDS powders, which had 27.7%, 11.5%, and 6.5% crystallinity, respectively (Table 5.3). Despite being largely amorphous, strictly speaking, these powders should be referred to as solid dispersions; but, for the sake of simplicity, we call all powders ASDs recognizing that some of them had notable crystalline content. The XRPD results overall suggest that (i) amorphous GF was molecularly dispersed in or solubilized by Sol matrix owing to their good miscibility even at 1:1 mass ratio regardless of the presence/absence of SDS, (ii) GF was only partially miscible with

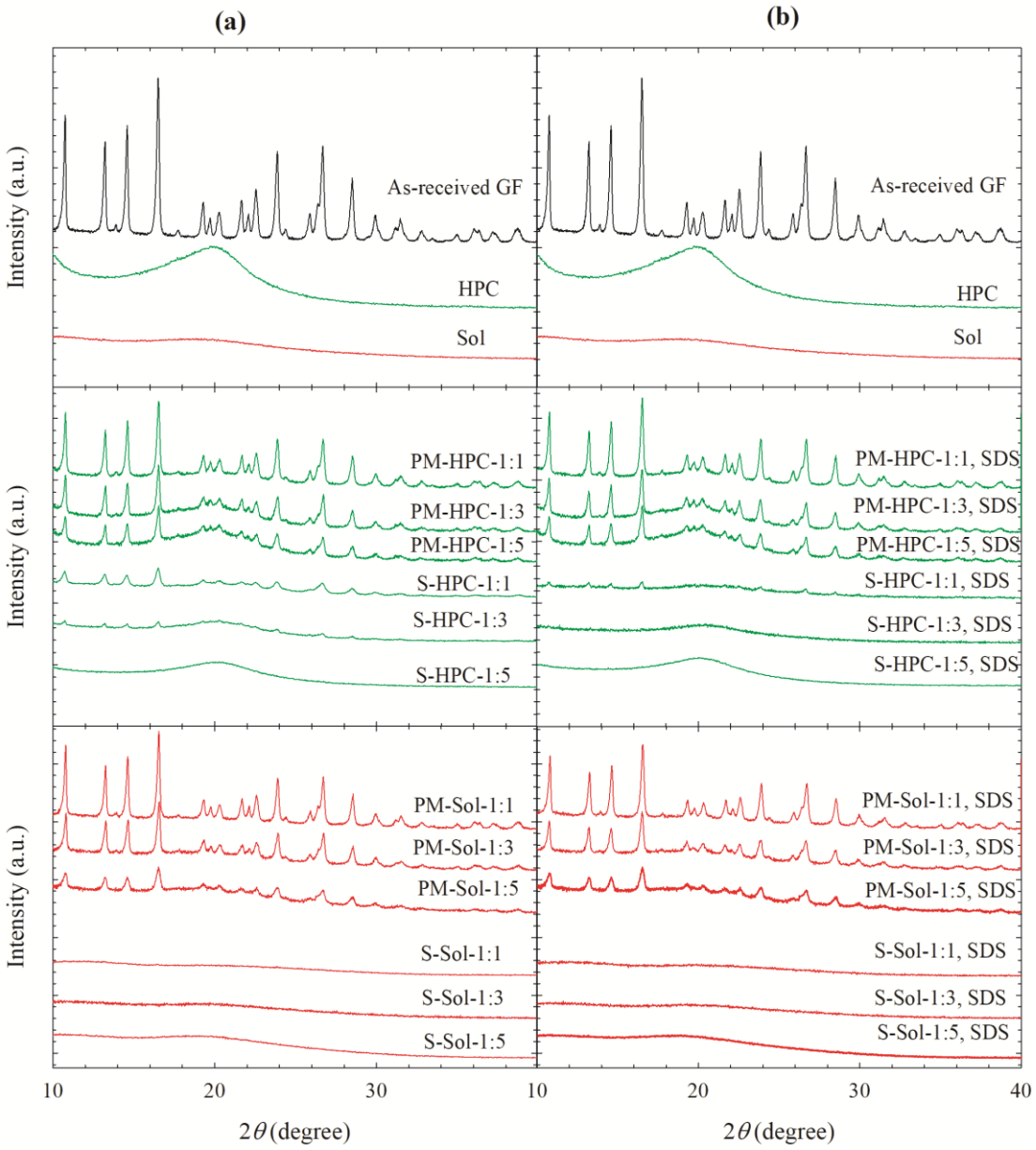

Figure 5.2 X-ray diffractograms of as-received GF, HPC, Sol, physical mixtures (PMs) of GF–HPC/Sol and the spray-dried powders prepared using the GF solution-based (S) feed with 1:1, 1:3, and 1:5 drug:polymer mass ratios: (a) without SDS and (b) with 0.125% SDS in the solution.

HPC, and required a high HPC loading (1:5 GF:HPC) to ensure formation of ASD; lower HPC loading could not prevent GF recrystallization during or right after spray drying, and (iii) SDS helped to disperse or solubilize GF in the HPC matrix, thus

allowing ASD formation at lower HPC loading (1:3 GF:HPC ratio). However, SDS could not prevent recrystallization when the GF:HPC mass ratio was 1:1. During spray drying, rapid evaporation of the solvents in the spray dryer increased viscosity instantaneously, resulting in kinetic arrest of the drug molecules in the amorphous polymer matrices, thus forming ASD (Baghel et al., 2016). Therefore, besides drug–polymer miscibility, fast drying kinetics in the spray dryer played a substantial role to produce ASD from solution-based (S) feeds, even for a partially miscible (GF–HPC) system.

The DSC thermograms in Figure 5.3 show an endothermic peak associated with melting of as-received GF, with a T_m of 220.1 °C and ΔH_f of 101.8 J/g; a glass transition for Sol (amorphous) at 72.4 °C, and a slight endothermic event around 170–200 °C for HPC likely due to the melting of the small crystalline domain of largely amorphous HPC (Sarode et al., 2013) (crystallinity was undetectable by XRPD). The T_g of HPC could not be measured (in the range of –25 to 0 °C (Sarode et al., 2013)) due to limitation of our equipment. A single T_g was observed confirming the formation of molecular level dispersion (Luebbert et al., 2017; Wlodarski et al., 2015) in all powders except S-HPC-1:1 with 28% GF crystallinity (see Table 5.3). While S-Sol-1:3, SDS, S-Sol-1:5, SDS, and S-Sol-1:5 exhibited only a glass transition, all other ASDs exhibited a glass transition followed by an exothermic event due to re-crystallization of amorphous GF, which was followed by the melting of the recrystallized GF (Figure 5.3a and Figure 5.3b). Recrystallization of GF from ASDs can occur during the heating step of DSC scan because above T_g amorphous drug molecules and amorphous polymer had higher mobility. The absence of

recrystallization and higher temperature of recrystallization transition T_{rc} (if it occurred at all) in the Sol-based powders than HPC-based powders suggest better miscibility and stronger molecular interactions between Sol–HPC than HPC–GF.

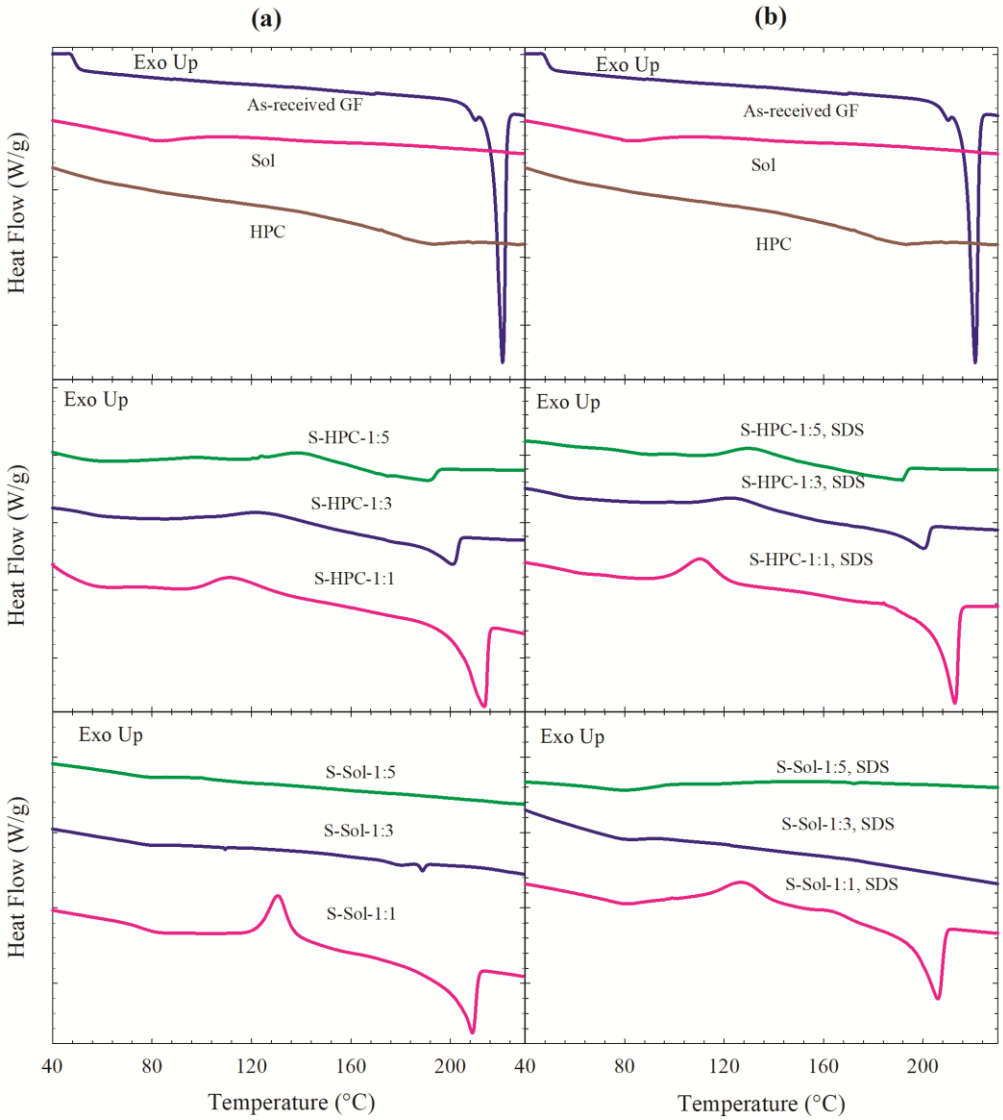

Figure 5.3 DSC thermograms of as-received GF, HPC, Sol, and the spray-dried powders prepared using the GF solution-based (S) feed with 1:1, 1:3, and 1:5 drug:polymer mass ratios: (a) without SDS and (b) with 0.125% SDS in the solution.

Table 5.3 Characteristic Temperatures–Enthalpy Values Obtained From DSC Thermograms and Crystallinity Estimated From XRPD Diffractograms

ID	Formulation[a]	T_g (ºC)[a,b]	T_{rc} (ºC) [a,b]	ΔH_{rc} (J/g) [a,b]	T_m (ºC) [a,b]	ΔH_f (J/g) [a,b]	Crystallinity (%)[b]
S1	S-Sol-1:5	80.6	ND	ND	ND	ND	ND
S2	S-Sol-1:3	80.4	ND	ND	189	0.64	ND
S3	S-Sol-1:1	77.7	131	–14.1	209	23.2	ND
S4	S-Sol-1:5, SDS	77.4	ND	ND	ND	ND	ND
S5	S-Sol-1:3, SDS	80.0	ND	ND	ND	ND	ND
S6	S-Sol-1:1, SDS	74.6	127	–9.26	206	25.4	ND
S7	S-HPC-1:5	52.9	139	–3.35	192	6.64	ND
S8	S-HPC-1:3	53.2	122	–4.36	201	13.2	11.5
S9	S-HPC-1:1	ND	111	–8.90	213	34.3	27.7
S10	S-HPC-1:5, SDS	51.7	130	–2.43	191	5.68	ND
S11	S-HPC-1:3, SDS	57.7	124	–1.71	200	10.5	ND
S12	S-HPC-1:1, SDS	58.9	109	–20.0	213	40.6	6.5

[a]S denotes solution-based feed, Sol denotes Soluplus; the ratios refer to the drug:polymer mass ratios. Other symbols: T_g, T_{rc}, and T_m stand for temperature for glass transition, recrystallization transition, and melting point, respectively, while ΔH_{rc} and ΔH_f respectively stand for recrystallization enthalpy and fusion enthalpy.
[b]ND: not detected.

For HPC-based powders, T_{rc} increased (recrystallization delayed to higher temperature) and ΔH_{rc} decreased when a higher polymer loading was used, which is in line with other studies (e.g., Wlodarski et al., 2015).

GF crystals have a T_m of 220.1 °C. The powders, whose DSC thermograms exhibited an endotherm due to melting of the existing GF crystals and/or GF crystals formed during the heat treatment of the DSC scan, also exhibited significant melting point depression (Figure 5.3). The significant melting point depression in drug–polymer mixtures is an indicator of drug–polymer miscibility (Baird et al., 2012; Newman et al., 2008). Table 5.3 indicates that higher polymer loading (lower GF:polymer mass ratio) led to lower T_m as compared with the as-received GF crystals, higher melting point depression, and lower ΔH_f, regardless of the presence/absence of SDS. Moreover, without exceptions, having identical polymer/SDS composition, the spray-dried powders with Sol had either no melting point or had a higher melting point depression and lower ΔH_f than those with HPC, which could be explained by (i) stronger molecular interactions and better miscibility for GF–Sol than GF–HPC, (ii) higher initial amorphous content in the Sol-based powders than in the HPC-based powders, and (iii) higher extent of drug solubilization during the thermal treatment when the polymer loading was higher. Compared with the clear trends regarding the impact of polymer loading for formulations with/without SDS, the trends for SDS impact were not as strong. At the same loading for a given polymer, the presence of SDS either led to disappearance of the melting point or slightly higher melting point depression, which suggests that SDS appears to help GF molecular dispersion or solubilization. These findings from DSC

thermograms are largely in agreement with the findings from the XRPD diffractograms regarding the impacts of GF–polymer miscibility and the impact of polymer loading and presence of SDS on the solid state of GF.

The observed Raman spectra in Figure 5.4 for as-received GF and PMs of GF are largely in agreement with Fourier transform Raman data of ref. (Feng et al., 2008) and Raman data of ref. (Żarów et al., 2011) for crystalline GF. The Raman spectra of all the spray-dried samples (Figure 5.4) show that the GF line at 1606 cm^{-1} disappeared, and the peaks at other characteristic frequencies shifted to new positions that are characteristic of amorphous GF, e.g., the peak shift from 1623 to 1620 cm^{-1} (see Żarów et al., 2011), signifying formation of amorphous GF and molecular level interactions between GF and polymers in the ASD. While the GF line at 1606 cm^{-1} disappeared in the Raman spectra of S-HPC-1:3 with and w/o SDS (Figure 5.4a and Figure 5.4b), the shifts in other peaks were subtler than those for the Raman spectra of S-Sol-1:3 with and w/o SDS, which could suggest stronger molecular interactions between GF–Sol than GF–HPC.

It is suggested that if the solubility parameter difference between a drug and polymer is <7.0 $MPa^{1/2}$, they are likely to be miscible; if the difference is >10 $MPa^{1/2}$, they are considered immiscible, and if the difference is in between 7.0 and 10, they exhibit partial miscibility (Forster et al., 2001; Greenhalgh et al., 1999). The solubility parameters of GF, HPC, and Sol are 12.2 (Thakral and Thakral, 2013), 24.0 (Choi et al., 1994), and 19.4 (Kolter et al., 2012) $MPa^{1/2}$, respectively. The solubility parameter differences between GF–Sol and GF–HPC are 7.2 and 11.8 $MPa^{1/2}$, respectively, which suggests that GF–Sol is borderline miscible, whereas GF–HPC is

immiscible. The solubility parameter prediction is fairly accurate for Sol–GF as XRPD, DSC, and Raman spectroscopy results suggests GF–Sol are miscible and molecularly interact more than GF–HPC. However, GF–HPC exhibits partial miscibility unlike what the solubility parameters of GF–HPC suggest. As the

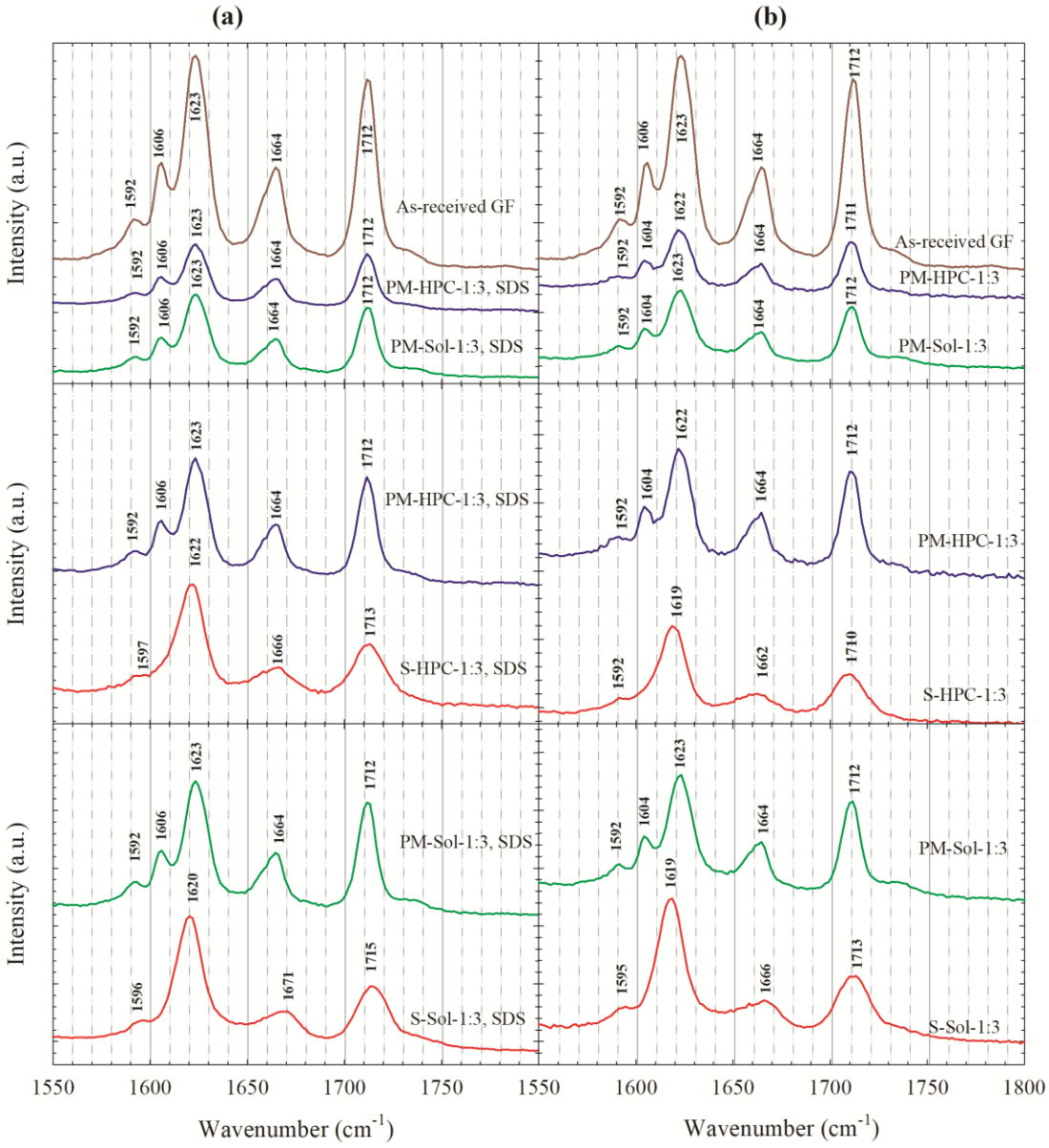

Figure 5.4 Raman spectra of as-received GF, physical mixtures (PMs) of GF–HPC/Sol at 1:3 drug:polymer ratio, and the spray-dried powders prepared using the GF solution-based (S) feed with 1:3 GF:polymer mass ratio: (a) with 0.125% SDS and (b) without SDS in the solution.

theoretical models behind the solubility parameter prediction are applicable for simple molecular structures wherein van der Waals force plays a predominant role, while for drug–polymer systems which are known to form highly directional interactions (e.g., hydrogen bonding) or long range interactions (e.g., ionic interaction), this approach can be erroneous (Ambike et al., 2005; Forster et al., 2001). Indeed, the absence of diffraction peaks in XRPD in several HPC-based powders and significant melting depression in DSC along with the Raman line shifts suggest that HPC molecularly interacts with GF, resulting in partial miscibility unlike the prediction from the solubility parameters.

5.2.3 Dissolution Performance of the Spray-Dried Powders Under Non-Supersaturating Condition

The temporal evolution of GF release from the spray-dried powders and the PM with the highest polymer loading (1:5 GF:polymer) containing 8.9 mg equivalent GF dose in 1000 mL deionized water at 37 ºC was investigated. The bulk dissolution medium will not supersaturate for this low drug dose as the GF solubility is 14.2 mg/L. We note from Figure 5.5 that as-received (micronized) GF microparticles with d_{50}: 9.74 ± 0.23 µm and d_{90}: 27.4 ± 0.1 µm dissolved very slowly: <20% GF dissolved at 20 min and <33% at 60 min. The mere blending of as-received GF particles with HPC/Sol (1:5 GF:polymer mass ratio) with and without SDS, i.e., led to the physical mixture, which enhanced GF release rate. This could be partly explained by the wetting enhancement of the hydrophobic drug (GF) in the presence of dissolved HPC/Sol–SDS (see Table 5.4) and deaggregation of the large drug aggregates present in the as-received drug (Letchford and Burt, 2007), and partly by the higher solubility of GF in the dissolution medium. For example, the thermodynamic solubility of the GF

microparticles at 37 °C was measured to be 14.2 mg/L, 17.8 mg/L, and 18.3 mg/L in the deionized water, aqueous medium of 1:3 GF:Sol with SDS, and aqueous medium of 1:3 GF:HPC with SDS, respectively.

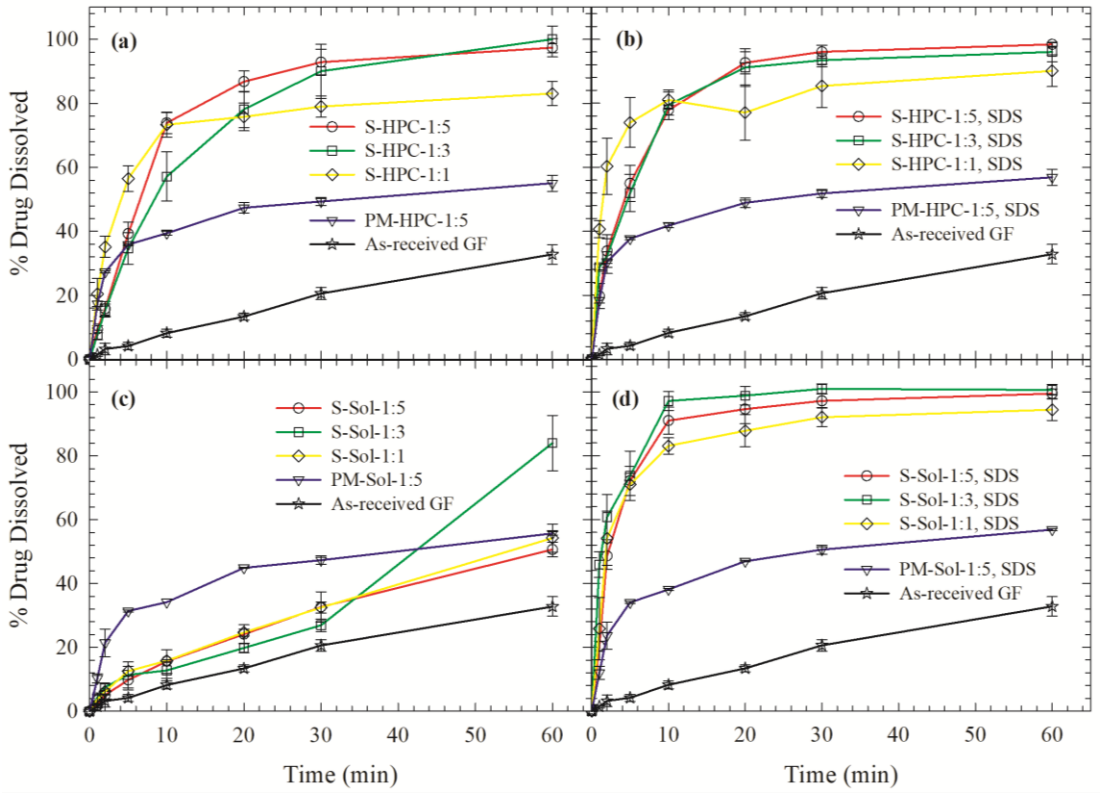

Figure 5.5 Evolution of drug release from as-received GF, physical mixture (PM) with 1:5 GF:polymer mass ratio, and spray-dried powders prepared using GF solution-based (S) feeds with 1:1, 1:3, and 1:5 drug:polymer mass ratios: (a) HPC without SDS, (b) HPC with SDS, (c) Sol without SDS, and (d) Sol with SDS. Dissolution sample size equivalent to 8.9 mg GF dose (low dose, non-supersaturating condition in the bulk dissolution medium).

Table 5.4 Properties of Drug-Saturated Deionized Water and Aqueous Polymer–SDS Solutions and Wetting Effectiveness Factor Determined Using the Modified Washburn Method

Formulation	η (cP)	ρ (g/mL)	γ (mN/m)	Slope, (g^2/s)	R^2	$\cos\theta_{ss}/\cos\theta_w$
Water	0.89	1.00	66.5	7.0×10^{-3}	0.990	1.00
SDS	0.94	1.00	37.1	7.2×10^{-3}	0.975	1.94
Sol	8.76	1.01	41.4	1.2×10^{-3}	0.989	2.65
Sol–SDS	13.5	1.01	40.5	1.5×10^{-3}	0.991	4.65
HPC	53.2	1.01	39.9	1.5×10^{-3}	0.998	20.9
HPC–SDS	58.3	1.01	34.8	2.4×10^{-3}	0.999	42.1

The spray-dried powders released GF faster than the PM (except S-Sol powders without SDS, see Figure 5.5c) owing to the presence of amorphous GF in the former that has higher kinetic solubility than crystalline GF in the PM. The poor wettability of S-Sol formulation hindered the dissolution of Sol and erosion of the spray-dried particles, which in turn retarded the drug release. Inclusion of SDS in the ASDs led to significant increase in the rate of GF release, but the increase was more notable for the Sol-based ASDs than the HPC-based ASDs. The analysis of the wetting effectiveness factors obtained from the modified Washburn method (Table 5.4) shed some light on this observation. Presence of SDS has almost doubled the wetting effectiveness of the dissolved polymer in water and the rank order of wettability enhancement is HPC–SDS > HPC > Sol–SDS > Sol > SDS, which is in accordance with the hydrophilic nature of HPC and amphiphilic nature of Sol. Hence, poor wettability of Sol-based ASDs was mitigated upon incorporation of SDS, which led to significant dissolution improvement. On the other hand, HPC-based ASDs did not significantly benefit from the incorporation of SDS as HPC is hydrophilic. The initial fast GF release within 10 min followed by a much slower dissolution in the

following 50 min for S-HPC-1:1 (Figure 5.5a) and S-HPC-1:1, SDS (Figure 5.5b) could be explained by their smallest particle sizes among the S-HPC formulations (see Table 5.1), which led to initial fast release of amorphous GF followed by the slow dissolution of their crystalline component, i.e., 27.7% and 6.5%, respectively (see Table 5.2).

5.2.4 Dissolution Performance of the Spray-Dried Powders Under Supersaturating Condition

The temporal evolution of GF release from the spray-dried powders and the PM with the highest polymer loading (1:5 GF:polymer) containing 100 mg equivalent GF dose in 1000 mL deionized water at 37 ºC was investigated. The bulk dissolution medium could supersaturate for this high drug dose as the GF solubility is 14.2 mg/L. Unless otherwise specified, all supersaturation values are relative to aqueous thermodynamic solubility of GF and calculated at 210 min. Figure 5.6 shows that only slight supersaturation (max. ~50%) was achieved fast upon dissolution of HPC-based ASDs. An increase in polymer loading (lower GF:HPC mass ratio) led to slight increase in the supersaturation attained. Similarly, presence of SDS only increased supersaturation for the lowest HPC S-HPC-1:1; at higher polymer loadings, the effect of SDS was not notable. A cursory look at Figure 5.7 and Figure 5.6 suggests that Sol-based ASDs exhibited higher GF supersaturation than HPC-based ASDs, and inclusion of SDS as a minor component of ASD had a drastic impact on the attainment of high supersaturation fast: e.g., 430% supersaturation at 30 min for S-Sol-1:5, SDS, which attained 570% supersaturation at 180 min. In fact, that ASD maintained supersaturation way above 430% for 180 min.

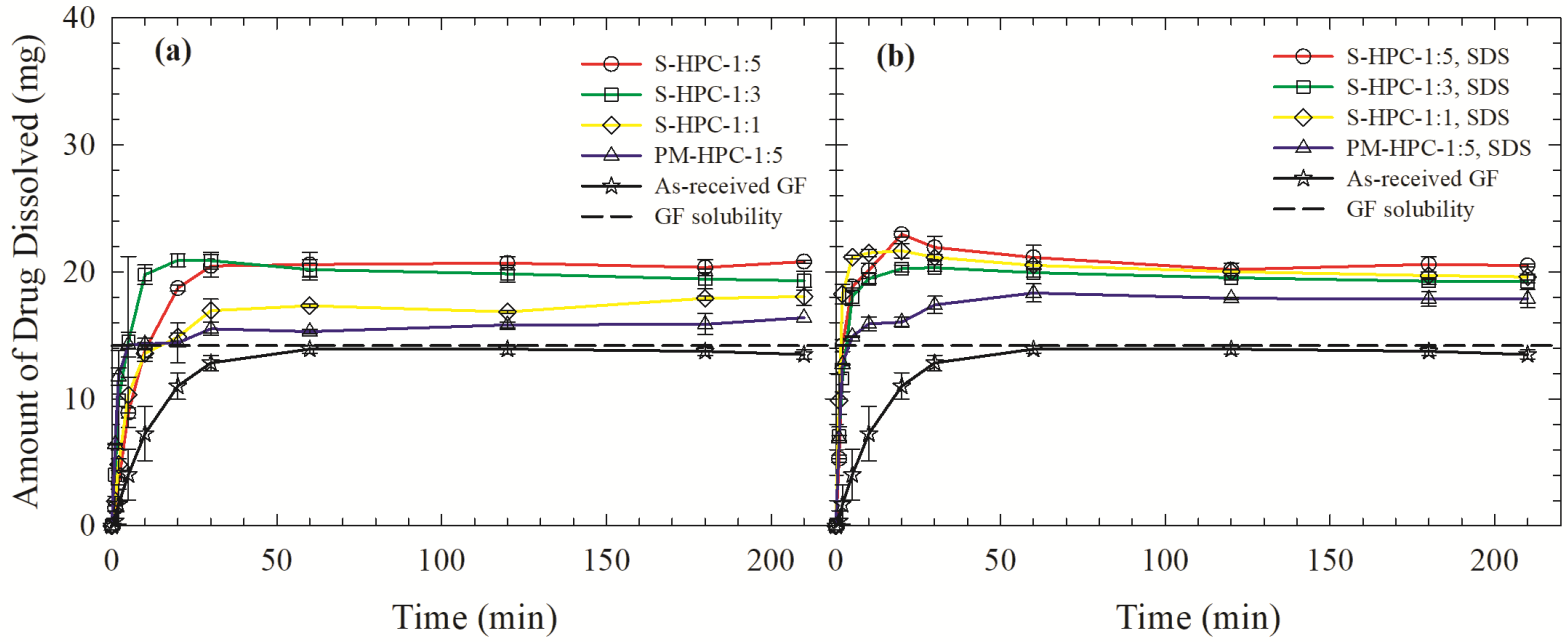

Figure 5.6 Evolution of drug release from as-received GF, physical mixture (PM) with 1:5 GF:HPC mass ratio, and spray-dried powders prepared using GF solution-based (S) feeds with 1:1, 1:3, and 1:5 GF:HPC mass ratios: (a) HPC without SDS, (b) HPC with SDS. Dissolution sample size equivalent to 100 mg GF dose (high dose, supersaturating condition in the bulk dissolution medium).

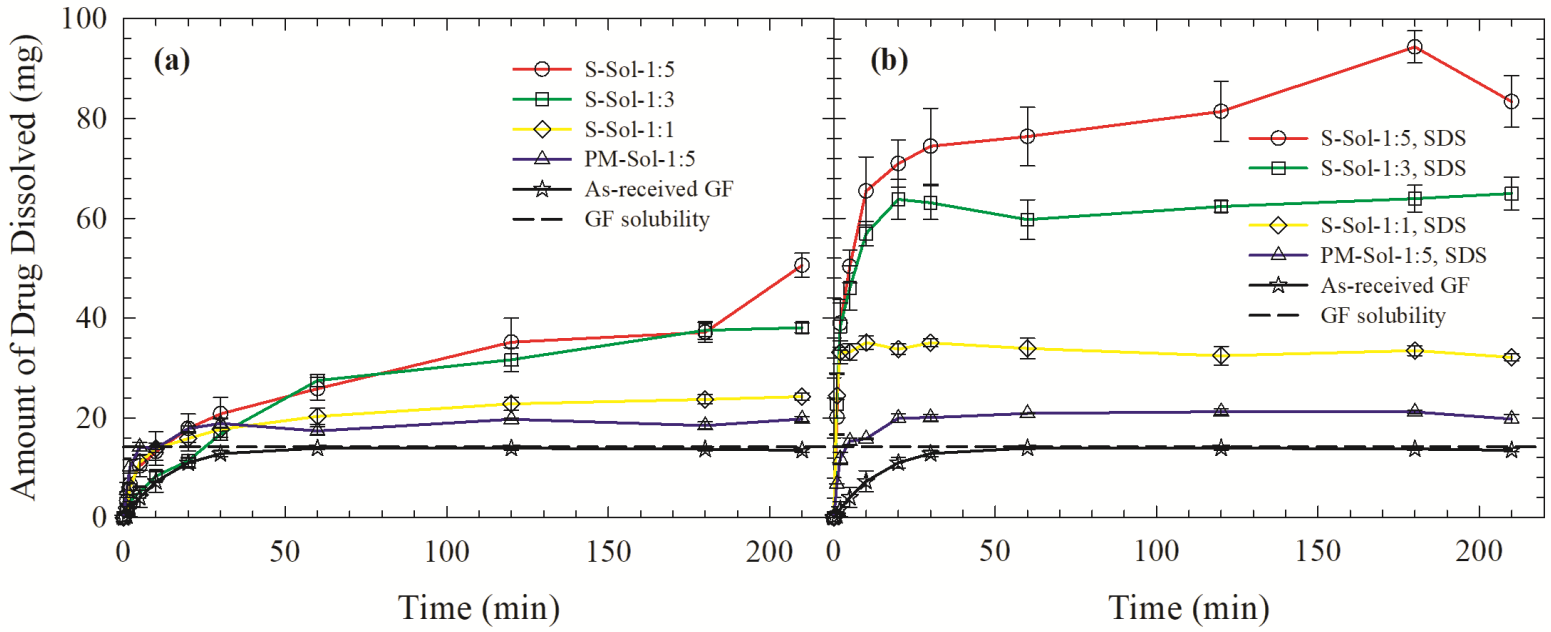

Figure 5.7 Evolution of drug release from as-received GF, physical mixture (PM) with 1:5 GF:Sol mass ratio, and spray-dried powders prepared using GF solution-based (S) feeds with 1:1, 1:3, and 1:5 GF:Sol mass ratios: (a) Sol without SDS, (b) Sol with SDS. Dissolution sample size equivalent to 100 mg GF dose (high dose, supersaturating condition in the bulk dissolution medium).

Maintaining the API in its amorphous state without precipitation during the intestinal transit time (>180 min) would often be sufficient for achieving the necessary bioavailability (Matsui et al., 2016).

The remarkably high GF supersaturation achieved by Sol-based ASDs as compared with HPC-based ASDs can be explained by the higher GF solubilization in Sol micelles, which increased with a higher Sol loading, and excellent GF recrystallization inhibition imparted by Sol as compared with HPC. To make the latter point more lucid, let us examine the PLM images (Figure 5.8) of loose ASD compacts imbibed with a 20 µL deionized water droplet. The addition of water to S-HPC-1:3, SDS compact (Figure 5.8a) and S-HPC-1:3 compact (Figure 5.8c) resulted in immediate dissolution of the compact and recrystallization of amorphous GF (see the shiny crystals in the respective images). On the other hand, for S-Sol-1:3, SDS compact (Figure 5.8b) and S-Sol-1:3 (Figure 5.8d), the swollen ASD particles eroded from the compact gradually released amorphous GF from the Sol matrix. The images show spherical, swollen ASD particles. Even after 5 min of water addition, no recrystallization of the amorphous GF observed, which implies that the phase separation did not occur and the undissolved ASD powders stayed in the amorphous form and facilitated the supersaturation generation of GF (Figure 5.8b and Figure 5.8c). It is inferred from these observations that due to fast and extensive recrystallization of GF in HPC-based ASDs upon exposure to water and low thermodynamic solubility of the GF crystals, only limited supersaturation was achieved by HPC-based ASDs.

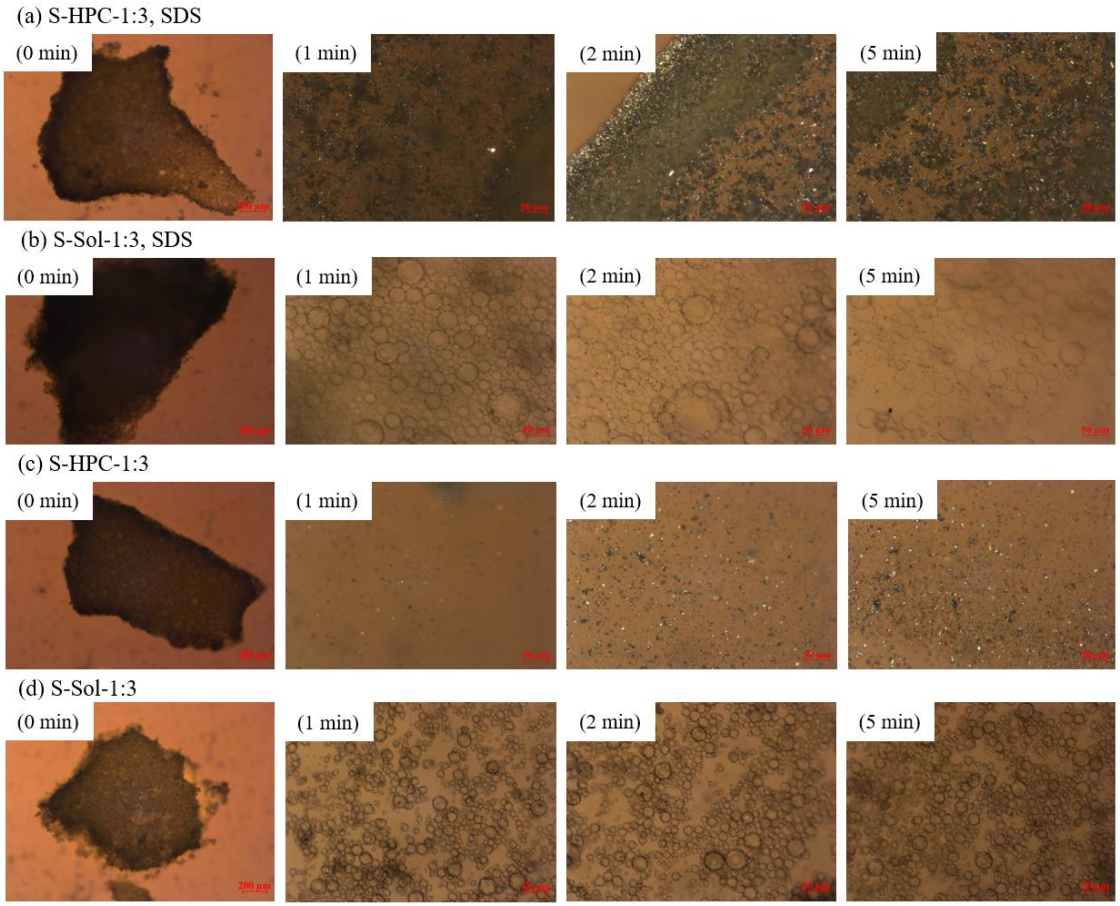

Figure 5.8 PLM images of a loose compact of the spray-dried ASD particles with 1:3 drug:polymer mass ratio in 20 µL deionized water: (a) HPC with SDS, (b) Sol with SDS, (c) HPC without SDS, and (d) Sol without SDS. The images were taken at 0 (before adding water), 1, 2, and 5 min after the addition of deionized water addition. Except 0 min image (5X magnification, scale bar: 200 µm), which focused on the compact, all other images focused on particles that emanated from the surface, which were captured at 20X magnification (scale bar: 50 µm).

To gain further insights into the GF recrystallization and supersaturation maintenance, desupersaturation experiments were performed *via* the solvent-shift method. 20 mL of 5 mg/mL GF solution in acetone was mixed with 1000 mL of aqueous solutions of 100 µg/mL, 300 µg/mL, and 500 µg/mL polymer with 0.0005%/0.125% SDS or without SDS. These concentrations and volume correspond to the formulation of fully dissolved ASDs with 1:1, 1:3, and 1:5 GF:polymer mass ratio, respectively, and SDS in the dissolution medium or in the initial solution fed to the spray dryer. The addition of GF solution led to a supersaturation spike; 76–99 µg/mL GF dissolved within 2 min (see Figure 5.9). HPC with or w/o SDS could not prevent depletion of supersaturation (desupersaturation) due to recrystallization of GF. It appears that for HPC-based ASDs, SDS promoted nucleation (earlier commencement of desupersaturation), but led to slower GF desupersaturation. In the absence of polymers, SDS alone also promoted nucleation, but appeared to cause slightly slower desupersaturation compared to the desupersaturation without any inhibitor. Finally, Sol was able to maintain high GF supersaturation for at least 180 min with a small drop at 210 min. The presence of SDS and higher Sol led to slightly higher supersaturation; but, these differences are small and within the experimental errors. In the presence of 0.125% SDS alone or with 500 µg/mL Sol in the dissolution medium, very fast nucleation and recrystallization occurred (see Figure 5.9b), which confirms that high concertation of SDS promotes recrystallization from the supersaturated GF solution. In summary, no adverse impact of SDS on GF recrystallization was observed when it was used along with Sol as a minor component (e.g., 1:3:0.05 GF:Sol:SDS). SDS promoted drug recrystallization in the presence of

PVP-VA (Liu et al., 2016) and crystal growth in the presence of PVP (Mosquera-Giraldo et al., 2014). These adverse effects could be absent partly due to low SDS concentration in the desupersaturation and dissolution tests (SDS being a minor component in the ASD) besides the specific interactions among GF–Sol–SDS.

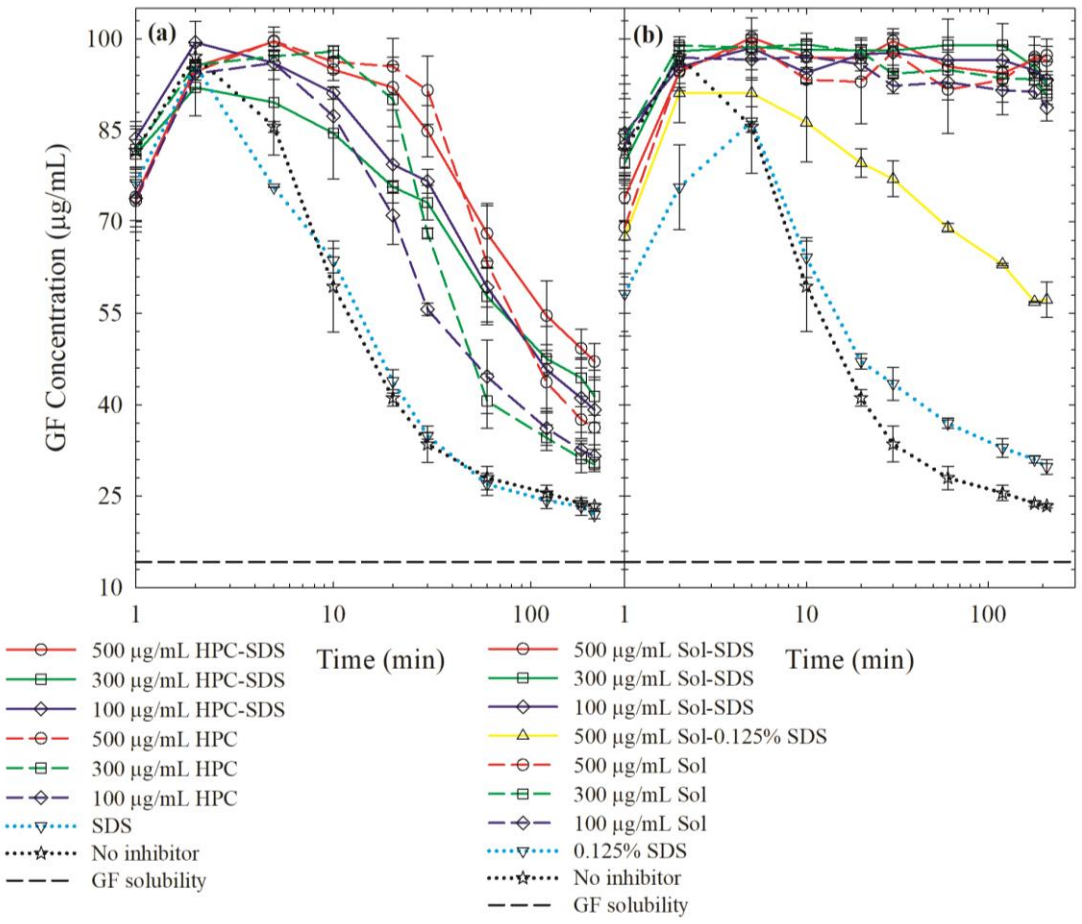

Figure 5.9 GF desupersaturation curves for a supersaturated 20 mL GF–acetone solution mixed with 1000 mL aqueous solution of 500 µg/mL, 300 µg/mL, and 100 µg/mL of HPC/Sol–SDS or w/o SDS (corresponding to 1:5, 1:3, and 1:1 drug:polymer formulations), SDS only, and deionized water without any recrystallization inhibitor: (a) HPC, and (b) Sol. Unless otherwise indicated, 0.0005% w/v (5 µg/mL) SDS was used for the formulation with SDS. With 500 µg/mL Sol, both 0.0005% w/v and 0.125% w/v SDS were used. The initial concentration of GF right after mixing was targeted at 100 µg/mL.

It is well-established that depending on the drug–polymer miscibility and interactions, amorphous drug may phase-separate and recrystallize upon contact of ASDs with water in the dissolution medium (Alonzo et al., 2011; Chen et al., 2015). Once imbibed into the ASD matrix, water acts as a plasticizing agent, enhancing the mobility of the drug molecules by reducing the T_g of the ASD (Chen et al., 2015). HPC-SSL has sub-ambient T_g (Sarode et al., 2013) (lower than T_g of Sol: 73 ± 2 °C) and its ASDs have lower T_g than Sol-based ASDs (see Table 5.3). Moreover, due to partial immiscibility of HPC with GF, its relatively weak molecular interactions with GF as compared with Sol (miscible with GF), as well as its poor GF nucleation/crystal growth inhibition (refer to Figure 5.9), it is no surprise that the amorphous GF recrystallized from HPC-based ASDs during the dissolution test, which also explains the drastically lower supersaturation generated by HPC-based ASDs than by Sol-based ASDs. PLM images of a loose compact of the ASD particles in Figure 5.8 corroborated the formation of GF crystals from S-HPC-1:3 ASD upon its exposure to water, whereas no recrystallization was observed for S-Sol-1:3.

To further elucidate the impact of SDS in Sol-based ASDs, S-Sol-1:5 (without SDS) was dissolved in 1000 mL of deionized water, aqueous solution of 0.0005% SDS solution, aqueous solution of 0.125% SDS solution. In these cases, SDS was introduced to ASDs externally, outside the ASD particles. In S-Sol-1:5, SDS, the SDS was in the ASD particles, whose dissolution in water would yield a 0.0005% SDS. Figure 5.10 shows that the external addition of 0.0005% SDS significantly improved the GF release of S-Sol-1:5, which corroborates the wettability

enhancement mechanism. Adding 0.125% SDS led to even faster supersaturation due to faster wettability; however, the released GF recrystallized, which is in line with the desupersaturation test (Figure 5.9b). When too much surfactant is used either in the ASD or in the dissolution medium, SDS molecules compete with drug molecules to interact with Sol molecules, which interferes with the crystallization inhibiting capability of Sol, leading to GF recrystallization (Liu et al., 2016). The fastest supersaturation occurred when SDS was internally added or incorporated into the ASD (S-Sol-1:5, SDS dissolution in water). It is likely that the presence of SDS in the ASD particle led to faster wettability enhancement as the GF is already available at the surface locally obviating the need for SDS molecules adsorbing onto ASD microparticles from the dissolution medium. Also, the higher local SDS concentration in the ASD particle and its boundary layer will facilitate water imbibition into Sol matrix and its faster erosion, leading to faster release of GF. Interestingly, despite exhbiting a much slower build-up of superstation in 0.0005% SDS solution, S-Sol-1:5 ASD (without SDS) tend to a plateau supersaturation at 210 min, which is slightly below the supersaturation achieved by S-Sol-1:5, SDS ASD (with SDS) in water. This finding suggests that having the SDS along with GF–Sol in the ASD led to slightly higher kinetic solubility of GF in Sol–SDS of the ASD.

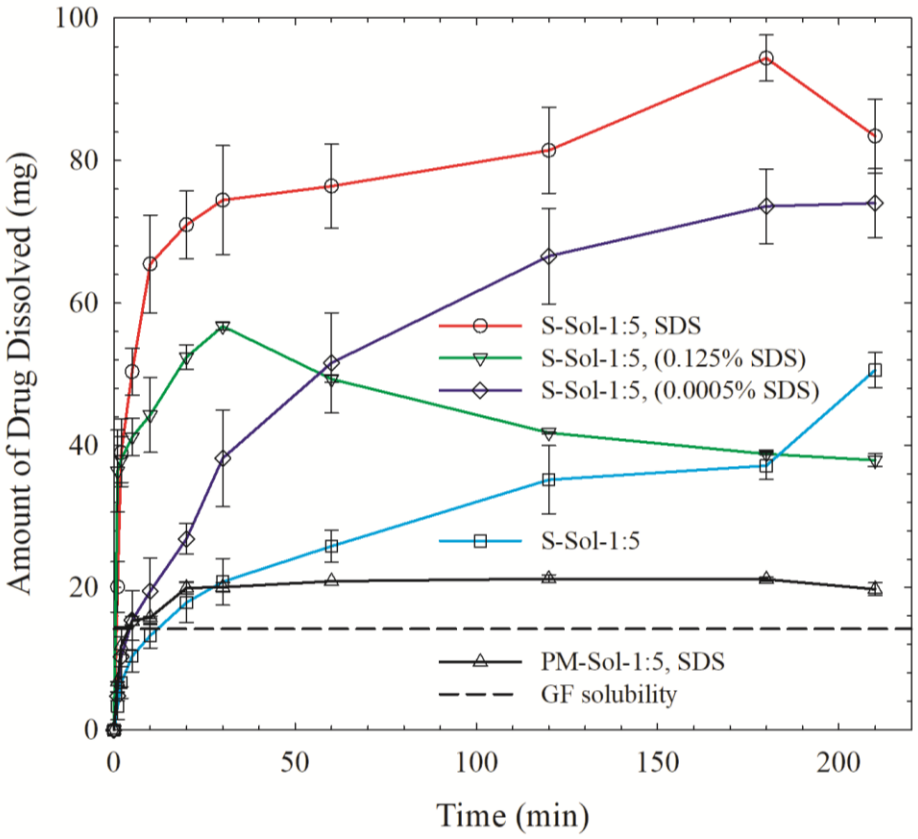

Figure 5.10 Evolution of drug release from physical mixture (PM) with SDS and spray-dried powders prepared using GF solution-based (S) feeds with 1:5 drug:polymer mass ratio with and without SDS in the formulation. Deionized water was used as the medium for the formulation with SDS (S-Sol-1:5, SDS) and physical mixture. For the formulation without SDS (S-Sol-1:5), aqueous solution of 0.125% w/v SDS, aqueous solution of 0.0005% w/v SDS, and deionized water were used as dissolution media. Dissolution sample size equivalent to 100 mg GF dose (high dose, supersaturating condition in the bulk dissolution medium).

5.3 Conclusions

We have demonstrated that the use of SDS as a minor component along with a drug-miscible polymer (Sol) as major component, which provides significant solubilization of the drug (GF) and supersaturation maintenance *via* recrystallization inhibition, could boost drug supersaturation from the ASDs *via* mainly wettability enhancement and some additional drug solubilization. The ASD with 1:5:0.05 GF:Sol:SDS

composition achieved 430% GF supersaturation within 30 min and maintained it for 3 h. Unlike the use of SDS as carriers/solubilizers, the use of SDS as a minor component dramatically improved the wettability of the ASD, without having any deleterious impact on drug recrystallization, which is a common problem in polymer–surfactant carrier systems. Also, the use of such low concentrations of SDS even in high-dose applications of ASDs alleviates any concern associated with the toxicity of anionic surfactants.

The high GF supersaturation was only possible owing to the highly favorable properties of Sol because very limited supersaturation was achieved by HPC-based ASDs with or without SDS. Sol-based ASDs have higher T_g owing to higher T_g of Sol (73 ± 2 °C) than HPC-SSL; Sol has greater miscibility and stronger molecular interactions with GF, as revealed by XRPD, DSC, and Raman spectroscopy analysis; and it is an excellent GF recrystallization inhibitor, as suggested by the desupersaturation experiments. The only drawback of Sol was its amphiphilic nature, and ensuing poor wettability of the Sol-based ASDs that contain a hydrophobic drug. Adding SDS as a minor component alleviated that problem, which enabled fast supersaturation from Sol-based ASDs. A future study entails examining the stability of these ASD formulations and optimizing the SDS concentration for various high drug doses. Also, the generality of the use of anionic surfactants as a minor component will be tested with other drug–polymer–surfactants to assess supersaturation generation–maintenance benefits.

CHAPTER 6

SYNERGISTIC EFFECTS OF HYDROPHILIC POLYMER–AMPHIPHILIC POLYMER COMBINATION IN ENHANCING GRISEOFULVIN RELEASE FROM AMORPHOUS SOLID DISPERSIONS

As discussed in Chapter 1, formulating an amorphous solid dispersion (ASD) with high drug loading that releases drug rapidly, while generating and maintaining high supersaturation over at least three hours is challenging. To overcome this challenge in this study, we prepared ternary drug ASDs using a combination of a hydrophilic polymer that provides significant wettability enhancement to drug and an amphiphilic polymer that provides supersaturation maintenance and compared their *in vitro* dissolution release to binary drug ASDs prepared using each polymer separately. Griseofulvin (GF) was selected as a challenging, fast-crystallizing poorly soluble drug; hydroxypropyl cellulose (HPC) and Kollidon VA64 (VA64) were the hydrophilic polymers, while Soluplus® (Sol) was the amphiphilic polymer. In the ASDs, GF:total polymer mass ratio was fixed at 1:3 to yield 25% GF loading. XRPD, DSC, and Raman spectroscopy confirmed the formation of ASDs from GF–Sol, GF–HPC, and GF–VA64 and their binary polymer combinations. Sol-based ASD generated supersaturation very slowly and achieved 170% supersaturation in 210 min. HPC-based ASD exhibited fast recrystallization in the matrix; whereas VA64-based ASD achieved 220% supersaturation in 10 min followed by rapid desupersaturation due to recrystallization in the medium. The modified Washburn experiments revealed the significant wettability enhancement of GF by HPC/VA64 and inadequate enhancement by Sol, which explains the rapid burst in VA64-based ASD and slow supersaturation build-up in Sol-based ASD. Slow drying of a droplet of GF–

polymer(s) solutions and desupersaturation experiments revealed the poor recrystallization inhibition by the hydrophilic polymers. In most cases, combination of Sol with HPC/VA64 led to a trade-off between rapid drug release and high supersaturation. A strong synergistic effect emerged for the ASD with 11:1 Sol:VA64, which led to 230% supersaturation within 30 min and maintained it over three hours. Contrary to existing literature, the inclusion of a hydrophilic polymer as a minor component in an amphiphilic, precipitation-inhibiting polymer of a ternary ASD exhibited optimal drug release.

6.1 Materials and Methods

6.1.1 Materials

BP/EP grade, micronized griseofulvin (GF) purchased from Letco Medical (Decatur, AL, USA) was used as a challenging Biopharmaceutics Classification System (BCS) Class II drug because it is a fast-crystallizing poorly soluble drug (Baird et al., 2010). Its solubility is ~8.9 mg/L at 25 °C and ~14.2 mg/L at 37 °C, melting point T_m 220 °C, and a glass transition temperature T_g of 89 °C (Baird et al., 2010). Hydroxypropyl cellulose (HPC, SSL grade, Nisso America Inc., New York, NY) and PVP-VA64 (Kollidon VA64) were used as the hydrophilic polymers, while Soluplus® (Sol) was used as the amphiphilic polymer. HPC is a semi-crystalline polymer with low crystallinity and amorphous domains of very low T_g (Sarode et al., 2013). It has been widely used as a matrix polymer in drug nanocomposites (solid nanodispersions) that allows for fast drug nanoparticle recovery and rapid drug release (Bhakay et al., 2018). Kollidon VA64 (VA64) is a vinylpyrrolidone-vinyl acetate copolymer with a

glass transition temperature of 101 °C (Kolter et al., 2012). Soluplus® (Sol, BASF, Tarrytown, NY) is an amphiphilic graft copolymer produced from polyvinyl caprolactam–polyvinyl acetate–polyethylene glycol having a single glass transition temperature of 73 ± 2 °C (Terife et al., 2012). Acetone (ACS reagent, ≥ 99.5%) and ethanol (reagent alcohol, ≥ 95%) were purchased from BDH Analytical chemicals (VWR, GA) and used as solvent to prepare drug–polymer solutions.

6.1.2 Drug–Polymer Solution Preparation and Spray Drying

The formulations of the solution-based (S) feeds to the spray dryer are provided in Table 6.1. The drug concentration was set at 2.5% (w/v), which was measured with respect to the total volume (240 mL) of the solution (mixture of acetone–water/acetone–ethanol–water), in all formulations. For both binary and tertiary ASDs, the drug:total polymer mass ratio was kept constant at 1:3. To prepare the solution-based (S) feed, a common solvent mixture was selected where drug, and polymers (HPC/Sol/VA64) can be dissolved completely. A mixture of acetone–water was used for dissolving GF–HPC/Sol, whereas a ternary solvent mixture (acetone–water–ethanol) was used to dissolve formulations with VA64. After dissolving the drug–polymer(s) into the solvent mixture using a magnetic stirrer, the solutions were sonicated for 30 min to ensure complete solubilization of the solid components before feeding to the spray dryer.

Table 6.1 Formulations and Compositions of the Drug–Polymer Solutions (S) Used in Spray Drying Experiments

ID	Formulation[a]	GF (% w/v)[b]	Polymers (% w/v)[b]			Water (mL)	Acetone (mL)	Ethanol (mL)
			HPC	Sol	VA64			
S1	S-Sol	2.5	-	7.5	-	40	200	0
S2	S-HPC	2.5	7.5	-	-	40	200	0
S3	S-VA64	2.5	-	-	7.5	40	140	60
S4	S-Sol-HPC-1:1	2.5	3.75	3.75	-	40	200	0
S5	S-Sol-HPC-5:1	2.5	1.25	6.25	-	40	200	0
S6	S-Sol-HPC-9:1	2.5	0.75	6.75	-	40	200	0
S7	S-VA64-HPC-1:1	2.5	3.75	-	3.75	40	140	60
S8	S-VA64-HPC-5:1	2.5	1.25	-	6.25	40	140	60
S9	S-VA64-HPC-9:1	2.5	0.75	-	6.75	40	140	60
S10	S-Sol-VA64-1:5	2.5	-	1.25	6.25	40	140	60
S11	S-Sol-VA64-1:1	2.5	-	3.75	3.75	40	140	60
S12	S-Sol-VA64-3:1	2.5	-	5.62	1.88	40	140	60
S13	S-Sol-VA64-5:1	2.5	-	6.25	1.25	40	140	60
S14	S-Sol-VA64-11:1	2.5	-	6.87	0.63	40	140	60

[a]S denotes solution-based feed. Sol denotes Soluplus; VA64 denotes polyvinylpyrrolidone vinyl-acetate (6:4). The ratios refer to the polymer1:polymer2 mass ratio.

[b]% w/v, with respect to the total solvent volume (240 mL). All formulations had a drug:total polymer mass ratio of 1:3.

6.2 Characterization Techniques

6.2.1 Particle Size Measurement

The particle sizes of the spray-dried powders were measured by a Rodos/Helos laser diffraction system (Sympatec, NJ, USA) based on Fraunhofer theory following the procedure described in Li et al. (2016b). About 1 g of the powder sample was placed on top of the sample chute of the Rodos dispersing system and the sample chute was vibrated at a 100% setting, and 0.1 bar dispersion pressure was used to suck in the falling powder through the sample cell of the laser diffraction system. For further confirmation of the particle sizes, spray-dried particles were placed on a glass slide and observed by Axio Scope.A1 polarized light microscope (PLM, Carl Zeiss Microscopy GmbH, Göttingen, Germany).

6.2.2 Solid State Characterization and Drug–Polymer Interactions

To analyze the crystallinity of the as-received GF, HPC, Sol, VA64, spray-dried powders with single and binary polymers, and physical mixtures of GF–HPC/Sol/VA64, X-ray powder diffraction (XRPD) (PANanalytical, Westborough, MA, USA), provided with Cu K_α radiation (λ= 1.5406 Å) was used. The samples were scanned at a rate of 0.165 s^{-1} for 2θ ranging from 5° to 40°. The total area under three distinct, non-overlapping peaks of GF, if they exist, at characteristic diffraction angles of 13.2°, 14.6°, and 16.5° was calculated for both the physical mixtures and the spray-dried powders using the equipment's HighScore Plus software, which was then used to estimate the crystallinity.

Differential scanning calorimetry (DSC) of the as-received GF, Sol, HPC, VA64, and spray-dried powders with single and binary polymers was performed

using a Mettler-Toledo polymer analyzer (PolyDSC, Columbus, OH, USA) with integrated STARe 10 software. ~6.0–7.0 mg powder sample was placed in an aluminum pan with a hole in the lid and loaded into the DSC machine. As-received GF was heated at a rate of 10 °C/min from 25 °C to 250 °C. All other samples were heated from 25 °C to 70 °C and the temperature was held for 2 min at 70 °C, then cooled back to 25 °C to remove any residual solvent in the sample. In the final step, the samples were heated from 25 °C to 250 °C at 10 °C/min. Nitrogen gas was used as the purge gas and protective gas at a flow rate of 50 mL/min and 150 mL/min, respectively. Thermogravimetric analysis (TGA) was performed to measure the residual water/solvent content using a TGA/DSC1/SF Stare system (Mettler Toledo, Inc., Columbus, OH). ~6.0–7.0 mg of each spray-dried sample was placed in a ceramic crucible and heated from 25 °C to 150 °C at a heating rate of 10 °C/min under nitrogen flow.

Raman spectroscopy was conducted using a Fergie Imaging Spectrometer System (Princeton Instruments, Trenton, NJ) with a 500-mW external diode laser processing at 785 nm wavelength. Data acquisition time for all spectra was 15 s per scanned spectrum (100–1800 cm^{-1}) and each spectrum acquired was averaged over two scans. The data was presented for the range of 1550–1800 cm^{-1} wavenumber.

6.2.3 Characterization of Drug Recrystallization

To assess the recrystallization inhibition capability of the polymer(s) qualitatively, a droplet of 20 µL of the GF–polymer(s) solutions was put onto a hot glass slide at 75 °C and kept for drying in quiescent air. After about one min drying, the slides were

placed under the polarized light microscope (PLM) to observe if any drug recrystallization occurred.

6.2.4 Drug Content in the Spray-Dried Powders and *In Vitro* Dissolution Tests

The drug content in the dried powders varied based on the drug:polymer mass ratios. To measure the actual drug content, an assay testing was performed by dissolving 100 mg of the sample powders in 20 mL methanol under 30 min of sonication, followed by overnight storage to ensure complete solubilization of the drug. An aliquot of 100 µL was taken from the GF solution and diluted up to 10 mL using methanol. The absorbance of the samples was measured at 292 nm using UV spectrophotometer (Agilent, Santa Clara, CA, USA), and the drug concentration was calculated from a pre-established calibration curve. Six replicates were tested for each formulation to calculate the mean drug content along with the relative standard deviation (RSD).

Drug release from the as-received GF, various physical mixtures (PMs) prepared by blending, and spray-dried powders was determined *via* a Distek 2100C dissolution tester (North Brunswick, NJ, USA), following the USP II paddle method. 1000 mL deionized water at 37 °C was stirred at 50 rpm paddle speed. Spray-dried powder samples containing 100 mg GF (above the thermodynamic solubility of as-received GF particles) were weighed and added to the dissolution medium and 4 mL samples were taken out manually at 1, 2, 5, 10, 20, 30, 60, 120, 180, and 210 min. These aliquots were filtered with a 0.1 µm PVDF membrane-type syringe filter before UV-spectroscopy measurements to minimize any confounding effect of the undissolved drug clusters (Bhakay et al., 2014; Li et al., 2016b). The filtered samples were diluted with 37 °C deionized water at a ratio of 1 to 5 before UV measurement.

Dissolved GF amount was measured by UV spectroscopy at 296 nm wavelength and calculated using a pre-established calibration curve. Deionized water was used as the blank before UV measurement and six replicates of each sample were performed. In this paper, relative % supersaturation is reported based on GF concentration at 210 min and thermodynamic solubility of as-received GF particles, unless otherwise indicated.

6.2.5 Drug Wettability Enhancement by Single and Binary Polymer Solutions

Aqueous wettability of GF particles was investigated by analyzing the penetration rate of drug-saturated polymer solutions into a packed bed of GF particles inside a cylindrical column according to the Washburn method (Hołownia et al., 2008; Washburn, 1921). Attension Sigma 700 (Biolin Scientific, Linthicum, MD, USA) set-up was used to measure the mass of the liquid penetrated the GF powder bed as a function of time. Experimental methods were adapted from Bilgili et al. (2018) and Li et al. (2017) and the details can be found in Section E.1 of the Appendix E. In the current study, liquids and powder refer to GF-saturated aqueous solutions of 15% polymer (single or binary polymer) and as-received GF, respectively. All percentages are (% w/w) with respective to deionized water. The aqueous polymer(s) solution and deionized water were saturated with griseofulvin (GF) and stirred overnight. After overnight stirring, the saturated solutions were used for further characterization. The apparent shear viscosity and surface tension of the liquids were measured using R/S Plus Rheometer (Brookfield Engineering, Middleboro, MA, USA) and Attension Sigma 700 (Biolin Scientific, Linthicum, MD, USA), respectively. The ratio of the cosine of contact angles $\cos\theta_{ss}/\cos\theta_{w}$ was calculated using the modified Washburn

equation and used as a wetting effectiveness factor. Here, θ_{ss} is the contact angle between GF and the polymer(s) solutions and θ_w is the contact angle between GF and deionized water. The ratio was used as a rough measure of the drug wettability enhancement upon use of different polymer (HPC/Sol/VA64 and their combinations) in water with respect to the GF–water wettability.

6.2.6 Drug Supersaturation Maintenance Ability of the Polymers

Drug (GF) supersaturation maintenance ability of HPC/Sol/VA64 and their combination was examined in separate desupersaturation tests (similar to Konno et al. (2008)) based on the solvent-shift method. A GF solution was prepared by dissolving 100 mg of as-received GF into 20 mL of acetone via sonication for 40 min. This solution was subsequently added to a 1000 mL of pre-dissolved HPC/Sol/VA64 solution having 300 µg/mL total polymer concentrations to mimic 1:3 drug:polymer mass ratio in the USP II paddle type dissolution tester. In the case of binary polymers, polymer concentrations were adjusted following the formulation compositions in Table 6.1, while keeping the total polymer concentration fixed at 300 µg/mL. The addition resulted in 92–98 µg/mL supersaturated solution of GF initially (target: 100 µg/mL, corresponding to complete dissolution of 100 mg drug during dissolution testing). Any subsequent desupersaturation during the following 210 min was tracked via GF concentration measurements. The experimental conditions and concentration measurements were identical to those in the dissolution test. All measurements were carried out in triplicate.

6.3 Results and Discussion

6.3.1 Size, Morphology, and Drug–Moisture Content of the Spray-Dried Powders

Drug–polymer solutions with single and binary polymers were dried using a spray dryer. Despite the relatively short residence time in the spray dryer (5.0 s), the spray-dried powders were completely dried, as indicated by the TGA, which shows weight loss of ~2.0% for the samples. The extremely large surface area generated by atomization of the feed coupled with the fast convective heat–mass transfer at high air temperature enabled fast drying of the droplets. The slightly lower drug content as compared with the theoretical value can be attributed to preferential drug loss during handling, poor separation of finer particles in the cyclone separator of the spray dryer, and presence of the residual moisture after drying (Azad et al., 2015b; Bilgili et al., 2018). RSD values of drug content were below 6%, which signifies pharmaceutically acceptable content uniformity. The median sizes of the spray-dried powders were measured to be in the range of 8.69–15.4 μm (Table 6.2). The microscopic images (Figure 6.1) illustrate that spray-dried particles have rounded–donut shapes, and their sizes are in rough agreement with the size ranges presented in Table 6.2.

Table 6.2 Particle Size Statistics of the Spray-Dried Powders and Their Drug Content

ID	Formulation[a]	Size of the spray-dried powders (μm)			Actual drug content, RSD (%w/w, %)[b]
		d_{10} ± SD	d_{50} ± SD	d_{90} ± SD	
S1	S-Sol	6.08±0.1	14.3±0.0	32.4±0.1	22.1, 1.76
S2	S-HPC	5.87±0.1	15.4±0.3	33.5±0.1	24.0, 1.51
S3	S-VA64	4.21±0.1	10.3±0.2	21.3±0.2	22.5, 2.15
S4	S-Sol-HPC-1:1	4.01±0.0	10.9±0.0	22.7±0.0	22.4, 3.85
S5	S-Sol-HPC-5:1	4.52±0.1	11.2±0.1	24.3±0.6	21.7, 1.60
S6	S-Sol-HPC-9:1	4.21±0.0	11.5±0.0	27.7±0.1	21.7, 3.93
S7	S-VA64-HPC-1:1	4.35±0.0	9.90±0.5	21.6±0.7	22.1, 2.15
S8	S-VA64-HPC-5:1	4.11±0.1	9.34±0.2	19.7±0.2	22.6, 1.76
S9	S-VA64-HPC-9:1	3.27±0.1	8.69±0.1	17.4±0.1	22.3, 1.42
S10	S-Sol-VA64-1:5	4.40±0.0	12.1±0.1	27.3±0.1	20.9, 1.12
S11	S-Sol-VA64-1:1	4.61±0.1	10.2±0.2	20.6±0.1	21.3, 3.14
S12	S-Sol-VA64-3:1	3.71±0.1	9.76±0.3	22.8±0.2	23.1, 1.22
S13	S-Sol-VA64-5:1	4.58±0.0	12.0±0.0	28.9±0.1	22.8, 1.48
S14	S-Sol-VA64-11:1	3.47±0.1	13.0±0.1	30.9±0.2	22.3, 2.57

[a]S denotes solution-based feed. Sol denotes Soluplus; VA64 denotes polyvinylpyrrolidone vinyl-acetate (6:4). The ratios refer to the polymer1:polymer2 mass ratio.
[b]% w/v, with respect to the total solvent volume (240 mL). All formulations had a drug:total polymer mass ratio of 1:3.

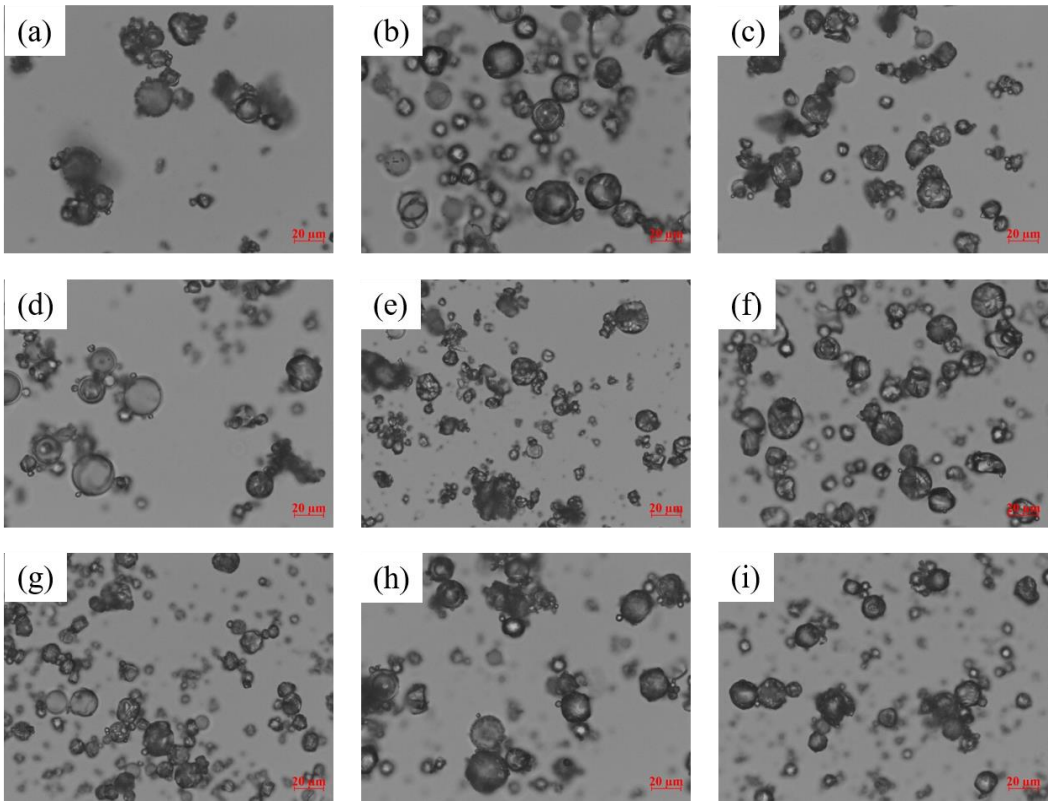

Figure 6.1 Microscope images of the spray-dried powders prepared using GF solution-based (S) feeds with a single polymer and binary polymers with various polymer1:polymer2 mass ratios: (a) S-HPC, (b) S-Sol, (c) S-VA64, (d) S-Sol-HPC-9:1, (e) S-VA64-HPC-9:1, (f) S-Sol-VA64-1:5, (g) S-Sol-VA64-1:1, (h) S-Sol-VA64-5:1, and (i) S-Sol:VA64-15:1. All formulations had 1:3 drug:polymer mass ratio. The images were taken at 50X magnification (scale bar: 20 µm).

6.3.2 Formation of Drug ASDs Upon Spray Drying

The solid state of GF in the spray-dried powders was investigated *via* XRPD (see Figure 6.2) and DSC (see Figure 6.3). Table 6.3 presents the summary of DSC thermal events and estimated crystallinity *via* XRPD. X-ray diffractograms depict that as-received GF exhibited intense peak characteristics of a crystalline material, whereas HPC/Sol/VA64 exhibited halo pattern indicating amorphous structure

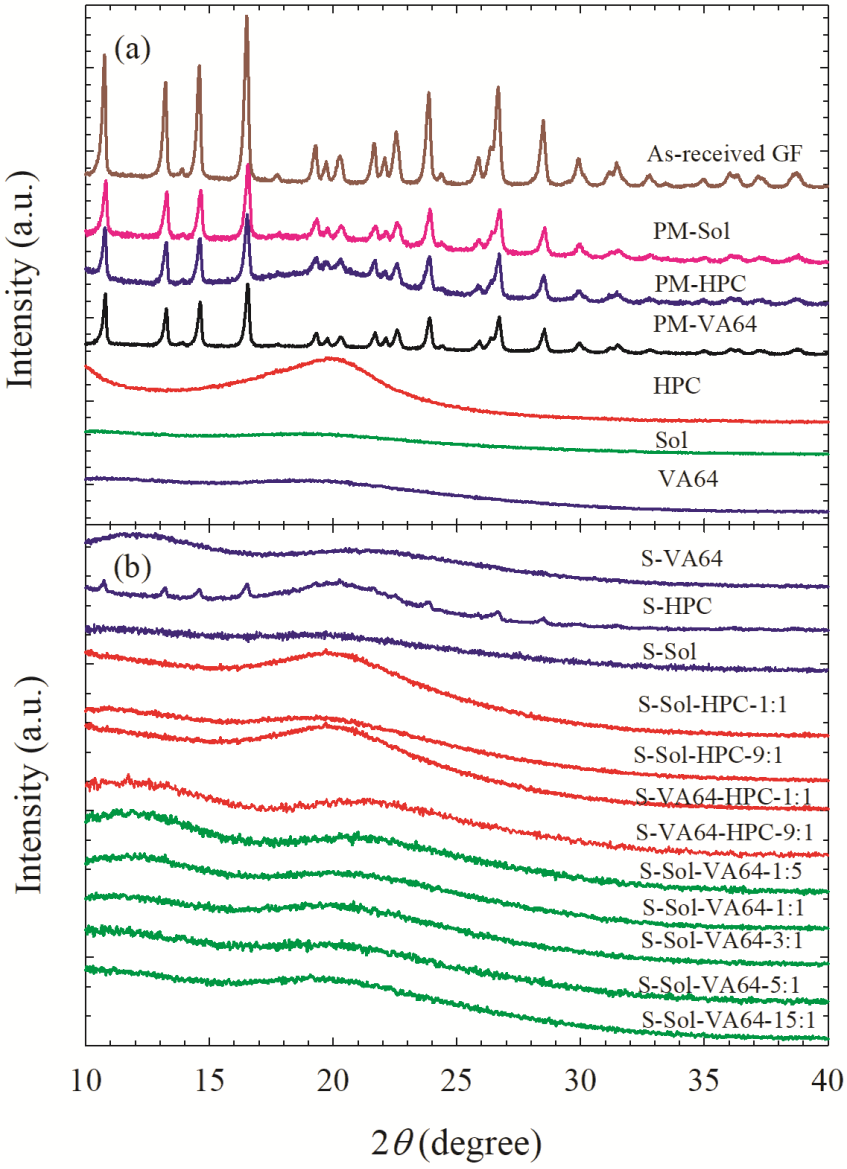

Figure 6.2 X-ray diffractograms of (a) as-received GF, HPC, Sol, VA64, and physical mixtures (PMs) of GF–HPC/Sol/VA64; (b) spray-dried powders prepared using the GF solution-based (S) feeds with a single polymer and binary polymers with various polymer1:polymer2 mass ratios. All formulations had 1:3 drug:polymer mass ratio.

(Figure 6.2a). The physical mixtures (PMs), prepared by blending, exhibited peaks at the same diffraction angles as those of as-received GF, albeit with reduced peak intensity (Figure 6.2a), which can be attributed to the dilution and surface coverage of GF microparticles with HPC/Sol/VA64. XRPD diffractograms (Figure 6.2b) of the

spray-dried powders prepared using the drug–polymer solutions showed halo pattern instead of any characteristic diffraction peaks of GF (except S-HPC). These halo patterns confirm that amorphous GF dispersed molecularly into the polymer matrix forming amorphous solid dispersions (ASDs). On the other hand, the peaks in the XRPD diffractogram of S-HPC and 11.5% crystalline GF could be explained by the partial miscibility of GF–HPC and insufficient HPC concentration to ensure complete dispersion of GF molecules in the polymer matrix; hence, recrystallization of GF during spray-drying occurred.

The DSC thermograms in Figure 6.3a show an endothermic peak associated with melting of as-received GF, with a T_m of 220.1 °C and ΔH_f of 101.8 J/g; a glass transition for Sol (amorphous) at 72.4 °C, a glass transition for VA64 (amorphous) at 102 °C and a slight endothermic event around 170–200 °C for HPC likely due to the melting of the small crystalline domain of largely amorphous HPC (Sarode et al., 2013) (crystallinity was undetectable by XRPD). The T_g of HPC could not be measured (in the range of –25 to 0 °C (Sarode et al., 2013)) due to limitation of our equipment. For the spray-dried powders prepared from the drug–polymer solutions, a single T_g was observed for all the formulations confirming the formation of molecular level dispersion (Luebbert et al., 2017; Wlodarski et al., 2015) (see Table 6.3). All spray-dried powders exhibited a glass transition and a small endothermic melting peak for GF. S-HPC had the highest value of fusion enthalpy due to presence of 12% crystals, as measured by XRPD. The small endothermic event for all other samples could be due to small amount of nuclei/crystals in the prepared ASDs, which could not be detected by XRPD or crystals generated during the heat treatment of DSC.

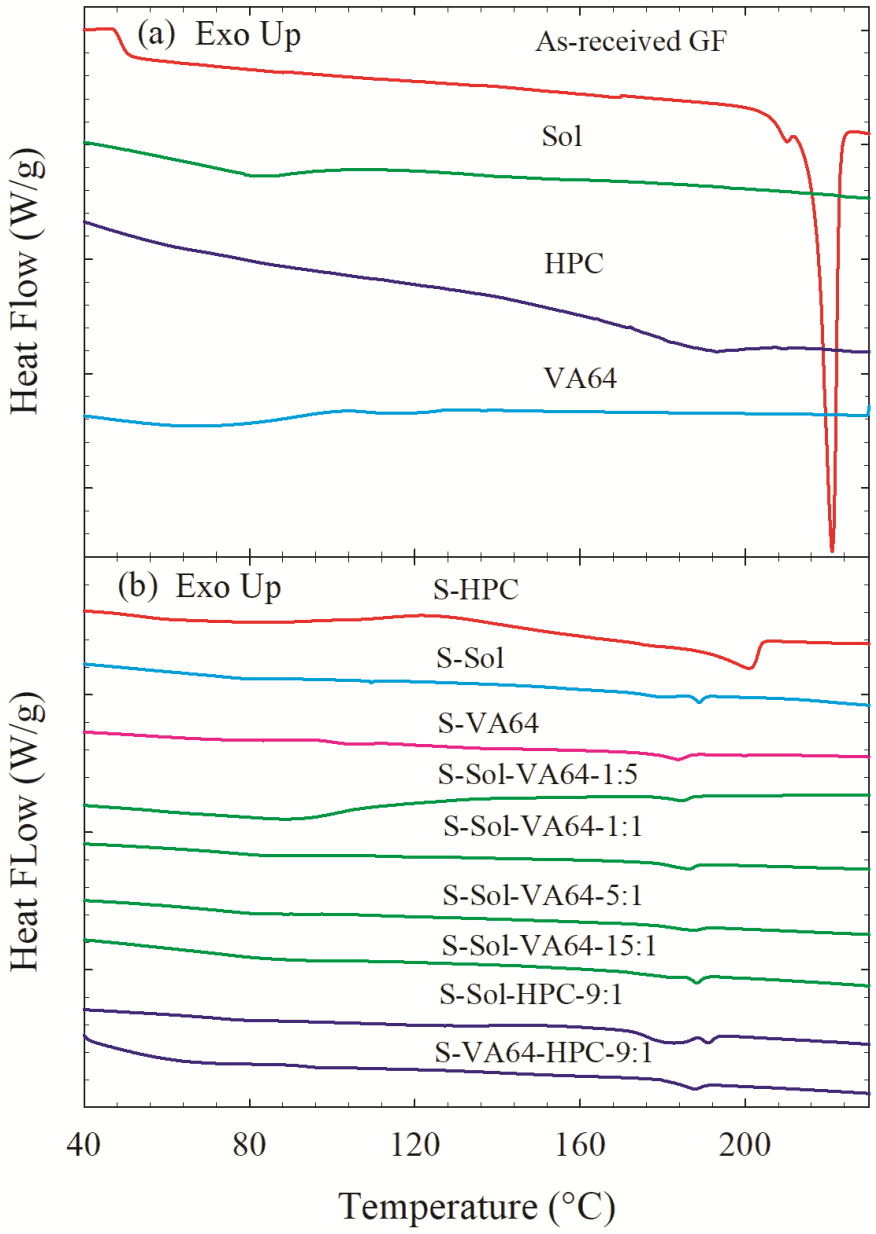

Figure 6.3 DSC thermograms of (a) as-received GF, HPC, Sol, and VA64; (b) spray-dried powders prepared using the GF solution-based (S) feeds with a single polymer and binary polymers with various polymer1:polymer2 mass ratios. All formulations had 1:3 drug:polymer mass ratio.

Table 6.3 Characteristic Temperatures–Enthalpy Values Obtained From DSC Thermograms and Crystallinity Estimated From XRPD Diffractograms

ID	Formulation[a]	T_g (ºC)[a,b]	T_{rc} (ºC) [a,b]	ΔH_{rc} (J/g) [a,b]	T_m (ºC) [a,b]	ΔH_f (J/g) [a,b]	Crystallinity (%)[b]
S1	S-Sol	80.4	ND	ND	189	0.64	ND
S2	S-HPC	53.2	122	–4.36	201	13.2	11.5
S3	S-VA64	100.4	ND	ND	184	0.94	ND
S4	S-Sol-HPC-1:1	77.6	135	–6.38	195	7.45	ND
S6	S-Sol-HPC-9:1	75.1	ND	ND	191	4.64	ND
S7	S-VA64-HPC-1:1	93.7	ND	ND	187	2.26	ND
S9	S-VA64-HPC-9:1	94.1	ND	ND	188	1.11	ND
S10	S-Sol-VA64-1:5	85.9	ND	ND	185	1.06	ND
S11	S-Sol-VA64-1:1	86.1	ND	ND	186	1.31	ND
S12	S-Sol-VA64-3:1	82.8	ND	ND	186	0.62	ND
S13	S-Sol-VA64-5:1	82.7	ND	ND	188	0.74	ND

[a]S denotes solution-based feed, Sol denotes Soluplus; the ratios refer to the polymer1:polymer2 mass ratio. Other symbols: T_g, T_{rc}, and T_m stand for temperature for glass transition, recrystallization transition, and melting point, respectively, while ΔH_{rc} and ΔH_f respectively stand for recrystallization enthalpy and fusion enthalpy.

[b]ND: not detected.

However, significant depression in the melting point of the spray-dried samples compared to the respective physical mixtures confirm the miscibility of the drug–polymers. S-HPC and S-Sol-HPC-1:1 exhibited a glass transition followed by an exothermic event due to the recrystallization of amorphous GF followed by the melting of the existing crystals and/or recrystallized GF (Figure 6.3c). Recrystallization occurred during the heating step of DSC scan because above T_g amorphous drug molecules and amorphous polymer had higher mobility, which may cause GF recrystallization. Since GF–HPC are partially miscible, above T_g GF molecules can easily phase separate and recrystallize. Due to strong molecular interactions and good miscibility of GF–Sol and GF–VA64, recrystallization event at high temperature was not observed for the formulations with Sol, VA64, and their combinations during the DSC scan.

The observed Raman spectra in Figure 6.4a for as-received GF and PMs of GF are largely in agreement with Fourier transform Raman data of ref. (Feng et al., 2008) and Raman data of ref. (Żarów et al., 2011) for crystalline GF. The Raman spectra of all the spray-dried samples (Figure 6.4b) show that the GF line at 1606 cm^{-1} disappeared, and the peaks at other characteristic frequencies shifted to new positions that are characteristic of amorphous GF, e.g., the peak shift from 1623 to 1620 cm^{-1} (see (Żarów et al., 2011)), signifying formation of amorphous GF and molecular level interactions between GF and polymers in the ASD. While the GF line at 1606 cm^{-1} disappeared in the Raman spectra of S-HPC (Figure 6.4b), the shifts in other peaks were subtler than those for the Raman spectra of S-Sol and S-VA64, which could suggest stronger molecular interactions between GF–Sol and GF–VA64

than GF–HPC. For all the spray-dried formulations produced from binary polymers, noticeable peaks shift also suggest stronger molecular interactions between GF–binary polymers (Figure 6.5).

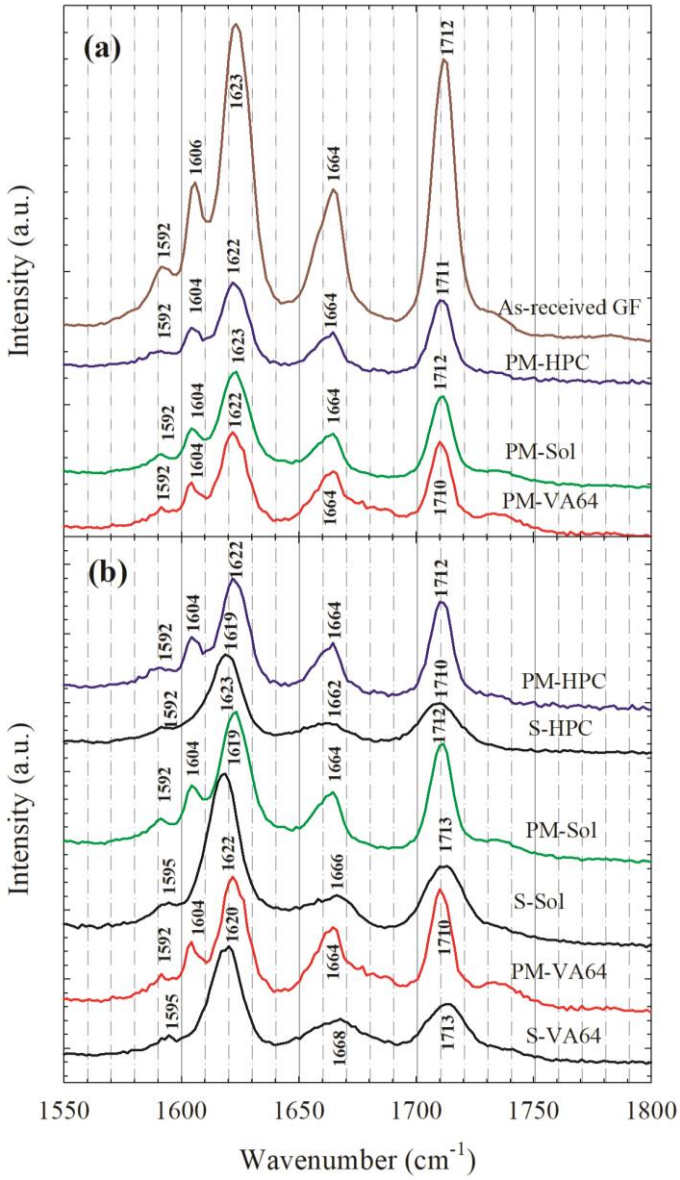

Figure 6.4 Raman spectra of (a) as-received GF, physical mixtures (PMs) of GF–HPC, GF–Sol, and GF–VA64 at 1:3 drug:polymer mass ratio; (b) physical mixtures (PMs) and spray-dried powders prepared using GF solution-based (S) feeds of GF–HPC, GF–Sol, and GF–VA64 with 1:3 drug:polymer mass ratio.

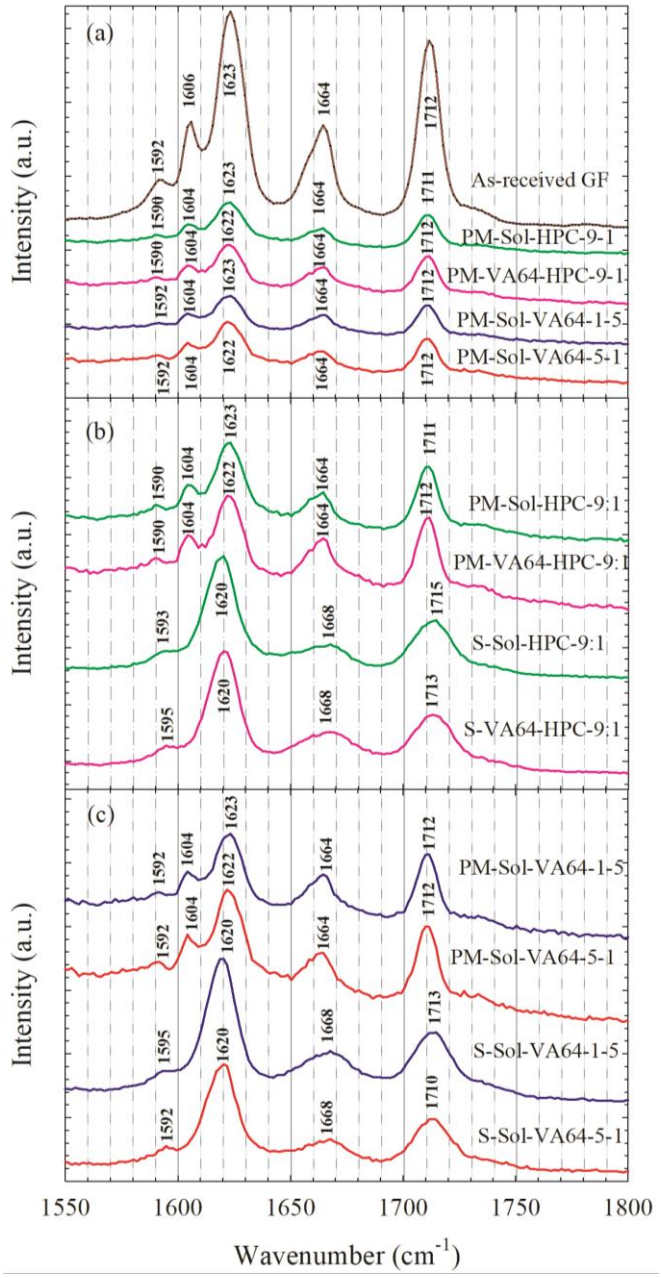

Figure 6.5 Raman spectra of (a) as-received GF, physical mixtures (PMs) of GF–binary polymers at various polymer1:polymer2 mass ratios; (b) physical mixtures (PMs) of GF–Sol–HPC and GF–VA64–HPC and their respective spray-dried powders with 9:1 mass ratio of Sol:HPC and VA64:HPC, respectively; (c) physical mixtures (PMs) of GF–Sol–VA64 and their respective spray-dried powders with 5:1 and 1:5 mass ratios of Sol:VA64. All formulations had 1:3 drug:polymer mass ratio.

Overall, XRPD, DSC, and Raman spectroscopy results (i) confirm that the spray-drying of drug–polymer(s) solutions produced ASDs and (ii) suggest stronger GF–polymer interactions and miscibility for GF–Sol and GF–VA64 than GF–HPC. It is suggested that if the solubility parameter difference between a drug and polymer is <7.0 $MPa^{1/2}$, they are likely to be miscible; if the difference is >10 $MPa^{1/2}$, they are considered immiscible; and if the difference is in between 7.0 and 10, they exhibit partial miscibility (Forster et al., 2001; Greenhalgh et al., 1999). The solubility parameters of GF, HPC, Sol, and VA64 are 12.2 (Thakral and Thakral, 2013), 24.0 (Choi et al., 1994), 19.4, and 19.7 (Kolter et al., 2012) $MPa^{1/2}$, respectively. The solubility parameter differences between GF–Sol and GF–VA64, and GF–HPC are 7.2, 7.5, and 11.8 $MPa^{1/2}$, respectively, which suggests that GF–Sol is borderline miscible, GF–VA64 is partially miscible, whereas GF–HPC is most likely immiscible. While being useful, the solubility parameters do not account for all drug–polymer interactions such as contributions from hydrogen bonding, hydrophobic interactions, etc., and hence should be used with caution as rough estimates of drug–polymer miscibility. The solubility parameter prediction appears to be accurate for GF–Sol and GF–VA64 as XRPD, DSC, and Raman spectroscopy results suggests GF–Sol and GF–VA64 are miscible and molecularly interact more than GF–HPC. However, GF–HPC exhibits partial miscibility unlike what the solubility parameters of GF–HPC suggest. As the theoretical models behind the solubility parameter prediction are applicable for simple molecular structures wherein van der Waals force plays a predominant role, while for drug–polymer systems which are known to form highly directional interactions (e.g., hydrogen bonding) or long range interactions

(e.g., ionic interaction), this approach can be erroneous (Baird et al., 2010; Meng et al., 2015). Indeed, the absence of diffraction peaks in XRPD for 1:5 GF:Sol ASD (not shown) and significant melting point depression with respect to physical mixtures based on DSC (not shown) along with the Raman line shifts suggest that HPC molecularly interacts with GF, resulting in partial miscibility unlike the prediction from the solubility parameters.

6.3.3 Assessment of the Recrystallization Inhibition Capability of the Polymers

In the drug–polymer solutions, GF and polymer (s) were completely dissolved in acetone–water/acetone–water–ethanol mixture, which allowed molecular level interaction in the solution before spray drying. Due to fast evaporation of the solvents in the spray dryer, viscosity increases rapidly causing entrapment of the drug molecules in the polymer matrices, which appears to have retarded phase separation even in the case of GF–HPC (immiscible or partially miscible) and enables the ASD formation.

To assess the recrystallization inhibition capability of the polymers qualitatively, we have devised a slower drying method: a single droplet of GF–polymer (s) solution was dried on a heated glass slide at 75 ºC, i.e, the same temperature as that of hot air in the spray-drying. However, the droplet was dried in quiescent air, which makes external mass transfer of solvent vapor in air controlling the evaporation rate, making drying slower compared to spray drying. This slow drying is quite conservative regarding the crystallization inhibition capability of the polymers as it gives ample time for dissolved drug to precipitate and form crystals. The drying took less than 40 s, whereas the drying occurred less than ~5 s in the

spray dryer. The PLM images in Figure 6.6 illustrate that GF crystals formed during the slow drying of all solutions. On the other hand, the slow drying of S-Sol and S-VA64 solution yielded few small crystals, whereas that of S-HPC solution yielded significant number of long needle-shaped crystals. The extent of recrystallization was much higher in HPC than in Sol or VA64. HPC could not inhibit the nucleation/crystal growth of GF from the supersaturated solution as evaporation proceeded during the spray-drying. Figure 6.6d and 6.6e show that Sol is a better precipitation inhibitor than VA64 in the presence of HPC. An increase in Sol:VA64 mass ratio led to smaller and fewer crystals suggesting that Sol could be a good GF crystal inhibitor. While all images in Figure 6.6 shows presence of crystals due to slow drying, fast spray-drying did not allow much time for precipitation; thus, all GF–polymer(s) led to ASD, except ASD with 1:3 GF:HPC mass ratio.

It is known that the phase separation and recrystallization involve diffusion and nucleation of drug molecules, both of which require molecular mobility and can be restricted by polymer molecules as inhibitor (Baghel et al., 2016). Strong drug–polymer interactions can reduce the molecular mobility and delay crystallization onset time and the extent of crystallization (Mistry et al., 2015). To gain additional insights into the GF recrystallization inhibition capability of Sol/HPC in supersaturated drug solutions, desupersaturation experiments were performed. In the desupersaturation tests (Figure 6.7a), only Sol was able to maintain the GF supersaturation for ~3 h, whereas GF concentration drastically decreased after 10 min in the case of VA64 or HPC upon GF recrystallization. These results suggest that the

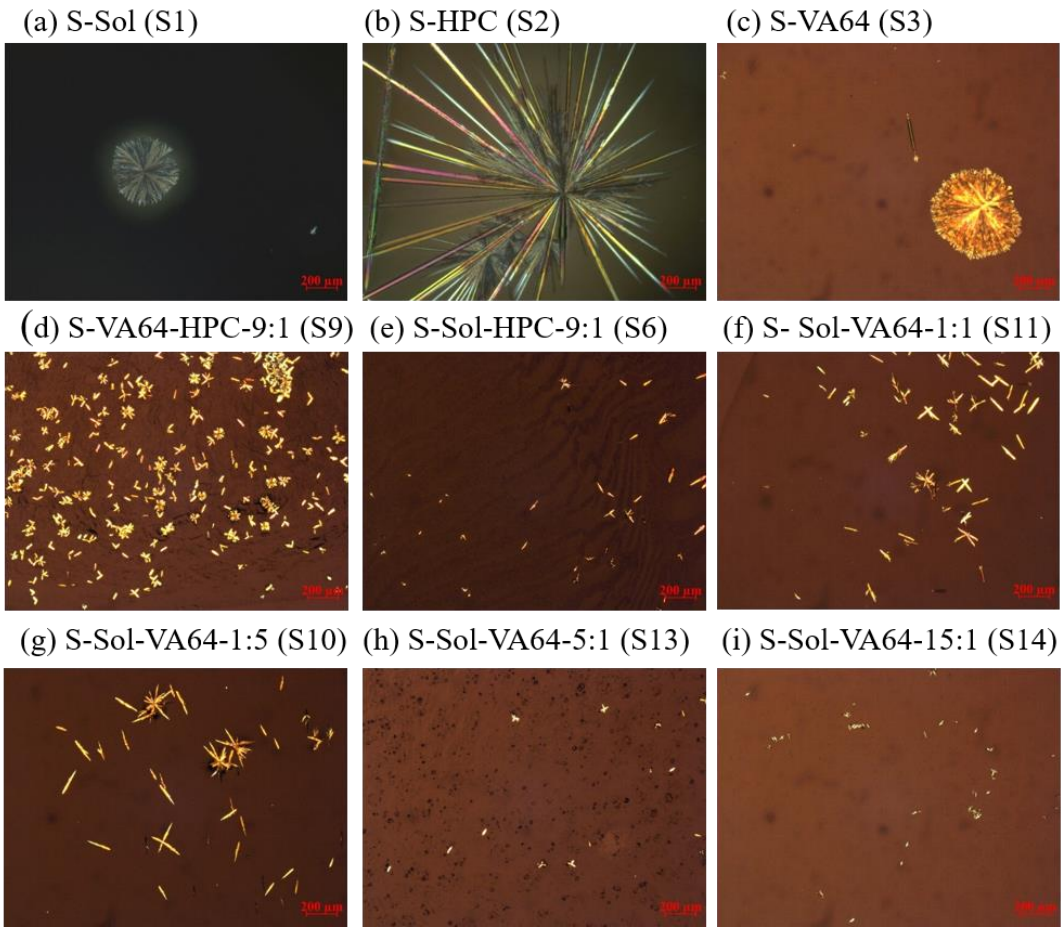

Figure 6.6 Polarized light microscope images of a droplet of GF solution-based (S) feed of (a) S-Sol, (b) S-HPC, (c) S-VA64, (d) S-VA64-HPC-9:1, (e) S-Sol-HPC-9:1, (f) S-Sol-VA64-1:1, (g) S-Sol-VA64-1:5, (h) S-Sol-VA64-5:1, and (i) S-Sol-VA64-15:1 after slow drying. The droplets were dried on a glass slide at room temperature. All formulations had 1:3 drug:polymer mass ratio. The images were taken at 5X zoom (scale bar: 200 µm).

superior GF recrystallization inhibition and supersaturation maintenance capability of Sol over HPC and VA64 (Figure 6.7a). Excellent nucleation inhibition and supersaturation maintenance capability of Sol was reported earlier (Guan et al., 2019a; Guan et al., 2019b). Figure 6.7 also corroborates the fast recrystallization tendency of GF (Baird et al., 2010) without inhibitors. Among binary polymers, Sol–

VA64 and Sol–HPC were able to maintain the supersaturation, whereas VA64–HPC could not maintain the supersaturation. In other words, the ASDs without Sol, as the

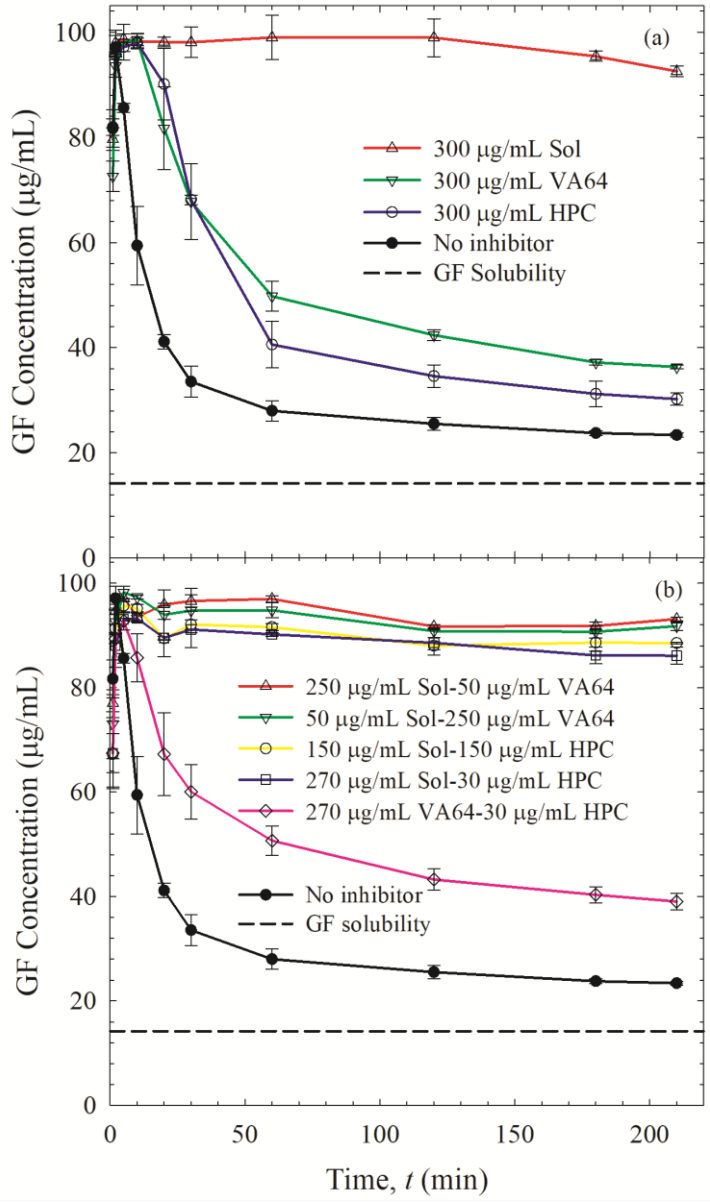

Figure 6.7 GF desupersaturation curves for a 20 mL GF–acetone solution mixed with (a) 1000 mL aqueous solutions of 300 µg/mL Sol/VA64/HPC and deionized water and (b) 1000 mL aqueous solutions of 250 µg/mL Sol–50 µg/mL VA64, 50 µg/mL Sol–250 µg/mL VA64, 150 µg/mL Sol–150 µg /mL HPC, 270 µg/mL Sol–30 µg/mL HPC, 270 µg/mL VA64–30 µg/mL HPC, and deionized water. Deionize water has no recrystallization inhibitor. The initial concentration of GF right after mixing was targeted at 100 µg/mL.

crystallization inhibitor is not expected to provide or maintain a high supersaturation. These findings suggest that having an amphiphilic polymer like Sol as the crystallization inhibitor is a must as the rather hydrophilic polymers like VA64–HPC do not have much inhibitory effect.

6.3.4 Dissolution Performance of the Spray-Dried Powders

The temporal evolution of GF release from the binary ASDs with single polymer and ternary ASDs with binary polymers combinations and the PM with the binary polymer combinations containing 100 mg equivalent GF dose in 1000 mL deionized water at 37 ºC was investigated. The bulk dissolution medium could supersaturate for this high drug dose as the GF solubility is 14.2 mg/L. Unless otherwise specified, all supersaturation values are relative to aqueous thermodynamic solubility of GF and calculated at 210 min.

Figure 6.8 shows that the GF ASDs prepared *via* spray-drying of the drug–polymer solutions with single polymer enhanced the dissolution rate and extent of GF release compared to the as-received GF. The initial drug release rate was significantly higher for S-HPC ASD and S-VA64 ASD than S-Sol ASD. At 10 min, 220% and 40% GF supersaturation were achieved by S-VA64 and S-HPC, respectively, whereas S-Sol could not even reach the saturation solubility (14 mg/L). These observations can be explained by the hydrophilicity of the polymers and their relative wetting effectiveness (see Table 6.4). The relative wetting effectiveness factor for HPC, VA64, and Sol measured to be 20.9, 16.1, and 2.65, respectively, which is in line with the relatively more hydrophilic nature of HPC/VA64 than Sol, based on the functional groups of the respective groups (not shown). Therefore, in the aqueous

dissolution medium, HPC and VA64 allowed for excellent wetting of hydrophobic GF molecules and their ASDs exhibited rapid release of GF and the hydrophilic polymer. Unlike HPC/VA64, Sol does not allow for good wetting of the GF particles, which hinders Sol/GF dissolution.

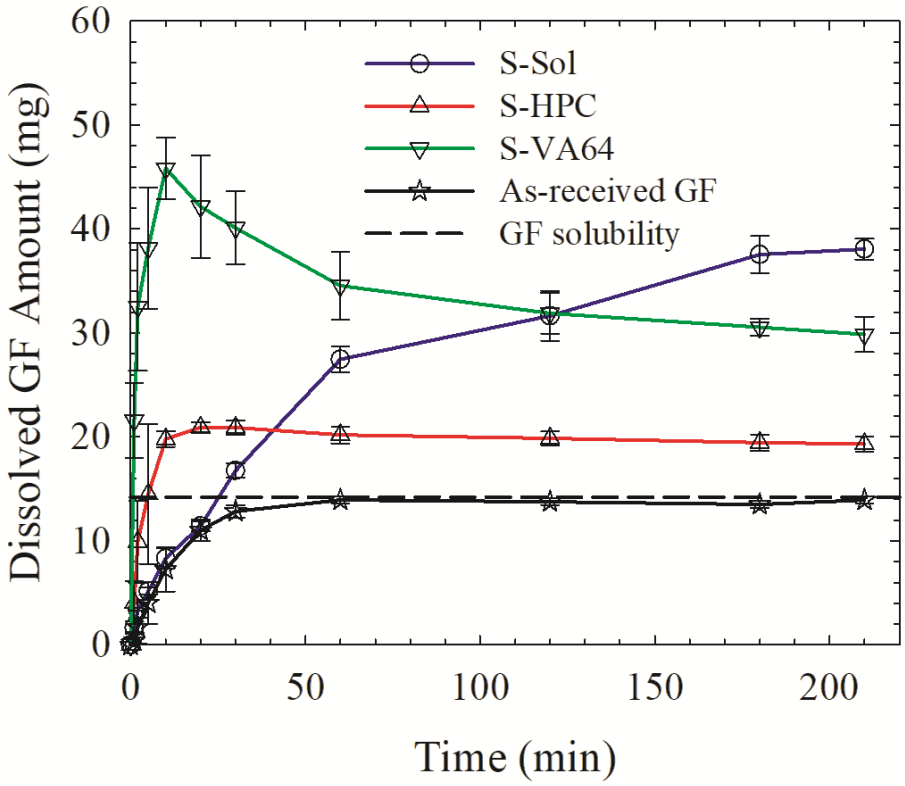

Figure 6.8 Evolution of drug release from as-received GF and spray-dried powders prepared using solution-based (S) feeds of GF–HPC, GF–Sol, and GF–VA64 with 1:3 drug:polymer mass ratio.

Table 6.4 Properties of Drug-Saturated Deionized Water–Aqueous Polymer Solutions and Wetting Effectiveness Factor Determined Using the Modified Washburn Method

Formulation	η (cP)	ρ (g/mL)	γ (mN/m)	Slope, (g^2/s)	R^2	$\cos\theta_{ss}/\cos\theta_w$
Water	0.89	1	66.5	7.0×10^{-3}	0.990	1[a]
HPC	53.2	1.01	39.9	1.5×10^{-3}	0.998	20.9
Sol	8.76	1.01	41.4	1.2×10^{-3}	0.989	2.65
VA64	7.80	1.01	39.6	7.8×10^{-3}	0.999	16.1
Sol-HPC-1:1	35.0	0.98	41.0	7.3×10^{-4}	0.997	6.93
Sol-HPC-9:1	10.9	1.01	41.9	2.0×10^{-3}	0.989	5.44
Sol-VA64-1:5	7.41	1.01	40.8	6.1×10^{-3}	0.996	11.6
Sol-VA64-5:1	8.05	1.01	41.9	2.9×10^{-3}	0.993	5.83
VA64-HPC-1:1	23.0	1.01	38.9	4.2×10^{-3}	0.999	26.9
VA64-HPC-9:1	10.6	1.01	36.8	7.3×10^{-3}	0.999	22.0

[a]The slope of the water penetration data was used as reference for wettability enhancement by the stabilizer solutions.

There is a drastic difference between S-HPC and S-VA64 in their GF release (Figure 6.8): after S-VA64 achieved 220% GF supersaturation at 10 min, the GF concentration displayed exponential decay in time due to recrystallization of the drug in the supersaturated dissolution medium because VA64 is not a good crystallization inhibitor (refer to Section 6.3.3 for recrystallization inhibition). On the other hand, S-HPC could not provide any further supersaturation after 10 min. It is well-established that depending on the drug–polymer miscibility and interactions, amorphous drug in an ASD may phase-separate and recrystallize upon contact of ASDs with water in the dissolution medium (Alonzo et al., 2011; Chen et al., 2015). Once imbibed into the ASD matrix, water acts as a plasticizing agent, enhancing the mobility of the drug molecules by reducing the T_g of the ASD (Chen et al., 2015). HPC-SSL has sub-ambient T_g (Sarode et al., 2013) (lower than T_g of Sol: 73 °C and T_g of VA64: 101 °C,

Kolter et al., 2012) and its ASDs have lower T_g than Sol-based and VA64-based ASDs (see Table 6.3). Moreover, due to partial immiscibility of HPC with GF, its relatively weak molecular interactions with GF as compared with Sol/VA64 (miscible with GF), as well as its poor GF nucleation/crystal growth inhibition, it is likely that the amorphous GF most likely crystallized in the S-HPC matrix rather than in the dissolution medium, unlike the case for S-VA64 ASD. Interestingly, at the end of the dissolution test (210 min), S-Sol was able to reach higher supersaturation (170%) compared to S-VA64 (110%) and S-HPC (40%). Owing to the high T_g of Sol and its ASD (see Table 6.3), its strong intermolecular interactions and relatively good miscibility with GF, Sol could achieve high GF supersaturation; however, the GF release rate from S-Sol is controlled by the relatively poor wettability, which led to slow, monotonic build-up of supersaturation, eventually after 210 min leading to the highest GF supersaturation in Figure 6.8.

Analysis of Figure 6.7 and Figure 6.8 and Table 6.4 overall suggests that binary polymers Sol–VA64 in a ternary ASD could potentially complement each other in achieving rapid drug release by VA64 and maintenance of high GF supersaturation by Sol, which will be evaluated *via* dissolution tests with ternary ASDs. Since HPC could not generate or maintain high extent of supersaturation, it was not used as a major component in the ternary ASDs. For both VA64–HPC and Sol–HPC combinations, 1:1, 5:1, and 9:1 VA64/Sol:HPC mass ratios were used. Due to its unfavorable characteristics mentioned earlier, using HPC either with VA64 or Sol did not appear to improve desirable dissolution performance (Figure 6.9a and

Figure 6.9b). The extent of supersaturation at 210 min for all ternary ASDs with HPC was lower than those for the binary ASDs: S-VA64 and S-Sol. Augmenting HPC with

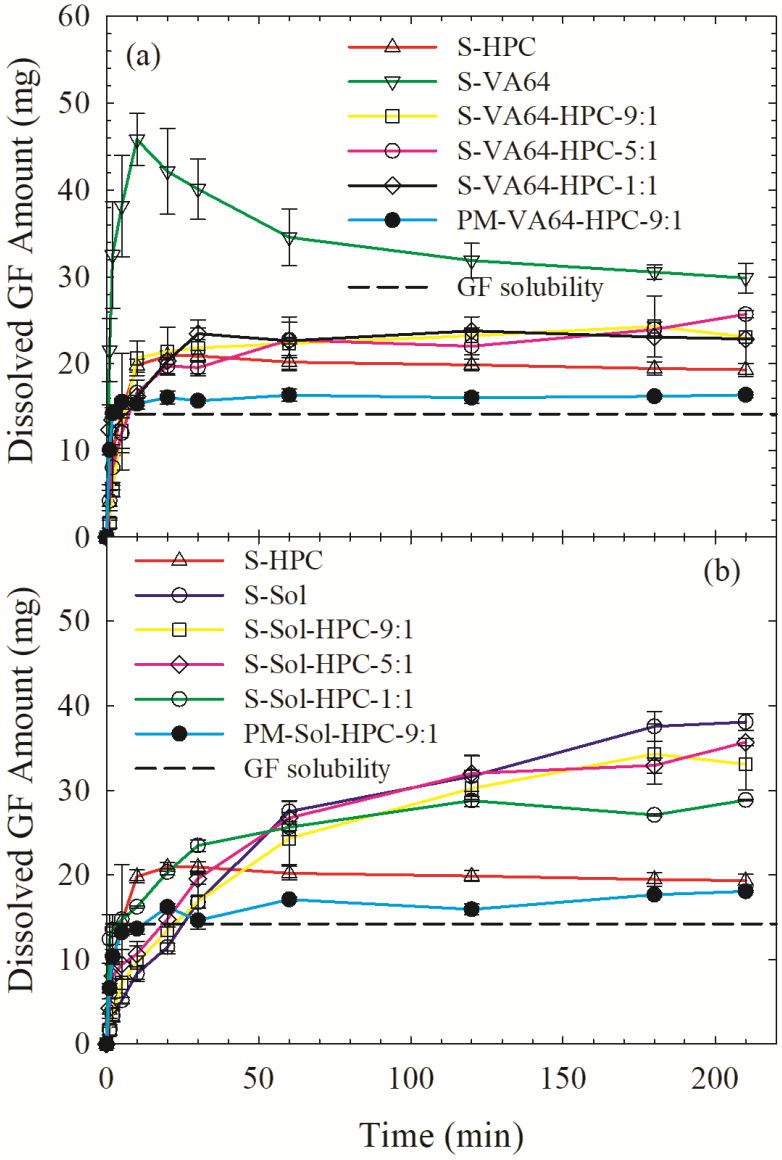

Figure 6.9 Evolution of drug release from physical mixture (PM) of GF–binary polymers and spray-dried powders prepared using GF–polymer solutions with a single polymer and binary polymers with various polymer1:polymer2 mass ratios: (a) VA64/HPC was each used as a single polymer and as binary polymers with 1:1, 5:1, and 9:1 VA64:HPC mass ratios; (b) Sol/HPC was each used as a single polymer and as binary polymers with 1:1, 5:1, and 9:1 Sol:HPC mass ratios. All formulations had 1:3 drug:polymer mass ratio.

VA64 deteriorated extent of supersaturation drastically (Figure 6.9a). For the Sol–HPC binary blends, the ternary ASDs had slightly faster initial GF release than the S-Sol, but this benefit came at the expense of reduced extent of supersaturation at longer times. These poor drug dissolution performance of the ternary ASDs with HPC stems from the rapid matrix crystallization of GF caused by low T_g of HPC and its relatively poor miscibility with GF. The detrimental impact of HPC was more marked for its ternary ASD with VA64 than that with Sol because Sol could at least inhibit recrystallization in the matrix to a certain extent, however, VA64 could not.

Ternary ASD of GF with Sol–VA64 exhibited desirable GF release characteristics such as initial, rapid GF release and build-up of supersaturation and its prolonged maintenance over 3 h when Sol was used as the major polymer component and VA64 as the minor component, i.e., 5:1 Sol:VA64 mass ratio (Figure 6.10). At 210 min, 230% relative supersaturation was achieved from S-Sol-VA64-5:1, whereas the relative supersaturation was 170% and 110% from S-Sol and S-VA64, respectively. It is inferred that ternary ASD with 5:1 Sol-VA64 exhibited significant synergistic enhancement upon combined use of an amphiphilic polymer (Sol, crystallization inhibitor) as a *major component* and the hydrophilic polymer (VA64) as a *minor component*. Apparently, this is contrary to the strategy proposed by Xie and Taylor, (2016a, b) based on their work on celecoxib. In fact, following their strategy, one would expect S-Sol-VA64-1:5 ASD to perform the best; yet, it led to the lowest extent of supersaturation among all ASDs with Sol–VA64 (Figure 6.10). Apparently, due to the obvious complexity of ternary ASDs, a “universal” formulation strategy is not likely to apply to all drugs because of the specificity of

drug–polymer1–polymer2 molecular interactions and their relative impact on wettability, drug recrystallization inhibition within the ASD matrix and in the dissolution medium, their diffusivities and dissolution rates relative to the drug, etc. Although increasing Sol concentration helped to improve the extent of supersaturation, there is a Sol:VA64 ratio after which the improvement is trivial, e.g., relative supersaturation 130%, 210%, 230%, and 260% was achieved at 210 min by varying Sol:VA64 mass ratio 1:1, 3:1, 5:1, and 11:1, respectively.

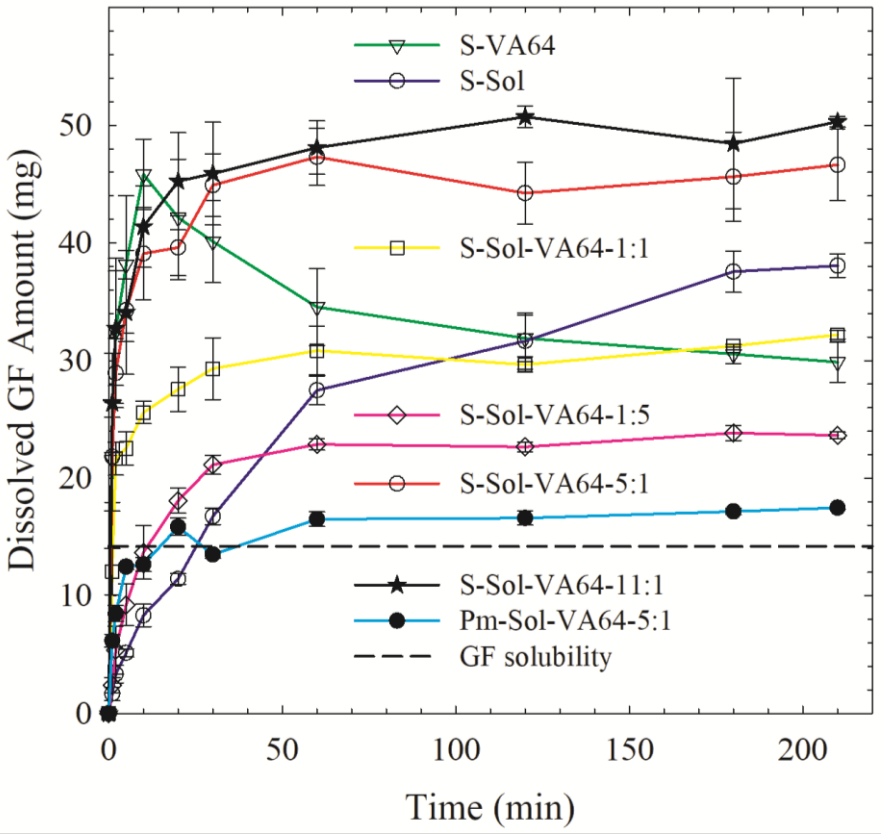

Figure 6.10 Evolution of drug release from physical mixture (PM) of GF–binary polymers and spray-dried powders prepared using GF–polymer solutions with a single polymer and binary polymers with different Sol:VA64 mass ratios: Sol/VA64 was each used as a single polymer and as binary polymers with 1:1, 5:1, 11:1, and 1:5 Sol:VA64 mass ratios.

6.4 Conclusions

Ternary ASDs of a poorly soluble fast crystallizing drug (GF) with binary combinations of HPC/VA64/Sol and binary ASDs of GF with the corresponding individual polymers, all having 1:3 GF:total polymer mass ratio, were prepared using spray-drying. XRPD, DSC, and Raman spectroscopy confirmed the molecular dispersion of GF in the matrices of single or binary polymers. Although binary ASDs with single polymer showed dissolution enhancement compared to as-received GF and physical mixtures, a desirable dissolution profile, i.e., rapid GF release concurrently generating fast supersaturation that lasts 3 hours, was not achieved. Despite being an excellent crystallization inhibitor, Sol did not allow for good wettability and hence its ASD could not achieve rapid drug release. Moreover, owing to its strong intermolecular interactions and miscibility with GF, it could generate a high GF supersaturation, albeit slowly. VA64, on the other hand, provided excellent wettability to the hydrophobic drug within the ASD and thus its ASD achieved fast initial release of the drug/polymer, with a burst. However, it is a poor crystallization inhibitor and could not sustain the initial high supersaturation. Unfortunately, having a sub-ambient T_g with low partial miscibility with GF, HPC (SSL grade) could not suppress the mobility of amorphous GF molecules upon contact of ASD with water, and fast recrystallization within the ASD matrix occurred.

The dissolution profiles of the ternary ASDs of binary polymers were mostly reflective of the deficiencies of the polymers in terms of wettability enhancement and recrystallization inhibition in the ASD matrix and the dissolution medium. As expected, the combination of the two hydrophilic polymers HPC–VA64 without an

amphiphilic crystal-inhibiting polymer (Sol) led to low supersaturation, below 80%. Being an effective crystallization inhibitor Sol compensated for HPC's inability to prevent recrystallization; but there was no synergistic positive impact. Any increase in initial drug release rate upon use of HPC was nullified by lower extent of supersaturation. Finally, based on the results regarding GF release from ternary ASDs with Sol-VA64, we conclude that a ternary ASD of GF could exhibit synergistic enhancement of drug release rate and its extent upon combined use of an amphiphilic polymer (Sol, as a crystallization inhibitor) as a *major component* and the hydrophilic polymer (VA64) as a *minor component* that provides wettability enhancement. Future work will focus on the application of such strategy to other poorly water-soluble drugs.

CHAPTER 7

RELEASE OF ITRACONAZOLE FROM SPRAY-DRIED NANOCRYSTAL–AMORPHOUS SOLID DISPERSIONS (HyNASDs) and ASDs

To elucidate the generality of the findings from the research on GF regarding HyNASDs formation and impact of SDS in the dissolution enhancement, here another BCS Class II drug, Itraconazole (ITZ) is selected, which has very low aqueous solubility (0.002 µg/mL). Hydroxypropyl cellulose (HPC), Kollidon VA64 (VA64), and Soluplus® (Sol) were used as suspension stabilizers and matrix-forming polymers. To elucidate the impact of a surfactant in on drug release from HyNASDs, an anionic surfactant, sodium dodecyl sulfate (SDS), was selected. 2.5% wet-milled ITZ suspensions containing 1:5 GF:polymer mass ratios, with 0.125% SDS (below CMC) and without SDS, were spray-dried. Hydroxypropyl cellulose (HPC) and Soluplus (Sol) were used as suspension stabilizers and matrix-forming polymers. To prepare ASDs, ITZ–Sol/HPC/VA64 solutions having identical composition to the nanosuspensions were spray dried. Examination of particle sizes in the milled suspensions revealed the criticality of SDS in the synergistic stabilization of GF nanoparticles. XRPD and DSC results suggest that nanocomposites and nanocomposites with notable amorphous ITZ, HyNASDs, were formed upon spray-drying. For 100 mg ITZ dose (above thermodynamic solubility), up to 840% relative supersaturation was achieved from Sol-based HyNASDs at 210 min, whereas with SDS, this value went up to 1230%. Sol-based HyNASDs outperformed HPC and VA64, which could be explained partly by the stronger molecular interaction between ITZ–Sol than ITZ–HPC/VA64 and partly by the micellar solubilization by Sol as well

as its recrystallization inhibition in the superstrated drug solutions. ITZ-Sol-ASD generated ~2000% supersaturation, which is higher that generated by HyNASDs (1230%). Nonetheless, such high supersaturation from nanoparticle-based formulation has not been achieved in literature before. So, HyNASDs boost the performance drug nanoparticle-based formulations and render them competitive to ASDs. Therefore, this study demonstrates the generality of the findings in Chapter 3 and Chapter 4, by using another poorly soluble drug, ITZ and the presence of SDS in the formulation significantly improved the extent of supersaturation in the dissolution medium, similar to the GF-HyNASDs.

7.1 Materials and Methods

7.1.1 Materials

Itraconazole (ITZ) was used as Biopharmaceutics Classification System (BCS) Class II drug and was purchased from Jai Radhe Sales (Ahmedabad, India). Solubility of pure ITZ in deionized water and 0.1 N HCl are around 0.002 µg/mL and ~ 4 µg/mL, respectively (Ghazal et al., 2009) at 37 ºC. The glass transition and melting temperature of ITZ are reported to be 59 ºC (Zhang et al., 2016) and 171 ºC (Bilgili et al., 2018), respectively. Hydroxypropyl cellulose (HPC, SSL grade, Nisso America Inc., New York, NY) is a semi-crystalline polymer with low crystallinity and amorphous domains of very low T_g. It is widely used as a stabilizer during milling and matrix former in the nanocomposites (Azad et al., 2015b; Bhakay et al., 2014a). Soluplus® (Sol) is an amphiphilic graft copolymer produced from polyvinyl caprolactam–polyvinyl acetate–polyethylene glycol having a single glass transition

temperature of 73 ± 2 °C (Terife et al., 2012). Kollidon VA64 (VA64) is a hydrophilic polymer produced from the combination of vinylpyrrolidone (hydrophilic in nature) and vinyl acetate (lyophilic in nature) and has a single glass transition temperature of 101 °C (Kolter et al., 2012). Even 15% w/v aqueous solutions of all three polymers have less than 60 cP viscosity at 25 °C, which allowed us to perform milling and spray drying without any likely processing issues such as pressure build-up in wet media milling and nozzle clogging in spray drying. Sodium dodecyl sulfate (SDS), an anionic surfactant with a CMC of 8.0 mM, purchased from GFS Chemicals, Inc. (Columbus, OH) was used as a wetting agent, which also helps to stabilize GF nanosuspensions. Dichloromethane, DCM (ACS reagent, ≥ 99.5%) was purchased from BDH Analytical chemicals (VWR, GA) and used as the solvent to prepare drug–polymer solutions. Wear resistant yttrium zirconia beads (Zirmil Y, Saint Gobain ZirPro, Mountainside, NJ, USA) with a median size of 430 µm was used as the milling media.

7.1.2 Preparation of Suspension-Based (W) and Solution-Based (S) feeds of ITZ and Their Spray Drying

Aqueous suspension-based (W:water) feeds of ITZ prepared by wet milling were fed to the spray dryer for the preparation of drug nanocomposites. Table 7.1 presents the formulations used in the precursor feeds. The concentration of ITZ and SDS was kept at 2.5% w/v and 0.125% w/v, respectively, in all suspensions. The concentration was calculated with respect to the 240 mL suspension liquid (deionized water). ITZ suspensions were prepared with three different polymers (HPC, Sol, and VA64) with drug:polymer mass ratios of 1:5 to examine the impact of polymer type on ITZ release in the dissolution tests. Finally, to investigate the impact of SDS in the

stabilization of the milled ITZ suspensions and ITZ release during dissolution tests, surfactant-free suspensions having the same drug:polymer mass ratios were also prepared for comparative analysis.

Table 7.1 Formulations and Compositions of the Suspension-Based (W) Feeds Used in Spray Drying Experiments

ID	Formulation[a]	GF (% w/v)[b]	SDS (% w/v)[b]	Polymers (% w/v)[b]			Water (mL)
				Sol	HPC	VA64	
W1	W-Sol	2.5	0	12.5	-	-	240
W2	W-HPC	2.5	0		12.5	-	240
W3	W-VA64	2.5	0	-	-	12.5	240
W4	W-Sol-SDS	2.5	0.125	12.5	-	-	240
W5	W-HPC-SDS	2.5	0.125		12.5	-	240
W6	W-VA64-SDS	2.5	0.125	-	-	12.5	240

[a]W denotes suspension-based feed; drug:polymer mass ratio was fixed at 1:5 in all the formulations; Sol denotes Soluplus; VA64 denotes polyvinylpyrrolidone vinyl-acetate (6:4).
[b]% w/v, with respect to the total solvent volume (240 mL).

In each milling experiment, a shear mixer (Fisher Scientific Laboratory Stirrer, Catalog No. 14-503, Pittsburgh, PA) was used to disperse as-received ITZ particles in aqueous stabilizer (HPC/Sol/VA64) solutions with and w/o SDS. The resultant GF pre-suspensions were transferred to the holding tank of a Microcer wet stirred media mill (WSMM) (Netzsch Fine Particle Technology, LLC, Exton, PA, USA) having 80 mL chamber. Milling conditions were adapted from our prior work on wet media milling (Afolabi et al., 2014; Bilgili et al., 2016; Bilgili et al., 2018). 50 mL of the milling chamber was filled with zirconia beads, and a screen with 200 μm opening was used at the outlet of the chamber to hold the beads in the chamber. A peristaltic pump was used to recirculate the suspension through the chamber at a rate of 126 mL/min and the suspension was milled for 64 min at a rotor speed of 4000 rpm. A chiller (Advantage Engineering Greenwood, IN, USA) was used to maintain

the milling chamber temperature below 35 °C throughout the milling. A portion of each suspension was separated in a vial and stored for 7-days at 8 °C to assess the short-term physical stability. Also, the milled suspensions were refrigerated at 8 °C overnight before spray drying.

The formulations of the solution-based (S) feeds to the spray dryer are provided in Table 7.2. The drug concentration was kept constant at 2.5% (w/v) in all the formulations, which was measured with respect to the total volume of the DCM (240 mL). ITZ solutions were prepared with three polymers (HPC, Sol, and VA64), while keeping the drug:polymer mass ratio constant at 1:5. After dissolving the drug–polymer into DCM using a magnetic stirrer, the solutions were sonicated for 30 min to ensure complete solubilization of the solid components before feeding to the spray dryer.

Table 7.2 Formulations and Compositions of the Solution-Based (S) Feeds Used in Spray Drying Experiments

ID	Formulation[a]	GF (% w/v)[b]	Polymers (% w/v)[b]			DCM (mL)
			Sol	HPC	VA64	
S1	S-Sol	2.5	12.5	-	-	240
S2	S-HPC	2.5	-	12.5	-	240
S3	S-VA64	2.5	-	-	12.5	240

[a] S denotes solution-based feed; drug:polymer mass ratio was fixed at 1:5 in all the formulations; the ratios refer to the polymer:polymer mass ratio; Sol denotes Soluplus; VA64 denotes polyvinylpyrrolidone vinyl-acetate (6:4).
[b] % w/v, with respect to the total solvent volume (240 mL).

7.2 Characterization Techniques

7.2.1 Particle Size Measurement

Drug particle size distributions (PSDs) in the suspensions were measured using a laser diffraction (LS 13 320, Beckman Coulter, Miami, FL) based on Mie scattering

theory following the procedure described in (Bilgili et al., 2016). Particle sizes were measured at various time points: right after milling, after 1-day and 7-day storage at 8 °C in a refrigerator. During the measurement, the intensity was maintained 40–50% while the obscuration was maintained below 8.0%. Refractive index values are 1.68 for ITZ (drug) and 1.33 for deionized water (medium). For each measurement, a 2.0 mL suspension sample was diluted with 5.0 mL of the respective stabilizer solution and mixed using a vortex mixer (Fisher Scientific Digital Vortex Mixer, Model No: 945415, Pittsburgh, PA) at 1500 rpm for 1 min.

The particle sizes of the spray-dried powders were measured by a Rodos/Helos laser diffraction system (Sympatec, NJ, USA) based on Fraunhofer theory following the procedure described in (Li et al., 2016b). About 1 g of the powder sample was placed on top of the sample chute of the Rodos dispersing system and the sample chute was vibrated at a 100% setting, and 0.1 bar dispersion pressure was used to suck in the falling powder through the sample cell of the laser diffraction system.

7.2.2 Solid State Characterization and Drug –Polymer Interactions

To analyze the crystallinity of the as-received ITZ, HPC, Sol, VA64, spray-dried powders, and physical mixtures of ITZ–polymer with or w/o SDS, X-ray powder diffraction (XRPD) (PANanalytical, Westborough, MA, USA), provided with Cu K_α radiation (λ= 1.5406 Å) was used. The samples were scanned at a rate of 0.165 s^{-1} for 2θ ranging from 5° to 40°.

Differential scanning calorimetry (DSC) of the as-received ITZ, Sol, HPC, VA64, spray-dried powders, and physical mixtures (PM) was performed using a

Mettler-Toledo polymer analyzer (PolyDSC, Columbus, OH, USA) with integrated STARe 10 software. ~6.0–7.0 mg powder sample was placed in an aluminum pan with a hole in the lid and loaded into the DSC machine. All the samples were heated at a rate of 10 °C/min from 25 °C to 200 °C. Nitrogen gas was used as the purge gas and protective gas at a flow rate of 50 mL/min and 150 mL/min, respectively. Thermogravimetric analysis (TGA) was performed to measure the residual water/solvent content using a TGA/DSC1/SF Stare system (Mettler Toledo, Inc., Columbus, OH). ~6.0–7.0 mg of each spray-dried sample was placed in a ceramic crucible and heated from 25 °C to 150 °C at a heating rate of 10 °C/min under nitrogen flow.

7.2.3 Drug Content in the Spray-Dried Powders and *In Vitro* Dissolution Tests

To measure the actual drug content, an assay testing was performed by dissolving 100 mg of the sample powders in 20 mL DCM under 30 min of sonication, followed by overnight storage to ensure complete solubilization of the GF particles. An aliquot of 100 µL was taken from the ITZ solution and diluted up to 10 mL using DCM. The absorbance of the samples was measured at 260 nm using UV spectrophotometer (Agilent, Santa Clara, CA, USA), and the drug concentration was calculated from a pre-established calibration curve. Six replicates were tested for each formulation to calculate the mean drug content along with the relative standard deviation (RSD).

Drug release from the spray-dried powders and physical mixtures (PMs) prepared by blending was determined *via* a Distek 2100C dissolution tester (North Brunswick, NJ, USA), following the USP II paddle method. 1000 mL of 0.1 N HCl solution at 37 °C was selected as the dissolution medium and stirred at 50 rpm paddle

speed. Considering the thermodynamic aqueous solubility of ITZ in 0.1 N HCl, i.e., 4.0 µg/mL at 37 °C (Ghazal et al., 2009), a high dose (100 mg) of ITZ would allow for supersaturating dissolution conditions. 100 mg ITZ equivalent spray-dried powders were poured into the dissolution medium and 4 mL samples were taken out manually at 1, 2, 5, 10, 20, 30, 60, 120, 180, and 210 min. These aliquots were filtered with a 0.1 µm PVDF membrane-type syringe filter before UV-spectroscopy measurements to minimize any confounding effect of the undissolved coarse drug aggregates (Bhakay et al., 2014a; Li et al., 2016b). The filtered samples were diluted with 0.1 N HCl solution kept at 37 ºC at a ratio of 1 to 10 before UV measurement. Dissolved GF amount was measured by UV-vis spectroscopy at 255 nm wavelength and calculated using a pre-established calibration curve. 0.1 N HCl solution was used as blank before UV measurement, and three replicates were performed for each sample. In this chapter, relative % supersaturation is reported based on GF concentration at 210 min and thermodynamic solubility of as-received ITZ particles, unless otherwise indicated.

7.2.4 Drug Wettability Enhancement by Sol and HPC Solutions With or W/O SDS

ITZ wettability was investigated by analyzing the penetration rate of stabilizer solutions into a packed bed of ITZ particles inside a cylindrical column according to the Washburn method (Hołownia et al., 2008; Washburn, 1921). Attension Sigma 700 (Biolin Scientific, Linthicum, MD, USA) set-up was used to measure the mass of the liquid penetrated the ITZ powder bed as a function of time. Experimental methods were adapted from Bilgili et al. (2018) and Li et al. (2017) and the details can be found in Section F.1 of the Appendix F. In the current study, liquids and powder refer to

aqueous solutions of 15% Sol/HPC/VA64 with 0.125% SDS or w/o SDS and as-received ITZ, respectively. All percentages are (% w/w) with respective to deionized water. The apparent shear viscosity and surface tension of the liquids were measured using R/S Plus Rheometer (Brookfield Engineering, Middleboro, MA, USA) and Attension Sigma 700 (Biolin Scientific, Linthicum, MD, USA), respectively. The ratio of the cosine of contact angles $\cos\theta_{ss}/\cos\theta_{w}$ was calculated using the modified Washburn equation and used as a wetting effectiveness factor. Here, θ_{ss} is the contact angle between ITZ and the stabilizer solutions and θ_{w} is the contact angle between ITZ and deionized water. This ratio or its logarithmic value provides a rough measure of the drug wettability enhancement upon use of various stabilizers in water.

7.2.5 Drug Supersaturation Maintenance Ability of the Polymers

Drug (ITZ) supersaturation maintenance ability of HPC/Sol/VA64 with or w/o SDS was examined in separate desupersaturation tests (similar to Konno et al., 2008). A concentrated solution of ITZ was prepared by adding 100 mg of as-received ITZ into 60 mL of methanol *via* sonication for 40 min. Unfortunately, 60 mL methanol did not completely dissolve 100 mg ITZ and a turbid solution was formed. The turbid solution was subsequently added to a 1000 mL of pre-dissolved HPC/Sol/VA64 in aqueous solution of 0.1 N HCl solution having 500 µg/mL concentrations to maintain 1:5 drug:polymer ratios (similar to the formulations in Table 7.1 and 7.2), respectively, with or w/o SDS in the USP II paddle type dissolution tester. The addition resulted in 69–78 µg/mL supersaturated solution of ITZ initially. This lower concentration of ITZ as compared with the targeted (100 µg/mL) resulted from both incomplete dissolution of IZT in methanol and inhomogeneous mixing of methanol

solution with the aqueous solution. Any subsequent desupersaturation during the following 210 min was tracked *via* ITZ concentration measurements. The experimental conditions and concentration measurements were identical to those in the dissolution test. All measurements were carried out in triplicate.

7.3 Results and Discussion

7.3.1 Properties of ITZ Suspensions Prepared *via* Wet Stirred Media Milling

Six ITZ suspensions with HPC/Sol/VA64 with 1:5 drug:polymer mass ratios and 0.125% SDS (W4–W6) and without SDS (W1–W3) were wet media milled. Table 7.3 shows the characteristic particle sizes of the 64 min milled suspensions and after 7-day storage. As-received ITZ particles had d_{50}: 15.5 µm and d_{90}: 45.8 µm, measured *via* Rodos/Helos laser diffraction system. After milling for 64 min, median particle sizes d_{50} were in the range of 0.16–0.24 µm for W4–W6 (Sol/HPC/VA64–SDS) and 0.21–0.80 µm for W1–W3 (Sol/HPC/VA64) formulations. Unless properly stabilized, milled drug nanoparticles are known to form micron-sized aggregates in aqueous suspensions (Bilgili and Afolabi, 2012; Bilgili et al., 2018). Table 7.3 suggests that only the formulations with SDS, ITZ nanosuspensions with median sizes d_{50} less than 200 nm were formed (except for W-VA64-SDS, W6), and the small changes in their d_{50} and d_{90} during the 7-day storage suggest that these suspensions were physically stable. Among the suspensions with the three polymers, VA64-based suspension had the coarsest particles in the presence/absence of SDS. Also, VA64-based suspension exhibited notable size increase upon 7-day storage, which resulted in d_{90} greater than 1 µm even in the presence of SDS (see Table 7.3).

Due to their relatively neutral charge, stabilizing capability of Sol/HPC/VA64 solely depends on their steric effects, which in turn is modulated by their adsorption onto ITZ nanoparticle surfaces. The adsorption is dependent on free polymer concentration in the suspension, and usually the adsorption is higher at high polymer concentrations until a saturation point is reached (Bilgili and Afolabi, 2012; Knieke et al., 2013).

Table 7.3 Particle Size Statistics of the Milled GF Suspensions After 64 min and 7-day Storage at 8 ºC

ID	Formulation[a]	After 64 min (μm)		After 7-day storage	
		d_{50} ± SD	d_{90} ± SD	d_{50} ± SD	d_{90} ± SD
W1	W-Sol	0.26±0.0	1.85±0.1	0.37±0.0	2.16±0.2
W2	W-HPC	0.21±0.0	0.32±0.0	0.23±0.0	0.35±0.0
W3	W-VA64	0.80±0.1	2.19±0.1	0.96±0.1	2.18±0.2
W4	W-Sol-SDS	0.16±0.0	0.25±0.0	0.18±0.0	0.25±0.0
W5	W-HPC-SDS	0.18±0.0	0.25±0.0	0.18±0.0	0.25±0.0
W6	W-VA64-SDS	0.24±0.0	0.45±0.0	0.27±0.0	1.81±0.1

[a] W denotes solution-based feed; drug:polymer mass ratio was fixed at 1:5 in all the formulations; the ratios refer to the polymer:polymer mass ratio; Sol denotes Soluplus; VA64 denotes Kollidon VA64.

Clearly, presence of 0.125% in the suspensions had the most dramatic effect on the stabilization and extent of nanoparticle aggregation. HPC–SDS was reported to have synergistic stabilizing effect on multiple BCS Class II drug nanosuspensions during milling and storage (Bilgili et al., 2016). HPC, Sol, and VA64 imparted steric stabilization by adsorbing on drug nanoparticles (Bilgili and Afolabi, 2012; Bilgili et al., 2018; Yang et al., 2014), while the anionic surfactant (SDS) enhanced ITZ wettability/deaggregation and helped to stabilize the ITZ nanosuspensions *via* electrostatic repulsion. As can be seen from Table 7.4, polymers alone and polymer–SDS combination reduce the surface tension and enhanced the ITZ wettability by water. As indicated by the higher wetting effectiveness factor, HPC (hydrophilic polymer) renders ITZ more wettable by water than VA64 and Sol (amphiphilic

polymer), and SDS enhances the wettability even further when used in combination with both polymers. The wettability is important to deggregation of the aggregates formed during milling, which allows for full exposure of ITZ particle surfaces for polymer adsorption. The lower wettability of ITZ by Sol and VA64 as compared with HPC could be another reason for the large aggregates in VA64 and Sol-based suspensions. On the other hand, with SDS, finer suspensions were obtained with Sol than with HPC, which suggests differing interaction between polymer–SDS. While wettability results here helped us to explain the milling results, they should be used with caution for interpreting the impact of polymers/surfactant on the wettability enhancement because the dissolution medium was 0.1 N HCl whereas the modified Washburn experiment was conducted with deionzied water as the penetrating liquid.

Table 7.4 Properties of Deionized Water–Aqueous Stabilizer Solutions and Wetting Effectiveness Factor Determined Using the Modified Washburn Method

Formulation	η, (cP)	ρ, (g/mL)	γ, (mN/m)	Slope, (g^2/s)	R^2 (-)	$\cos\theta_{ss}/\cos\theta_w$	$\log(\cos\theta_{ss}/\cos\theta_w)$
Water	0.89[a]	1	70.8	6.5×10^{-6}	0.995	1	0
Sol	8.21	1.02	41.6	1.9×10^{-3}	0.996	4430	3.65
HPC	54.4	1.02	40.5	7.0×10^{-4}	0.999	11120	4.01
VA64	6.75	1.02	40.0	4.1×10^{-3}	0.998	8180	3.91
Sol–SDS	13.3	1.01	38.6	2.0×10^{-3}	0.999	8310	3.92
HPC–SDS	63.2	1.01	39.4	9.0×10^{-4}	0.999	17410	4.24
VA64-SDS	8.76	1.01	38.2	4.9×10^{-3}	0.999	13550	4.13

[a]The slope of the water penetration data was used as reference for wettability enhancement by the stabilizer solution.

7.3.2 Size, Morphology, and Drug–Moisture Content of the Spray-Dried Powders

Despite the relatively short residence time (4 s and 5 s), the powders produced form both suspension-based (W) and solution-based (S) feeds were completely dried, as indicated by TGA, which shows weight loss of 2.0 ± 0.3% for the samples. The high surface area generated by atomization of the feed coupled with the convective heat–mass transfer at high air temperature enabled fast drying of the droplets in the drying chamber. The mean (actual) drug content after spray-drying was close or slightly higher than the theoretical drug content; all RSD values were below 6%: 0.49–5.23%, which signifies pharmaceutically acceptable content uniformity (see Table 7.5). Table 7.5 shows that for a given polymer, the ITZ suspension without SDS (W1–W3) had smaller particles than that with SDS (W4–W6) and the ITZ solution (S1–S3). The presence of aggregated ITZ particles and the aqueous viscosity–surface tension of the base-polymer/SDS appeared to have a joint effect on the particle size of the suspension-based spray-dried powders. Despite an increase in base viscosity, the presence of SDS resulted in lower surface tension (Table 7.4) and smaller ITZ aggregates (Table 3), which could explain the smaller spray-dried particles in the presence of SDS.

Table 7.5 Particle Size Statistics of the Spray-Dried Powders and Their Drug Content

ID	Formulation[a]	Size of the spray-dried powders (μm)			Theoretical drug content (%w/w)[b]	Actual drug content, RSD (%w/w, %)[b]
		d_{10}±SD	d_{50}±SD	d_{90}±SD		
W1	W-Sol	9.65±0.1	28.8±0.0	57.9±0.1	16.7	16.7, 0.49
W2	W-HPC	7.33±0.1	23.0±0.3	56.4±0.1	16.7	17.2, 3.56
W3	W-VA64	3.20±0.1	18.7±0.2	41.5±0.2	16.7	16.9, 4.31
W4	W-Sol-SDS	5.20±0.0	13.5±0.0	38.2±0.0	16.5	16.8, 5.10
W5	W-HPC-SDS	7.93±0.1	14.7±0.1	35.9±0.6	16.5	16.7, 4.37
W6	W-VA64-SDS	4.21±0.0	11.5±0.0	37.7±0.1	16.5	16.9, 1.93
S1	S-Sol	4.20±0.0	15.8±0.5	48.6±0.7	16.7	17.1, 2.02
S2	S-HPC	4.90±0.1	12.3±0.2	39.7±0.2	16.7	16.9, 5.23
S3	S-VA64	3.27±0.1	5.1±0.1	37.6±0.1	16.7	17.0, 3.41

[a]S denotes solution-based feed; W denotes suspensions-based feed; drug:polymer mass ratio was fixed at 1:5 in all the formulations; the ratios in the formulations refer to the polymer:polymer mass ratio; Sol denotes Soluplus; VA64 denotes polyvinylpyrrolidone vinyl-acetate (6:4).
[b]%w/w with respect to the total weight of the solid content.

7.3.3 Formation of Drug HyNASDs and ASDs Upon Spray Drying

Figures 7.1 and 7.2 illustrate the XRPD diffractograms of the spray-dried powders. X-ray diffractograms depict that as-received ITZ exhibited intense peak characteristics of a crystalline material. The physical mixtures (PMs), prepared by blending of as-received ITZ with HPC/Sol/VA64 or HPC/Sol/VA64–SDS powders, exhibited peaks at the same diffraction angles as those of as-received ITZ, albeit with reduced intensity. The diffractograms of the spray-dried powders with SDS (Figure 7.1a) and without SDS (Figure 7.1b) did not remarkably differ, except for peak intensities; they exhibit patterns similar to those of the physical mixtures. The peak intensities of ITZ in the PMs were lower than those of the as-received ITZ powder, which can be attributed to the dilution and surface coverage of ITZ microparticles with HPC/Sol/VA64. Similar XRPD diffractograms to those of the PMs were observed for the spray-dried powders produced from suspension-based feeds

confirming that spray-drying of the milled suspensions led to formation of nanocomposites that are crystalline in nature. Interestingly, the diffractograms of the spray-dried powders show significant peak broadening and reduction in intensities as compared with their respective PMs, beyond the aforementioned dilution effect of the polymers. This peak reduction points to the possibility that wet media milling followed by spray-drying led to reduction of crystallinity and formation of notable amorphous ITZ (similar to the observations in Chapter 3 and Chapter 4 for GF). However, unlike for the GF nanocomposites, the crystallinity has not been quantified here for the ITZ nanocomposites. It is conjectured that wet media milling does not cause any detectable amorphization of as-received ITZ, in the absence of stabilizers, due to plasticization effect of water (Bilgili et al., 2018; Li et al., 2018b). In the presence of high polymer loading in the suspensions here, however, amorphization of ITZ seemed to have taken place during the spray drying. Looking at the XRPD diffractograms (Figure 7.1a and 7.1b), the reduction in the peak intensity and peaks broadening confirm some extent of amorphization of ITZ occurred. Taking a close look, it is visible that the reduction in peak intensity is more pronounced for the ITZ–Sol formulation than for the ITZ–HPC/VA64 formulations with/without SDS.

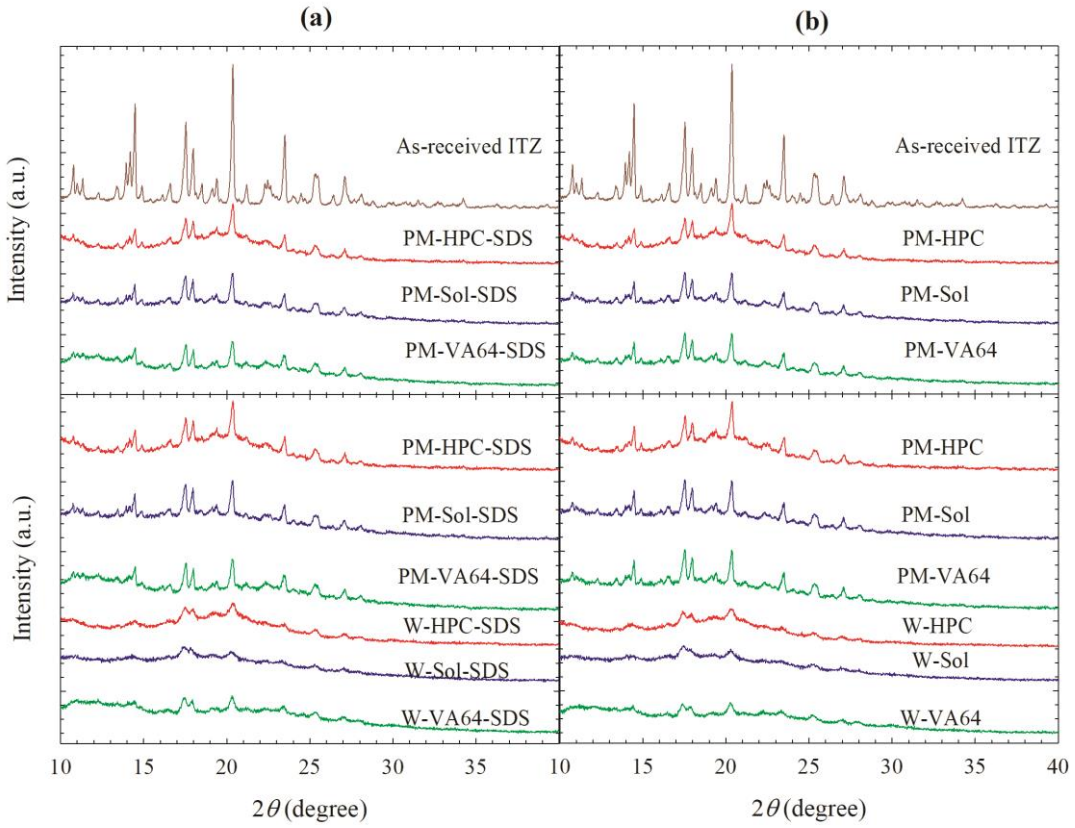

Figure 7.1 X-ray diffractograms of as-received ITZ, physical mixtures (PMs) of GF–HPC/Sol/VA64 and the spray-dried powders prepared using the ITZ suspension-based (W) feed with 1:5 drug:polymer mass ratios: (a) without SDS and (b) with 0.125% SDS in the suspension.

These findings imply that (i) amorphous ITZ formed due to ITZ–polymer molecular interactions and/or solubilization of the surface layer of nanoparticles by the polymer during the spray-drying and (ii) Sol appears to favor the amorphization of ITZ more than HPC and VA64, which implies stronger Sol–ITZ molecular interactions/miscibility than HPC/VA64–ITZ. It is likely that presence of ITZ nanoparticles and their aggregates with large surface area and higher polymer loading (more ITZ–polymer interactions and higher ITZ solubilization in the polymer) could have favored the formation of amorphous GF. Based on our findings and Kayaert and Van den Mooter, 2012, it is proposed that the polymeric matrix of the spray-dried

particles encapsulates drug nanocrystals/aggregates, surrounded by a layer of amorphous ITZ molecularly dispersed in the polymer. Formation of amorphous content upon drying of drug nanosuspensions was first noted by Kayaert and Van den Mooter, 2012, albeit to a lower extent, and was regarded as "unfavorable". Nonetheless, the impact of such amorphous content on drug release from the nanocomposites has not been studied at all. As the dissolution tests will reveal, despite being crystalline in nature, these nanocomposites with relatively high polymer loading (low drug:polymer ratio) allow for much higher supersaturation than traditional nanocomposites, similar to the supersaturation levels observed for ASDs; hence, we coin the term hybrid nanocrystal–ASD (HyNASD) for this special class of nanocomposites.

XRPD diffractograms (Figure 7.2) of the spray-dried powders produced from solution-based (S) feeds showed halo pattern instead of any characteristic diffraction peaks of ITZ. These halo patterns confirm that amorphous ITZ dispersed molecularly into the polymer matrix forming amorphous solid dispersions (ASDs).

Generally, it is suggested that if the solubility parameter difference between a drug and polymer is <7.0 $MPa^{1/2}$, they are likely to be miscible; if the difference is >10 $MPa^{1/2}$, they are considered immiscible (Forster et al., 2001; Greenhalgh et al., 1999). The solubility parameters of ITZ, HPC, Sol, and VA64 are 22.6 (Kolter et al., 2012), 24.0 (Choi et al., 1994), 19.4, and 19.7 (Kolter et al., 2012) $MPa^{1/2}$, respectively. The solubility parameter differences between ITZ–Sol and ITZ–VA64, and ITZ–HPC are 3.2, 2.9, and 1.4 $MPa^{1/2}$, respectively, which suggests that ITZ–Sol/VA64/HPC all are miscible based on the solubility parameter difference and very

likely to produce amorphous solid dispersions of ITZ. While being useful, the solubility parameters do not account for all drug–polymer interactions such as contributions from hydrogen bonding, hydrophobic interactions, etc., and hence should be used with caution as rough estimates of drug–polymer miscibility.

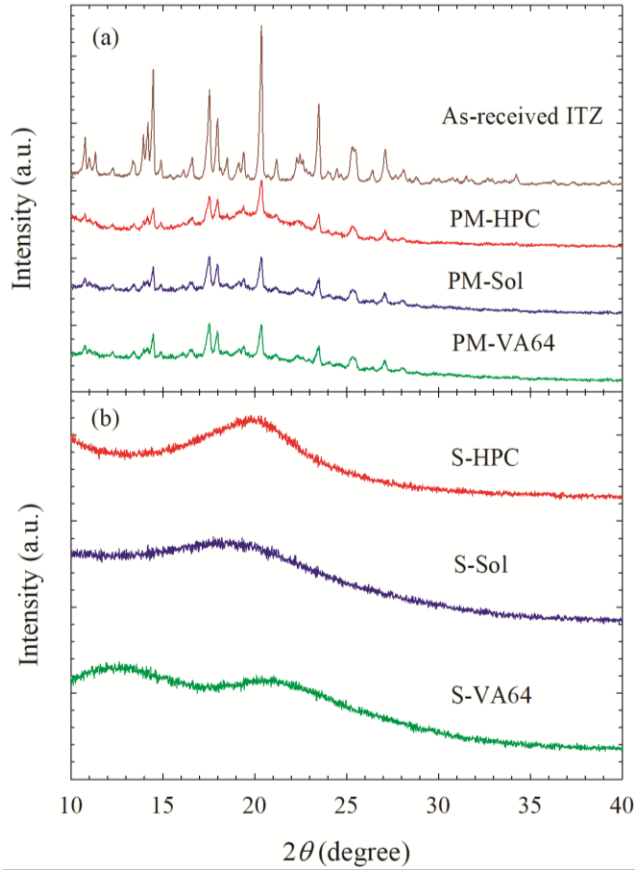

Figure 7.2 X-ray diffractograms of as-received ITZ, and physical mixtures (PMs) of GF–HPC/Sol/VA64 (a); spray-dried powders prepared using the ITZ solution-based (S) feeds with 1:5 drug:polymer mass ratio (b).

The DSC thermograms in Figure 7.3 show an endothermic peak associated with melting of as-received ITZ, with a melting point temperature T_m of 171 °C and a fusion enthalpy ΔH_f of 70.9 J/g; a glass transition for Sol (amorphous) at 72.4 °C, a glass transition for VA64 (amorphous) at 102 °C and a slight endothermic event

around 170–200 °C for HPC likely due to the melting of the small crystalline domain of largely amorphous HPC (Sarode et al., 2013) (crystallinity was undetectable by XRPD). The T_g of HPC could not be measured as it is in the range of –25 to 0 °C (Sarode et al., 2013) and our DSC equipment is limited. The spray-dried powders exhibited a melting endotherm only, corresponding to the fusion of their ITZ crystals. The absence of any recrystallization event during the heating could suggest that the amorphous ITZ in HyNASDs did not recrystallize due to ITZ–polymer molecular interactions as the amorphous content was in the ASD surrounding the drug crystals.

The DSC thermograms in Figure 7.3 and the data in Table 7.6 show that spray-drying of ITZ suspensions led to drastic melting point depression (high ΔT_m), up to 37 ºC, and reduction of ΔH_f even if the values were corrected for dilution with polymer and reduced crystallinity (not shown for brevity). Higher ΔT_m and lower ΔH_f of the spray-dried powders than those of the PMs suggest that the amorphous ITZ content of the spray-dried powders was lower. The significant melting point depression in drug–polymer mixtures is indicator of drug–polymer miscibility (Baird and Taylor, 2012; Newman et al., 2008). Moreover, without exceptions, having identical polymer/SDS composition, the spray-dried powders with Sol had higher ΔT_m and lower ΔH_f than those with HPC and VA64, which could be explained by (i) stronger ITZ–Sol interactions, (ii) higher initial amorphous content in the Sol-based spray-dried powders, and (iii) higher extent of solubilization of ITZ in the polymer melt at high temperatures due to the thermal treatment during the DSC scan. Compared with the clear trends regarding the impact of different polymers for

formulations with/without SDS, the trends for SDS impact were not as strong and as clear.

Table 7.6 Characteristic Temperatures–Enthalpy Values Obtained From DSC Thermograms

ID	Formulation[a]	T_g (ºC)[a,b]	T_m (ºC) [a,b]	ΔH_f (J/g) [a,b]
ITZ	As-received ITZ	ND	171	70.9
W1	W-Sol	ND	134	1.02
W2	W-HPC	ND	160	6.32
W3	W-VA64	ND	141	3.00
W4	W-Sol-SDS	ND	137	1.35
W5	W-HPC-SDS	ND	159	4.91
W6	W-VA64-SDS	ND	141	5.17
S1	S-Sol	72.3	ND	ND
S2	S-HPC	ND	ND	ND
S3	S-VA64	99.6	ND	ND

[a]S denotes solution-based feed, Sol denotes Soluplus; the ratios refer to the polmer:polymer mass ratios. Other symbols: T_g, T_{rc}, and T_m stand for temperature for glass transition, recrystallization transition, and melting point, respectively, while ΔH_{rc} and ΔH_f respectively stand for recrystallization enthalpy and fusion enthalpy.
[b]ND: not detected.

For the spray-dried powders prepared from the drug–polymer solutions (Figure 7.4), a single T_g was observed for all the formulations confirming the formation of molecular level dispersion (Luebbert et al., 2017; Wlodarski et al., 2015) (Table 7.6). Due to strong molecular interactions and good miscibility of ITZ–Sol, ITZ–HPC, and ITZ–VA64, recrystallization event at high temperature was not observed for the any of the formulations during the DSC scan. However, for S-VA64 formulation, at higher temperature (around 170 ºC) there was a thermal event observed, which might be due to phase separation of the drug and the polymer. Overall, the XRPD and DSC results suggest that spray-drying of ITZ–polymer

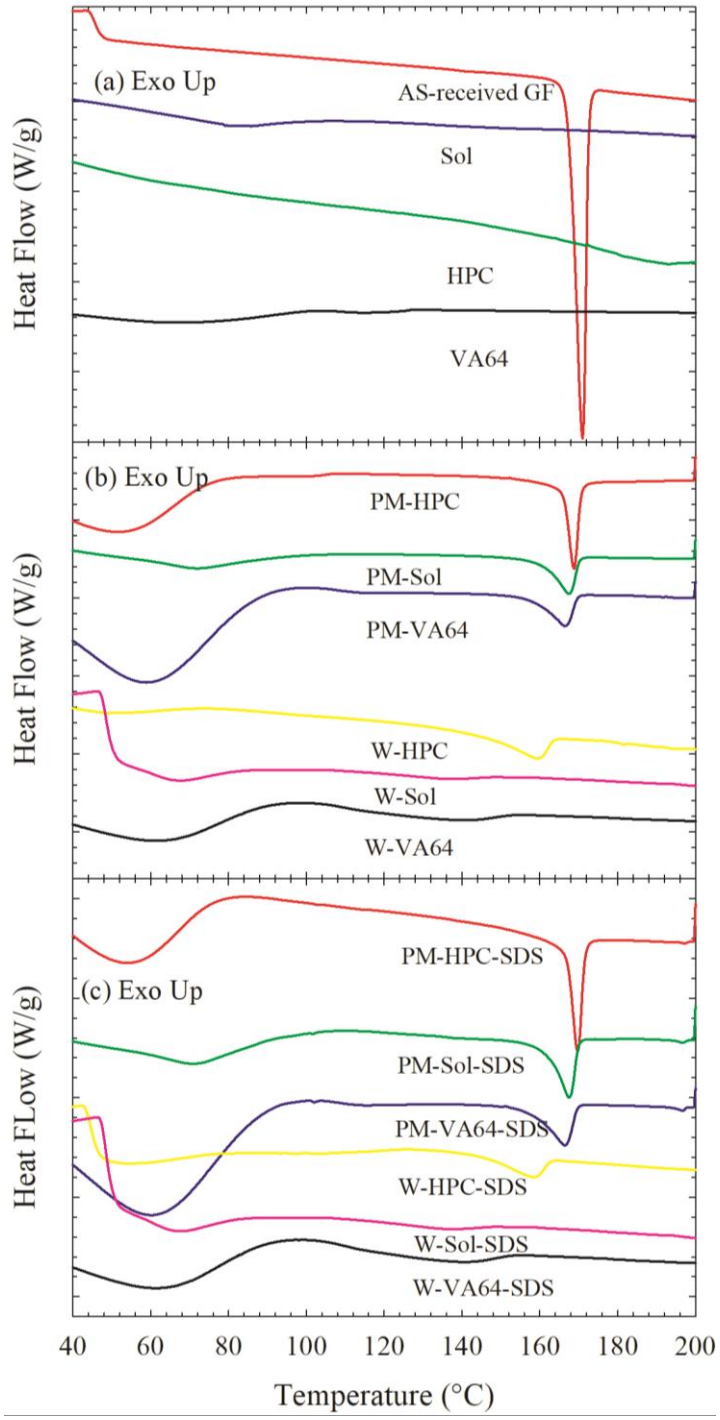

Figure 7.3 DSC thermograms of as-received ITZ, HPC, Sol, and VA64 (a); physical mixtures (PMs), and spray-dried powders prepared using the ITZ suspension-based (W) feed with 1:5 drug:polymer mass ratio: (b) without SDS and (c) with 0.125% SDS in the suspension.

nanosuspensions with/without SDS led to formation of drug HyNASDs and ITZ–polymer solutions led to formation of ASDs. Therefore, as a general observation, similar to Chapter 3 and Chapter 4, we note that spray-drying of a drug nanosuspension with a lower drug:polymer mass ratio (high polymer concertation) than typically used (see e.g., Table 1.2) and the use of a strongly miscible polymer that interacts with the drug nanoparticles and solubilizes them during the spray drying favor the formation of HyNASDs.

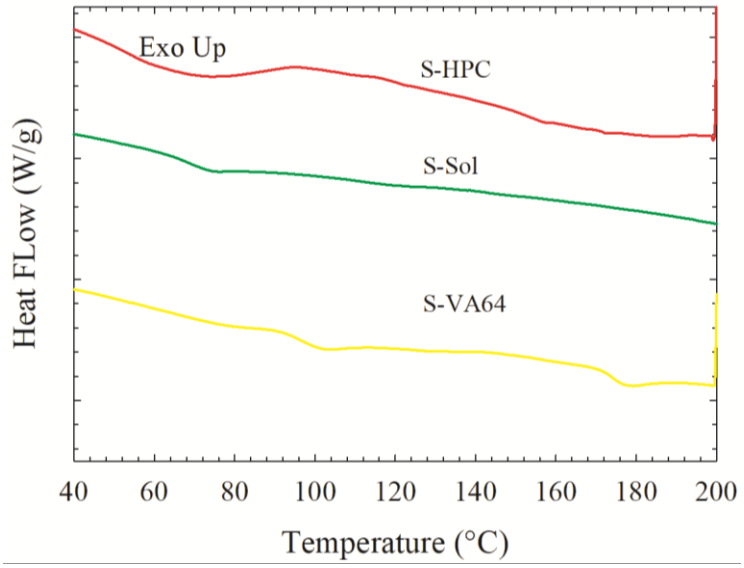

Figure 7.4 DSC thermograms of spray-dried powders prepared using the ITZ solution-based (S) feed with 1:5 drug:polymer mass ratio.

7.3.4 Dissolution performance of the Spay-Dried Powders in Supersaturating Condition

The temporal evolution of ITZ release from the spray-dried powders and the PM with the highest polymer loading (1:5 ITZ:polymer) containing 100 mg equivalent ITZ dose in 1000 mL 0.1 N HCl solution at 37 ºC was investigated. The bulk dissolution medium could supersaturate for this high drug dose as the ITZ solubility is ~4.0

mg/L. Unless otherwise specified, all supersaturation values are relative to aqueous thermodynamic solubility of ITZ and calculated at 210 min.

Considering that the major shortcoming of traditional drug nanocomposites with low polymer loading as compared with amorphous solid dispersions (ASDs) is their limited supersaturation capability in dissolution media, the examination of drug dissolution under supersaturating condition is critical. The most striking feature of Figure 7.5a and 7.5b is that Sol-based HyNASDs, nanocomposites with notable amorphous content, achieved 840% and 1230% ITZ supersaturation without SDS and with SDS, respectively. Such high supersaturation has not been reported for drug nanocomposites before, but for ASDs. A cursory look at Figure 7.5 also reveals some general trends: (i) the spray-dried powder could generate ITZ superstation more than the corresponding PM for 1:5 GF:Sol with and w/o SDS, (ii) the ITZ supersaturation was higher for spray-dried powders with SDS than those without SDS, and (iii) Sol-based formulations generated much higher supersaturation than HPC/VA64-based formulations especially when the formulation included SDS. These results point to the criticality of the wettability of the spray-dried powder, which is enhanced by SDS, ITZ–polymer interaction and solubilization of the ITZ by the polymer. The smaller ITZ nanoparticle sizes and the smaller spray-dried particle sizes in the presence of SDS could explain why the powders with SDS released ITZ faster besides the obvious wettability enhancement imparted by SDS (see Table 7.4).

During the dissolution test, as water wets and imbibes into the spray-dried particles, their polymer dissolves and the particles redisperse into smaller ITZ–polymer/SDS clusters depending on the wettability, while their amorphous ITZ

fraction contributes to the dissolution. In the polymer/SDS-rich microenvironment of the particles and releases clusters, ITZ could be solubilized by the polymer/SDS, and the rate of this process depends on the cluster/particle size as well as ITZ particle size inside these clusters as well as the drug:polymer mass ratio and presence/absence of SDS. Unfortunately, depending on the polymer–drug miscibility and interactions, amorphous content of the HyNASDs may phase-separate and recrystallize upon contact with water in the dissolution medium (Alonzo et al., 2011; Chen et al., 2015)

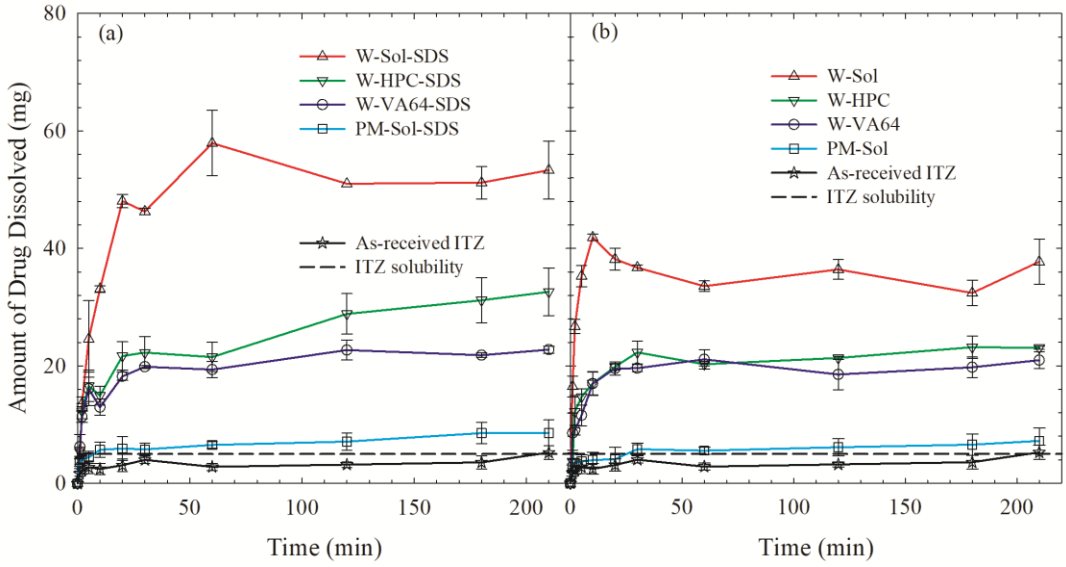

Figure 7.5 Evolution of drug release from as-received ITZ, physical mixture (PM) with 1:5 ITZ:Sol mass ratio, and spray-dried powders prepared using GF suspension-based (W) feeds with 1:5 drug:polymer mass ratios: (a) with 0.125% SDS in the ITZ suspensions and (b) without SDS. Dissolution sample size equivalent to 100 mg ITZ dose.

because water acts as a plasticizing agent, reducing the glass transition of the ASD component of HyNASDs and enhancing the mobility of the drug molecules (Chen et al., 2015). Finally, the supersaturated ITZ in the dissolution medium and the released drug nanoparticles form a metastable system, and ITZ could recrystallize on existing

ITZ nanoparticles and cause their growth in time, which in turn could cause reduced supersaturation. Strong drug–polymer interactions can reduce the molecular mobility and delay recrystallization onset time and the extent of recrystallization (Mistry et al., 2015).

With the hope of additional insights into the ITZ recrystallization inhibition capability of Sol/HPC/VA64 with and w/o SDS in supersaturated ITZ solutions, desupersaturation experiments were performed during which the dissolved ITZ shifts from methanol (high solubility) to methanol–water mixture (low solubility), thus creating supersaturation (see Figure 7.6). A peak ITZ supersaturation was attained fast upon mixing the ITZ solution with deionized water, and it was maintained up to ~210 min with all the polymers with and w/o SDS. SDS did not in the supersaturation maintenance is not significant compared to the polymers. In the absence of any inhibitor, ITZ recrystallized fast and its concentration exponentially decayed to an equilibrium concentration in 60 mL methanol–1000 mL water mixture (~21 µg/mL). Unfortunately, methanol volume was so high to affect the solubility in the desupersaturation experiment. Moreover, to be more predictive of the dissolution test, 0.1 N HCl rather than deionized water should have been used. Unfortunately, these results do not discern the inhibition capability of the polymers, nor do they confidently suggest that all polymers were good crystallization inhibitors of ITZ because a high supersaturation that mimics the saturation level in the dissolution vessel could not be achieved using 60 mL methanol in the desupersaturation experiment. It appears that a better solvent than methanol for ITZ is required and that solvent must be miscible with water and should be used at a lower solvent:antisolvent

mass ratio to generate high supersaturation. With such a caveat in mind, it may be fair to assert that in the presence of the polymers, ITZ recrystallization did not occur from the solutions with the specific supersaturation levels studied here.

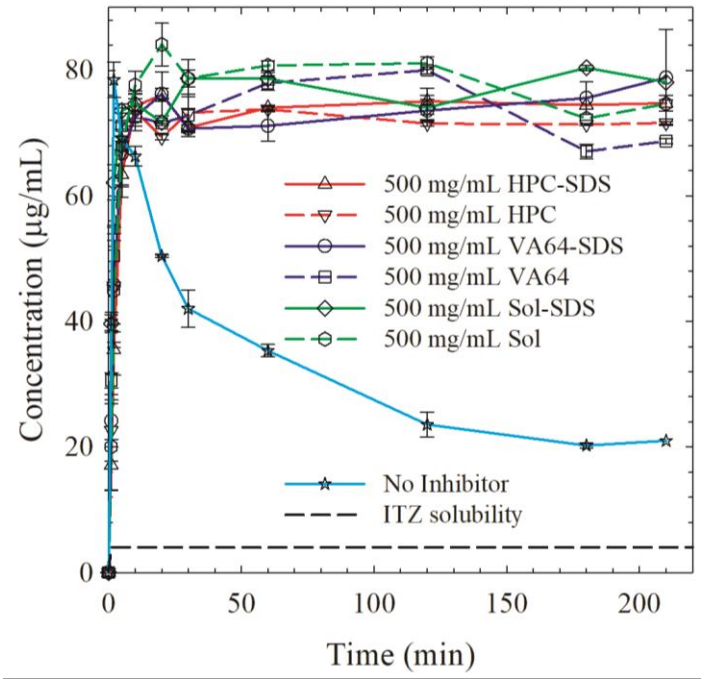

Figure 7.6 ITZ desupersaturation curves for a 60 mL ITZ–methanol solution mixed with 940 mL aqueous solutions of 500 µg/mL of HPC/Sol/VA64–5 µg/mL SDS or w/o SDS (corresponding to 1:5 drug:polymer formulations). The initial concentration of GF right after mixing was targeted at 100 µg/mL.

A comparison of Figure 7.7a (ASDs) and Figure 7.7b (HyNASDs) indicates that ASDs outperform HyNASDs owing to the presence of 100% amorphous ITZ in the former. However, it is amazing to see such high supersaturation (up to 840%) from the HyNASDs/ Figure 7.7a also shows that 1220%, 1340%, and 1980% relative supersaturation was achieved by HPC-based, VA64-based, and Sol-based ASDs with SDS, respectively, at 210 min. Interestingly, even after 210 min of dissolution, the profile is still rising, which signifies that if the dissolution test was run longer than

210 min, the extent of supersaturation would be even higher. Before an attempt is to be made to explain these results, some caveats regarding the interpretation of dissolution results in view of the desupersaturation and wettability results must be mentioned. It is speculated based on the somewhat inconclusive desupersaturation test results (refer to Figure 7.6) that all three polymers are capable of maintaining the supersaturation in the dissolution medium. Also, since the Washburn experiments were carried out with deionized water rather than 0.1 N HCl, relating the ITZ wettability enhancement to the dissolution results are somewhat confounded due to the pH effect. Since the reduced pH in the acidic media results in ionization of ITZ (weak base), it is likely that surface properties and wettability changed with the pH. It should also be noted that the dissolution profiles in Figure 7.7a did not plateau within 210 min; hence, longer dissolution time is needed to glean the impact of potential recrystallization.

The solubility parameter differences suggest all polymers are miscible with ITZ, while the melting point depression results (refer to Table 7.6) suggest the miscibility of ITZ with Sol > VA64 > HPC. The supersaturation generation in Figure 7.7a correlated positively with the ITZ–polymer miscibility inferred from DSC. The remarkably high ITZ supersaturation achieved by Sol-based ASDs as compared with HPC/VA64-based ASDs can be explained by the greater miscibility with ITZ and higher ITZ solubilization in Sol micelles in the dissolution medium. It is well-established that depending on the drug–polymer miscibility and interactions, amorphous drug may phase-separate and recrystallize upon contact of ASDs with water in the dissolution medium (Alonzo et al., 2011; Chen et al., 2015). Once

imbibed into the ASD matrix, water acts as a plasticizing agent, enhancing the mobility of the drug molecules by reducing the T_g of the ASD (Chen et al., 2015). HPC-SSL has sub-ambient T_g (Srode et al., 2013) (lower than T_g of Sol: 73 ± 2 °C and VA64: 101 ºC) and its ASDs have lower T_g (was not possible to detect) than Sol-based ASDs (Table 7.6). Owing to good miscibility of ITZ–HPC, no phase separation and recrystallization appeared in Figure 7.7a within 210 min (rising profile).

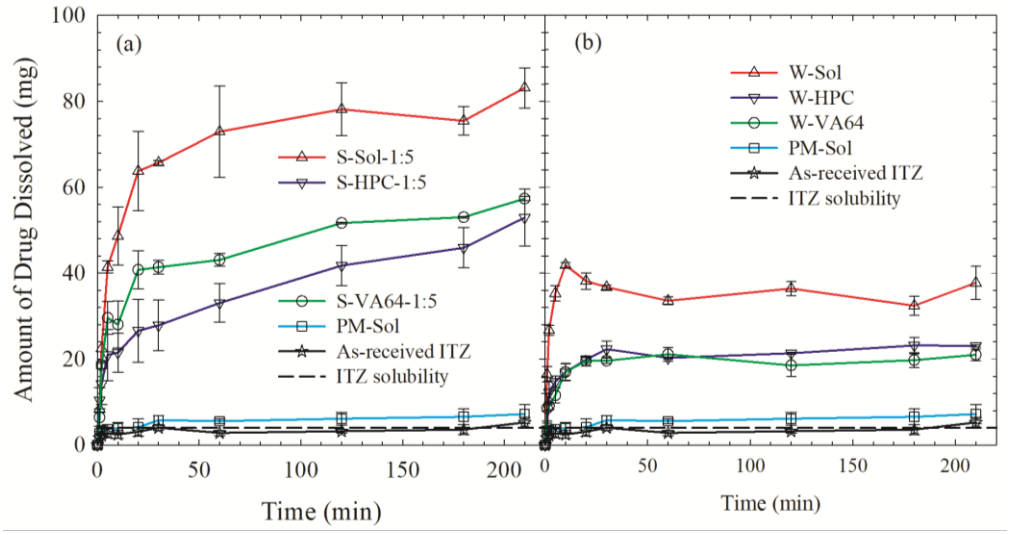

Figure 7.7 Evolution of drug release from as-received ITZ, physical mixture (PM) with 1:5 ITZ:Sol mass ratio, and spray-dried powders prepared from: (a) ITZ solution-based (S) feeds and (b) ITZ suspension-based (W) feeds with 1:5 drug:polymer mass ratios. Dissolution sample size equivalent to 100 mg ITZ dose.

7.4 Conclusion

Spray-drying of wet-milled ITZ suspensions with high polymer loading (1:5 ITZ:polymer mass ratio) with HPC/Sol/VA64 and with/without SDS led to formation of a special class of nanocomposites, HyNASDs, which contain drug nanocrystals and aggregates surrounded by notable amorphous content molecularly dispersed in the polymeric matrix. XRPD and DSC thermogram shed light on the HyNASD

formation and revealed miscibility of ITZ with Sol/HPC/VA64. However, the interaction seems to be stronger in the case of ITZ–Sol than ITZ–HPC/VA64 from XRPD and DSC results. Presence of SDS in the formulation enhanced the relative wetting effectiveness of the polymers significantly and in the dissolution test helped to reach higher extent of supersaturation. This higher extent of supersaturation may be explained by the solubilizing effect of SDS, but due to the inconclusive nature of the Washburn experiments and desupersaturation experiments in deionized water, the roles of SDS could not be well-elucidated. Without SDS in the formulation, 480%, 430%, and 840% relative supersaturation was achieved from HPC, VA64, and Sol-based formulation, respectively, at 210 min. On the other hand, presence of SDS in the formulation resulted 720%, 470%, and 1230% relative supersaturation from HPC, VA64, and Sol-based formulation, respectively. Therefore, the results here for ITZ are in line with our previous observations in Chapter 2 and Chapter 3, where significant supersaturation generation from drug nanocomposites was possible by forming HyNASDs and presence of SDS boosted up the supersaturation level. Although ASD formulations generated higher extent of supersaturation (up to 1980%) than HyNASDs, 840% relative supersaturation from a largely crystalline formulation is an interesting, novel, and impactful finding.

CHAPTER 8

CONCLUSIONS AND FUTURE WORK

8.1 Conclusions

This thesis research has identified two major challenges in the bioavailability enhancement of BCS Class II drugs *via* drug nanocomposites and amorphous solid dispersions (ASDs): (i) the major drawback of nanocomposites is their inability to attain high drug supersaturation during *in vitro* (<50% relative supersaturation) and *in vivo* dissolution; (ii) formulating an amorphous solid dispersion (ASD) with high drug loading (>20%) that releases drug rapidly, while generating and maintaining high supersaturation over at least three hours is challenging. The goal of this thesis was to develop a fundamental understanding of the impact of anionic surfactants–polymers on *in vitro* drug release from nanocomposites and ASDs, while addressing the aforementioned challenges. This dissertation has developed a processing–formulation approach to produce both nanocomposites and ASDs with identical formulation, which has allowed us to have a true head-to-head comparison of nanocomposites and ASDs.

Spray drying of milled drug nanosuspensions with high polymer loading (unlike traditional drug nanosuspension formulations) enabled us to produce a new class of drug nanocomposites titled hybrid nanocrystal–ASD (HyNASD). HyNASDs contain a notable fraction (5–22%) of amorphous drug molecularly dispersed in the polymeric matrix that encapsulates drug nanoparticles. They generated high drug supersaturation rapidly (~300% within 20 min) in the dissolution tests unlike traditional nanocomposites (max. 50%), which could render nanoparticle

formulations more competitive to ASDs in bioavailability enhancement of poorly soluble drugs. The supersaturation generation capability of HyNASDs is largely controlled by drug–polymer interactions/miscibility as well as the size of the drug (nano)crystals in the polymeric matrix. While HyNASDs did not generate as high saturation as ASDs (480%), they can be rendered competitive to ASDs upon further formulation–process optimization.

In wet media milling of drugs, various hydrophilic/amphiphilic polymers along with an anionic surfactant provided excellent physical stability to drug nanoparticles *via* electrosteric mechanisms. In the absence of the surfacatant, large aggregates of the drug nanoparticles formed. Significant supersaturation generation and maintenance was achieved by HyNASDs for high drug dose (100 mg). On the other hand, the supersaturation generation capability of HyNASDs was largely controlled by the anionic surfactant either in the formulation or in the dissolution medium, drug–polymer interactions/miscibility as well as the size of the drug (nano)crystals in the polymeric matrix.

Inclusion of an anionic surfactant as a minor component along with a drug-miscible polymer (major component), which can provide significant solubilization of the drug and supersaturation maintenance *via* recrystallization inhibition, could boost drug supersaturation from the ASDs *via* mainly wettability enhancement and some additional drug solubilization. Unlike the use of surfactant as carriers/solubilizers, the use of an anionic surfactant as a minor component dramatically improved the wettability of the drug ASDs, without having any deleterious impact on drug recrystallization, which is a common problem in polymer–surfactant carrier systems.

Also, the use of low concentrations of an anionic surfactant even in high-dose applications of ASDs alleviates any concern associated with the toxicity of anionic surfactants.

Ternary ASDs of a poorly soluble fast crystallizing drug (GF) with binary combinations of HPC/VA64/Sol and binary ASDs of GF with the corresponding individual polymers, all having 1:3 GF:total polymer mass ratio, were prepared using spray-drying. Although binary ASDs with single polymer showed dissolution enhancement compared to as-received GF and physical mixtures, a desirable dissolution profile, i.e., rapid GF release concurrently generating fast supersaturation that lasts 3 hours, was not achieved. The dissolution profiles of the ternary ASDs of binary polymers were mostly reflective of the deficiencies of the polymers in terms of wettability enhancement and recrystallization inhibition in the ASD matrix and the dissolution medium. As expected, the combination of the two hydrophilic polymers HPC–VA64 without an amphiphilic crystal-inhibiting polymer (Sol) led to low supersaturation, below 80%. Being an effective crystallization inhibitor, Sol compensated for HPC's inability to prevent recrystallization; but there was no synergistic positive impact. Any increase in initial drug release rate upon use of HPC was nullified by lower extent of supersaturation. Finally, based on the results regarding GF release from ternary ASDs with Sol-VA64, we conclude that a ternary ASD of GF could exhibit synergistic enhancement of drug release rate and its extent upon combined use of an amphiphilic polymer (Sol, as a crystallization inhibitor) as a major component and the hydrophilic polymer (VA64) as a minor component that provides wettability enhancement.

General findings from the research on GF regarding HyNASD formation and impact of SDS were applicable to another poorly water-soluble, BCS Class II drug, Itraconazole (ITZ) as well. Spray drying of wet media milled drug nanosuspensions with high polymer loading led to formation of ITZ HyNASDs, which exhibited high supersaturation, and the presence of the anionic surfactant favored the ITZ supersaturation generation. Based on the success of the HyNASDs for two completely different BCS Class II drugs, i.e., GF and ITZ, Figure 8.1 presents a preliminary decision tree for the selection of nanocomposites, HyNASDs, and ASDs for BCS Class II drugs based on the current knowledge-base generated in this thesis. Obviously, the construction of this decision tree presumes that the physical stability of the HyNASDs is not worse than ASDs of the same drug, and the stability aspects of HyNASDs will be examined in future work.

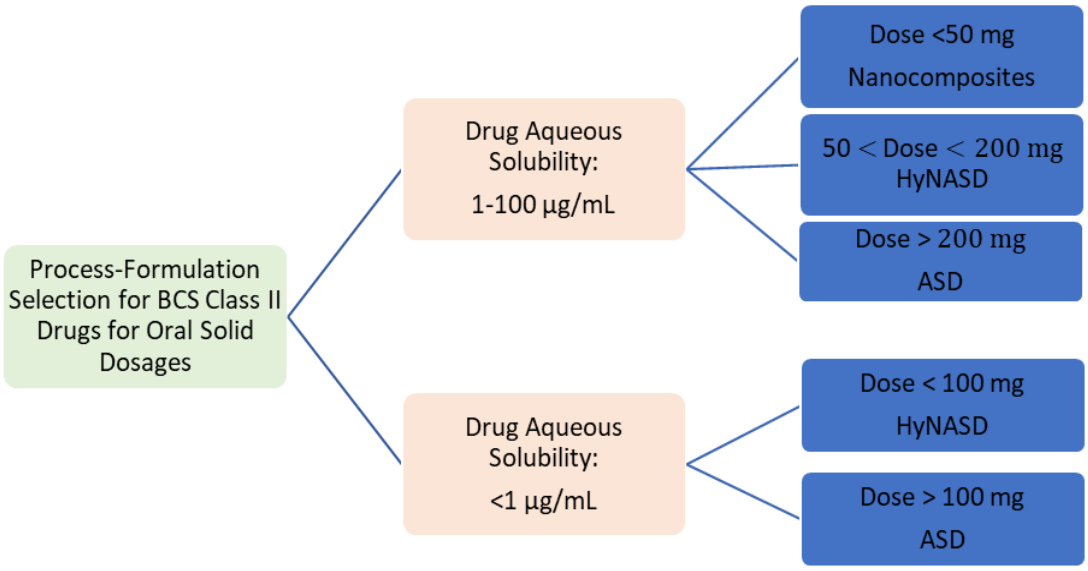

Figure 8.1 A preliminary decision tree for the selection of drug nanocomposites, HyNASDs, and ASDs based on the aqueous and dose of the drug.

Overall, this dissertation has established a platform approach (spray-drying) for a scientific comparison of drug nanocomposites *vs.* ASDs and generated the prerequisite processing–materials knowledge and methodology needed. The following objectives have been realized: (i) drug release from drug (GF) nanocomposites and ASDs with identical formulation, i.e., low drug GF:polymer (HPC/Soluplus) mass ratios (1:1 to 1:5) and an anionic surfactant (SDS), were examined, (2) the impact of anionic surfactant on drug release from hybrid nanocrystal–amorphous solution dispersions (HyNASDs) has been investigated, (3) rapidly supersaturating ternary ASDs of GF with HPC/Sol and SDS as a minor component were prepared, and (4) GF release from ternary ASDs of GF with a hydrophilic, wettability-enhancing polymer (HPC/PVP-VA64) as a minor component and an amphiphilic polymer as drug precipitation inhibitor was examined, and (5) the fundamental knowledge generated on GF was applied to another drug, itraconazole (ITZ). While this dissertation addressed the major shortcoming of the drug nanocomposites, i.e., limited supersaturation capability in the dissolution media compared with ASDs, elucidated the roles/impact of anionic surfactants and binary polymers on drug release from ASDs, there are still various areas for further research and investigation, which are summarized below.

8.2 Future Work

8.2.1 Investigation on Storage Stability of HyNASDs *vs.* ASDs Under Various Environmental Conditions

In current dissertation, we have introduced a new class of particles called Hybrid Nanocrystals–Amorphous Solid Dispersions (HyNASDs) by spray-drying an aqueous

GF nanosuspension with higher polymer concertation (1:1–1:5 drug:polymer mass ratio) than conventional drug nanosuspensions, where 1:0.02–1:0.8 drug:polymer mass ratio is used. This special class of nanoparticles has significant amount of amorphous content (>10%), which allowed us to increase the apparent solubility of the poorly water-soluble drugs significantly and achieve supersaturation during dissolution. Also, significant improvement in the drug release rate was achieved by producing ASDs of the poorly soluble drugs. Since amorphous drugs are thermodynamically unstable in nature, they can recrystallize during storage and dissolution. Therefore, investigation into the storage stability of HyNASDs *vs.* ASDs should be conducted under various environmental (RH, T) conditions.

8.2.2 Production of HyNASDs with Various Drug–Polymer Pairs and Their Comparative Assessment

In the current dissertation, HyNASDs of GF (griseofulvin) and ITZ (itraconazole) were produced using HPC, Sol, and VA64, which worked as stabilizer/carrier/matrix formers. Dissolution enhancement of a poorly soluble drug from HyNASDs requires some extent of drug–polymer miscibility or interactions. As shown in Chapter 4, due its good miscibility with GF and higher glass transition temperature, Sol achieved significant supersaturation from HyNASDs, whereas due to the low glass transition temperature and poor miscibility, HyNASDs with GF–HPC could not provide high GF supersaturation. In Chapter 7, HyNASDs of ITZ were also produced using HPC, Sol, and VA64, where very high extent of supersaturation was attained in the dissolution tests. To generalize the concept of supersaturation generation from drug nanoparticle-based formulation using HyNASDs, multiple drug–polymer pairs should be used.

8.2.3 Systematic Investigation of the Impact of Various Surfactants for HyNASDs *vs.* ASDs

In Chapters 4, 5, and 7, the impact of an anionic surfactant, sodium dodecyl sulfate (SDS) has been studied in the production and dissolution performance of GF and ITZ from HyNASDs and ASDs. It was found that the inclusion of a surfactant at low concentration in the formulation can significantly improve the stabilization of drug nanosuspensions during milling and it has remarkable impact in the drug release rate due to the wettability enhancement. However, the role of SDS in the HyNASDs and ASDs was different. Investigation on various surfactants and their impact in the production of HyNASDs/ASDs and drug release performance should be conducted for better understanding of the roles of surfactants. This understanding can help the formulation scientist in the selection of surfactant for the development of drug ASDs *vs*. HyNASDs formulations.

8.2.4 Investigating the Impact of Various Drug Nanoparticle Sizes in the Range of 50–1000 nm on Drug Supersaturation from HyNASDs

As shown in Chapters 3, 4, and 7, drug median particle sizes in the nanosuspensions were less than 200 nm when SDS was included in the formulation. In the absence of SDS, the particles were severely aggregated during milling (depending on the stabilizers type and concertation) and the size of the particles varied up to few microns in the final milled drug suspensions. Also, it was very evident from the studies in Chapters 4 and 7 that the final milled particles sizes played a significant role in the supersaturation generation besides the amorphous content of the drug in the final spray-dried powders. Consequently, a systematic study in the impact of drug

nanoparticles sizes in the range of 50–1000 nm will provide better understanding about the drug particle size impact in the supersaturation generation.

8.2.5 Characterize the Thermodynamic Solubility of Crystalline Drug and Kinetic Solubility of the Amorphous Drug in the ASD and Drug Nanoparticles

The thermodynamic solubility of the as-received crystalline drug particles in the presence of various polymers/surfactants must be determined. Kinetic solubility of the amorphous drug in different ASD formulation as well as drug nanoparticles must be measured separately.

8.2.6 Detailed Characterization of HyNASDs and ASDs

Drug–polymer intermolecular interactions should be studied *via* FTIR spectroscopy. Miscibility of polymer1–polymer2 in ternary ASDs should be studied by preparing films of pure polymer1, polymer2, and their known mixtures and using such films in FTIR spectroscopy. Modulated DSC should be used to determine glass transition temperature more accurately.

8.2.7 Study of High Dose Effects in Drug Release from HyNASDs and ASDs

In this thesis research, only 9 mg and 100 mg drug doses were considered in the dissolution testing. Hence, at least two other higher drug doses (200 mg and 400 mg) should be used in dissolution testing to address the needs of pharmaceutical industry.

8.2.8 Characterization of the Dissolution/Redispersion Medium after Testing of HyNASDs and ASDs

Characterization of particle sizes in the dissolution vessel following a dissolution experiment with HyNASDs and ASDs could provide significant insights as to the size of drug nanoparticles in HyNASDs. Similar information can be gleaned from

redispersion medium following the test. Also, any residue from the dissolution or redispersion should be characterized using polarized light microscopy, DSC, and XRPD.

8.2.9 Development of a Decision Tree for Process–Formulation Selection

As the invention of HyNASDs has been shown the performance of drug nanocomposites, it is likely that HyNASDs will be competitive to ASDs in the future upon for development and optimization. While in Section 8.1 has presented a preliminary decision tree for HyNASDs *vs.* ASDs, a more streamlined and robust decision tree should be developed based on the storage stability of HyNASDs in comparison to ASDs.

APPENDIX A

IMPACT OF POLYMERS ON THE AGGREGATION OF WET-MILLED ITRACONAZOLE AND THEIR DISSOLUTION FROM SPRAY-DRIED NANOCOMPOSITES

In appendix A, detail of the modified Washburn method to measure the relative wetting effectiveness of the stabilizer/dispersant solutions are provided. Also, to confirm the size of the redispersed drug particles form the drug the polymeric matrix of the drug nanocomposites, microscopic images are also shown here.

A.1 Experimental Details of the Drug Wettability Measurements

Penetration of a liquid into a packed powder bed of drug particles inside a cylindrical column allows for measurement of the drug powder wettability, based on the modified Washburn method (Hołownia et al., 2008; Washburn, 1921). In the current study, liquids and powder refers to aqueous solutions of dispersants (HPC, PVP K30, HPMC E3, SDS, HPC SL–SDS) and Itraconazole (ITZ), respectively. All percentages are w/w with respective to deionized water. Dispersant concentrations in the solutions were identical to those in the respective wet-milled suspensions in Table 2.1 of main text. The apparent shear viscosity and surface tension of the solutions were measured as described below. Then, the drug wettability was quantified based on fitting of the experimental data on the temporal evolution of the liquid mass penetrated into the drug powder bed by the modified Washburn equation.

A.1.1 Apparent Shear Viscosity and Surface Tension of the Dispersant Solutions

The apparent shear viscosity of the aqueous dispersant solutions was measured using an R/S Plus Rheometer (Brookfield Engineering, Middleboro, MA, USA) with a

water jacket assembly Lauda Eco (Lauda-Brinkmann LP, Delran, NJ, USA). A coaxial cylinder (CC40) was used to provide a controlled shear rate on the samples from 0 to 1000 1/s for 60 s. The temperature of the jacket was kept constant at 25 ± 0.5 °C. The raw data were analyzed using the Rheo 3000 software (Brookfield Engineering, Middleboro, MA, USA) of the equipment to obtain the apparent shear viscosity as a function of the shear rate. For solutions with low viscosities (< 10 cP) such as 2.5% HPC SL, 4.5% HPC SSL, and 4.5% PVP solutions, a Kinexus Ultra Plus Rotational Rheometer (Malvern Panalytical, Southborough, MA, USA) with higher sensitivity/accuracy was used. 40 mm rotational parallel plates with 0.75 mm gap were used to provide a controlled shear rate on the samples from 0 to 1000 1/s. The viscosity value at ~100 1/s shear rate was used in the wetting effectiveness factor calculations. The viscosities of water and the 0.2% SDS solution were taken from Korson et al. (1969) and Kushner et al. (1952), respectively.

The surface tension of deionized water and the aforementioned solutions was measured using Attension Sigma 700 (Biolin Scientific, Linthicum, MD, USA). The Attention software calculates surface tension from force measurements of interaction of a probe (Wilhelmy plate) at the boundary between air and a liquid, i.e., the deionized water or the dispersant solution.

A.1.2 Drug Wettability with the Dispersant Solutions

Attension Sigma 700 set-up (Biolin Scientific, Linthicum, MD, USA) was used to study the penetration of water/aforementioned dispersant solutions into a packed powder bed of drug (ITZ) particles inside a cylindrical column and determine the drug powder wettability, based on the Washburn method. The assembly consists of a

sample holder in the form of a cylindrical metallic tube with small holes at the bottom as well as a hook at the top of the cover equipped with screw threads. About 0.8 g of ITZ powder was packed uniformly into the tube before each measurement. A filter paper was placed at the perforated end of the sample holder to support the drug powder sample. A petri dish containing deionized water/dispersant solution was placed below the perforated end of the holder on the mechanical platform.

Upon contact of the sample holder with deionized water/dispersant solution, the liquid penetrated into the drug powder bed, while Attension Sigma 700 recorded the mass of liquid penetrated into the drug powder bed as a function of time. The contact angle for the deionized water/dispersant solution and drug can be determined using the modified Washburn equation, which provides a relationship between mass of liquid penetrated and contact angle θ, i.e., $M^2 = \left(C\rho^2\gamma\cos\theta/\eta\right)T$, where T, M, η, ρ, and γ are time after contact, mass of the liquid penetrated into the drug powder bed, viscosity of the liquid, density of the liquid, and surface tension of the liquid, respectively. C is a characteristic parameter of the powder sample (ITZ powder in the current study), which could have been determined independently using a completely wetting liquid such as hexane, heptane, etc. Since ITZ was used as the only powder sample and C depends only on powder packing (identical packing procedure used), C is assumed to remain invariant for various dispersant solutions and deionized water studied. This approach allows us to eliminate C and calculate the ratio of $\cos\theta_{ds}/\cos\theta_w$ as a wetting effectiveness factor, in which θ_{ds} is the contact angle between ITZ and the dispersant solution and θ_w is the contact angle between ITZ and deionized water. The wettability enhancement upon use of different dispersants (polymers/surfactant)

on the wetting of ITZ particles can be assessed by using this ratio or its logarithmic value, taking the wettability by water as a basis of comparison.

Experimental liquid penetration data (M^2 vs. T) for water and various dispersant solutions are presented in Figure A.1. Penetration of water into ITZ bed is extremely slow because of the highly hydrophobic (lipophilic) nature of ITZ, which is indicated by the log-partition coefficient (logP) value of 7.3. The use of dispersant in water increased the penetration rate (slope) markedly with respect to that of water. The slope was obtained by fitting the linear region of liquid penetration curve. Initial ~20 s was not considered due to transient behavior, and data points that deviated from the linear region, which may correspond to structural change in the bed, were excluded. The modified Washburn equation fitted the data almost perfectly ($R^2 \geq 0.995$). Using the slope, η, ρ, and γ for different dispersant solutions and water, $\log(\cos\theta_{ds}/\cos\theta_{w})$ was calculated.

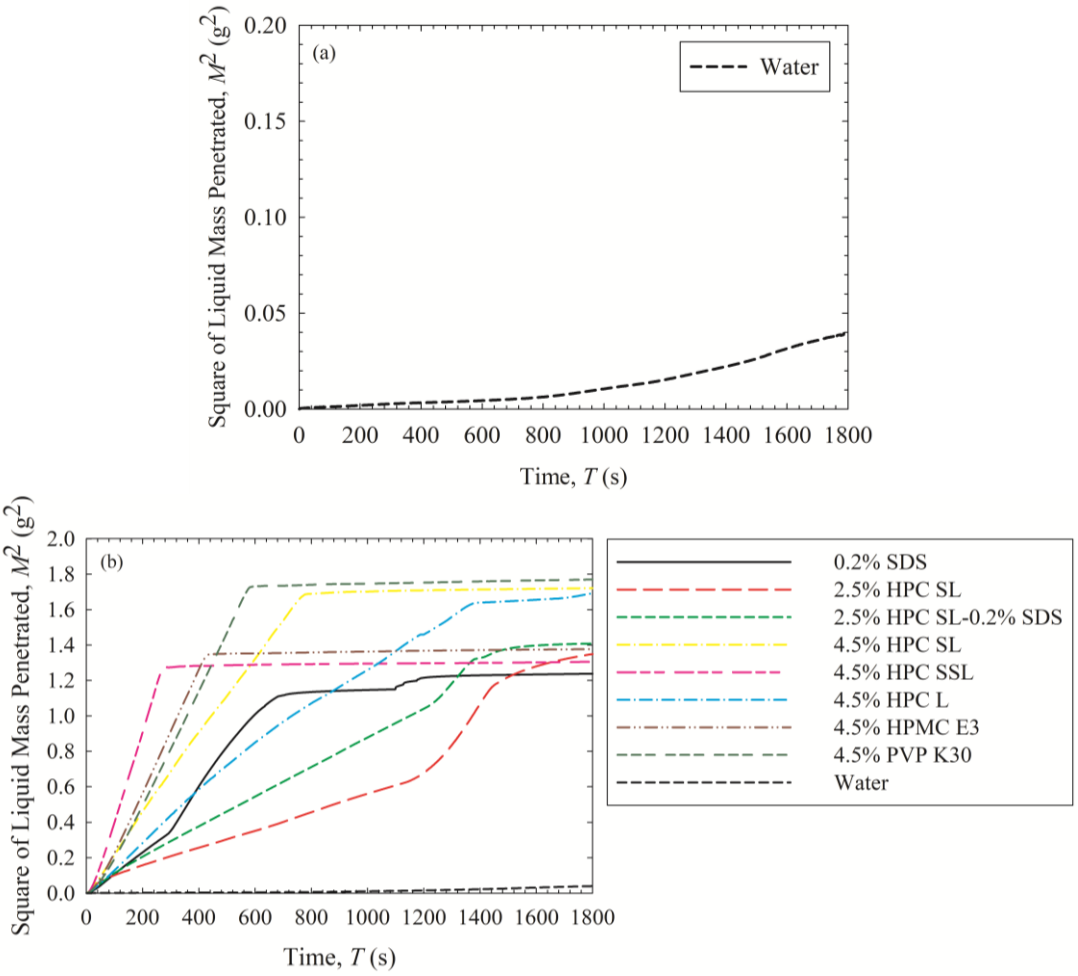

Figure A.1 Temporal evolution of the liquid mass penetrated into a packed bed of as-received ITZ particles for (a) water only and (b) various dispersant solutions such as 0.2% SDS, 2.5% HPC SL, 2.5% HPC SL–SDS, 4.5% HPC SL, 4.5% HPC SSL, 4.5% HPC L, 4.5% HPMC E3, and 4.5% PVP K30, as well as water.

A.2. Impact of the Nanocomposite Particle Size on the ITZ Release

We spray-dried the milled 4.5% HPC SL suspension (F4) using a larger nozzle tip size (1.2 mm vs. 0.6 mm) at a lower atomization pressure (1.5 bar vs. 2 bar) as compared with the baseline drying conditions. The so-formed nanocomposite particles were coarser (d_{50}: 20.7 µm and d_{90}: 40.6 µm) than the baseline nanocomposites (d_{50}: 16.2 µm and d_{90}: 32.3 µm). The dissolution profiles (Figure A.2) suggest that despite ~30% increase in d_{50} and d_{90}, (i) both the coarser and

baseline nanocomposites exhibited fast, immediate release and (ii) there is no statistically significant impact of the nanocomposite particle size on ITZ release (f_1 = 0.93 and f_2 = 91.8) within the particle size range studied. The differences are within the variability of drug assay and dissolution measurements.

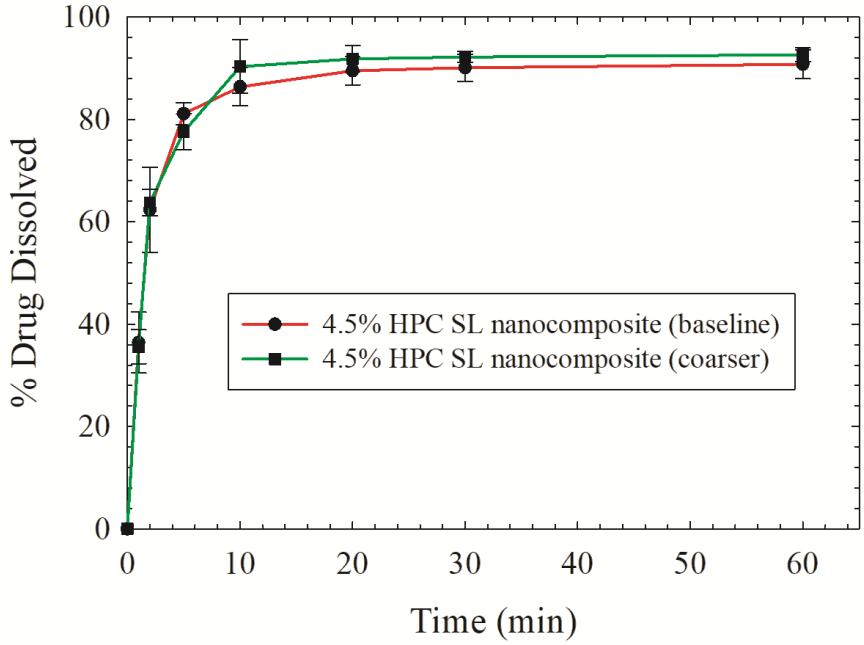

Figure A.2 Drug dissolution from the nanocomposites prepared *via* spray-drying with different processing conditions for the same milled ITZ suspension with 4.5% HPC SL (F4).

A.3. Optical Microscopic Images of Redispersed Nanocomposites

In the redispersion test, about 0.5 g of nanocomposites was weighed and dispersed in 30 mL of 3 g/L aqueous SDS solution inside a 60 mL beaker and stirred at 400 rpm for 60 min with a paddle-stirrer (CAT R18, Scientific Instrument Center Limited, Winchester, UK). ~0.5 mL aliquot of redispersed sample was taken at 2, 10 and 60 min while stirring, and particle size was measured using laser diffraction. At the same time, a droplet of each sample was dropped on a glass slide and dried immediately using a hot air gun (Steinel Professional, Bloomington, MN, USA). After drying,

Axio Scope.A1 polarizing microscope (Carl Zeiss Microscopy GmbH, Göttingen, Germany) was used to capture images of redispersed particles (Figure A3).

When redispersion was slow and incomplete, the rounded/spherical nanocomposite particles appeared in the images even after 60 min (e.g., 2.5% HPC SL) because the nanocomposite matrix slowly eroded or did not erode at all, keeping the shape/morphology intact. On the other hand, fast redispersion was associated with complete erosion of the nanocomposite matrix, leading to disappearance of the nanocomposite particles in the images (e.g., 2.5% HPC SL–0.2% SDS). In the latter case, ITZ nanoparticles/clusters, whose sizes are mostly below the detection limit of the optical microscope, were released upon disappearance of the matrix. These findings are in good agreement with the laser diffraction measurements of the redispersed nanocomposites (see Figure 2.9 of the main text).

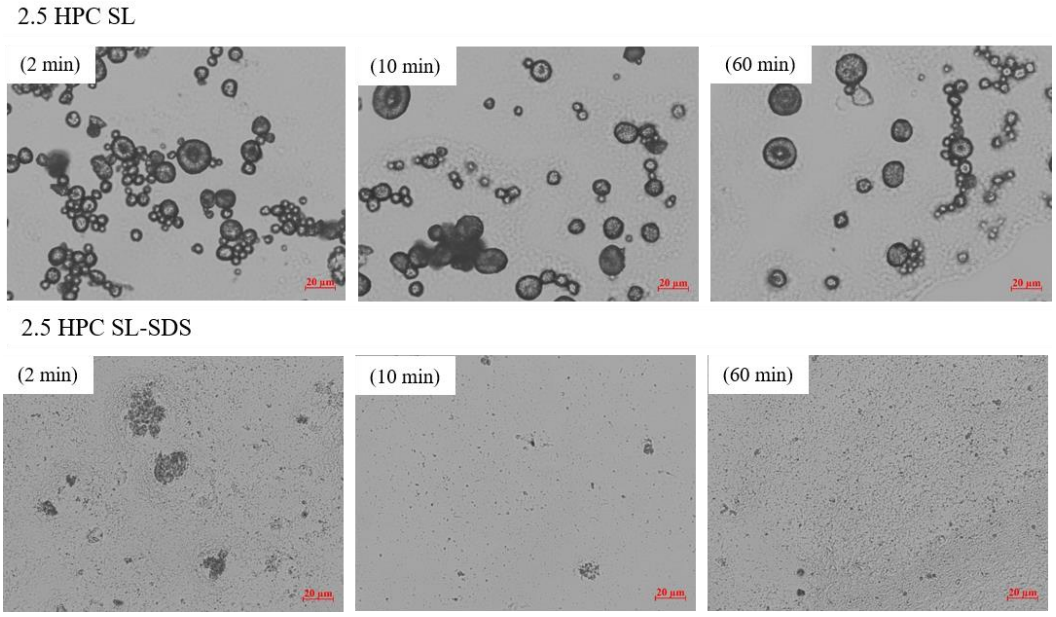

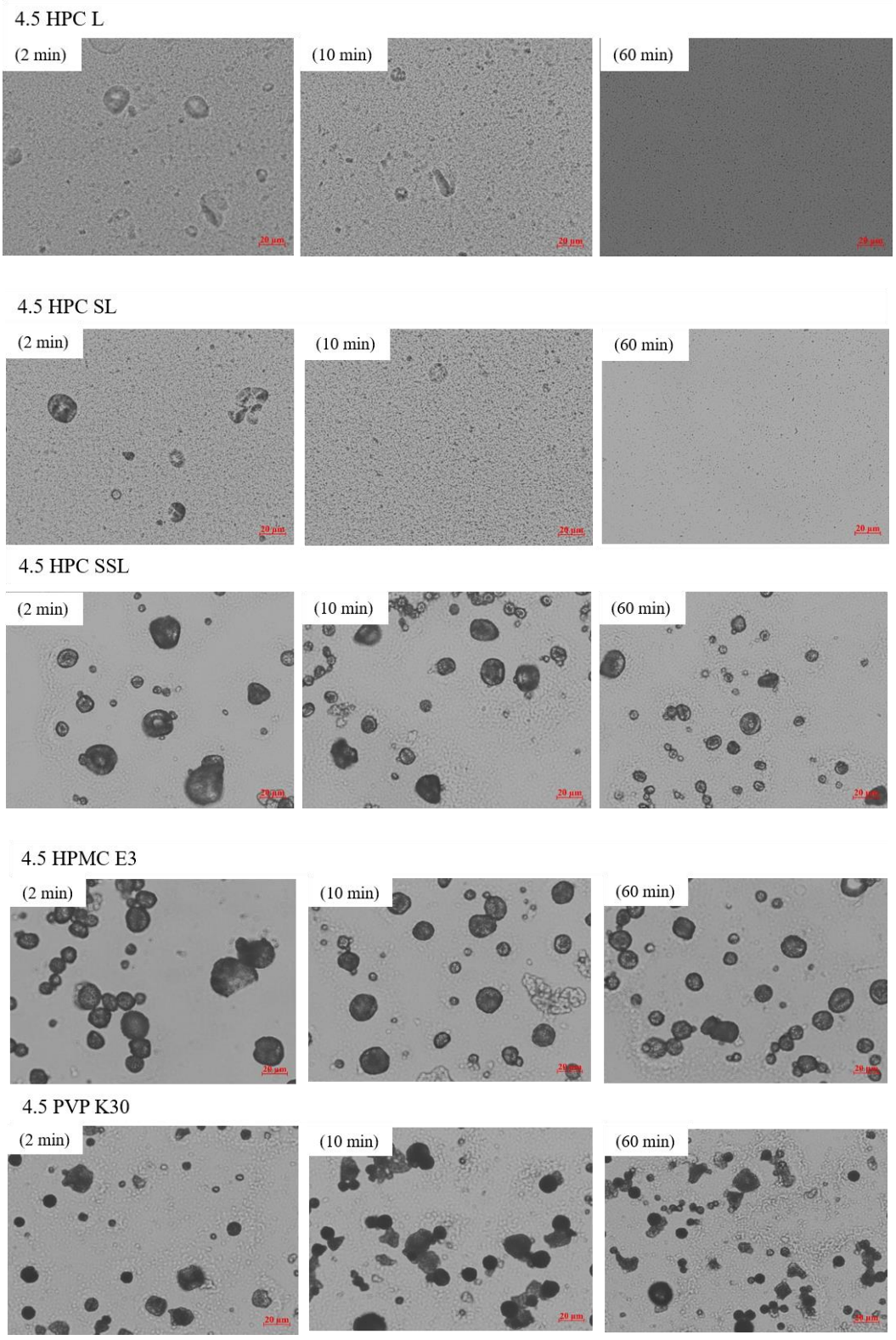

Figure A.3 Optical microscope images of the nanocomposites with various dispersants redispersed in 3 g/L SDS solution at 2 min, 10 min, and 60 min (marker size: 20 µm).

A.4 Difference (f_1) and similarity (f_2) factors for dissolution profiles of ITZ nanocomposites

Table A.1 Difference (f_1) and similarity (f_2) factors for dissolution profiles of ITZ nanocomposites with various dispersants (F1, F2, F4–F8) as compared with that of F3

Difference and similarity factors	Formulation ID						
	F1	F2	F4*	F5	F6	F7	F8
f_1	68.6	71.7	3.73	48.2	24.5	44.7	41.5
f_2	29.0	28.0	83.5	36.2	54.4	37.7	38.1

*****This formulation had statistically similar dissolution profile to that of F3.

Table A.2 Difference (f_1) and similarity (f_2) factors for dissolution profiles of ITZ nanocomposites with various dispersants (F1, F2, F4–F8) as compared with that of F4

Difference and similarity factors	Formulation ID						
	F1	F2	F3*	F5	F6	F7	F8
f_1	67.4	70.6	3.88	46.2	21.4	42.5	39.2
f_2	30.4	29.2	83.5	38.0	58.0	39.6	40.0

*****This formulation had statistically similar dissolution profile to that of F4.

APPENDIX B

DISSOLUTION ENHANCEMENT *VIA* DRUG HYBRID NANOCRYSTALS–AMORPHOUS SOLID DISPERSIONS (HyNASDs) *VS*. ASDs DISSOLUTION

In appendix B, particle size statistics of the spray-dried powders before and after redispersions is shown. To confirm the size of the redispersed drug particle, microscopic images are also shown here.

B.1. Redispersion of the Spray-Dried Powders

Aqueous redispersion of the spray-dried powders prepared using the nanosuspension-based (W) feeds, i.e., the HyNASD particles, was performed following a previously established method (Bhakay et al., 2014; Li et al., 2016; Bilgili et al., 2018). About 0.5 g spray-dried powder was weighed and dispersed in 30 mL of deionized water inside a 60 mL beaker and stirred at 500 rpm for 60 min with a paddle-stirrer (CAT R18, Scientific Instrument Center Limited, Winchester, UK). ~1.0 mL aliquot of redispersed sample was taken at 2, 10 and 60 min while stirring, and particle size was measured using laser diffraction (LS 13 320, Beckman Coulter, Miami, FL). At the same time, a droplet of each redispersed sample was dried immediately by dropping on a preheated glass slide on a hot plate at 100 °C. After drying, Zeiss Axio Scope.A1 polarizing microscope (Carl Zeiss Microscopy GmbH, Göttingen, Germany) was used to capture images of the redispersed particles (Figure B.2). 30 mL of deionized water was selected purposefully so that the polymer in the sample dissolved fully, while releasing the GF nanoparticles/clusters with minimal dissolution. Indeed, the maximum amount of GF that can dissolve was estimated to be small (e.g., 1.1% of GF from W-Sol-1-3).

In general, GF nanoparticles with sizes similar to those particles in the milled suspensions were recovered within 2 min upon redispersion of the spray-dried powders (Figure B.1). Since the spray-dried powders contain SDS, they got wetted fast and their polymer content dissolved quickly, thus releasing GF nanoparticles/clusters. The particles released are mostly below the detection limit of the optical microscope; hence, they are barely discernible in the optical microscope images (see Figure B.2). Overall, both the laser diffraction measurements and the optical microscope images suggest that HyNASDs release drug nanoparticles fast upon redispersion in water.

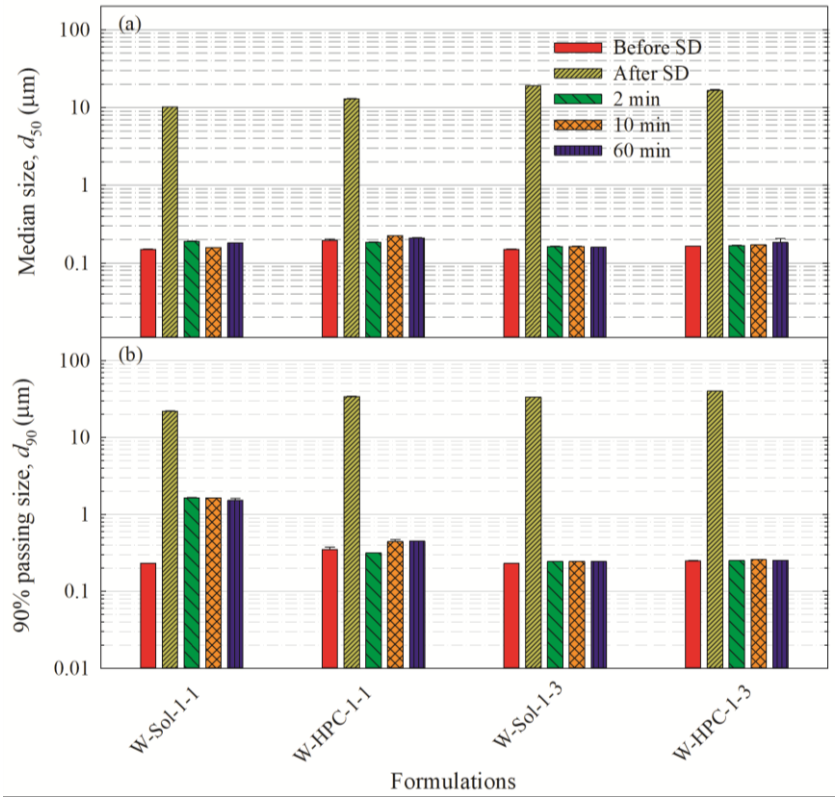

Figure B.1 Volume-based particle size statistics of the nanosuspension-based (W) feeds of GF–Sol and GF–HPC before spray drying (SD) (after 1 day of milling), after spray drying (HyNASDs), and the HyNASD particles redispersed in deionized water at 2 min, 10 min, and 60 min: (a) Median particle size d_{50}, and (b) 90% passing size d_{90}. All feeds have 2.5% w/v GF and 0.125% w/v SDS.

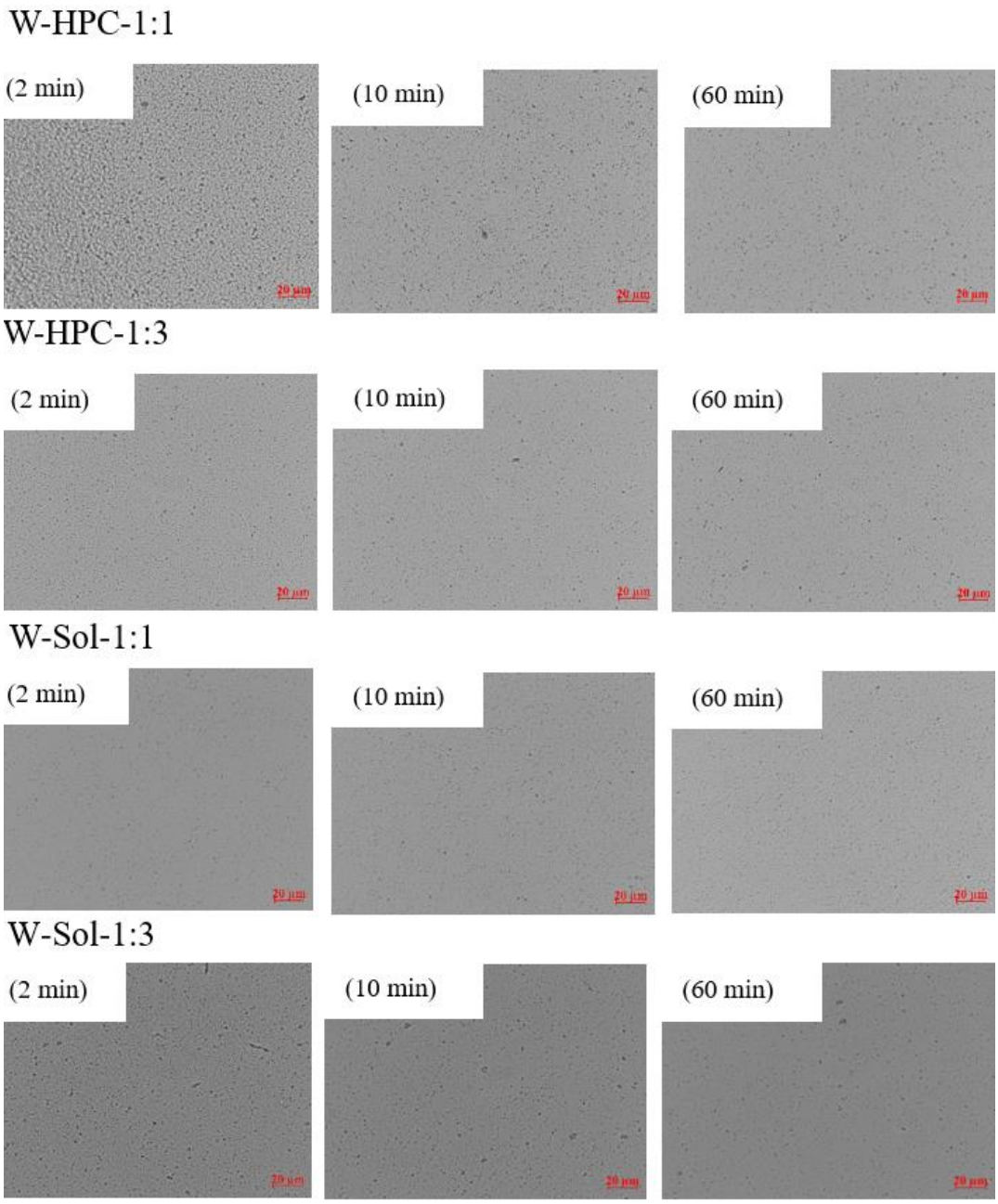

Figure B.2 Optical microscope images of the HyNASD particles, prepared using the nanosuspension-based (W) feeds, after redispersion in deionized water at 2 min, 10 min, and 60 min (marker size: 20 µm). All feeds have 2.5% w/v GF and 0.125% w/v SDS.

APPENDIX C

DRUG RELEASE FROM SPRAY-DRIED HYBRID NANOCRYSTAL–AMORPHOUS SOLID DISPERSIONS (HyNASDs): IMPACT OF SDS

In appendix C, detail of the modified Washburn method to measure the relative wetting effectiveness of the stabilizer/dispersant solutions are provided. Also, to confirm the size of the redispersed drug particles form the drug the polymeric matrix of the drug nanocomposites, microscopic images are also shown here.

C.1 Details of the Characterization Methods Used for Drug Wettability Measurements

Penetration of a liquid into a packed powder bed of a drug inside a cylindrical column allows for measurement of the drug powder wettability, based on the Washburn method (Hołownia et al., 2008; Washburn, 1921). The method presented here was adapted from Bilgili et al. (2018) and Li et al. (2017). In the current study, liquids and powder refer to GF (griseofulvin)-saturated aqueous solutions of 15% Soluplus (Sol)/HPC with 0.125% SDS or w/o SDS and GF powder, respectively. All percentages are (% w/w) with respective to deionized water. This polymer concentration was selected to measure the viscosity accurately in our viscometer set-up instead of the maximum viscosity of 12.5% used in the stabilizer solutions. The solutions and deionized water were saturated with griseofulvin (GF) and stirred overnight. After overnight stirring, the saturated solutions were used for further characterization. The apparent shear viscosity and surface tension of the solutions were measured using R/S Plus Rheometer (Brookfield Engineering, Middleboro, MA, USA) and Attension Sigma 700 (Biolin Scientific, Linthicum, MD, USA) respectively, as described below; then, the drug wettability by the drug-saturated

solutions was quantified *via* a wetting effectiveness factor using the modified Washburn equation.

C.1.1 Apparent Shear Viscosity of the Solutions

The apparent shear viscosity of the GF-saturated aqueous solutions of the stabilizers was measured using an R/S Plus Rheometer (Brookfield Engineering, Middleboro, MA, USA) with a water jacket assembly Lauda Eco (Lauda-Brinkmann LP, Delran, NJ, USA). A coaxial cylinder (CC40) was used to provide a controlled shear rate on the samples and shear rate 0 to 1000 1/s for 60 s was used for all the samples. The temperature of the jacket was kept constant at 25 ± 0.5 °C. The raw data were analyzed using the Rheo 3000 software (Brookfield Engineering, Middleboro, MA, USA) of the equipment to obtain the apparent shear viscosity as a function of the shear rate. The apparent shear viscosity at ~100 1/s was used as a representative low shear rate value. The viscosity of water was taken from Korson et al. (1969).

C.1.2 Surface Tension of the Solutions

The surface tension of the GF-saturated deionized water and the GF-saturated aqueous solutions of the stabilizers was measured using Attension Sigma 700 (Biolin Scientific, Linthicum, MD, USA). The Attention software calculates surface tension from force measurements of interaction of a probe (Wilhelmy plate) at the boundary between air and a liquid.

C.1.3 Drug Wettability with the Solutions

Attension Sigma 700 set-up (Biolin Scientific, Linthicum, MD, USA) was used to study the penetration of GF-saturated deionized water/GF-saturated aqueous solutions

of the stabilizers into a packed powder bed of GF inside a cylindrical column and determine the GF wettability, based on the modified Washburn method. The assembly consists of a sample holder in the form of a cylindrical metallic tube with small holes at the bottom as well as a hook at the top of the cover equipped with screw threads. About 0.8 g of GF powder was packed uniformly into the tube before each measurement. A filter paper was placed at the perforated end of the sample holder to support the GF powder sample. A petri dish containing deionized water/stabilizer solution was placed below the perforated end of the holder on the mechanical platform.

Upon contact of the sample holder with the liquid, the liquid penetrated the GF powder bed, while Attension Sigma 700 recorded the mass M of the liquid penetrated as a function of time T. The cosine of the contact angle θ for the GF-saturated deionized water/GF-saturated aqueous stabilizer solution and drug can be determined using the modified Washburn equation, which provides a relationship between liquid penetration rate and contact angle, *via* $M^2 = \left(\frac{C\rho^2\gamma\cos\theta}{\eta}\right)T$, where η, ρ, and γ stand for viscosity of the liquid, density of the liquid, and surface tension of the liquid, respectively. C is a characteristic parameter of the powder sample, which could have been determined independently using a completely wetting liquid such as hexane, heptane, etc. Since the same drug powder (GF) was used as the powder sample and C depends only on powder packing–size, C remained invariant for different liquids studied here. This allows us to calculate the ratio of $\cos\theta_{ss}/\cos\theta_{w}$ as a wetting effectiveness factor from the slopes of M^2 vs. T for deionized water and the stabilizer solution. Here, θ_{ss} is the contact angle between GF and the polymer–SDS stabilizer

solution and θ_w is the contact angle between GF and deionized water. The wettability enhancement upon the use of different stabilizers (polymers/surfactant) on the wetting of GF particles can be assessed by using this ratio, taking the wettability by water as a basis for comparison.

Experimental liquid penetration data (M^2 vs. T) for various liquids are presented in Figure C.1. The slope of the modified Washburn equation, i.e., $\frac{C\rho^2\gamma\cos\theta}{\eta}$, was obtained by fitting the linear region of the liquid penetration curve. Initial ~20 s was not considered due to transient behavior; data points that deviated from the linear region, which may correspond to structural change in the bed, were excluded. The modified Washburn equation fitted the data well ($R^2 \geq 0.990$). Using the slope for the different stabilizer solutions and water, $\cos\theta_{ss}/\cos\theta_w$ was calculated. The viscosity, surface tension, and calculated wetting effectiveness factor are reported in Table 4.3 of the main text.

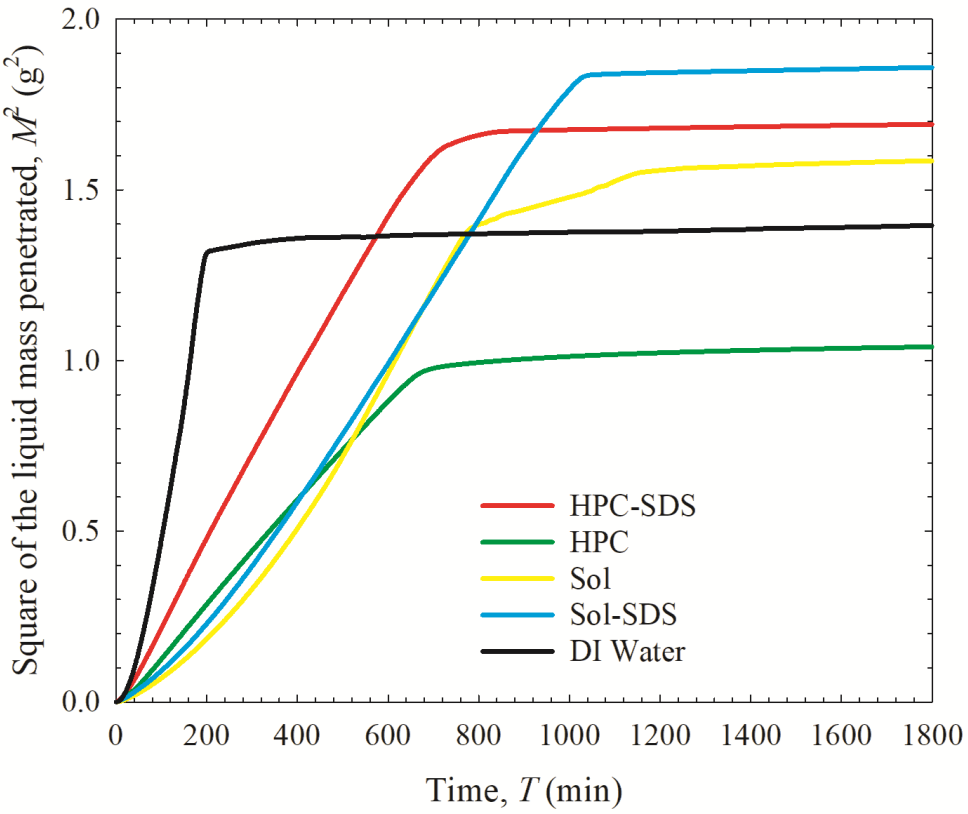

Figure C.1 Temporal evolution of the liquid mass penetrated into a packed bed of as-received GF particles for GF-saturated deionized (DI) water and various GF-saturated aqueous solutions of 15% HPC/Sol with 0.125% SDS and without SDS.

C.2 Optical Microscopic Images of the Spray-Dried Particles Redispersed in Deionized Water

The redispersion test method was adapted from Bhakay et al. (2014) and Li et al. (2016). About 0.5 g of nanocomposites was weighed and dispersed in 30 mL of deionized water inside a 60 mL beaker and stirred at 500 rpm for 60 min with a paddle-stirrer (CAT R18, Scientific Instrument Center Limited, Winchester, UK). 30 mL of deionized water was selected purposefully so that the polymer could dissolve fully, while releasing the GF nanoparticles/clusters with minimal GF dissolution. ~1.0 mL aliquot of redispersed sample was taken at 2, 10 and 60 min while stirring, and particle size was measured using laser diffraction (see Figure 4.7 and 4.8 of the

main text). At the same time, a droplet of each redispersed sample was dried immediately by dropping on a preheated glass slide at 100 °C using a hot plate. After drying, Zeiss Axio Scope.A1 polarizing microscope (Carl Zeiss Microscopy GmbH, Göttingen, Germany) was used to capture images of the redispersed particles (Figure C.2).

Since only few images were taken per sample during the redispersion, the microscopic imaging of the redispersion should could only provide qualitative information. When redispersion was slow and incomplete due to poor wettability of the spray-dried particles as in most W-formulations without SDS, the rounded/spherical particles with some aggregates appeared in the images even after 60 min redispersion. The matrix of such particles appears to be slowly eroded, keeping the shape/morphology somewhat intact. On the other hand, fast redispersion was associated with complete erosion of the spray-dried particles (W-formulations with SDS), leading to their disappearance from the images. Note that due to inability of the microscope to detect nanoparticles, some images do not have many particles. The microscopic imaging of the redispersion shows that presence of SDS imparts excellent wettability to the spray-dried particles and helped to release drug nanoparticles faster than the particles w/o SDS. These findings are largely in good agreement with the laser diffraction measurements presented in Figure 4.7 and 4.8 of the main text.

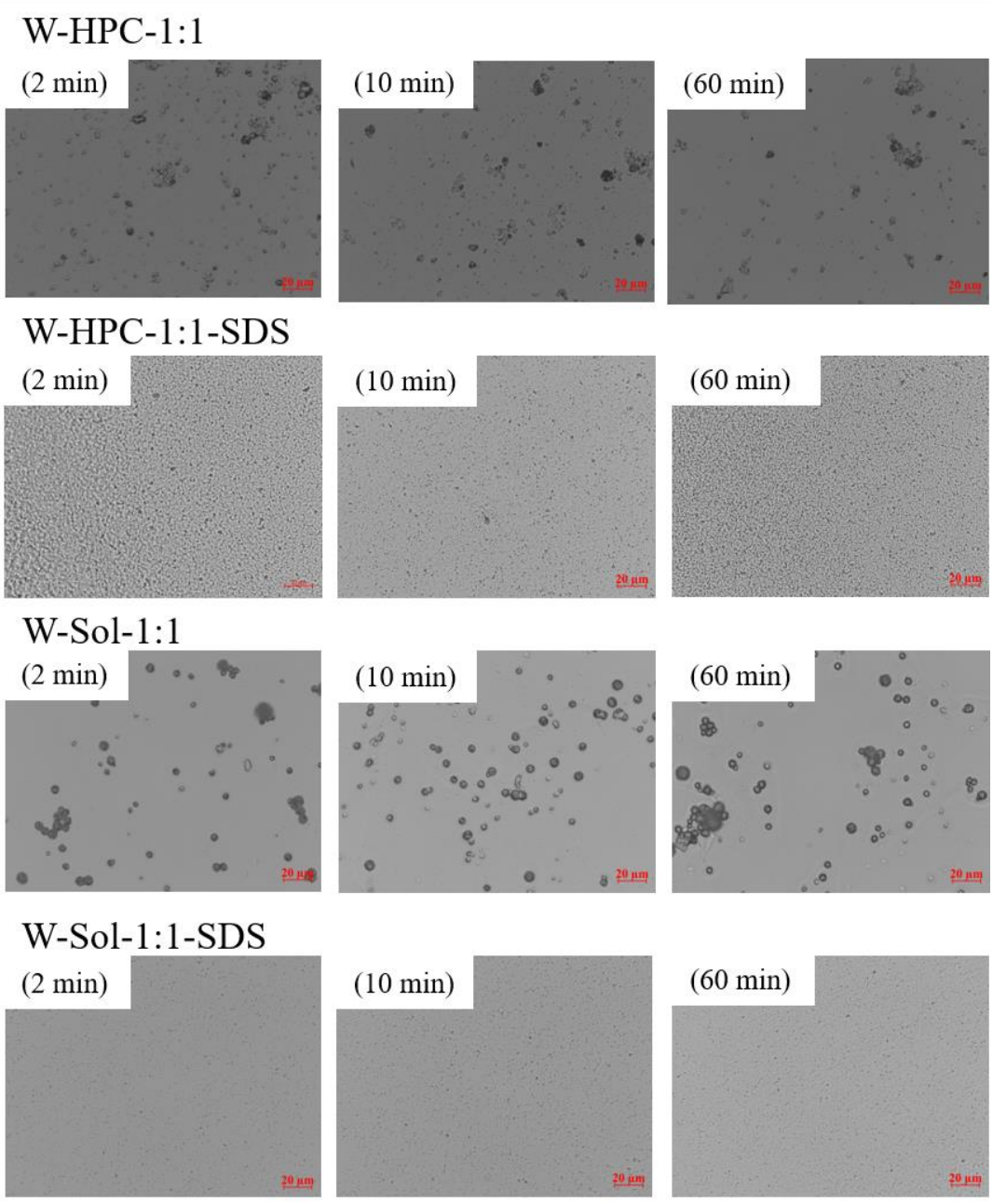
W-HPC-1:1
(2 min)
(10 min)
(60 min)
W-HPC-1:1-SDS
(2 min)
(10 min)
(60 min)
W-Sol-1:1
(2 min)
(10 min)
(60 min)
W-Sol-1:1-SDS
(2 min)
(10 min)
(60 min)

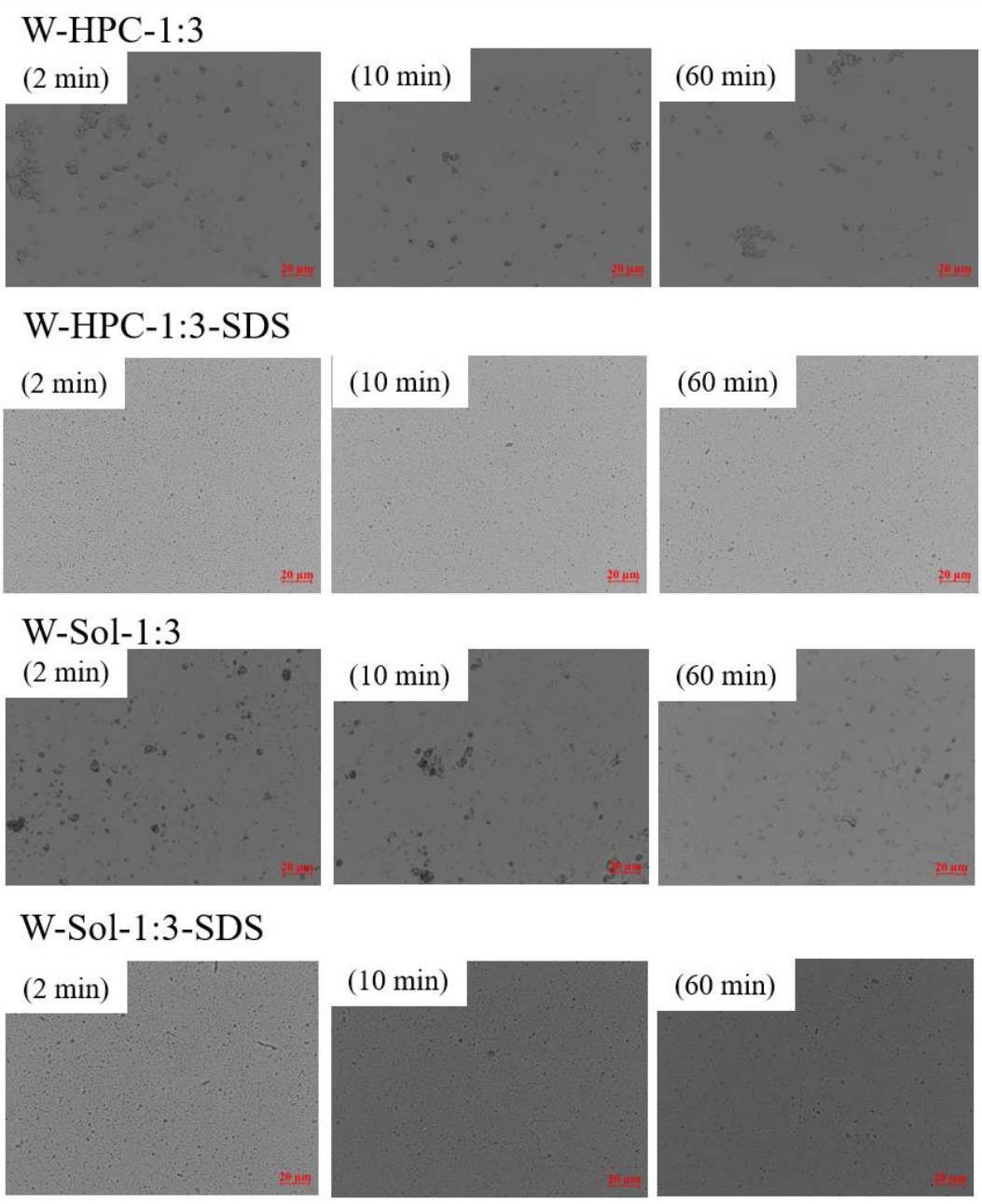
W-HPC-1:3
(2 min)
(10 min)
(60 min)
W-HPC-1:3-SDS
(2 min)
(10 min)
(60 min)
W-Sol-1:3
(2 min)
(10 min)
(60 min)
W-Sol-1:3-SDS
(2 min)
(10 min)
(60 min)

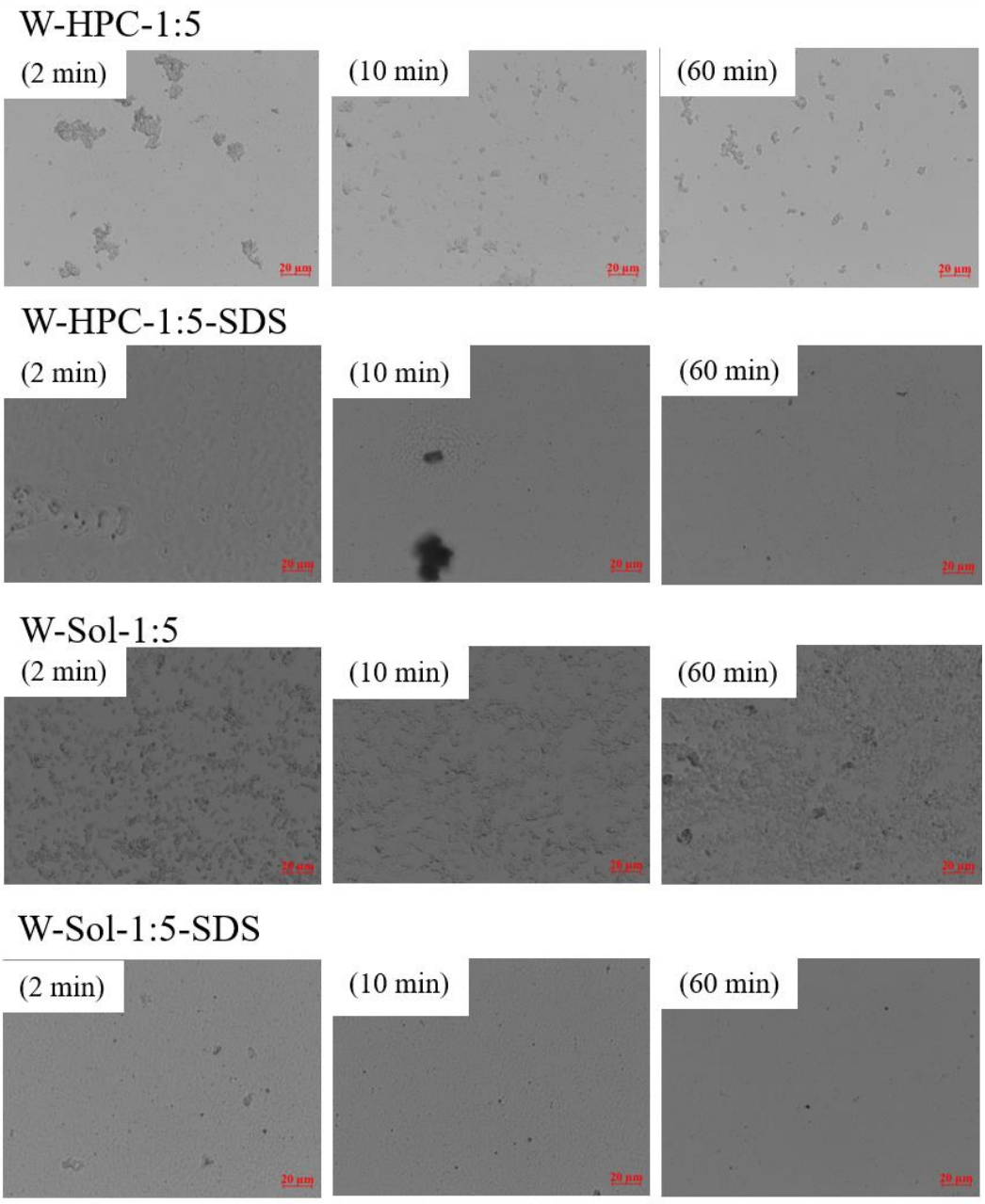

Figure C.2 Microscopic images of the spray-dried particles with 1:1, 1:3, and 1:5 GF:polymer (Sol/HPC) mass ratios having SDS and no SDS after redispersion in DI water at 2 min, 10 min, and 60 min (marker size: 20 µm).

APPENDIX D

IMPACT OF SDS ON GRISEOFULVIN RELEASE FROM SPRAY-DRIED AMORPHOUS SOLID DISPERSIONS WITH HPC–SOLUPLUS

In appendix D, detail of the modified Washburn method to measure the relative wetting effectiveness of the stabilizer/dispersant solutions are provided.

D.1 Details of the Characterization Methods Used for Drug Wettability Measurements

Penetration of a liquid into a packed powder bed of a drug inside a cylindrical column allows for measurement of the drug powder wettability, based on the Washburn method (Hołownia et al., 2008; Washburn, 1921). The method presented here was adapted from Bilgili et al. (2018) and Li et al. (2017). In the current study, liquids and powder refer to GF (griseofulvin)-saturated aqueous solutions of 15% Soluplus (Sol)/HPC with 0.125% SDS or w/o SDS and GF powder, respectively. All percentages are (% w/w) with respective to deionized water. This polymer concentration was selected to measure the viscosity accurately in our viscometer set-up instead of the maximum viscosity of 12.5% used in the solutions. The solutions and deionized water were saturated with griseofulvin (GF) and stirred overnight. After overnight stirring, the saturated solutions were used for further characterization. The apparent shear viscosity and surface tension of the solutions were measured using R/S Plus Rheometer (Brookfield Engineering, Middleboro, MA, USA) and Attension Sigma 700 (Biolin Scientific, Linthicum, MD, USA) respectively, as described below; then, the drug wettability by the drug-saturated solutions was quantified *via* a wetting effectiveness factor using the modified Washburn equation.

D.1.1 Apparent Shear Viscosity of the Solutions

The apparent shear viscosity of the GF-saturated aqueous solutions of the polymer/surfactant was measured using an R/S Plus Rheometer (Brookfield Engineering, Middleboro, MA, USA) with a water jacket assembly Lauda Eco (Lauda-Brinkmann LP, Delran, NJ, USA). A coaxial cylinder (CC40) was used to provide a controlled shear rate on the samples and shear rate 0 to 1000 1/s for 60 s was used for all the samples. The temperature of the jacket was kept constant at 25 ± 0.5 °C. The raw data were analyzed using the Rheo 3000 software (Brookfield Engineering, Middleboro, MA, USA) of the equipment to obtain the apparent shear viscosity as a function of the shear rate. The apparent shear viscosity at ~100 1/s was used as a representative low shear rate value. The viscosity of water was taken from Korson et al. (1969).

D.1.2 Surface Tension of the Solutions

The surface tension of the GF-saturated deionized water and the GF-saturated aqueous solutions of the polymer/surfactant was measured using Attension Sigma 700 (Biolin Scientific, Linthicum, MD, USA). The Attention software calculates surface tension from force measurements of interaction of a probe (Wilhelmy plate) at the boundary between air and a liquid.

D.1.3 Drug Wettability with the Solutions

Attension Sigma 700 set-up (Biolin Scientific, Linthicum, MD, USA) was used to study the penetration of GF-saturated deionized water/GF-saturated aqueous solutions of the polymer/surfactant into a packed powder bed of GF inside a cylindrical column and determine the GF wettability, based on the modified Washburn method. The

assembly consists of a sample holder in the form of a cylindrical metallic tube with small holes at the bottom as well as a hook at the top of the cover equipped with screw threads. About 0.8 g of GF powder was packed uniformly into the tube before each measurement. A filter paper was placed at the perforated end of the sample holder to support the GF powder sample. A petri dish containing deionized water or polymer/surfactant solution was placed below the perforated end of the holder on the mechanical platform.

Upon contact of the sample holder with the liquid, the liquid penetrated the GF powder bed, while Attension Sigma 700 recorded the mass M of the liquid penetrated as a function of time T. The cosine of the contact angle θ for the GF-saturated deionized water/GF-saturated aqueous polymer/surfactant solution and drug can be determined using the modified Washburn equation, which provides a relationship between liquid penetration rate and contact angle, *via* , where η, ρ, and γ $M^2 = \left(\frac{C\rho^2\gamma\cos\theta}{\eta}\right)T$ stand for viscosity of the liquid, density of the liquid, and surface tension of the liquid, respectively. C is a characteristic parameter of the powder sample, which could have been determined independently using a completely wetting liquid such as hexane, heptane, etc. Since the same drug powder (GF) was used as the powder sample and C depends only on powder packing–size, C remained invariant for different liquids studied here. This allows us to calculate the ratio of $\cos\theta_{ss}/\cos\theta_w$ as a wetting effectiveness factor from the slopes of M^2 vs. T for deionized water and the polymer/surfactant solution. Here, θ_{ss} is the contact angle between GF and the polymer–surfactant solution and θ_w is the contact angle between GF and deionized water. The wettability enhancement upon the use of different

polymers/surfactant on the wetting of GF particles can be assessed by using this ratio, taking the wettability by water as a basis for comparison.

Experimental liquid penetration data (M^2 vs. T) for various liquids are presented in Figure D.1. The slope of the modified Washburn equation, i.e., $c\rho^2\gamma\cos\theta/\eta$, was obtained by fitting the linear region of the liquid penetration curve. Initial ~20 s was not considered due to transient behavior; data points that deviated from the linear region, which may correspond to structural change in the bed, were excluded. The modified Washburn equation fitted the data well ($R^2 \geq$ 0.990). Using the slope for the different polymer/surfactant solutions and water, $\cos\theta_{ss}/\cos\theta_w$ was calculated. The viscosity, surface tension, and calculated wetting effectiveness factor are reported in Table 5.5 of the main text.

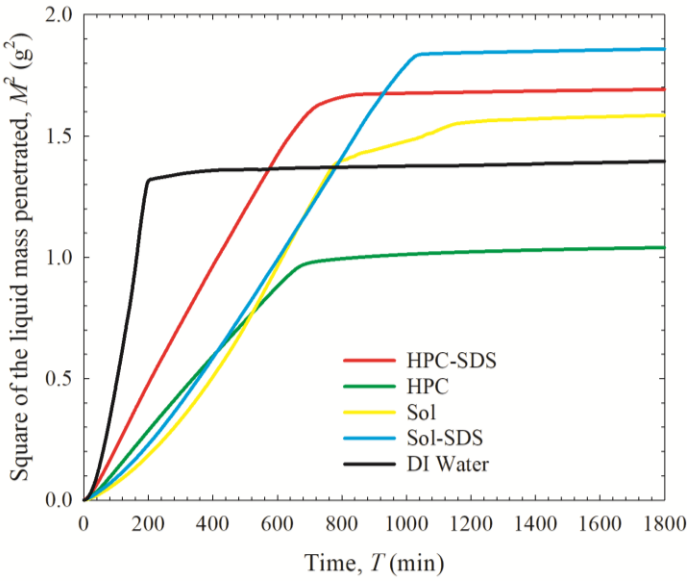

Figure D.1 Temporal evolution of the liquid mass penetrated into a packed bed of as-received GF particles for GF-saturated deionized (DI) water and various GF-saturated aqueous solutions of 15% HPC/Sol with 0.125% SDS and without SDS.

APPENDIX E

SYNERGISTIC EFFECTS OF HYDROPHILIC POLYMER–AMPHIPHILIC POLYMER COMBINATION IN ENHANCING GRISEOFULVIN RELEASE FROM AMORPHOUS SOLID DISPERSIONS

In appendix E, detail of the modified Washburn method to measure the relative wetting effectiveness of the stabilizer/dispersant solutions are provided.

E.1 Details of the Characterization Methods used for Drug Wettability Measurements

Penetration of a liquid into a packed powder bed of a drug inside a cylindrical column allows for measurement of the drug powder wettability, based on the Washburn method (Hołownia et al., 2008; Washburn, 1921). The method presented here was adapted from Bilgili et al. (2018) and Li et al. (2017). In the current study, liquids and powder refer to GF (griseofulvin)-saturated aqueous solutions of 15% single or binary polymers and GF powder, respectively. Single polymer includes Soluplus (Sol)/HPC/Kollidon VA64 (VA64). In the preparation of aqueous solutions of binary polymers, Sol–HPC were combined at 1:1 and 9:1 mass ratio, Sol–VA64 were combined at 1:5 and 5:1 ratio, and VA64–HPC were combined at 1:1 and 9:1 ratio. All percentages are (% w/w) with respective to deionized water. This polymer concentration was selected to measure the viscosity accurately in our viscometer set-up instead of the maximum viscosity of 7.5% used in the polymer solutions. The solutions and deionized water were saturated with griseofulvin (GF) and stirred overnight. After overnight stirring, the saturated solutions were used for further characterization. The apparent shear viscosity and surface tension of the solutions were measured using R/S Plus Rheometer (Brookfield Engineering, Middleboro, MA,

USA) and Attension Sigma 700 (Biolin Scientific, Linthicum, MD, USA) respectively, as described below; then, the drug wettability by the drug-saturated solutions was quantified *via* a wetting effectiveness factor using the modified Washburn equation.

E.1.1 Apparent Shear Viscosity of the Solutions

The apparent shear viscosity of the GF-saturated aqueous solutions of the polymers was measured using an R/S Plus Rheometer (Brookfield Engineering, Middleboro, MA, USA) with a water jacket assembly Lauda Eco (Lauda-Brinkmann LP, Delran, NJ, USA). A coaxial cylinder (CC40) was used to provide a controlled shear rate on the samples and shear rate 0 to 1000 1/s for 60 s was used for all the samples. The temperature of the jacket was kept constant at 25 ± 0.5 °C. The raw data were analyzed using the Rheo 3000 software (Brookfield Engineering, Middleboro, MA, USA) of the equipment to obtain the apparent shear viscosity as a function of the shear rate. The apparent shear viscosity at ~100 1/s was used as a representative low shear rate value. The viscosity of water was taken from Korson et al. (1969).

E.1.2 Surface Tension of the Solutions

The surface tension of the GF-saturated deionized water and the GF-saturated aqueous solutions of the polymers was measured using Attension Sigma 700 (Biolin Scientific, Linthicum, MD, USA). The Attention software calculates surface tension from force measurements of interaction of a probe (Wilhelmy plate) at the boundary between air and a liquid.

E.1.3 Drug Wettability with the Solutions

Attension Sigma 700 set-up (Biolin Scientific, Linthicum, MD, USA) was used to study the penetration of GF-saturated deionized water/GF-saturated aqueous solutions of the polymers into a packed powder bed of GF inside a cylindrical column and determine the GF wettability, based on the modified Washburn method. The assembly consists of a sample holder in the form of a cylindrical metallic tube with small holes at the bottom as well as a hook at the top of the cover equipped with screw threads. About 0.8 g of GF powder was packed uniformly into the tube before each measurement. A filter paper was placed at the perforated end of the sample holder to support the GF powder sample. A petri dish containing deionized water/polymer solution was placed below the perforated end of the holder on the mechanical platform.

Upon contact of the sample holder with the liquid, the liquid penetrated the GF powder bed, while Attension Sigma 700 recorded the mass M of the liquid penetrated as a function of time T. The cosine of the contact angle θ for the GF-saturated deionized water/GF-saturated aqueous polymer solution and drug can be determined using the modified Washburn equation, which provides a relationship between liquid penetration rate and contact angle, *via* $M^2 = \left(\frac{C\rho^2\gamma\cos\theta}{\eta}\right)T$, where η, ρ, and γ stand for viscosity of the liquid, density of the liquid, and surface tension of the liquid, respectively. C is a characteristic parameter of the powder sample, which could have been determined independently using a completely wetting liquid such as hexane, heptane, etc. Since the same drug powder (GF) was used as the powder sample and C depends only on powder packing–size, C remained invariant for

different liquids studied here. This allows us to calculate the ratio of $\cos\theta_{ss}/\cos\theta_w$ as a wetting effectiveness factor from the slopes of M^2 vs. T for deionized water and the polymer solution. Here, θ_{ss} is the contact angle between GF and the polymer/SDS solution and θ_w is the contact angle between GF and deionized water. The wettability enhancement upon the use of different polymers on the wetting of GF particles can be assessed by using this ratio, taking the wettability by water as a basis for comparison.

Experimental liquid penetration data (M^2 vs. T) for various liquids are presented in Figure E.1. The slope of the modified Washburn equation, i.e., $c\rho^2\gamma\cos\theta/\eta$, was obtained by fitting the linear region of the liquid penetration curve. Initial ~20 s was not considered due to transient behavior; data points that deviated from the linear region, which may correspond to structural change in the bed, were excluded. The modified Washburn equation fitted the data well ($R^2 \geq$ 0.990). Using the slope for various polymer solutions and water, $\cos\theta_{ss}/\cos\theta_w$ was calculated. The viscosity, surface tension, and calculated wetting effectiveness factor are reported in Table 6.4 of the main text.

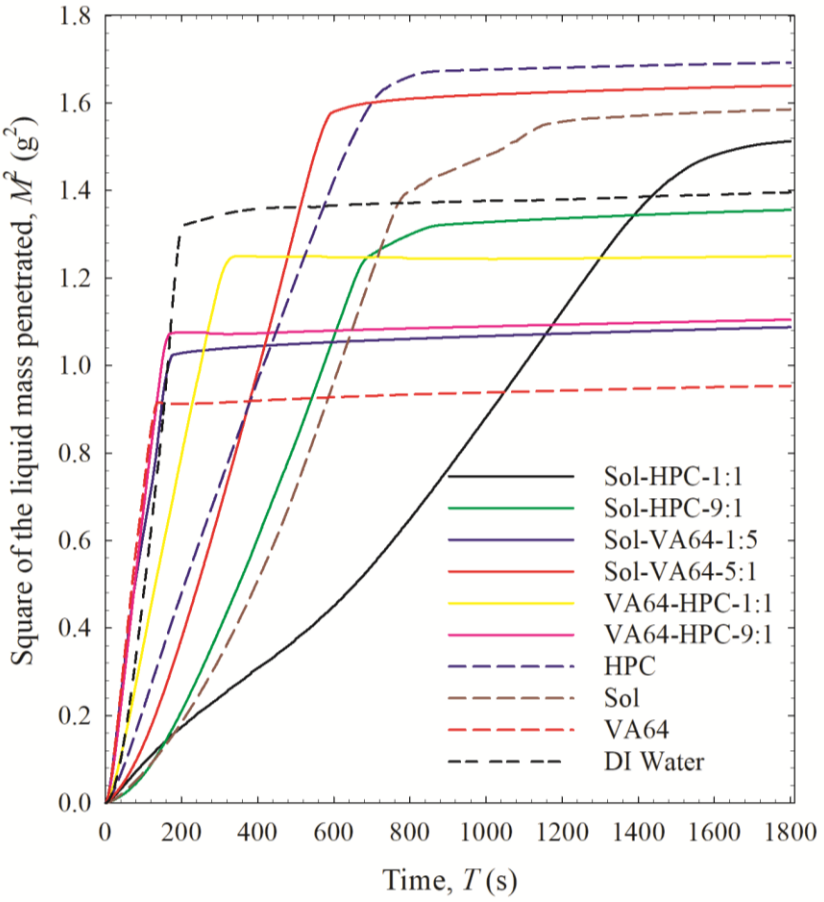

Figure E.1 Temporal evolution of the liquid mass penetrated into a packed bed of as-received GF particles for GF-saturated deionized (DI) water and various GF-saturated aqueous solutions of 15% HPC/Sol/VA64 (single polymer) and 15% Sol–HPC/VA64–HPC/Sol–VA64 (binary polymer) with varied polymer1:polymer2 mass ratios.

APPENDIX F

RELEASE OF ITRACONAZOLE FROM SPRAY-DRIED NANOCRYSTAL–AMORPHOUS SOLID DISPERSIONS (HyNASDs) AND ASDs

In appendix F, detail of the modified Washburn method to measure the relative wetting effectiveness of the stabilizer/dispersant solutions are provided.

F.1 Details of the Characterization Methods used for Drug Wettability Measurements

Penetration of a liquid into a packed powder bed of a drug inside a cylindrical column allows for measurement of the drug powder wettability, based on the Washburn method (Hołownia et al., 2008; Washburn, 1921). The method presented here was adapted from Bilgili et al. (2018) and Li et al. (2017). In the current study, liquids and powder refer to aqueous solutions of 15% polymers (Soluplus (Sol)/HPC/Kollidon VA64 (VA64)) and ITZ powder, respectively. All percentages are (% w/w) with respective to deionized water. This polymer concentration was selected to measure the viscosity accurately in our viscometer set-up instead of the maximum viscosity of 7.5% used in the polymer solutions. After dissolving the polymers, the solutions were stirred overnight. After overnight stirring, the solutions were used for further characterization. The apparent shear viscosity and surface tension of the solutions were measured using R/S Plus Rheometer (Brookfield Engineering, Middleboro, MA, USA) and Attension Sigma 700 (Biolin Scientific, Linthicum, MD, USA) respectively, as described below; then, the drug wettability by the drug-saturated solutions was quantified *via* a wetting effectiveness factor using the modified Washburn equation.

F.1.1 Apparent Shear Viscosity of the Solutions

The apparent shear viscosity of the aqueous solutions of the polymers was measured using an R/S Plus Rheometer (Brookfield Engineering, Middleboro, MA, USA) with a water jacket assembly Lauda Eco (Lauda-Brinkmann LP, Delran, NJ, USA). A coaxial cylinder (CC40) was used to provide a controlled shear rate on the samples and shear rate 0 to 1000 1/s for 60 s was used for all the samples. The temperature of the jacket was kept constant at 25 ± 0.5 °C. The raw data were analyzed using the Rheo 3000 software (Brookfield Engineering, Middleboro, MA, USA) of the equipment to obtain the apparent shear viscosity as a function of the shear rate. The apparent shear viscosity at ~100 1/s was used as a representative low shear rate value. The viscosity of water was taken from Korson et al. (1969).

F.1.2 Surface Tension of the Solutions

The surface tension of the water and the aqueous solutions of the polymers was measured using Attension Sigma 700 (Biolin Scientific, Linthicum, MD, USA). The Attention software calculates surface tension from force measurements of interaction of a probe (Wilhelmy plate) at the boundary between air and a liquid.

F.1.3 Drug Wettability with the Solutions

Attension Sigma 700 set-up (Biolin Scientific, Linthicum, MD, USA) was used to study the penetration of deionized water/ aqueous solutions of the polymers into a packed powder bed of ITZ inside a cylindrical column and determine the ITZ wettability, based on the modified Washburn method. The assembly consists of a sample holder in the form of a cylindrical metallic tube with small holes at the bottom as well as a hook at the top of the cover equipped with screw threads. About 0.8 g of

ITZ powder was packed uniformly into the tube before each measurement. A filter paper was placed at the perforated end of the sample holder to support the ITZ powder sample. A petri dish containing deionized water/polymer solution was placed below the perforated end of the holder on the mechanical platform.

Upon contact of the sample holder with the liquid, the liquid penetrated the ITZ powder bed, while Attension Sigma 700 recorded the mass M of the liquid penetrated as a function of time T. The cosine of the contact angle θ for the deionized water/ aqueous polymer solution and drug can be determined using the modified Washburn equation, which provides a relationship between liquid penetration rate and contact angle, *via* $M^2 = \left(\frac{C\rho^2\gamma\cos\theta}{\eta}\right)T$, where η, ρ, and γ stand for viscosity of the liquid, density of the liquid, and surface tension of the liquid, respectively. C is a characteristic parameter of the powder sample, which could have been determined independently using a completely wetting liquid such as hexane, heptane, etc. Since the same drug powder (ITZ) was used as the powder sample and C depends only on powder packing–size, C remained invariant for different liquids studied here. This allows us to calculate the ratio of $\cos\theta_{ss}/\cos\theta_w$ as a wetting effectiveness factor from the slopes of M^2 vs. T for deionized water and the polymer solution. Here, θ_{ss} is the contact angle between ITZ and the polymer/SDS solution and θ_w is the contact angle between ITZ and deionized water. The wettability enhancement upon the use of different polymers on the wetting of ITZ particles can be assessed by using this ratio, taking the wettability by water as a basis for comparison.

Experimental liquid penetration data (M^2 vs. T) for various liquids are presented in Figure F.1. The slope of the modified Washburn equation, i.e.,

$c\rho^2\gamma\cos\theta/\eta$, was obtained by fitting the linear region of the liquid penetration curve. Initial ~20 s was not considered due to transient behavior; data points that deviated from the linear region, which may correspond to structural change in the bed, were excluded. The modified Washburn equation fitted the data well ($R^2 \geq$ 0.990). Using the slope for various polymer solutions and water, $\cos\theta_{ss}/\cos\theta_w$ was calculated. The viscosity, surface tension, and calculated wetting effectiveness factor are reported in Table 7.4 of the main text.

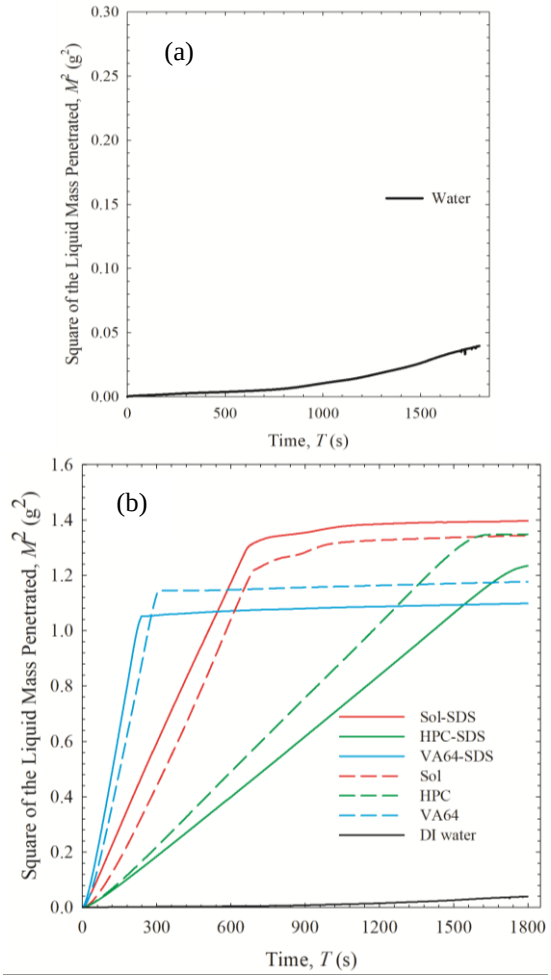

Figure F.1 Temporal evolution of the liquid mass penetrated into a packed bed of as-received ITZ particles for (a) water only and (b) various aqueous solutions of 15% HPC/Sol/VA64–0.125% SDS or w/o SDS.

REFERENCES

Abdelwahed, W., Degobert, G., Fessi, H., 2006. Investigation of nanocapsules stabilization by amorphous excipients during freeze-drying and storage. Eur. J. Pharm. Biopharm. 63, 87–94.

Adamson, A., Gast, A., 1997. Physical chemical of surfaces. John Wiley & Son, Inc., New York.

Afolabi, A., Akinlabi, O., Bilgili, E., 2014. Impact of process parameters on the breakage kinetics of poorly water-soluble drugs during wet stirred media milling: a microhydrodynamic view. Eur. J. Pharm. Sci. 51, 75–86.

Albadarin, A.B., Potter, C.B., Davis, M.T., Iqbal, J., Korde, S., Pagire, S., Paradkar, A., Walker, G., 2017. Development of stability-enhanced ternary solid dispersions *via* combinations of HPMCP and Soluplus® processed by hot melt extrusion. Int. J. Pharm. 532, 603–611.

Aleandri, S., Schönenberger, M., Niederquell, A., Kuentz, M., 2018. Temperature-induced surface effects on drug nanosuspensions. Pharm. Res. 35, 69.

Aleem, O., Kuchekar, B., Pore, Y., Late, S., 2008. Effect of β-cyclodextrin and hydroxypropyl β-cyclodextrin complexation on physicochemical properties and antimicrobial activity of cefdinir. J. Pharm. Biomed. Anal. 47, 535–540.

Alhalaweh, A., Alzghoul, A., Mahlin, D., Bergström, C.A., 2015. Physical stability of drugs after storage above and below the glass transition temperature: Relationship to glass-forming ability. Int. J. Pharm. 495, 312–317.

Alonzo, D.E., Gao, Y., Zhou, D., Mo, H., Zhang, G.G., Taylor, L.S., 2011. Dissolution and precipitation behavior of amorphous solid dispersions. J. Pharm. Sci. 100, 3316–3331.

Alonzo, D.E., Zhang, G.G., Zhou, D., Gao, Y., Taylor, L.S., 2010. Understanding the behavior of amorphous pharmaceutical systems during dissolution. Pharm. Res. 27, 608–618.

Ambike, A.A., Mahadik, K., Paradkar, A., 2005. Spray-dried amorphous solid dispersions of simvastatin, a low T g drug: in vitro and in vivo evaluations. Pharm. Res. 22, 990–998.

Azad, M., Afolabi, A., Bhakay, A., Leonardi, J., Davé, R., Bilgili, E., 2015a. Enhanced physical stabilization of fenofibrate nanosuspensions *via* wet co-milling with a superdisintegrant and an adsorbing polymer. Eur. J. Pharm. Biopharm. 94, 372–385.

Azad, M., Arteaga, C., Abdelmalek, B., Davé, R., Bilgili, E., 2015b. Spray drying of drug-swellable dispersant suspensions for preparation of fast-dissolving, high drug-loaded, surfactant-free nanocomposites. Drug Dev. Ind. Pharm. 41, 1617–1631.

Azad, M., Moreno, J., Bilgili, E., Davé, R., 2016. Fast dissolution of poorly water soluble drugs from fluidized bed coated nanocomposites: Impact of carrier size. Int. J. Pharm. 513, 319–331.

Baghel, S., Cathcart, H., O'Reilly, N.J., 2016. Polymeric amorphous solid dispersions: a review of amorphization, crystallization, stabilization, solid-state characterization, and aqueous solubilization of biopharmaceutical classification system class II drugs. J. Pharm. Sci. 105, 2527–2544.

Baird, J.A., Taylor, L.S., 2012. Evaluation of amorphous solid dispersion properties using thermal analysis techniques. Adv. Drug Delivery Rev. 64, 396-421.

Baird, J.A., Van Eerdenbrugh, B., Taylor, L.S., 2010. A classification system to assess the crystallization tendency of organic molecules from undercooled melts. J. Pharm. Sci. 99, 3787–3806.

Barthelmes, G., Pratsinis, S.E., Buggisch, H., 2003. Particle size distributions and viscosity of suspensions undergoing shear-induced coagulation and fragmentation. Chem. Eng. Sci. 58, 2893–2902.

Basa, S., Muniyappan, T., Karatgi, P., Prabhu, R., Pillai, R., 2008. Production and in vitro characterization of solid dosage form incorporating drug nanoparticles. Drug Dev. Ind. Pharm. 34, 1209–1218.

BASF, 2019. Crystallization inhibition for enhanced bioavailability – BASF functional solutions for solid and liquid formulations.

Berglund, K.D., Przybycien, T.M., Tilton, R.D., 2003a. Coadsorption of sodium dodecyl sulfate with hydrophobically modified nonionic cellulose polymers. 1. Role of polymer hydrophobic modification. Langmuir 19, 2705–2713.

Berglund, K.D., Przybycien, T.M., Tilton, R.D., 2003b. Coadsorption of sodium dodecyl sulfate with hydrophobically modified nonionic cellulose polymers. 2. Role of surface selectivity in adsorption hysteresis. Langmuir 19, 2714–2721.

Bernhardt, C., Reinsch, E., Husemann, K., 1999. The influence of suspension properties on ultra-fine grinding in stirred ball mills. Powder Technol. 105, 357–361.

Bhakay, A., Merwade, M., Bilgili, E., Dave, R.N., 2011. Novel aspects of wet milling for the production of microsuspensions and nanosuspensions of poorly water-soluble drugs. Drug Dev. Ind. Pharm. 37, 963–976.

Bhakay, A., Davé, R., Bilgili, E., 2013. Recovery of BCS Class II drugs during aqueous redispersion of core–shell type nanocomposite particles produced *via* fluidized bed coating. Powder Technol. 236, 221–234.

Bhakay, A., Azad, M., Bilgili, E., Dave, R., 2014a. Redispersible fast dissolving nanocomposite microparticles of poorly water-soluble drugs. Int. J. Pharm. 461, 367–379.

Bhakay, A., Azad, M., Vizzotti, E., Dave, R.N., Bilgili, E., 2014b. Enhanced recovery and dissolution of griseofulvin nanoparticles from surfactant-free nanocomposite microparticles incorporating wet-milled swellable dispersants. Drug Dev. Ind. Pharm. 40, 1509–1522.

Bhakay, A., Vizzotti, E., Li, M., Davé, R., Bilgili, E., 2016. Incorporation of fenofibrate nanoparticles prepared by melt emulsification into polymeric films. J. Pharm. Innovation 11, 53–63.

Bhakay, A., Davé, R., Bilgili, E., 2018a. Quiescent and agitated redispersion as a tool for evaluating dispersant effectiveness in dissolution enhancement of drug-laden nanocomposites. AAPS PharmSciTech 19, 436–447.

Bhakay, A., Rahman, M., Dave, R.N., Bilgili, E., 2018b. Bioavailability enhancement of poorly water-soluble drugs *via* nanocomposites: Formulation processing aspects and challenges. Pharmaceutics 10.

Bilgili, E., Hamey, R., Scarlett, B., 2004. Production of pigment nanoparticles using a wet stirred mill with polymeric media. China Particuology 2, 93–100.

Bilgili, E., Afolabi, A., 2012. A combined microhydrodynamics–polymer adsorption analysis for elucidation of the roles of stabilizers in wet stirred media milling. Int. J. Pharm. 439, 193–206.

Bilgili, E., Li, M., Afolabi, A., 2016. Is the combination of cellulosic polymers and anionic surfactants a good strategy for ensuring physical stability of BCS Class II drug nanosuspensions? Pharm. Dev. Technol. 21, 499–510.

Bilgili, E., Rahman, M., Palacios, D., Arevalo, F., 2018. Impact of polymers on the aggregation of wet-milled itraconazole particles and their dissolution from spray-dried nanocomposites. Adv. Powder Technol. 9, 2941–2956.

Bitterlich, A., Laabs, C., Busmann, E., Grandeury, A., Juhnke, M., Bunjes, H., Kwade, A., 2014. Challenges in nanogrinding of active pharmaceutical ingredients. Chem. Eng. Technol. 37, 840-846.

Boateng, J.S., Matthews, K.H., Auffret, A.D., Humphrey, M.J., Stevens, H.N., Eccleston, G.M., 2009. In vitro drug release studies of polymeric freeze-dried wafers and solvent-cast films using paracetamol as a model soluble drug. Int. J. Pharm. 378, 66–72.

Bose, S., Schenck, D., Ghosh, I., Hollywood, A., Maulit, E., Ruegger, C., 2012. Application of spray granulation for conversion of a nanosuspension into a dry powder form. Eur. J. Pharm. Sci. 47, 35–43.

Brough, C., Williams, R., 2013. Amorphous solid dispersions and nano-crystal technologies for poorly water-soluble drug delivery. Int. J. Pharm. 453, 157–166.

Cerdeira, A.M., Mazzotti, M., Gander, B., 2010. Miconazole nanosuspensions: influence of formulation variables on particle size reduction and physical stability. Int. J. Pharm. 396, 210–218.

Cerdeira, A.M., Mazzotti, M., Gander, B., 2013. Formulation and drying of miconazole and itraconazole nanosuspensions. Int. J. Pharm. 443, 209–220.

Chang, T.-L., Zhan, H., Liang, D., Liang, J.F., 2015. Nanocrystal technology for drug formulation and delivery. Frontiers of Chemical Science and Engineering 9, 1–14.

Chaubal, M.V., Popescu, C., 2008. Conversion of nanosuspensions into dry powders by spray drying: a case study. Pharm. Res. 25, 2302–2308.

Chen, Y., Liu, C., Chen, Z., Su, C., Hageman, M., Hussain, M., Haskell, R., Stefanski, K., Qian, F., 2015. Drug–polymer–water interaction and its implication for the dissolution performance of amorphous solid dispersions. Molecular Pharmaceutics 12, 576–589.

Cheow, W.S., Ng, M.L.L., Kho, K., Hadinoto, K., 2011. Spray freeze-drying production of thermally sensitive polymeric nanoparticle aggregates for inhaled drug delivery: effect of freeze-drying adjuvants. Int. J. Pharm. 404, 289–300.

Chin, W.W.L., Parmentier, J., Widzinski, M., Tan, E.H., Gokhale, R., 2014. A brief literature and patent review of nanosuspensions to a final drug product. J. Pharm. Sci. 103, 2980–2999.

Choi, J.-Y., Park, C.H., Lee, J., 2008. Effect of polymer molecular weight on nanocomminution of poorly soluble drug. Drug Delivery 15, 347–353.

Choi, P., Kavassalis, T.A., Rudin, A., 1994. Estimation of Hansen solubility parameters for (hydroxyethyl) and (hydroxypropyl) cellulose through molecular simulation. Industrial & Engineering Chemistry Research 33, 3154–3159.

Costa, P., Lobo, J.M.S., 2001. Modeling and comparison of dissolution profiles. Eur. J. Pharm. Sci. 13, 123–133.

Craig, D.Q., 2002. The mechanisms of drug release from solid dispersions in water-soluble polymers. Int. J. Pharm. 231, 131–144.

Crowley, K.J., Zografi, G., 2002. Water vapor absorption into amorphous hydrophobic drug/poly (vinylpyrrolidone) dispersions. J. Pharm. Sci. 91, 2150-2165.

Cui, Y., 2007. A material science perspective of pharmaceutical solids. Int. J. Pharm. 339, 3-18.

Dave, R.H., Patel, H.H., Donahue, E., Patel, A.D., 2013. To evaluate the change in release from solid dispersion using sodium lauryl sulfate and model drug sulfathiazole. Drug Dev. Ind. Pharm. 39, 1562–1572.

Davis, M.T., Potter, C.B., Walker, G.M., 2018. Downstream processing of a ternary amorphous solid dispersion: The impacts of spray drying and hot melt extrusion on powder flow, compression and dissolution. Int. J. Pharm. 544, 242–253.

De Smet, L., Saerens, L., De Beer, T., Carleer, R., Adriaensens, P., Van Bocxlaer, J., Vervaet, C., Remon, J.P., 2014. Formulation of itraconazole nanococrystals and evaluation of their bioavailability in dogs. Eur. J. Pharm. Biopharm. 87, 107–113.

De Waard, H., Hinrichs, W., Frijlink, H., 2008. A novel bottom–up process to produce drug nanocrystals: controlled crystallization during freeze-drying. J. Controlled Release 128, 179–183.

Di, L., Kerns, E.H., Carter, G.T., 2009. Drug-like property concepts in pharmaceutical design. Current Pharmaceutical Design 15, 2184–2194.

Duddu, S.P., Sokoloski, T.D., 1995. Dielectric analysis in the characterization of amorphous pharmaceutical solids. 1. Molecular mobility in poly (vinylpyrrolidone)–water systems in the glassy state. J. Pharm. Sci. 84, 773-776.

Elder, D.P., Holm, R., de Diego, H.L., 2013. Use of pharmaceutical salts and cocrystals to address the issue of poor solubility. Int. J. Pharm. 453, 88–100.

Eskin, D., Zhupanska, O., Hamey, R., Moudgil, B., Scarlett, B., 2005. Microhydrodynamics of stirred media milling. Powder Technol. 156, 95-102.

Evertsson, H., Nilsson, S., 1997. Microviscosity in clusters of ethyl hydroxyethyl cellulose and sodium dodecyl sulfate formed in dilute aqueous solutions as determined with fluorescence probe techniques. Macromolecules 30, 2377–2385.

Ewing, A.V., Clarke, G.S., Kazarian, S.G., 2014. Stability of indomethacin with relevance to the release from amorphous solid dispersions studied with ATR-FTIR spectroscopic imaging. Eur. J. Pharm. Sci. 60, 64-71.

Fakes, M.G., Vakkalagadda, B.J., Qian, F., Desikan, S., Gandhi, R.B., Lai, C., Hsieh, A., Franchini, M.K., Toale, H., Brown, J., 2009. Enhancement of oral bioavailability of an HIV-attachment inhibitor by nanosizing and amorphous formulation approaches. Int. J. Pharm. 370, 167–174.

Fasano, A., 1998. Innovative strategies for the oral delivery of drugs and peptides. Trends Biotechnol. 16, 152–157.

Feng, T., Pinal, R., Carvajal, M.T., 2008. Process induced disorder in crystalline materials: differentiating defective crystals from the amorphous form of griseofulvin. J. Pharm. Sci. 97, 3207–3221.

Forster, A., Hempenstall, J., Rades, T., 2001. Characterization of glass solutions of poorly water‐soluble drugs produced by melt extrusion with hydrophilic amorphous polymers. J. Pharm. Pharmacol. 53, 303‐315.

França, M.T., Pereira, R.N., Riekes, M.K., Pinto, J.M.O., Stulzer, H.K., 2018. Investigation of novel supersaturating drug delivery systems of chlorthalidone: The use of polymer-surfactant complex as an effective carrier in solid dispersions. Eur. J. Pharm. Sci. 111, 142–152.

Galli, C., 2006. Experimental determination of the diffusion boundary layer width of micron and submicron particles. Int. J. Pharm. 313, 114–122.

Ghazal, H.S., Dyas, A.M., Ford, J.L., Hutcheon, G.A., 2009. In vitro evaluation of the dissolution behaviour of itraconazole in bio-relevant media. Int. J. Pharm. 366, 117–123.

Ghosh, I., Bose, S., Vippagunta, R., Harmon, F., 2011. Nanosuspension for improving the bioavailability of a poorly soluble drug and screening of stabilizing agents to inhibit crystal growth. Int. J. Pharm. 409, 260–268.

Greenhalgh, D.J., Williams, A.C., Timmins, P., York, P., 1999. Solubility parameters as predictors of miscibility in solid dispersions. J. Pharm. Sci. 88, 1182–1190.

Gupta, R.B., Kompella, U.B., 2006. Nanoparticle technology for drug delivery. Taylor & Francis, New York, USA.

Gupta, S., Kesarla, R., Omri, A., 2013. Formulation strategies to improve the bioavailability of poorly absorbed drugs with special emphasis on self-emulsifying systems. ISRN Pharmaceutics 2013, 848043.

Ha, E.-S., Baek, I.-h., Cho, W., Hwang, S.-J., Kim, M.-S., 2014. Preparation and evaluation of solid dispersion of atorvastatin calcium with Soluplus® by spray drying technique. Chem. Pharm. Bull. 62, 545–551.

Hancock, B.C., Parks, M., 2000. What is the true solubility advantage for amorphous pharmaceuticals? Pharm. Res. 17, 397–404.

Hancock, B.C., Zografi, G., 1994. The relationship between the glass transition temperature and the water content of amorphous pharmaceutical solids. Pharm. Res. 11, 471-477.

Hauss, D.J., Fogal, S.E., Ficorilli, J.V., Price, C.A., Roy, T., Jayaraj, A.A., Keirns, J.J., 1998. Lipid‐based delivery systems for improving the bioavailability and lymphatic transport of a poorly water‐soluble LTB4 inhibitor. Journal of pharmaceutical sciences 87, 164-169.

Hecq, J., Deleers, M., Fanara, D., Vranckx, H., Amighi, K., 2005. Preparation and characterization of nanocrystals for solubility and dissolution rate enhancement of nifedipine. Int. J. Pharm. 299, 167–177.

Hoffman, J.D., 1958. Thermodynamic driving force in nucleation and growth processes. The Journal of Chemical Physics 29, 1192-1193.

Hołownia, D., Kwiatkowska, I., Hupka, J., 2008. An investigation on wetting of porous materials. Physicochem. Prob. Miner. Process. 42, 251–262.

Hou, Y., Shao, J., Fu, Q., Li, J., Sun, J., He, Z., 2017. Spray-dried nanocrystals for a highly hydrophobic drug: Increased drug loading, enhanced redispersity, and improved oral bioavailability. Int. J. Pharm. 516, 372–379.

Huang, S., Williams, R.O., 2018. Effects of the preparation process on the properties of amorphous solid dispersions. AAPS PharmSciTech 19, 1971–1984.

Humberstone, A.J., Charman, W.N., 1997. Lipid-based vehicles for the oral delivery of poorly water soluble drugs. Adv. Drug Delivery Rev. 25, 103–128.

Ilevbare, G.A., Taylor, L.S., 2013. Liquid–liquid phase separation in highly supersaturated aqueous solutions of poorly water-soluble drugs: implications for solubility enhancing formulations. Crystal Growth & Design 13, 1497–1509.

Iurian, S., Bogdan, C., Tomuță, I., Szabó-Révész, P., Chvatal, A., Leucuța, S.E., Moldovan, M., Ambrus, R., 2017. Development of oral lyophilisates containing meloxicam nanocrystals using QbD approach. Eur. J. Pharm. Sci. 104, 356–365.

Jackson, M.J., Kestur, U.S., Hussain, M.A., Taylor, L.S., 2015. Dissolution of danazol amorphous solid dispersions: supersaturation and phase behavior as a

function of drug loading and polymer type. Molecular Pharmaceutics 13, 223–231.

Janssens, S., Van den Mooter, G., 2009. Physical chemistry of solid dispersions. J. Pharm. Pharmacol. 61, 1571-1586.

Jermain, S.V., Brough, C., Williams III, R.O., 2018. Amorphous solid dispersions and nanocrystal technologies for poorly water-soluble drug delivery–An update. Int. J. Pharm. 535, 379–392.

Jung, H.J., Ahn, H.I., Park, J.Y., Ho, M.J., Lee, D.R., Cho, H.R., Park, J.S., Choi, Y.S., Kang, M.J., 2016. Improved oral absorption of tacrolimus by a solid dispersion with hypromellose and sodium lauryl sulfate. Int. J. Biol. Macromol. 83, 282–287.

Jung, J.-Y., Yoo, S.D., Lee, S.-H., Kim, K.-H., Yoon, D.-S., Lee, K.-H., 1999. Enhanced solubility and dissolution rate of itraconazole by a solid dispersion technique. Int. J. Pharm. 187, 209–218.

Junghanns, J.-U.A., Müller, R.H., 2008a. Nanocrystal technology, drug delivery and clinical applications. Int. J. Nanomed. 3, 295–309.

Kagotani, R., Kinugawa, K., Nomura, M., Imanaka, H., Ishida, N., Imamura, K., 2013. Improving the physical stability of freeze‐dried amorphous sugar matrices by compression at several hundreds MPa. Journal of pharmaceutical sciences 102, 2187-2197.

Kayaert, P., Van den Mooter, G., 2012. Is the amorphous fraction of a dried nanosuspension caused by milling or by drying? A case study with Naproxen and Cinnarizine. Eur. J. Pharm. Biopharm. 81, 650–656.

Keck, C.M., Müller, R.H., 2006. Drug nanocrystals of poorly soluble drugs produced by high pressure homogenisation. Eur. J. Pharm. Biopharm. 62, 3–16.

Kemp, I.C., 2011. Fundamentals of energy analysis of dryers, Modern Drying Technology. WILEY-VCH Verlag GmbH & Co. KGaA, Weinheim, Germany, pp. 1–46.

Knieke, C., Azad, M., Davé, R., Bilgili, E., 2013. A study of the physical stability of wet media-milled fenofibrate suspensions using dynamic equilibrium curves. Chem. Eng. Res. Des. 91, 1245–1258.

Kesisoglou, F., Panmai, S., Wu, Y., 2007. Nanosizing—oral formulation development and biopharmaceutical evaluation. Adv. Drug Delivery Rev. 59, 631–644.

Kesisoglou, F., Wu, Y., 2008. Understanding the effect of API properties on bioavailability through absorption modeling. AAPS J. 10, 516–525.

Kim, D.S., Choi, H.G., Jin, S.G., 2018. Influence of Hydroxypropylmethylcellulose and Sodium Lauryl Sulfate on the Solubility and Dissolution of Sirolimus in Solvent‐evaporated Solid Dispersions. Bull. Korean Chem. Soc. 39, 778–783.

Kim, D.S., Choi, J.S., Kim, D.W., Kim, K.S., Seo, Y.G., Cho, K.H., Kim, J.O., Yong, C.S., Youn, Y.S., Lim, S.-J., 2016. Comparison of solvent wetted and kneaded l-sulpiride loaded solid dispersions: Powder characterization and in vivo evaluation. Int. J. Pharm. 511, 351–358.

Kim, S., Lee, J., 2010. Effective polymeric dispersants for vacuum, convection and freeze drying of drug nanosuspensions. Int. J. Pharm. 397, 218–224.

Kipp, J., 2004. The role of solid nanoparticle technology in the parenteral delivery of poorly water-soluble drugs. Int. J. Pharm. 284, 109–122.

Knieke, C., Azad, M., Davé, R., Bilgili, E., 2013. A study of the physical stability of wet media-milled fenofibrate suspensions using dynamic equilibrium curves. Chem. Eng. Res. Des. 91, 1245–1258.

Knieke, C., Rawtani, A., Davé, R.N., 2014. Concentrated fenofibrate nanoparticle suspensions from melt emulsification for enhanced drug dissolution. Chem. Eng. Technol. 37, 157–167.

Kolter, K., Karl, M., Gryczke, A., Ludwigshafen am Rhein, B., 2012. Hot-melt extrusion with BASF pharma polymers: extrusion compendium. BASF.

Konnerth, C., Braig, V., Ito, A., Schmidt, J., Lee, G., Peukert, W., 2017. Formation of mefenamic acid nanocrystals with improved dissolution characteristics. Chem. Ing. Tech. 89, 1060–1071.

Konno, H., Handa, T., Alonzo, D.E., Taylor, L.S., 2008. Effect of polymer type on the dissolution profile of amorphous solid dispersions containing felodipine. Eur. J. Pharm. Biopharm. 70, 493–499.

Korson, L., Drost-Hansen, W., Millero, F.J., 1969. Viscosity of water at various temperatures. J. Phys. Chem. 73, 34–39.

Kothari, K., Ragoonanan, V., Suryanarayanan, R., 2015. The role of polymer concentration on the molecular mobility and physical stability of nifedipine solid dispersions. Molecular Pharmaceutics 12, 1477–1484.

Krull, S.M., Ma, Z., Li, M., Davé, R.N., Bilgili, E., 2016. Preparation and characterization of fast dissolving pullulan films containing BCS class II drug nanoparticles for bioavailability enhancement. Drug Dev. Ind. Pharm. 42, 1073–1085.

Krull, S.M., Susarla, R., Afolabi, A., Li, M., Ying, Y., Iqbal, Z., Bilgili, E., Davé, R.N., 2015. Polymer strip films as a robust, surfactant-free platform for delivery of BCS Class II drug nanoparticles. Int. J. Pharm. 489, 45–57.

Kumar, S., Jog, R., Shen, J., Zolnik, B., Sadrieh, N., Burgess, D.J., 2015a. In vitro and in vivo performance of different sized spray-dried crystalline itraconazole. J. Pharm. Sci. 104, 3018–3028.

Kumar, S., Shen, J., Zolnik, B., Sadrieh, N., Burgess, D.J., 2015b. Optimization and dissolution performance of spray-dried naproxen nano-crystals. Int. J. Pharm. 486, 159–166.

Kumar, S., Xu, X., Gokhale, R., Burgess, D.J., 2014. Formulation parameters of crystalline nanosuspensions on spray drying processing: a DoE approach. Int. J. Pharm. 464, 34–45.

Kushner, L.M., Duncan, B.C., Hoffman, J.I., 1952. A viscometric study of the micelles of sodium dodecyl sulfate in dilute solutions. J. Res. Nat. Bur. Stand. 49, 85–90.

Lakshmi, P., Kumar, G.A., 2010. Nanosuspension technology: A review. Int. J. Pharm. Sci. 2, 35–40.

Langham, Z.A., Booth, J., Hughes, L.P., Reynolds, G.K., Wren, S.A., 2012. Mechanistic insights into the dissolution of spray‐dried amorphous solid dispersions. Journal of pharmaceutical sciences 101, 2798-2810.

Layre, A.-M., Couvreur, P., Richard, J., Requier, D., Eddine Ghermani, N., Gref, R., 2006. Freeze-drying of composite core-shell nanoparticles. Drug Dev. Ind. Pharm. 32, 839–846.

Lebhardt, T., Roesler, S., Uusitalo, H.P., Kissel, T., 2011. Surfactant-free redispersible nanoparticles in fast-dissolving composite microcarriers for dry-powder inhalation. Eur. J. Pharm. Biopharm. 78, 90–96.

Lee, J., 2003. Drug nano‐and microparticles processed into solid dosage forms: physical properties. J. Pharm. Sci. 92, 2057–2068.

Lee, J., Choi, J.-Y., Park, C., 2008. Characteristics of polymers enabling nano-comminution of water-insoluble drugs. Int. J. Pharm. 355, 328–336.

Lee, M.K., Kim, M.Y., Kim, S., Lee, J., 2009. Cryoprotectants for freeze drying of drug nano‐suspensions: Effect of freezing rate. J. Pharm. Sci. 98, 4808‐4817.

Leleux, J., Williams, R.O., 2014. Recent advancements in mechanical reduction methods: particulate systems. Drug Dev. Ind. Pharm. 40, 289–300.

Letchford, K., Burt, H., 2007. A review of the formation and classification of amphiphilic block copolymer nanoparticulate structures: micelles, nanospheres, nanocapsules and polymersomes. Eur. J. Pharm. Biopharm. 65, 259–269.

Leuner, C., Dressman, J., 2000. Improving drug solubility for oral delivery using solid dispersions. Eur. J. Pharm. Biopharm. 50, 47-60.

Li, M., Yaragudi, N., Afolabi, A., Dave, R., Bilgili, E., 2015. Sub-100 nm drug particle suspensions prepared *via* wet milling with low bead contamination through novel process intensification. Chem. Eng. Sci. 130, 207–220.

Li, M., Azad, M., Davé, R., Bilgili, E., 2016a. Nanomilling of drugs for bioavailability enhancement: a holistic formulation-process perspective. Pharmaceutics 8, 27.

Li, M., Lopez, N., Bilgili, E., 2016b. A study of the impact of polymer–surfactant in drug nanoparticle coated pharmatose composites on dissolution performance. Adv. Powder Technol. 27, 1625–1636.

Li, M., Zhang, L., Davé, R.N., Bilgili, E., 2016c. An intensified vibratory milling process for enhancing the breakage kinetics during the preparation of drug nanosuspensions. AAPS PharmSciTech 17, 389–399.

Li, M., Ioannidis, N., Gogos, C., Bilgili, E., 2017. A comparative assessment of nanocomposites vs. amorphous solid dispersions prepared *via* nanoextrusion for drug dissolution enhancement. Eur. J. Pharm. Biopharm. 119, 68–80.

Li, M., Alvarez, P., Orbe, P., Bilgili, E., 2018a. Multi-faceted characterization of wet-milled griseofulvin nanosuspensions for elucidation of aggregation state and stabilization mechanisms. AAPS PharmSciTech 19, 1789–1801.

Li, M., Suriel, I., Vekaria, J., Proske, J., Orbe, P., Armani, M., Dave, R., Bilgili, E., 2018b. Impact of dispersants on dissolution of itraconazole from drug-loaded, surfactant-free, spray-dried nanocomposites. Powder Technol. 339, 281–295.

Lipinski, C., 2002. Poor aqueous solubility—an industry wide problem in drug discovery. Am. Pharm. Rev. 5, 82–85.

Liu, C., Chen, Z., Chen, Y., Lu, J., Li, Y., Wang, S., Wu, G., Qian, F., 2016. Improving oral bioavailability of sorafenib by optimizing the “Spring” and “Parachute” based on molecular interaction mechanisms. Molecular Pharmaceutics 13, 599–608.

Liu, T., Müller, R.H., Möschwitzer, J.P., 2018. Production of drug nanosuspensions: effect of drug physical properties on nanosizing efficiency. Drug Dev. Ind. Pharm. 44, 233–242.

Liversidge, G.G., Cundy, K.C., 1995. Particle size reduction for improvement of oral bioavailability of hydrophobic drugs: I. Absolute oral bioavailability of nanocrystalline danazol in beagle dogs. Int. J. Pharm. 125, 91–97.

Lu, Y., Tang, N., Lian, R., Qi, J., Wu, W., 2014. Understanding the relationship between wettability and dissolution of solid dispersion. Int. J. Pharm. 465, 25–31.

Luebbert, C., Huxoll, F., Sadowski, G., 2017. Amorphous-amorphous phase separation in API/polymer formulations. Molecules 22, 296.

Malamatari, M., Taylor, K.M., Malamataris, S., Douroumis, D., Kachrimanis, K., 2018. Pharmaceutical nanocrystals: prodcution by wet media milling and applications. Drug Discovery Today 23, 534–547.

Marsac, P.J., Konno, H., Taylor, L.S., 2006. A comparison of the physical stability of amorphous felodipine and nifedipine systems. Pharm. Res. 23, 2306-2316.

Matsui, K., Tsume, Y., Amidon, G.E., Amidon, G.L., 2016. The evaluation of in vitro drug dissolution of commercially available oral dosage forms for itraconazole in gastrointestinal simulator with biorelevant media. J. Pharm. Sci. 105, 2804–2814.

Medarević, D., Djuriš, J., Ibrić, S., Mitrić, M., Kachrimanis, K., 2018. Optimization of formulation and process parameters for the production of carvedilol nanosuspension by wet media milling. Int. J. Pharm. 540, 150–161.

Meng, F., Trivino, A., Prasad, D., Chauhan, H., 2015. Investigation and correlation of drug polymer miscibility and molecular interactions by various approaches for the preparation of amorphous solid dispersions. Eur. J. Pharm. Sci. 71, 12–24.

Merisko-Liversidge, E., Liversidge, G.G., 2011. Nanosizing for oral and parenteral drug delivery: a perspective on formulating poorly-water soluble compounds using wet media milling technology. Adv. Drug Delivery Rev. 63, 427–440.

Merisko-Liversidge, E., Liversidge, G.G., Cooper, E.R., 2003. Nanosizing: a formulation approach for poorly-water-soluble compounds. Eur. J. Pharm. Sci. 18, 113–120.

Merisko-Liversidge, E.M., Liversidge, G.G., 2008. Drug nanoparticles: formulating poorly water-soluble compounds. Toxicologic Pathology 36, 43–48.

Mistry, P., Mohapatra, S., Gopinath, T., Vogt, F.G., Suryanarayanan, R., 2015. Role of the strength of drug–polymer interactions on the molecular mobility and crystallization inhibition in ketoconazole solid dispersions. Molecular Pharmaceutics 12, 3339–3350.

Mittal, G., Sahana, D., Bhardwaj, V., Kumar, M.R., 2007. Estradiol loaded PLGA nanoparticles for oral administration: effect of polymer molecular weight and copolymer composition on release behavior in vitro and in vivo. J. Controlled Release 119, 77–85.

Monteiro, A., Afolabi, A., Bilgili, E., 2013. Continuous production of drug nanoparticle suspensions *via* wet stirred media milling: a fresh look at the Rehbinder effect. Drug Dev. Ind. Pharm. 39, 266–283.

Moroi, Y., Motomura, K., Matuura, R., 1974. The critical micelle concentration of sodium dodecyl sulfate-bivalent metal dodecyl sulfate mixtures in aqueous solutions. J. Colloid Interface Sci. 46, 111–117.

Morrison, I.D., Ross, S., 2002. Colloidal Dispersions. Wiley-Interscience, New York, USA.

Müller, R.H., Gohla, S., Keck, C.M., 2011. State of the art of nanocrystals–special features, production, nanotoxicology aspects and intracellular delivery. Eur. J. Pharm. Biopharm. 78, 1–9.

Müller, R.H., Benita, S., Böhm, B.H., 1998. Nanosuspensions, in: Benita, S., Böhm, B.H. (Ed.), Emulsions and nanosuspensions for the formulation of poorly soluble drugs. Medpharm Scientific, Stuttgart, Germany, pp. 149–173.

Müller, R.H., Peters, K., 1998. Nanosuspensions for the formulation of poorly soluble drugs: I. Preparation by a size-reduction technique. Int. J. Pharm. 160, 229–237.

Müllertz, A., Ogbonna, A., Ren, S., Rades, T., 2010. New perspectives on lipid and surfactant based drug delivery systems for oral delivery of poorly soluble drugs. J. Pharm. Pharmacol. 62, 1622–1636.

Muster, T.H., Prestidge, C.A., 2005. Water adsorption kinetics and contact angles of pharmaceutical powders. J. Pharm. Sci. 94, 861–872.

Nakagami, H., 1991. Solid dispersions of indomethacin and griseofulvin in non-porous fumed silicon dioxide, prepared by melting. Chem. Pharm. Bull. 39, 2417–2421.

Newman, A., Engers, D., Bates, S., Ivanisevic, I., Kelly, R.C., Zografi, G., 2008. Characterization of amorphous API: Polymer mixtures using X‐ray powder diffraction. J. Pharm. Sci. 97, 4840‐4856.

Niwa, T., Danjo, K., 2013. Design of self-dispersible dry nanosuspension through wet milling and spray freeze-drying for poorly water-soluble drugs. Eur. J. Pharm. Sci. 50, 272–281.

Niwa, T., Miura, S., Danjo, K., 2011. Design of dry nanosuspension with highly spontaneous dispersible characteristics to develop solubilized formulation for poorly water-soluble drugs. Pharm. Res. 28, 2339–2349.

Noyes, A.A., Whitney, W.R., 1897a. The rate of solution of solid substances in their own solutions. J. Am. Chem. Soc. 19, 930–934.

Paradkar, A., Ambike, A.A., Jadhav, B.K., Mahadik, K., 2004. Characterization of curcumin–PVP solid dispersion obtained by spray drying. Int. J. Pharm. 271, 281–286.

Parmentier, J., Tan, E.H., Low, A., Möschwitzer, J.P., 2017. Downstream drug product processing of itraconazole nanosuspension: Factors influencing drug particle size and dissolution from nanosuspension-layered beads. Int. J. Pharm. 524, 443–453.

Peeters, J., Neeskens, P., Tollenaere, J.P., Van Remoortere, P., Brewster, M.E., 2002. Characterization of the interaction of 2‐hydroxypropyl‐β‐cyclodextrin with itraconazole at pH 2, 4, and 7. J. Pharm. Sci. 91, 1414‐1422.

Peltonen, L., Hirvonen, J., 2010. Pharmaceutical nanocrystals by nanomilling: Critical process parameters, particle fracturing and stabilization methods. J. Pharm. Pharmacol. 62, 1569–1579.

Peltonen, L., Hirvonen, J., 2018. Drug nanocrystals–Versatile option for formulation of poorly soluble materials. Int. J. Pharm. 537, 73–83.

Peppas, N., 1985. Analysis of Fickian and non-Fickian drug release from polymers. Pharm. Acta Helv. 60, 110–111.

Ploehn, H.J., Russel, W.B., 1990. Interactions between colloidal particles and soluble polymers. Adv. Chem. Eng. 15, 137–228.

Poozesh, S., Bilgili, E., 2019. Scale-up of pharmaceutical spray drying using scale-up rules: A review. Int. J. Pharm. 562, 271–292.

Prasad, D., Chauhan, H., Atef, E., 2016. Role of molecular interactions for synergistic precipitation inhibition of poorly soluble drug in supersaturated drug–polymer–polymer ternary solution. Molecular Pharmaceutics 13, 756–765.

Qian, F., Huang, J., Hussain, M.A., 2010. Drug–polymer solubility and miscibility: stability consideration and practical challenges in amorphous solid dispersion development. J. Pharm. Sci. 99, 2941–2947.

Rabinow, B.E., 2004. Nanosuspensions in drug delivery. Nature reviews. Drug discovery 3, 785.

Raghavan, S., Trividic, A., Davis, A., Hadgraft, J., 2001. Crystallization of hydrocortisone acetate: influence of polymers. Int. J. Pharm. 212, 213–221.

Rahman, Z., Zidan, A.S., Samy, R., Sayeed, V.A., Khan, M.A., 2012. Improvement of physicochemical properties of an antiepileptic drug by salt engineering. AAPS PharmSciTech 13, 793–801.

Riddick, T.M., 1968. Control of colloid stability through zeta potential. Zeta-Meter Inc. *via* Livingston Publishing Company, Lynnewood, PA, USA.

Ritger, P.L., Peppas, N.A., 1987a. A simple equation for description of solute release I. Fickian and non-fickian release from non-swellable devices in the form of slabs, spheres, cylinders or discs. J. Controlled Release 5, 23–36.

Ritger, P.L., Peppas, N.A., 1987b. A simple equation for description of solute release II. Fickian and anomalous release from swellable devices. J. Controlled Release 5, 37–42.

Rowe, R., 1986. The effect of the molecular weight of ethyl cellulose on the drug release properties of mixed films of ethyl cellulose and hydroxypropylmethylcellulose. Int. J. Pharm. 29, 37–41.

Rumondor, A.C., Stanford, L.A., Taylor, L.S., 2009. Effects of polymer type and storage relative humidity on the kinetics of felodipine crystallization from amorphous solid dispersions. Pharm. Res. 26, 2599–2606.

Rumondor, A.C., Dhareshwar, S.S., Kesisoglou, F., 2016. Amorphous solid dispersions or prodrugs: complementary strategies to increase drug absorption. J. Pharm. Sci. 105, 2498–2508.

Ryde, N.P., Ruddy, S.B., 2002. Solid dose nanoparticulate compositions comprising a synergistic combination of a polymeric surface stabilizer and dioctyl sodium sulfosuccinate. Google Patents.

Sarnes, A., Kovalainen, M., Häkkinen, M.R., Laaksonen, T., Laru, J., Kiesvaara, J., Ilkka, J., Oksala, O., Rönkkö, S., Järvinen, K., 2014. Nanocrystal-based per-oral itraconazole delivery: Superior in vitro dissolution enhancement versus Sporanox® is not realized in in vivo drug absorption. J. Controlled Release 180, 109–116.

Sarode, A., Wang, P., Cote, C., Worthen, D.R., 2013. Low-viscosity hydroxypropylcellulose (HPC) grades SL and SSL: versatile pharmaceutical polymers for dissolution enhancement, controlled release, and pharmaceutical processing. AAPS PharmSciTech 14, 151–159.

Schersch, K., Betz, O., Garidel, P., Muehlau, S., Bassarab, S., Winter, G., 2010. Systematic investigation of the effect of lyophilizate collapse on

pharmaceutically relevant proteins I: Stability after freeze‐drying. Journal of pharmaceutical sciences 99, 2256-2278.

Schönert, K., 1988. Size Reduction (Fundamentals)—Chap. 1, Ullmann's Encyclopedia of Industrial Chemistry, vol. B2. Vch Verlagsgesellschaft, Weinheim.

Sepassi, S., Goodwin, D., Drake, A., Holland, S., Leonard, G., Martini, L., Lawrence, M., 2007. Effect of polymer molecular weight on the production of drug nanoparticles. J. Pharm. Sci. 96, 2655–2666.

Serajuddin, A., 1999. Solid dispersion of poorly water‐soluble drugs: Early promises, subsequent problems, and recent breakthroughs. J. Pharm. Sci. 88, 1058‐1066.

Shah, D.A., Patel, M., Murdande, S.B., Dave, R.H., 2016. Influence of spray drying and dispersing agent on surface and dissolution properties of griseofulvin micro and nanocrystals. Drug Dev. Ind. Pharm. 42, 1842–1850.

Shah, N., Iyer, R.M., Mair, H.J., Choi, D.S., Tian, H., Diodone, R., Fähnrich, K., Pabst‐Ravot, A., Tang, K., Scheubel, E., 2013. Improved human bioavailability of vemurafenib, a practically insoluble drug, using an amorphous polymer‐stabilized solid dispersion prepared by a solvent‐controlled coprecipitation process. J. Pharm. Sci. 102, 967-981.

Shamblin, S.L., Tang, X., Chang, L., Hancock, B.C., Pikal, M.J., 1999. Characterization of the time scales of molecular motion in pharmaceutically important glasses. The Journal of Physical Chemistry B 103, 4113-4121.

Sharma, V., Yadav, O., Singh, J., 1996. Physicochemical studies of aqueous sodium dodecyl sulphate solutions in pyridine and isomeric picolines. Colloids and Surfaces A: Physicochemical and Engineering Aspects 110, 23–35.

Shchekin, A., Rusanov, A., 2008. Generalization of the Gibbs–Kelvin–Köhler and Ostwald–Freundlich equations for a liquid film on a soluble nanoparticle. The Journal of chemical physics 129, 154116.

Shegokar, R., Müller, R.H., 2010. Nanocrystals: industrially feasible multifunctional formulation technology for poorly soluble actives. Int. J. Pharm. 399, 129–139.

Shete, G., Jain, H., Punj, D., Prajapat, H., Akotiya, P., Bansal, A.K., 2016. Stabilizers used in nano-crystal based drug delivery systems. J. Excipients and Food Chem. 5, 184–200.

Shibata, Y., Fujii, M., Suzuki, A., Koizumi, N., Kanada, K., Yamada, M., Watanabe, Y., 2014. Effect of storage conditions on the recrystallization of drugs in solid dispersions with crospovidone. Pharm. Dev. Technol. 19, 468–474.

Sievens-Figueroa, L., Bhakay, A., Jerez-Rozo, J.I., Pandya, N., Romañach, R.J., Michniak-Kohn, B., Iqbal, Z., Bilgili, E., Davé, R.N., 2012. Preparation and characterization of hydroxypropyl methyl cellulose films containing stable BCS Class II drug nanoparticles for pharmaceutical applications. Int. J. Pharm. 423, 496–508.

Singh, A., Van den Mooter, G., 2016. Spray drying formulation of amorphous solid dispersions. Adv. Drug Delivery Rev. 100, 27–50.

Singh, S.K., Srinivasan, K., Gowthamarajan, K., Singare, D.S., Prakash, D., Gaikwad, N.B., 2011. Investigation of preparation parameters of nanosuspension by top-down media milling to improve the dissolution of poorly water-soluble glyburide. Eur. J. Pharm. Biopharm. 78, 441–446.

Six, K., Verreck, G., Peeters, J., Brewster, M., Van den Mooter, G., 2004. Increased physical stability and improved dissolution properties of itraconazole, a class II drug, by solid dispersions that combine fast‐ and slow‐dissolving polymers. J. Pharm. Sci. 93, 124‐131.

Sjökvist, E., Nyström, C., Aldén, M., 1991. Physicochemical aspects of drug release. XIII. The effect of sodium dodecyl sulphate additions on the structure and dissolution of a drug in solid dispersions. Int. J. Pharm. 69, 53–62.

Sommer, M., Stenger, F., Peukert, W., Wagner, N., 2006. Agglomeration and breakage of nanoparticles in stirred media mills—a comparison of different methods and models. Chem. Eng. Sci. 61, 135–148.

Srinarong, P., de Waard, H., Frijlink, H.W., Hinrichs, W.L., 2011. Improved dissolution behavior of lipophilic drugs by solid dispersions: the production process as starting point for formulation considerations. Expert Opin. Drug Delivery 8, 1121–1140.

Srivalli, K.M.R., Mishra, B., 2016. Improved aqueous solubility and antihypercholesterolemic activity of ezetimibe on formulating with hydroxypropyl-β-cyclodextrin and hydrophilic auxiliary substances. AAPS PharmSciTech 17, 272–283.

Sun, W., Ni, R., Zhang, X., Li, L.C., Mao, S., 2015. Spray drying of a poorly water-soluble drug nanosuspension for tablet preparation: formulation and process optimization with bioavailability evaluation. Drug Dev. Ind. Pharm. 41, 927–933.

Susarla, R., Afolabi, A., Patel, D., Bilgili, E., Davé, R.N., 2015. Novel use of superdisintegrants as viscosity enhancing agents in biocompatible polymer films containing griseofulvin nanoparticles. Powder Technol. 285, 25–33.

Suzuki, H., Sunada, H., 1998. Influence of water-soluble polymers on the dissolution of nifedipine solid dispersions with combined carriers. Chem. Pharm. Bull. 46, 482–487.

Suzuki, M., Machida, M., Adachi, K., Otabe, K., Sugimoto, T., Hayashi, M., Awazu, S., 2000. Histopathological study of the effects of a single intratracheal instillation of surface active agents on lung in rats. J. Toxicol. Sci. 25, 49–55.

Tanaka, Y., Inkyo, M., Yumoto, R., Nagai, J., Takano, M., Nagata, S., 2012. Nanoparticulation of probucol, a poorly water-soluble drug, using a novel wet-milling process to improve in vitro dissolution and in vivo oral absorption. Drug Dev. Ind. Pharm. 38, 1015–1023.

Terife, G., Wang, P., Faridi, N., Gogos, C.G., 2012. Hot melt mixing and foaming of soluplus® and indomethacin. Polymer Engineering & Science 52, 1629–1639.

Thakral, S., Thakral, N.K., 2013. Prediction of drug–polymer miscibility through the use of solubility parameter based Flory–Huggins interaction parameter and the experimental validation: PEG as model polymer. J. Pharm. Sci. 102, 2254–2263.

Toziopoulou, F., Malamatari, M., Nikolakakis, I., Kachrimanis, K., 2017. Production of aprepitant nanocrystals by wet media milling and subsequent solidification. Int. J. Pharm. 533, 324–334.

Truong, D.H., Tran, T.H., Ramasamy, T., Choi, J.Y., Choi, H.-G., Yong, C.S., Kim, J.O., 2015. Preparation and characterization of solid dispersion using a novel amphiphilic copolymer to enhance dissolution and oral bioavailability of sorafenib. Powder Technol. 283, 260–265.

Tuomela, A., Liu, P., Puranen, J., Rönkkö, S., Laaksonen, T., Kalesnykas, G., Oksala, O., Ilkka, J., Laru, J., Järvinen, K., 2014. Brinzolamide nanocrystal formulations for ophthalmic delivery: reduction of elevated intraocular pressure in vivo. Int. J. Pharm. 467, 34–41.

Van Drooge, D.J., Braeckmans, K., Hinrichs, W.L., Remaut, K., De Smedt, S.C., Frijlink, H.W., 2006. Characterization of the mode of incorporation of lipophilic compounds in solid dispersions at the nanoscale using fluorescence resonance energy transfer (FRET). Macromol. Rapid Commun. 27, 1149-1155.

Van Eerdenbrugh, B., Froyen, L., Martens, J., Blaton, N., Augustijns, P., Brewster, M., Van den Mooter, G., 2007. Characterization of physico-chemical properties and pharmaceutical performance of sucrose co-freeze–dried solid

nanoparticulate powders of the anti-HIV agent loviride prepared by media milling. Int. J. Pharm. 338, 198–206.

Van Eerdenbrugh, B., Froyen, L., Van Humbeeck, J., Martens, J.A., Augustijns, P., Van Den Mooter, G., 2008a. Alternative matrix formers for nanosuspension solidification: dissolution performance and X-ray microanalysis as an evaluation tool for powder dispersion. Eur. J. Pharm. Sci. 35, 344–353.

Van Eerdenbrugh, B., Froyen, L., Van Humbeeck, J., Martens, J.A., Augustijns, P., Van den Mooter, G., 2008b. Drying of crystalline drug nanosuspensions—the importance of surface hydrophobicity on dissolution behavior upon redispersion. Eur. J. Pharm. Sci. 35, 127–135.

Van Eerdenbrugh, B., Van den Mooter, G., Augustijns, P., 2008c. Top-down production of drug nanocrystals: nanosuspension stabilization, miniaturization and transformation into solid products. Int. J. Pharm. 364, 64–75.

Van Eerdenbrugh, B., Vercruysse, S., Martens, J., Vermant, J., Froyen, L., Van, J.H., den Mooter Van, G., Augustijns, P., 2008d. Microcrystalline cellulose, a useful alternative for sucrose as a matrix former during freeze-drying of drug nanosuspensions-a case study with itraconazole. Eur. J. Pharm. Biopharm. 70, 590–596.

Vasconcelos, T., Marques, S., das Neves, J., Sarmento, B., 2016. Amorphous solid dispersions: Rational selection of a manufacturing process. Adv. Drug Delivery Rev. 100, 85-101.

Vasconcelos, T., Sarmento, B., Costa, P., 2007. Solid dispersions as strategy to improve oral bioavailability of poor water soluble drugs. Drug Discovery Today 12, 1068–1075.

Vatanara, A., 2015. Spray drying of nanoparticles to form fast dissolving glipizide. Asian J. Pharm. 9, 213–218.

Vehring, R., 2008. Pharmaceutical particle engineering *via* spray drying. Pharm. Res. 25, 999–1022.

Verma, S., Kumar, S., Gokhale, R., Burgess, D.J., 2011. Physical stability of nanosuspensions: investigation of the role of stabilizers on Ostwald ripening. Int. J. Pharm. 406, 145–152.

Vo, C.L.-N., Park, C., Lee, B.-J., 2013. Current trends and future perspectives of solid dispersions containing poorly water-soluble drugs. Eur. J. Pharm. Biopharm. 85, 799-813.

Wang, B., Zhang, W., Zhang, W., Mujumdar, A.S., Huang, L., 2005. Progress in drying technology for nanomaterials. Drying Technol. 23, 7–32.

Wang, Y., Kho, K., Cheow, W.S., Hadinoto, K., 2012. A comparison between spray drying and spray freeze drying for dry powder inhaler formulation of drug-loaded lipid–polymer hybrid nanoparticles. Int. J. Pharm. 424, 98–106.

Wang, Y., Zheng, Y., Zhang, L., Wang, Q., Zhang, D., 2013. Stability of nanosuspensions in drug delivery. J. Controlled Release 172, 1126–1141.

Washburn, E.W., 1921. The dynamics of capillary flow. Phys. Rev. 17, 273–283.

Winnik, F.M., Winnik, M.A., 1990. The interaction of sodium dodecylsulfate with (hydroxypropyl) cellulose. Polym. J. 22, 482–488.

Wlodarski, K., Sawicki, W., Kozyra, A., Tajber, L., 2015. Physical stability of solid dispersions with respect to thermodynamic solubility of tadalafil in PVP-VA. Eur. J. Pharm. Biopharm. 96, 237–246.

Wu, L., Zhang, J., Watanabe, W., 2011. Physical and chemical stability of drug nanoparticles. Adv. Drug Delivery Rev. 63, 456–469.

Wu, T., Yu, L., 2006. Surface crystallization of indomethacin below T g. Pharm. Res. 23, 2350-2355.

Wu, W., Nancollas, G.H., 1998. A new understanding of the relationship between solubility and particle size. J. Solution Chem. 27, 521–531.

Xia, D., Yu, H., Tao, J., Zeng, J., Zhu, Q., Zhu, C., Gan, Y., 2016. Supersaturated polymeric micelles for oral cyclosporine A delivery: the role of Soluplus–sodium dodecyl sulfate complex. Colloids Surf. B Biointerfaces 141, 301–310.

Yalkowsky, S.H., Roseman, T.J., 1981. Techniques of solubilization of drugs. M. Dekker, New York.

Yamashita, K., Nakate, T., Okimoto, K., Ohike, A., Tokunaga, Y., Ibuki, R., Higaki, K., Kimura, T., 2003. Establishment of new preparation method for solid dispersion formulation of tacrolimus. Int. J. Pharm. 267, 79–91.

Yan, Y.-D., Sung, J.H., Kim, K.K., Kim, D.W., Kim, J.O., Lee, B.-J., Yong, C.S., Choi, H.-G., 2012. Novel valsartan-loaded solid dispersion with enhanced bioavailability and no crystalline changes. Int. J. Pharm. 422, 202–210.

Yang, H., Teng, F., Wang, P., Tian, B., Lin, X., Hu, X., Zhang, L., Zhang, K., Zhang, Y., Tang, X., 2014. Investigation of a nanosuspension stabilized by Soluplus® to improve bioavailability. Int. J. Pharm. 477, 88–95.

Yu, L., 2001. Amorphous pharmaceutical solids: preparation, characterization and stabilization. Adv. Drug Delivery Rev. 48, 27-42.

Żarów, A., Zhou, B., Wang, X., Pinal, R., Iqbal, Z., 2011. Spectroscopic and X-ray diffraction study of structural disorder in cryomilled and amorphous griseofulvin. Appl. Spectrosc. 65, 135–143.

Zhang, S., Lee, T.W., Chow, A.H., 2016. Crystallization of itraconazole polymorphs from melt. Crystal Growth & Design 16, 3791–3801.

Zhang, X., Guan, J., Ni, R., Li, L.C., Mao, S., 2014. Preparation and solidification of redispersible nanosuspensions. J. Pharm. Sci. 103, 2166–2176.

Zhang, X., Xing, H., Zhao, Y., Ma, Z., 2018. Pharmaceutical dispersion techniques for dissolution and bioavailability enhancement of poorly water-soluble drugs. Pharmaceutics 10, 74.

Zuo, B., Sun, Y., Li, H., Liu, X., Zhai, Y., Sun, J., He, Z., 2013. Preparation and in vitro/in vivo evaluation of fenofibrate nanocrystals. Int. J. Pharm. 455, 267–275.